Hydrotreatment of pyrolysis oils over nickel-based catalysts

Zur Erlangung des akademischen Grades eines

DOKTORS DER NATURWISSENSCHAFTEN

(Dr. rer. nat.)

der KIT-Fakultät für Chemie und Biowissenschaften

des Karlsruher Instituts für Technologie (KIT)

genehmigte

DISSERTATION

von

M.Sc. Chiara Boscagli

aus

Castel del Piano (Italien)

KIT-Dekan: Prof. Dr. Willem M. Klopper

Referent: Prof. Dr. Jan-Dierk Grunwaldt

Korreferent: Prof. Dr. Nicolaus Dahmen

Tag der Mündlichen Prüfung: 10. Februar 2017

It always seems impossible
until it's done.

Nelson Mandela

Acknowledgements

The years spent on this PhD project taught me how to work alone and organise myself, but especially they emphasised the importance in science of working with other people, who have helped me with discussions and collaborations, and given me feedback and criticism bringing new input and ideas. For this reason, this section will not be so brief, since I want to thank all of them.

Firstly, I would like to thank Prof. Dr. Jan-Dierk Grunwaldt for the possibility to do this work under his supervision, giving me complete freedom in organising the project and taking the commitment to revise my work.

Thanks go to Dr. Klaus Raffelt, who supported me in these years not only scientifically, but especially from a human point of view. I thank him for letting me work with freedom and letting me grow professionally, giving me responsibilities in managing independently my research project and supervising other students. I thank him for being every time available for discussion and actually for never having a boring day with him.

I would like to thank Prof. Dr.-Ing. Sauer and Prof. Dr. Dahmen for allowing me to carry out my PhD work at the Institute.

I would like to thank in general all the employees from IKFT for the good times spent together. In particular I thank Birgit Rolli and Gilbert Zwick for analysis support in gas chromatography. I thank Pia Griesheimer, Jessica Maier, Jessica Heinrich, Petra Janke and Melanie Frank for measurements of elemental analysis, Karl Fischer titration and TGA.

For use of the laboratory facilities, discussion about catalysts and nice lunch times together I thank Dr. Karin Walter, Dr. Martin Schubert, Dr. Konstantin Hengst, Benjamin Mutz and Dr. Kai Kalz. I thank Wolfgang Olbrich for the valuable help and the good times in the lab during his stay.

For further analysis, I want to thank Hermann Köhler for ICP-OES, Dr. Silke Behrens for TEM, Dr. Thomas Otto and Doreen Neumann-Walter for TPR, William Habicht and Dr. Michael Zimmermann for SEM-EDX, and Sigrid

Abstract

The era of an energy market dominated by fossil resources is destined to finish in the foreseeable future. The scarcity of petrol reserves, together with rising energy demands due to increasing population and living standards, is prompting exploration about the feasibility of renewable energies for producing electricity, heat, fuels and chemicals. In particular, biomass plays a crucial role in the production of fuels and chemicals since it is the only renewable carbon source. In this context, thermochemical conversion processes of lignocellulosic materials have been investigated in literature and among them, pyrolysis followed by hydrodeoxygenation (HDO) was identified as an energetically and economically favourable approach. However, while pyrolysis is a well-investigated process and ready for commercialisation, HDO is still in its infancy and faces challenges mainly related to catalyst stability over long term operation. For this reason, research has been addressed to develop a stable HDO catalyst, but so far no definitive solution has been reached for an optimal scale-up. Besides the intensively studied conventional hydrodesulphurisation (HDS) catalysts and noble metals, alternative catalysts have gained more importance. Nickel-based catalysts in particular are a promising system, with lower cost compared to noble metals, and potentially higher stability than HDS catalysts. The idea of using Ni-catalysts specifically for HDO is relatively new (6-7 years ago) and only few studies have been performed with these catalysts on model compounds or pyrolysis oils. Further research is therefore necessary in order to evaluate and understand the feasibility of Ni-catalysts for this process.

The aim of this thesis was to study the performance of different nickel-based catalysts in HDO, especially for upgrading of pyrolysis oils. Various pyrolysis oils were analysed and employed: a light and a heavy phase of a bio-oil from fast pyrolysis of wheat straw, a stable bio-oil from fast pyrolysis of wheat straw, a bio-oil from intermediate pyrolysis of wheat straw followed by hot-vapour filtration, and four bio-oils produced at different intermediate pyrolysis temperature (350, 400, 450 and

500 °C) followed by hot vapour filtration. At first the bio-oils were characterised by the combination of several complementary analytical techniques, including elemental analysis, Karl Fischer titration, solvent fractionation, gas chromatography and quantitative ^{1}H-NMR (employed in the bio-oil context here for the first time). Significant differences in composition were detected depending on the pyrolysis process used. Bio-oils produced from beech wood were more stable and easier to handle than those from wheat straw, and generally contained fewer heteroatoms and minerals. Intermediate pyrolysis produced bio-oils in lower yield than fast pyrolysis and containing molecules with a higher degree of fragmentation, but with lower oxygen content. Hot-vapour filtration used downstream from intermediate pyrolysis permitted the removal of solids and minerals, providing a substrate more appropriate for HDO. Higher pyrolysis temperatures decreased the oxygen content, but at the expense of the bio-oil yield.

Successively, different nickel-based catalysts were screened in the HDO of the light phase of fast-pyrolysis bio-oil produced from wheat straw, including Ni/Al_2O_3, $NiCu/Al_2O_3$, Ni/SiO_2, Ni/ZrO_2, NiW/AC (supported on activated carbon) and Ni/TiO_2. Ru/C was used as a benchmark, as the HDO activity of this catalyst is well described in literature. Hydrodeoxygenation was performed in a batch reactor at 250 °C (mild conditions) and 340 °C (deep HDO). The nickel catalysts provided similar deoxygenation levels, producing upgraded oils with 20-26% oxygen content in mild conditions and 12-15% in deep HDO, which is a significant decrease from 40% in the original feed. The level of deoxygenation using Ru/C was similar to the nickel catalysts, but Ru/C was more active in hydrogenation, resulting therefore in higher hydrogen consumption. Nickel-based catalysts were suitable for HDO, producing upgrading oils with a significant content of ketones and avoiding aromatic ring hydrogenation. In addition, they permitted the valorisation of a low value fraction (containing mainly sugar derivatives and water) to an upgraded oil with low oxygen content and high carbon recovery.

Further studies addressed the HDO of model compounds both in a pure solvent (water) and in bio-oil, in order to elucidate the different reactivity in the two media. Experiments over nickel catalysts showed that phenol in aqueous solution was easily converted with high selectivity at 250 °C to cyclohexanol and at 340 °C to cyclohexane. On the contrary, phenol inside pyrolysis oil showed only little reactivity under the same reaction conditions. For this reason, isotopically-labelled compounds in pyrolysis oil were employed to better understand the reactivity of some model compounds. Phenol-d_6 was used to represent lignin derivatives and

D-glucose-$^{13}C_6$ for cellulose. Phenol was not converted significantly, showing only exchange of deuterium atoms in ortho and para positions of the aromatic ring with the bio-oil medium. D-glucose was completely converted forming a complex mixture of products recovered mainly in the upgraded oil. On the other hand, D-glucose in aqueous solution was selectively converted to methane.

In order to understand the cause of the different behaviour of model compounds in pure solvent and pyrolysis oil, chemical and structural changes of the catalyst before and after the reaction were investigated. The main change in selectivity was attributed to adsorption of sulphur and formation of a Ni_3S_2 layer on the nickel nanoparticle surface, that resulted in selective production of ketones and inhibited hydrogenation of the aromatic ring. The catalyst could be regenerated with no drastic structural changes and with only a low decrease in activity (circa 15% compared to the fresh catalyst) if the sulphur amount in the feed was low and sulphur adsorption limited to the catalyst surface. In contrast, if the sulphur amount was too high, intense sintering of the catalyst was observed.

The last study of the thesis included a systematic variation of HDO temperature, catalyst, feedstock and pyrolysis temperatures, in order to assess the influence on the HDO product composition. Generally, olefins were converted at 80 °C and aldehydes at 150 °C. At 250 °C the main products were alcohols over Ru/C and ketones over NiCu/Al$_2$O$_3$. At 350 °C a significant fraction of hydrocarbons and alcohols were formed over Ru/C, whereas NiCu/Al$_2$O$_3$ mainly produced ketones, which were not further hydrodeoxygenated. Phenols were not significantly converted in the whole tested temperatures range over both catalysts. The pyrolysis feedstock had a considerable influence on the HDO products, mainly due to the sulphur amount, which reduced the catalyst stability during HDO of bio-oils from wheat straw with high sulphur content (0.3%). Pyrolysis temperature influenced the bio-oil composition, which in turn affected the properties of the upgraded oils. Higher pyrolysis temperatures produced bio-oils and upgraded oils with lower oxygen content.

In conclusion, nickel-based catalysts are promising systems for HDO of pyrolysis oil, but their activity is strongly influenced by the presence of sulphur, which impacts the selectivity of the process. Therefore, if the formation of Ni_3S_2 can be controlled, nickel catalysts may be used for selective production of ketones and phenols, which are fine chemicals with a higher economic value in comparison to fuels, and which require lower hydrogen consumption for their production. The upgraded oils had a low thermogravimetric residue, which can possibly enable product separation by

fractional distillation. Further studies on long term operation using nickel catalysts are needed in order to define the feasibility of HDO in an industrial context. For this purpose a trickle bed reactor was designed and is currently under construction at the IKFT/KIT.

Kurzfassung

Mittelfristig ist es absehbar, dass das Zeitalter eines von fossilen Energiequellen dominierten Energiemarkts enden wird. Erdölreserven sind begrenzt, gleichzeitig steigt der Energieverbrauch aufgrund der steigender Weltbevölkerung und steigender Lebensstandards. Daher werden erneuerbare Quellen für den Bedarf an Elektrizität, Wärme, Treibstoff, aber auch für Chemierohstoffe untersucht. Biomasse spielt bei der Erzeugung von Treibstoff und Chemikalien eine entscheidende Rolle, weil es die einzige erneuerbare Kohlenstoffquelle ist. In diesem Zusammenhang werden seit Jahrzehnten thermochemische Konversionsverfahren von Lignocellulose untersucht. Vielversprechend ist eine Schnellpyrolyse mit darauf folgender Hydrodeoxygenierung (HDO). Während die Schnellpyrolyse eine gut untersuchtes Verfahren an der Schwelle der Kommerzialisierung ist, steckt die Hydrodeoxygenierung noch in den Kinderschuhen. Die größte und bisher ungelöste Herausforderung stellt dabei die Katalysatorstabilität über längere Laufzeiten dar. Neben den intensiv untersuchten konventionellen Hydrodesulfurierungskatalysatoren und Edelmetallen gewinnen in den letzten Jahren auch alternative Materialien an Bedeutung. Auf Nickel basierende Katalysatoren sind vielversprechend, da sie weniger kosten als Edelmetalle und eine höhere Stabilität haben als HDS Katalysatoren. Die Idee, Nickelkatalysatoren zu verwenden ist relativ neu (6-7 Jahre), daher wurden bisher nur wenige Untersuchungen zu Nickel–katalysierter HDO von Pyrolyseölen oder deren Modellverbindungen veröffentlicht, sodass weitere Forschung notwendig ist.

In dieser Arbeit wird die Wirkung verschiedener Nickel–basierter Katalysatoren beim Upgrading durch HDO an Pyrolyseöl und geeigneten Modellsystemen untersucht. Verschiedene Pyrolyseöle wurden verwendet und zuvor einer chemischen Analyse unterzogen: Eine leichte und eine schwere Phase von Pyrolyseöl aus Weizenstroh, das in der bioliq–Pilotanlage gewonnen wurde. Außerdem Bio-Öle aus Weizenstroh und Buchenholz einer mittelschnellen Pyrolyse bei 350, 400, 450 und 500 °C gefolgt von einer Heißgasfiltration. Zuerst wird das Pyrolyseöl durch verschiedene sich ergänzende Analysemethoden charakterisiert:

Elementaranalyse, Karl-Fischer-Titration, Gaschromatographie und quantitative
^{1}H-NMR Spektroskopie. Letztere Methode wird in dieser Dissertation neu in die
Analytik von Pyrolyseöl und deren Upgrading – Produkte eingeführt. Es wurden
Unterschiede in der Zusammensetzung in Abhängigkeit des Pyrolyseprozesses
gefunden. Pyrolyseöle aus Buchenholz waren stabiler und einfacher zu handhaben
als Pyrolyseöle aus Weizenstroh, außerdem hatten sie weniger Anteile an
Heteroatomen. Verglichen mit der Schnellpyrolyse war bei der mittelschnellen
Pyrolyse die Ölausbeute geringer, die Moleküle waren stärker fragmentiert
und hatten einen niedrigeren Sauerstoffanteil. Durch Heißgasfiltration wurden
mineralische Feststoffe und Kokspulver vom Öl der mittelschnellen Pyrolyse
abgeschieden. Daher waren diese Einsatzstoffe besonders gut für die HDO geeignet.
Bei höherer Pyrolysetemperatur sank der Sauerstoffgehalt, allerdings bei ingesamt
geringerer Ölausbeute.

In einem Screening wurden verschiedene Nickel haltige Katalysatoren in der HDO
einer leichten und relativ wasserreichen Phase von Schnellpyrolyseöl aus Weizenstroh
getestet: Ni/Al_2O_3, $NiCu/Al_2O_3$, Ni/SiO_2, Ni/ZrO_2, Ni/TiO_2, NiW/AC
(AC:Aktivekohle) und Ru/C. Letzterer Katalysator wurde als Bezugspunkt gewählt,
da HDO Versuche an Pyrolyseölen mit diesem Katalysator in der Literatur gut
dokumentiert sind und dieser Katalysator eine hohe Aktivität hat. Die Reaktionen
wurden in einem Batch Autoklaven bei 250 °C (milde Bedingungen) und 340
°C (tiefe HDO) durchgeführt. Die Nickel Katalysatoren zeigten unterschiedliche
Deoxygenisierungsgrade. Unter milden Bedingungen hatte das Upgrading Produkt
einen Sauerstoffanteil von 20–26%, unter schärferen Bedingungen waren es 12-15%,
was ein deutlicher Unterschied zu ursprünglichen 40% im Pyrolyseöl darstellt.
Die Deoxygenierung mit dem Ru/C Katalysator brachte die gleichen Ergebnisse
wie die Nickel-haltigen Katalysatoren, allerdings findet man mit dem Ru/C
Katalysator eine höheren Hydrierung und stärkeren Wasserstoffverbrauch. Die
Nickelkatalysatoren zeigten eine hohe Selektivität zur Bildung von Ketonen,
während aromatische Ringe nicht angegriffen wurden. Mit diesen Katalysatoren
konnte eine heizwertarme Fraktion des Pyrolyseöls zu einem heizwertreichen Öl mit
niedrigem Wassergehalt upgegradet werden, während der hohe Wasseranteil durch
Phasentrennung abgeschieden wurde.

Um den Einfluss der chemischen Umgebung auf die Reaktivität zu beschreiben
wurden HDO Experimente von Modellsubstanzen in Wasser und in Bioöl
durchgeführt und miteinander verglichen. Mit Hilfe von Nickel-Katalysatoren wurde
phenol in wässriger Lösung mit hoher Selektivität bei 250 °C zu Cyclohexanol

und bei 340 °C zu Cyclohexan umgesetzt. Unter gleichen Bedingungen aber in Pyrolyseöl sind die untersuchten Nickel-Katalysatoren jedoch fast wirkungslos. Um die Reaktionen im Pyrolyseöl besser zu verstehen, wurden auch Experimente mit Isotopen – markierten Modellsubstanzen durchgeführt. Phenol-d_6 repräsentierte dabei die Lignin Derivate und D-glucose-$^{13}C_6$ die Cellulose. Das Phenol blieb bei der Reaktion stabil, allerdings wurden ^{1}H- Atome des Pyrolyseöls in ortho- und para- Position des Phenol-d_6 eingebaut. D-Glucose hingegen wurde vollständig zu einem komplexen Gemisch umgesetzt, das sich nach der HDO vor allem in der Ölphase wiederfindet. In wässriger Umgebung bekommt man bei der Reaktion selektiv Methan.

Um den Ursachen der unterschiedlichen Reaktivitäten in Wasser und im Pyrolyseöl auf den Grund zu gehen, wurden im nächsten Schritt chemische und strukturelle Änderungen des Katalysators vor und nach der Reaktion untersucht. Vor allem wurde Adsorption von Schwefel auf der Katalysatoroberfläche gefunden, sowie die Ausbildung einer Schicht aus Ni_3S_2 auf Nickel–Nanopartikeln. Diese Veränderungen scheinen also dafür verantwortlich zu sein, dass die Hydrogenierung auf der Stufe der Ketone verbleibt und dass der aromatische Ring nicht hydriert wird. Die Nickelkatalysatoren sind regenerierbar unter nur geringem Verlust der Aktivität (ca. 15%), falls der Schwefelgehalt im Pyrolyseöl nicht zu groß ist und der Schwefel nur an der Katalysatoroberfläche adsorbiert. Bei zu hohem Schwefelgehalt sintern jedoch schwefelhaltige Partikel auf der Katalysatoroberfläche und eine Regeneration des Katalysators war dann nicht mehr möglich.

Im letzten Teil der Dissertation wurden Pyrolysetemperatur, HDO Temperatur, Katalysator und Einsatzgut systematisch variiert, um den Einfluss der Gesamtheit der Verfahrensparameter auf die Zusammensetzung der HDO Produkte zu beschreiben. Olefine werden schon bei 80 °C hydriert, Aldehyde bei 150 °C reduziert. Bei 250 °C waren die Hauptprodukte bei Verwendung von Ru/C Alkohole, bzw. Ketone unter Einfluss von Nickelkatalysatoren. Bei 350 °C findet man mit Ru/C einen signifikanten Anteil an Kohlenwasserstoffen, während es bei den nickelhaltigen Katalysatoren bei der hohen Selektivität für Ketone bleibt und die Phenole nicht in ihrem aromatischen Kern angegriffen werden. Das Einsatzgut hatte insofern Einfluss auf die HDO Produkte, als Pyrolyseprodukte aus Weizenstroh einen so hohen Schwefelanteil haben, dass die Katalysatoraktivität signifikant erniedrigt wird. Die Pyrolysetemperatur beeinflusst das mittlere molekulare Gewicht des Pyrolyseöls und den Sauerstoffgehalt nach Upgrading.

Als Schlussfolgerung kann man ziehen, dass Nickel–haltige Katalysatoren ein

geeignetes Katalysatorsystem für die Hydrodeoxygenierung von Pyrolyseölen sind, dass aber der Schwefelgehalt den Erfolg der Reaktion maßgeblich bestimmt. Wenn der Schwefelgehalt kontrolliert werden kann, dann bieten Nickelkatalysatoren die vielversprechende Möglichkeit, Pyrolyseöl zu Ketonen und Phenolderivaten umzusetzen, die als Feinchemikalien einen höheren Verkaufswert haben, als Treibstoffe und deren Herstellung nur wenig Wasserstoff verbraucht. Die Pyrolyseöle bilden nach dem Upgrading nur einen sehr geringen Rückstand in der Thermogravimetrie. Es sollte also möglich sein, das HDO Produkt durch fraktionierte Destillation zu trennen und dadurch maßgeschneiderte Wertstoffströme zu erzeugen. Um die Machbarkeit der HDO von Pyrolyseölen über Nickelkatalysatoren in einem industriellen Maßstab zu beurteilen, sind weitere Untersuchungen über das Langzeitverhalten der Nickelkatalysatoren notwendig. Zu diesem Zweck wird im IKFT gerade ein Rieselbettreaktor in Betrieb genommen, der die Hydrodeoxygenierung von Pyrolyseöl im kontinuierlichen Betrieb erlaubt.

Contents

Chapter 1

Introduction

This chapter gives an overview of the research in the field of production of bio-fuels and chemicals from pyrolysis oil and its state of the art. Different methodologies for biomass conversion are described with a special focus on pyrolysis. The main characteristics of pyrolysis oils are reported together with the current challenges. Upgrading methods are introduced and a detailed description about hydrodeoxygenation and the catalyst employed in this process is presented. Finally, the motivation and an introduction of the topics developed in this thesis are exposed.

1.1 Biomass as the only renewable source of carbon: an overview on alternative production of fuels and chemicals

Increasing awareness of crude-oil depletion and the importance of environmental safeguards have driven the politics and economy of many countries to increase the use of renewable energies and to invest in their research and development [1]. Electricity and heating energy can be produced by various alternative and carbon-neutral power sources, such as solar, wind, hydro, geothermal, tidal and biomass [2]. However, transportation fuels (for aviation, ships, long-distance trucks) as well as chemicals are connected inseparably to carbon-based sources [2–5], and it is still currently inconceivable to substitute them with other forms of energy. This is because liquid carbon-based fuels contain a high energy density per volume (e.g. diesel circa 40 MJ/L), can be stored and transported easily with negligible losses, and used off-grid also in the most remote areas with basic equipment [6,7]. On the contrary, electric energy presents, even with the most advanced technology, significant losses in storage [8] and in transportation, and needs a complex system of infrastructure for use and transport. In addition, the petrochemical industry requires carbon base-sources for the production of materials and chemicals used in daily life [9].

In a future scenario without fossil sources, biomass represents the only renewable carbon-based source [10,11]. It has the advantage to be located more homogenously on the planet in comparison to crude oil and it contributes to a CO_2-neutral economy [12,13], since the CO_2 produced by the use of bio-fuel is reabsorbed by new plants, closing in this way the carbon cycle [2]. However, biomass alone is not enough to cover the global energy demand, due to the limitation of arable lands and considering factors like preservation of biodiversity and food supply [2]. Therefore a smart integration between different renewable forms of energy is required for the transition from fossil to renewable resources.

Up to now, three generations of bio-fuels are usually distinguished [3,14,15]. The first is constituted by bio-ethanol and bio-diesel, produced respectively from biomass with high sugar content (e.g. sugarcane and corn) and high lipid content (e.g. sunflower seeds and rapeseed). The production technology and the development of this generation are in an advanced state thanks to incentives and attention in the legislative field to promote this kind of fuels. However, their production has been dissuaded in the last decade for ethical reasons, which underline that bio-fuel
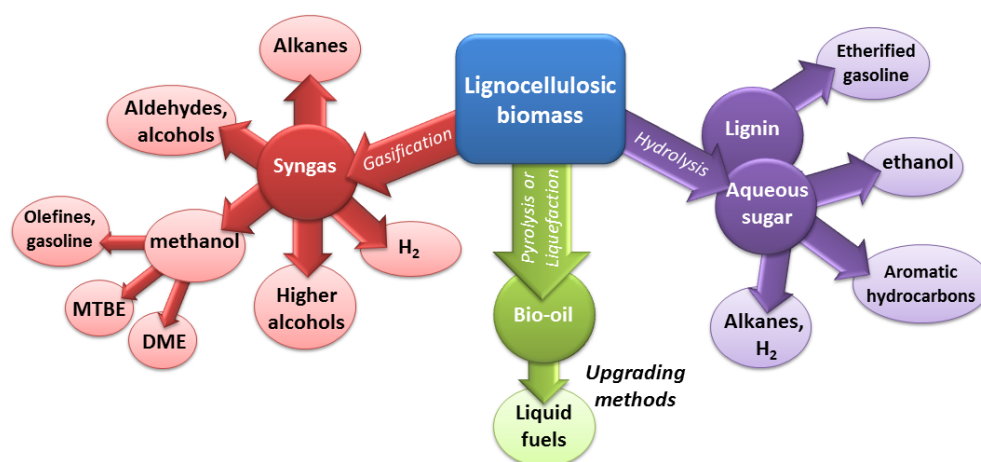
Figure 1.1: Possible routes for processing of lignocellulose biomass for bio-fuel production. Adapted with the permission of Ref. [3]. Copyright (2006) American Chemical Society.

production from edible biomass subtracts resources normally used for food [3,16].

Second generation bio-fuels are based on lignocellulosic materials [17,18], which are not in competition with food production. Usually agriculture and forestry residues, as well as other no-valuable waste can be used for the production of these bio-fuels, usually by thermochemical processes [4] or hydrolysis [3] (Figure 1.1).

Third generation bio-fuels are associated exclusively to algae [19–21], with a special focus on microalgae [22]. These have high growth rates and high solar energy capture (up to 10% in comparison to a maximum of 1% for other plants), and they grow in areas that are not in competition with other activities [3]. However, their big limitation that discourages this kind of bio-fuel is the high production costs, especially in terms of cultivation and harvesting [23].

Second generation bio-fuels receive a lot of attention and they can offer new perspectives in bio-fuel production [24]. Three main approaches have been considered for conversion of lignocellulosic biomass in bio-fuels [3,25] (Figure 1.1):

- gasification and subsequent synthesis from syngas [2, 26, 27], such as Fischer-Tropsch synthesis to obtain diesel fraction [28], synthesis through dimethylether/ methanol for gasoline or olefins [10], higher alcohols synthesis [29,30], hydrogen production by water-gas shift rection, etc;

- pyrolysis or hydrothermal liquefaction to obtain bio-oils, followed by an upgrading process [31–40];

- hydrolysis and processing of the aqueous phase containing sugars and of lignin

[2, 3]. The aqueous sugar can be converted to ethanol by fermentation, to aromatic hydrocarbons by dehydration, to alkanes and hydrogen by aqueous-phase processing, while the lignin can be upgraded to etherified gasoline [3].

Focusing on thermochemical conversion, the processes listed above are theoretically feasible, but some issues remain to be solved before scale-up and commercialisation. Biomass gasification suffers from tar formation and the syngas produced is difficult to clean efficiently to a purity degree required for subsequent synthesis [25]. On the other hand, fast pyrolysis technology is ready for commercialisation, but the upgrading process is only at its infancy [39, 40]. The challenge for upgrading pyrolysis oil (as well as bio-oil from hydrothermal liquefaction, despite being less complicated) is to find a catalyst that has long lifespan, low cost, resistance to coke formation and to leaching [32, 39, 41, 42].

From an economical and energetic point of view (considering the process thermal efficiency [3, 32]), pyrolysis followed by upgrading is the most convenient solution. Pyrolysis requires lower capital cost than liquefaction or gasification [3, 32], is a versatile process where different biomass feedstock can be used [28] and it constitutes an easy solution for energy densification [43]. For this reason, different projects developed the idea of performing pyrolysis in decentralised plants located near the biomass production point and of transporting the bio-oils to a central upgrading unit [25, 32–34, 36, 38, 44].

In the following sections, fast and intermediate pyrolysis will be presented and more details will be given about upgrading processes, specifically hydrodeoxygenation (HDO) as the main subject of this thesis.

1.2 Fast and intermediate pyrolysis: liquefaction of biomass into an energy-dense mixture

Pyrolysis is a thermal degradation reaction occurring in the absence of oxygen [31]. In the context of biomass pyrolysis, the decomposition is related to its building blocks, which are mainly cellulose, hemicellulose and lignin [45–48]. The products derived are a liquid phase (or sometimes multiple liquid phases), char and non-condensable gases. The yield and the composition of products are influenced by different process parameters, the most important ones being temperature, heating rate (correlated also mass and heat transfer) and residence time of the vapours

[31, 49–53].

Dependent on these parameters, different types of pyrolysis processes can be distinguished (Table 1.1). Fast pyrolysis is a process where the liquid production is maximised, obtaining a yield up to 70-75% of the mass of the original biomass. Usually the maximum liquid yield is reached at 500 °C with heating rates of circa 500 °C/s and vapour residence times around 1 s [31, 50]. Intermediate pyrolysis operates at similar temperatures as fast pyrolysis, but it uses more moderate heating rates (100-300 °C/min) and residence times of circa 5–30 s for the vapours and 5–20 min for the solids. The process is also finalised to maximise the liquid products. Usually two liquid phases appear in this process, an aqueous-rich phase and a bio-oil, with a total yield of circa 50%, a value that is inferior to that of fast pyrolysis. Despite the lower yield, the bio-oils produced are usually less viscous and with low tar content in comparison to fast pyrolysis oil. This technology is relatively new and only few data about it are available [2,54,55]. Torrefaction and carbonisation are pyrolysis processes using lower temperatures and residence times in order to maximise the solid yield. Gasification uses higher temperatures and the main product is gas [31].

Table 1.1: Typical conditions of different pyrolysis processes and respective product weight yield for wood pyrolysis (dry basis). Data from Bridgwater [31] reproduced with the permission of Elsevier.

Mode	Conditions	Liquid	Solid	Gas
Fast	$\sim$ 500 °C, short hot vapour residence time $\sim$ 1 s	75%	12% char	13%
Intermediate	$\sim$ 500 °C, hot vapour residence time $\sim$ 10-30 s	50% in 2 phases	25% char	25%
Carbonisation	$\sim$ 400 °C, long vapour residence hours to days	30%	35% char	35%
Gasification	$\sim$ 750-900 °C	5%	10% char	85%
Torrefaction	$\sim$ 290 °C, solids residence time $\sim$ 10-60 min	0% unless condensed, then up to 5%	80% solid	20%

One of the main interests in the field of bio-fuels is associated to fast pyrolysis, due to the higher liquid yield. For this process different reactor typologies have been developed. The most common reactors are fluidised bed, circulating fluid beds, ablative pyrolyzer, rotating cone and twin screw [56]. Commercial facilities exist already, like Ensyn Technologies (USA and Canada) [57], Dynamotive (Canada) [58], BTG (The Netherlands) [56] with the newest commercial plant Empyro (25 MW$_{th}$) operated since 2015 [59].

Fast pyrolysis oils appear as a dark brown viscous liquid with a characteristic smoky smell. The IEA Bioenergy Task 34 Pyrolysis provided the following description for fast pyrolysis bio-oils, recognised with the CAS number 1207435-39-9 [60]:

"Liquid condensate recovered by thermal treatment of lignocellulosic biomass at short hot vapour residence time (typically less than about 5 seconds) typically at between 450-600°C at near atmospheric pressure or below, in the absence of oxygen, using small (typically less than 5 mm) dry (typically less than 10% water) biomass particles. A number of engineered systems have been used to effect high heat transfer into the biomass particle and quick quenching of the vapour product, usually after removal of solid byproduct "char", to recover a single phase liquid product. Bio-oil is a complex mixture of, for the most part, oxygenated hydrocarbon fragments derived from the biopolymer structures. It typically contains 15-30% water. Common organic components include acetic acid, methanol, aldehydes and ketones, cyclopentenones, furans, alkyl-phenols, alkyl-methoxy-phenols, anhydrosugars, and oligomeric sugars and water-insoluble lignin-derived compounds. Nitrogen- and sulfur-containing compounds are also sometimes found depending on the biomass source."
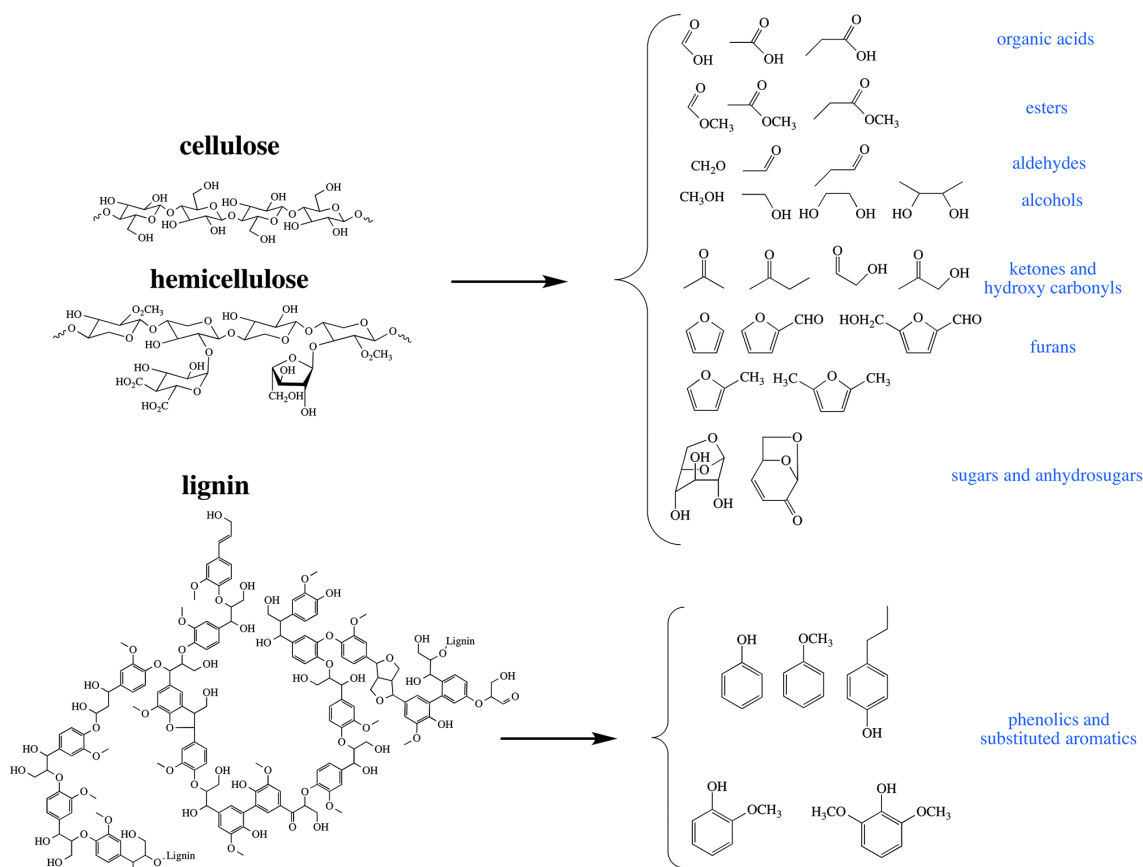
Figure 1.2: Typical products formed by pyrolysis of lignocellulosic materials. Reproduced from Ref. [61] with the permission of the Royal Society of Chemistry.

Bio-oils are therefore a complex mixture of relative polar oxygenated compounds, derived from the decomposition of the bio-polymers cellulose, hemicellulose and lignin (some representative components are reported in Figure 1.2). More than 300 components were identified, but still the main fraction has not been determined exactly. The main works in the field of pyrolysis oil characterisation have been done by Oasmaa et al. [62–64] with the development of the solvent fractionation methods and analysis standard and norms [65, 66], and by Meier et al. [50, 67, 68] with the development of gas chromatography methods for identification and quantification of several components.

Due to its polarity, pyrolysis oil is miscible with polar solvents like methanol and acetone, but not with crude oil. This is because its elemental composition is more similar to biomass than to crude oil (Table 1.2, [50, 62, 63, 66, 67]) and this constitutes a barrier for the direct processing of bio-oil in a conventional refinery [32]. The oxygen functionalities present in the organic molecules of the bio-oil are responsible for several characteristics, such as the polarity, acidity, relative low heating value, viscosity [35] and reactivity (polymerisation, aging). All these parameters can influence negatively its phase stability [69]. Another negative aspect is related to the water content, which decreases the heating value of the pyrolysis oil and can induce phase separation. The acidity constitutes a general problem in terms of material corrosion during transport, storage and processing [32]. In addition, since the different oxygen-containing functional groups in the bio-oils are rather reactive

Table 1.2: Comparison between bio-oil and crude-oil. Data reported by Mortensen et al. [32], reprinted with permission from Elsevier.

	Bio-oil	Crude-oil
Water (wt.%)	15–30	0.1
pH	2.8–3.8	–
ρ(kg/l)	1.05–1.25	0.86
μ_{50C} (cP)	40–100	180
HHV (MJ/kg)	16–19	44
C (wt.%)	55–65	83–86
O (wt.%)	28–40	<1
H (wt.%)	5–7	11–14
S (wt.%)	<0.05	<4
N (wt.%)	<0.4	<1
Ash (wt.%)	<0.2	0.1

already at low temperature, bio-oils are not distillable [64] due to their tendency to coking (polymerisation), making the separation of the bio-oil components very difficult.

Some upgrading methods, which will be described in the next Section 1.3, can decrease the oxygen content and increase the stability of the bio-oil.

1.3 Applications and upgrading of pyrolysis oil

Bio-oils with specific characteristics defined in the standard norm ASTM D7544 were demonstrated to be suitable for electricity and heat generation in static applications, like combustion in boilers, furnaces, engines and turbines [65, 70, 71]. In this case significant modifications of the combustion system should be applied in order to use bio-oils [35]. However, bio-oils can present several issues, including problems of ignition and combustion if the water content is too high, corrosion of the engine due to their acidity, coking and clogging due to carbon formation from reactive species and the solids present [38, 43, 72].

Especially for transport applications, bio-oil characteristics are not suitable, mainly due to the high content of oxygen and an upgrading process is necessary. Upgrading processes have been extensively reviewed and among them the work of Huber et al. [3], Elliott [35], Mortensen et al. [32], Bridgwater [31], and Zacher et al. [38] should be mentioned.

In general, upgrading processes are distinguished as physical, chemical and catalytic methods (Figure 1.3). The quality of the upgraded oils changes considerably dependent on the process used, and the upgrading method should be chosen to suit the desired application. Among the physical methods, filtration of the bio-oils permits the removal of solids and alkali metals (mainly concentrated in the char), which constitute a risk of fouling, corrosion, deposition and increasing of the viscosity. This pretreatment prevents eventual problems during combustion or in further treatment (like hydrotreatment), avoiding unnecessary breakdown and reducing operational costs [38]. A method demonstrated to be more successful is hot vapour filtration [73–76]. The pyrolysis vapours are filtrated downstream to the pyrolysis process, obtaining an oil with low content in char (less than 0.01%) and alkali (less than 10 ppm), with better performance compared to the employment of cyclones. However, the char trapped in the filter is catalytically active, enhancing further cracking of the vapour. This reduces the bio-oil yield and at the same time also the viscosity of the oil and the average molecular weight of the components [2].
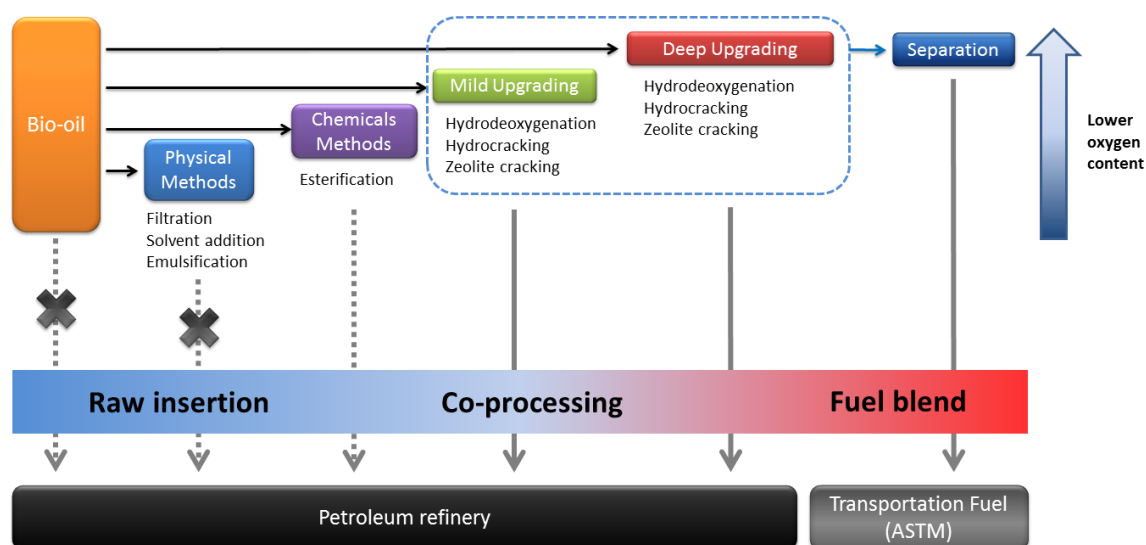
Figure 1.3: Upgrading methods and possible insertion of upgraded bio-oils in a petroleum refinery or blend with conventional fuels. Adapted from Ref. [38] with permission of The Royal Society of Chemistry.

Solvent addition is also a physical method. Diebold and Czernik [77] found that adding methanol to bio-oil increases the phase stability and the resistance to aging. On the other hand, addition of water induces a phase separation, as tested by Vispute et al [78, 79], de Miguel Mercader et al. [80] and patented by UOP [81] and Total [82]. This permits the separation of more-polar water-soluble compounds typical of the sugar derivatives fraction, from more-apolar ones derived from lignin. UOP proposed that the lignin fraction could be further hydroprocessed, while the sugar fraction could supply hydrogen by aqueous phase reforming for the hydrotreatment of the lignin fraction [78].

Emulsification with diesel was tested by Chiaramonti et al. [83, 84], demonstrating the stability of the emulsion, but high corrosion during the combustion in an unmodified diesel engine. Another disadvantage of this method is the surfactant cost and the energy invested in creating the emulsion.

Among the chemical methods, esterification of the carboxylic acids present in the bio-oil with additional alcohols (usually methanol, ethanol, or butanol) has been investigated [85–89]. Usually a catalyst is employed for this reaction and Amberlyst resins as solid acids are usually preferred, but a wide range of catalysts have been tested [89]. Esterification was demonstrated to decrease the acidity of bio-oil (and with it also the corrosion potential), the viscosity and to limit the aging, but complete neutralisation of the acidity could not be obtained due to the

thermodynamic equilibrium shifted by the presence of water.

In general physical methods do not modify substantially the elemental composition of the bio-oils, and the oxygen content remains high also using conventional chemical methods. They are potentially good methods for bio-oil stabilisation for combustion application, but the quality is neither sufficient for the production of transport fuels nor for insertion in a refinery [38]. For these purposes, the oxygen content should be further reduced, therefore catalytic upgrading is required [32].

Hydrodeoxygenation and zeolite cracking are the main catalytic upgrading methods. Hydrodexygenation has analogies with hydrodesulphurisation. It removes oxygen present in the organic molecules through the cleavage of the C-O bond forming water. The use of a catalyst, high pressure of hydrogen (up to 30 MPa) and relatively high temperatures (up 400 °C) are required. This process produces bio-oils with low oxygen content, but usually complete deoxygenation is never reached due to other competitive reactions. However, this oil is generally compatible with crude-oil and it can be further processed by FCC (Fluid Catalytic Cracking) or hydrocracking to obtain products comparable to those of a refinery [34, 38]. This process will be discussed in detail in the next Section 1.4.

Zeolite cracking removes oxygen mainly in the form of CO_2 and it related for some aspects to FCC [32]. This process works at atmospheric pressure and temperatures between 350 and 500 °C, usually over a zeolite with acid characteristics, like H-ZSM-5 [31, 32, 90–93]. The advantage of zeolite cracking in comparison to hydrodeoxygenation is that no H_2 is required (economically and energetically expensive) and it operates at atmospheric pressure, permitting low capital and operational costs. However, the upgraded oil produced contains more oxygen (therefore lower heating value), its yield is theoretically lower than the one obtained by HDO and practically this is further decreased by the formation of coke (14-23% [94]), which also causes poisoning of the catalyst [95]. Therefore hydrodeoxygenation is usually preferred as an upgrading methods despite the need for hydrogen addition. Zeolite cracking can be performed on the pyrolysis vapours downstream to the pyrolysis process, or ex situ revapourising the bio-oil, or using directly the liquid bio-oil. Catalytic pyrolysis is a similar process that uses ZSM-5 as catalyst, but it suffers from the same problems of coking. As alternative to this process, fast hydropyrolysis, which consists of a thermal decomposition in hydrogen atmosphere, has gain more importance for the advantages of stabilising radicals, removing oxygen (usually in presence of a catalyst), producing hydrocarbons and limiting

coke formation [96].

Another strategy to produce transport fuel is to gasify pyrolysis oil in order to obtain syngas [3, 31]. From this, different synthetic routes are possible, like Fischer Tropsch and synthesis of methanol, dimethylether, alcohols, olefins and gasoline. The bioliq® pilot plant [10] at the Karlsruhe Institute of Technology works on this principle. The pyrolysis plant (500 kg/h, 2 MW$_{th}$) was designed for installation in decentralised locations close to the biomass production point. This permits densification of the energy contained in the biomass in a smaller volume, for economical transportation to a central processing unit. There, slurries (char and bio-oil) can be gasified for syngas production, and subsequently synthesis of dimethylether and further to gasoline can be performed [10].

Hydrogen production could be obtained by Water Gas Shift reaction from syngas, providing hydrogen for HDO. Another hydrogen source from renewable resources can involve electrolysis of water performed by plants producing electricity, like photovoltaics or wind turbines [31, 32].

1.4 Hydrodeoxygenation

In order to increase the stability and decrease the oxygen content of the pyrolysis oil, hydrodeoxygenation (HDO) is one of the most studied and promising upgrading methods, which can provide a combustible mixture with a higher heating value and more similar composition to fossil fuels [32, 38]. The reaction is carried out under high hydrogen pressure (up to 30 MPa [32]), relatively high temperature (up to 400 °C [31]) and by employing a heterogeneous catalyst. The catalyst must be able to activate the diatomic hydrogen and to cleave the C-O bond, removing the oxygen atoms in the form of water, e.g. as illustrated schematically in Figure 1.4 for phenol. In the case of phenol and analogous compounds two routes have been observed depending on the temperature and on the catalyst. In general hydrogenation followed by acid-catalyzed dehydration (Route II) is the preferential pathway under mild-deep conditions [97], while the formation of benzene is observed only at high temperature (Route I [98, 99]). The catalyst support play also a fundamental role since it can coordinate the oxygenated compounds and its acidity can enhance the dehydration.

In general HDO of bio-oils is a slightly exothermic reaction. The high hydrogen pressure is required in order to increase the availability of hydrogen in the liquid and in proximity to the catalyst, since H$_2$ solubility is limited in liquid and especially
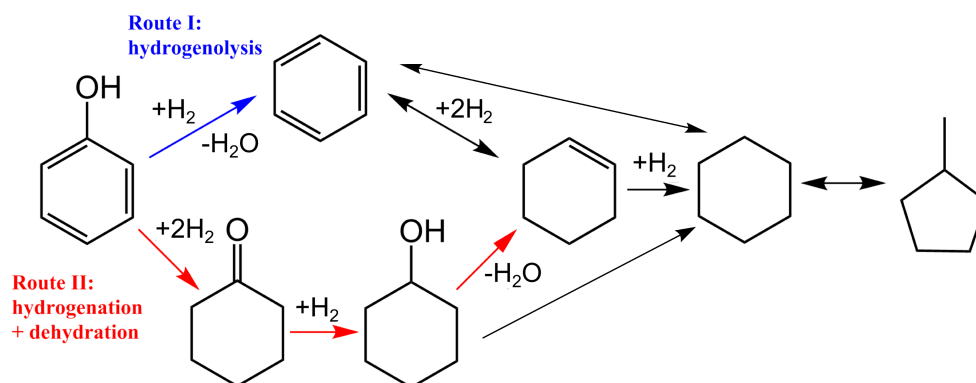
Figure 1.4: HDO of phenol according to the two routes proposed by Echendia et al. [98] (adapted with permission from Elsevier) and Mortensen et al. [97]. In general route II is favoured instead of Route I.

in polar media like pyrolysis oil. In addition, high pressure of hydrogen was demonstrated to limit polymerisation reactions, enhancing HDO.

The reaction can be simplified as:

$$CH_xO_y + (1 + y - x/2)H_2 \rightarrow 1"CH_2" + yH_2O \qquad (1.1)$$

where CH_xO_y describes the composition of a generic bio-oil and "CH_2" indicates a generic aliphatic hydrocarbon.

In reality, this formula gives no overview of the many reactions effectively happening. During HDO of bio-oils, a lot of competitive reactions can occur, like hydrogenation, hydrocracking, decarboxylation, decarbonylation, cracking, polymerisation and dehydration [32, 33, 38, 100]. Therefore it is recommendable to find a catalyst that can favour mainly HDO. In fact, hydrocracking and hydrogenation consume more hydrogen, which should be avoided because it increases the economic and energetic costs of the process and forms products with lower economical value [3]. For example, hydrogenation of the aromatic ring decreases the octane number, which is undesired if the products are bound to gasoline production [3]. On the other hand, reactions like decarbonylation, decarboxylation, polymerisation and cracking (in the case of gas formation) lower the recovery of carbon in the upgraded oil. If these parallel reactions do not occur, HDO has a theoretical carbon recovery up to 100%, which is an advantage in comparison to zeolite cracking, whose theoricatically value is much inferior. Usually, the main products of the bio-oil hydrotreating in deep conditions are similar to the naphtha fraction and further treatment, like FCC or hydrocracking, should be carried out in order to reach at transport fuel quality. In terms of mass and energy recovery,

Bridgwater [31, 93] reported that circa 25% of the weight or 55% in energy are typical yields of the naphtha fraction derived from biomass, but without including the hydrogen contribution. Considering that H_2 is produced by biomass gasification, the yield was as low as 15% of the weight and 33% of the energy.

1.4.1 HDO of different functional groups and process parameters

The challenge for the search of a catalyst selective for HDO is that different functional groups are present in the bio-oils and they have different reactivities, requiring various reaction conditions [35, 101, 102]. As reported in Figure 1.5 and described also by Grange et al. [103], each functional group has a different activation energy and reacts at a different temperature. The hydrogenation of olefins already occurs at low temperatures, followed by the hydrogenation of aldehyde and ketone groups to form alcohols. Ethers, alcohol, carboxylic acid, phenols and molecules with more substituted and hindered oxygen groups (like dibenzofuran) need gradually higher temperatures for HDO. In contrast to HDS, the temperatures used in HDO are lower and in general it is recommendable to operate around 340-350 °C. Here the upgraded oil yield and the deoxygenation degree are both high, while at higher temperature cracking reactions become more important [104], leading to product losses as gas. In addition, the exposure of the bio-oil directly to high temperatures can cause polymerisation reactions, which can be suppressed using a low-temperature HDO step for stabilisation before proceeding to the final temperature [35, 100].

The HDO product composition and yield can be different depending on the
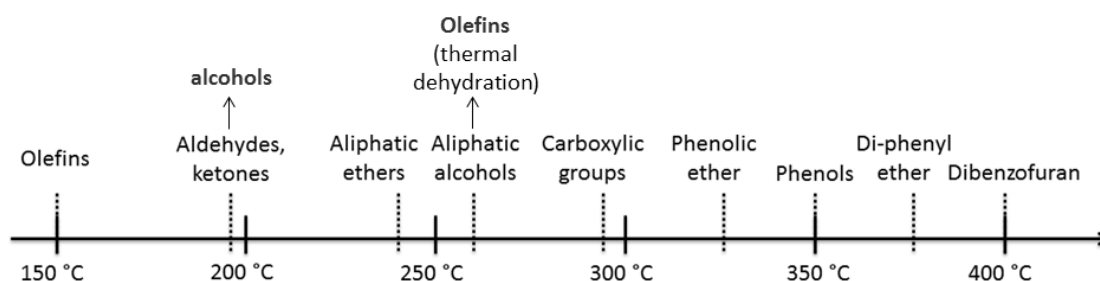
Figure 1.5: Reactivity of different functional groups present in the pyrolysis oil over sulfided NiMo catalyst as reported by Elliott [35]. Adapted with the permission of Ref. [35]. Copyright (2007) American Chemical Society.

reaction conditions used. The main products are an upgraded oil with a decreased oxygen content, and an aqueous phase containing mainly water and some soluble organic molecules. Usually gas and coke are by-products, but in general they are limited to low amount. Since bio-oil is a complex mixture of different molecules, it is normally not possible to determine the conversion of each component and other parameters are used to follow the reaction and understand the influence of the catalyst. Among them, the upgraded oil yield is used (Y_{oil}, eq. 1.2) and it constitutes the mass percentage of the upgraded oil (m_{oil}) derived from the original feed (m_{feed}).

$$Y_{oil} = \left(\frac{m_{oil}}{m_{feed}} \right) \cdot 100 \tag{1.2}$$

However, this parameter is not sufficient to describe HDO and it should always be considered together with the deoxygenation degree (D.O.D., eq.1.3), expressed as the percentage of oxygen removed (wt.%O_{feed} - wt.%O_{oil}) in comparison to that present in original feed (wt.%O_{feed}) [32]. This indicates how much oxygen is removed during the reaction.

$$D.O.D. = \left(1 - \frac{wt.\%O_{oil}}{wt.\%O_{feed}} \right) \cdot 100 \tag{1.3}$$

These two parameters are inversely correlated. Usually for a higher level of deoxygenation, the yield of the oil is decreased, since less oxygen is contained in the oil. Another parameter of interest connected to these two parameters is the recovery of carbon in the upgraded oil (R.C., eq.1.4), which gives an indication of the percentage of carbon (wt.%C_{oil}) recovered in comparison to that contained in the original pyrolysis oil((wt.%C_{feed}) (theoretical maximum 100%).

$$R.C. = \frac{wt.\%C_{oil} \cdot Y_{oil}}{wt.\%C_{feed}} \tag{1.4}$$

The van Krevelen plot [105], which is usually employed for fossil fuels classification, is also a good system to monitor the effectiveness of HDO of pyrolysis oils. In Figure 1.6, the van Krevelen plot shows that pyrolysis oil has an O/C ratio much higher than fossil fuels (e.g. gasoline or diesel) and a H/C ratio that is in general lower. The general purpose of HDO is to lower the O/C ratio, without decreasing too much the H/C (which is correlated to the mean molecular weight and the viscosity) in order to obtain from pyrolysis oil something compatible for mixing with fossil fuels.
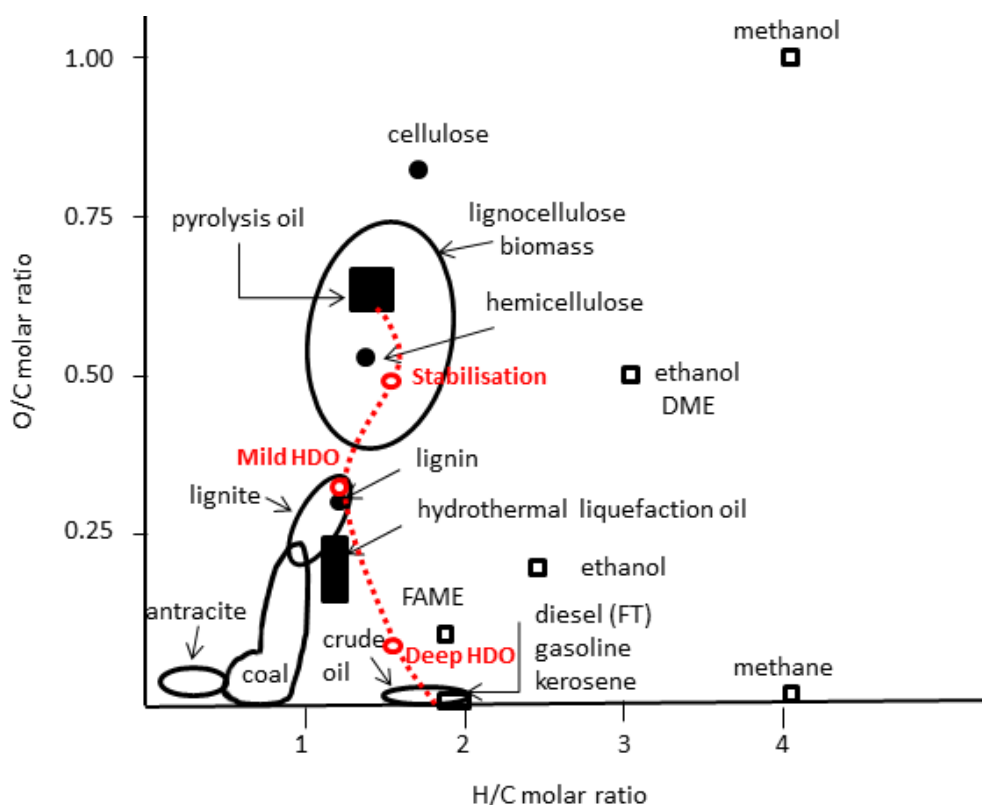
Figure 1.6: Van Krevelen plot of fossil and biomass derived material. An indication of the hydrotreatment effect on upgraded oil composition is reported in red dashed line (Venderbosch et al. [33]). Adapted from Kersten et al. [106] with the permission of John Wiley and Sons.

The dependency of the H_2 consumption versus the degree of deoxygenation was studied by Venderbosch et al. [33] and it was found not to be linear (Figure 1.7). A distinction was made between stabilisation (<200 °C), mild HDO or mild hydrotreatment (up to 250°C) mainly for co-processing, and deep HDO (up to 400°C) for fuel blend or other refinery processes. At low temperature (175 °C) the hydrogen consumption was higher in comparison to the extrapolated value, due to hydrogenation reactions. For higher D.O.D. the hydrogen consumption was lower than the estimated value and this was explained by dehydration reactions and phase separation occurring already at mild HDO. De Miguel Mercader et al. [44] found that the higher heating value (HHV) of the final product was directly proportional to the H_2 consumption in a quantity equal to 1 MJ/kg per mol/g H_2.
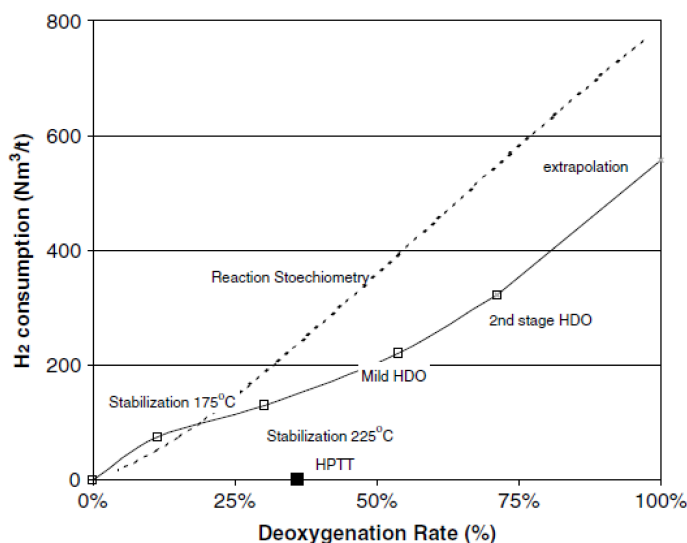
Figure 1.7: Dependency of the hydrogen consumption from the deoxygenation degree as reported by Venderbosch et al. [33], reproduced with the permission of John Wiley and Sons.

1.4.2 Reactors and strategies for HDO

In the design of a reactor for HDO, different important aspects have to be considered. The reactor should be able to operate at high temperature (up to 400 °C), high pressure (up to 40 MPa) in order to favour hydrogen solubility and in the acidic environment of bio-oils (pH 2-4). This means that an appropriate choice of the materials and of the structure design should be done. A good mixing is fundamental in order to avoid mass transfer limitations, especially in the case of a three-phase reaction system. In this case the relatively high viscosity of the bio-oil can be problematic especially at low temperature, while using higher temperatures permits the decrease of the bio-oil viscosity. Other issues during operation are connected to the tendency of bio-oils to polymerise, form coke and provoke clogging the reactors. Higher amount of hydrogen usually limits coke formation. The operation conditions and the catalyst choice should be done considering that different functional groups with different reactivities are present in the bio-oils. One of the big challenge remains the stability of the catalyst, as previously reported.

In the literature various studies on HDO of model compounds and different pyrolysis oils have been reported. The most common systems employed were batch and trickle bed reactors. The latter exhibits a higher level of complexity but are more suitable for further developments and scale-up. Long reaction times are required, in general between 3-4 hours [107] for batch reactors and liquid hourly space velocity

(LHSV) between 0.1-1.5 h^{-1} for continuous reactors [35,104,108]. Different catalysts have been tested and an overview will be given in Section 1.5.

The group of Elliott at the Pacific Northwest National Laboratory (PNNL) has strongly advanced the engineering aspects [38]. Elliott and Baker [109] patented in 1989 a two step hydrotreating process, which consists of a first stabilisation step to minimise coke formation in a temperature range between 250-280 °C, followed by higher temperature for effective HDO in the range of 370-400 °C. Typically a HDS catalyst (CoMo/γ-Al$_2$O$_3$ or NiMo/γ-Al$_2$O$_3$) was used for both stages. The two step hydrotreating has been accepted and applied in the majority of HDO studies regarding continuous reactors and pyrolysis oils. In some experiments in batch reactors, the reaction was carried out already during the heating ramp, providing in this way the stabilisation of the bio-oil [34].

In 2009, Elliott et al. [104] reported a D.O.D between 98-99 % for pyrolysis oil derived from different feedstocks. This was obtained using a down flow reactor with a catalyst bed of Pd/C for the hydrodeoxygenation (two steps at 310 and 370 °C, 14 MPa H$_2$) and a proprietary sulphided catalyst for hydrocracking at 405 °C and 10 MPa H$_2$. The same results were obtained using a non-isothermal configuration at 250-410 °C and 14 MPa H$_2$. For these studies an excess of hydrogen (35-420 mol H$_2$/kg bio-oil) in comparison to the theoretical stoichiometric value (25 mol H$_2$/kg bio-oil calculated by Venderbosch et al. [33]) was used.

Recent studies were performed in a two stage non-isothermal reactor [110]. The first stage is carried out at 150-200 °C with RuS/C catalyst and the second stage at 350-410 °C (14 MPa H$_2$), obtaining a D.O.D. between 94 and 99.5%. A further stabilisation step at lower temperature ($<$17 MPa) before the non-isothermal hydrotreating was demonstrated to increase the lifetime of the catalyst [110]. The untreated pyrolysis oil showed plugging after 50 hours, while the stabilised pyrolysis oil was resistant for more than 70 hours.

While PNNL worked mainly in deep hydrotreatment, a European project, BIOCOUP, evaluated both mild and deep HDO conditions in order to define the standard for a bio-oil for insertion in a conventional crude-oil refinery. In the context of the project, de Miguel Mercader et al. [80] investigated the hydrotreatment of the two bio-oil fractions obtained by phase separation, induced by adding water. Processing the two phases separately resulted in lower yield of the total upgraded oil compared to the process with the whole bio-oil, but it can present advantages for the co-processing through an efficient tailoring of the upgraded oil.

De Miguel Mercader at al. [44] also evaluated the co-processing of the upgraded

oils in a Micro-Activity Test (MAT) unit simulating FCC. The goal of co-processing is to prepare oils suitable for insertion in a refinery with the minimum needed pretreatment, therefore minimum invest of H_2 and energy. After a HDO at 230–340 °C, the upgraded oils, which contained 17-28 wt.% of oxygen (dry basis), were tested in a MAT reactor as a 20% mixture with VGO (Vacuum Gas Oil) fraction and they were found to be suitable as FCC feed. The products obtained were similar to those produced by the VGO fraction alone, without driving to an excessive polymerisation and coke formation. This demonstrated the feasibility of co-processing. However, undiluted upgraded oils showed excessive coking when treated alone in a FCC simulating unit. Co-processing upgraded bio-oils in a crude-oil refinery has the advantage of exploiting an existing infrastructure compared to deep hydrodeoxygenation for the production of fuel or fuel blender, which requires new facilities, leading to higher the capital costs.

Other subtasks of the BIOCOUP project dealt with testing and preparing alternative catalysts to the conventional HDS ones. Wildschut et al. [107,111,112] and Ardiyanti et al. [113–117] tested, prepared and developed noble-metal catalysts and nickel-based catalysts. This subject will be presented in detail in the next Section 1.5.

1.5 Catalysts for hydrotreating: state of the art and new perspectives

Since HDO has analogies to HDS, the first class of catalysts tested was the same employed in HDS processes, like sulphide CoMo/γ-Al$_2$O$_3$ and NiMo/γ-Al$_2$O$_3$. However, the oxygen content is largely higher in bio-oil than in crude oil. While crude oil has less than 1% oxygen, bio-oils contain circa 40% and this large amount can result in poisoning of the catalyst. Hence, several studies were focussed on prolonging the catalyst lifetime and/or preparation of alternative catalysts. In fact, the big challenge that blocks commercialisation of HDO is the development of a catalyst with a good stability in contact with bio-oil, long lifetime, good conversion at relatively low temperature, low coke formation, and preferably cheap for minimising the costs of a plant. [39].

In this section, an overview of different catalysts employed in literature will be given, dealing with conventional HDS catalysts (Section 1.5.1), noble metals (Section 1.5.2), non-noble metal catalysts based on nickel (Section 1.5.3) and in addition a

summary of the main deactivation processes (Section 1.5.4).

1.5.1 Conventional HDS catalysts

Catalysts for HDS of crude oil, such as sulphided CoMo/γ-Al$_2$O$_3$ and NiMo/γ-Al$_2$O$_3$, have been widely tested in HDO reactions of model compounds and pyrolysis oils [32, 42, 118].

According to the mechanism suggested by Romero et al. [119], Co and Ni act as promoters, which modify the electronic properties of Mo and weaken the Mo-S bond (Figure 1.8). This permits the formation of sulphur vacancies (coordinatively unsaturated sites of Mo) very reactive on the slab edge, which are the active sites. Hydrogen adsorbs on a site near to the vacancy, reducing Mo and forming S-H and Mo-H. On the vacancy, the molecule adsorbs, coordinating to Mo through the oxygen functionality. The S-H group donates a proton to the active oxygenated compound, forming a carbocation and promoting the cleavage of the C-O bond. After the elimination of water from the active site, the vacancy is restored. These catalysts work very well in the context of HDS related to crude oil and a lot of studies were performed in order to understand the complex structure and the mechanism during the hydrotreatment of crude oil fractions [120–126].
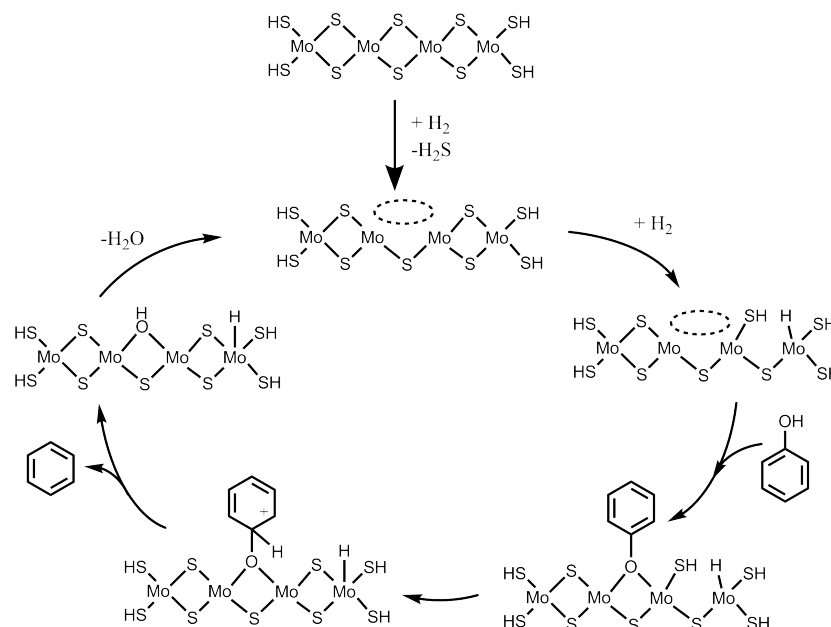
Figure 1.8: Hydrogenation mechanism of phenol over a conventional sulphided HDS catalyst, according to Romero et al. [119]. Adapted from Ref. [32] with permission of Elsevier.

In HDO, conventional HDS catalysts have shown satisfying performance in terms of oxygen removal, as demonstrated in different studies with model compounds and pyrolysis oil [35,110,111,118,127–130], but not in terms of catalyst stability [32,98, 131–134]. The deactivation of these catalysts is associated to the transformation of the active sulphur species in oxide, due to the low amount of sulphur and high oxygen content present naturally in the pyrolysis oil [32,37]. Co-feeding of H_2S during the HDO reaction regenerates the active sites, restoring the catalytic activity. However, the products are contaminated by the presence of thiols and sulphides [135–137]. Water formed during the reaction also exhibits a negative influence on the catalyst activity. Water blocks some active sites by adsorption on them and in addition it reduces the stability of the support by converting the γ-alumina into boehmite [138–140]. Another important deactivation route is associated to the deposition of carbonaceous species on the catalyst surface [32, 37, 140]. On the other hand, if suitable operating conditions are used, the catalyst can resist for relative long period of operation. For example Olarte et al. [141] reported for a proprietary sulfided catalyst an operation time over 700 hours.

Since the sulphide form of the conventional HDS catalysts is not stable, MoO_3 was suggested by DFT (Density Functional Theory) as a possible substitute [142], but this showed lower activity in the HDO of 4-methylphenol due to the strong Mo-O bond [143]. Another suggestion from DFT was WO_3, which was tested by Echendia et al. [98] also in combination with nickel on carbon support. The combination of tungsten with nickel produced high conversion with HDO selectivety of phenol and low carbon formation, showing promising results.

The substitution of the γ-alumina with other less acidic and more water-stable supports reduces coke formation and increases the stability of the catalysts. A good candidate can be carbon support [32, 98, 111, 144, 145] but also inorganic supports like silica, zirconia, ceria were found suitable in activating the oxygen-containing compounds, and they have lower tendency to coke production than γ-alumina [32].

1.5.2 Noble metals

As an alternative to HDS catalysts, which have the disadvantage of requiring H_2S co-feeding and getting deactivated in the presence of water, noble metals were tested in HDO reactions. These constitute a sulphide free solution, more environmentally friendly and they resulted in having high activity. The mechanism of these catalysts involve activation of hydrogen on the metal surface, followed by adsorption and

deoxygenation of the oxygenated substrate (Figure 1.9). Adsorption of oxygenated compounds could happen on the metal surface or on the support-metal interface [32, 42]. This latter step is still not well comprehended and both mechanisms were suggested [146–148].

Supported noble metals have been studied by several groups with model compounds and pyrolysis oil. Gutierrez et al. [149] studied the HDO of guaiacol in a batch reactor. The highest activity was attributed to Rh/ZrO_2, showing a performance superior to that of conventional HDS catalyst, while Pd/ZrO_2 and Pt/ZrO_2 were less active.

Wildschut et al. [111] found Ru/C as the most active catalyst in HDO of pyrolysis oil, with only 6% oxygen in the upgraded oils (batch reactor, 350 °C, 10 MPa H_2), followed by Pd/C. Further studies on Ru/C in a batch reactor investigated the stability and optimised the reaction time and other parameters [150, 151]. De Miguel Mercader et al. [80] used Ru/C for pretreatment HDO studies of bio-oil fractions for co-processing, while Venderbosch et al. [33] tested this catalyst in a continuous plant, obtaining upgraded oils with higher oxygen content (14% vs 6%) in comparison to the batch experiment, probably because the reaction time was lower [38].

Ardiyanti et al. [115] tested different noble metals, such as Rh, Pd, Pt, RhPt, RhPd, PdPt on zirconia in a batch reactor at 350 °C and 8.5 MPa H_2. Their activity was comparable to the conventional HDS catalyst on a gram basis catalyst, but was higher per gram of active metal.

Elliott et al. [152] patented the use of Pd/C for bio-oil hydroprocessing. In different studies Ru/C was used as a catalyst for low temperature stabilisation [110] or studied in model compounds until 300 °C [102] (also Pd/C), showing good activity
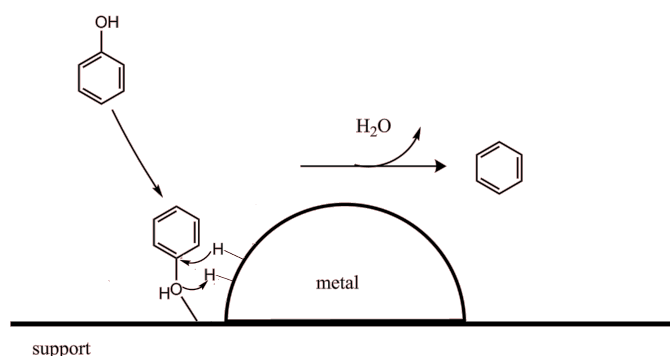
Figure 1.9: One of the possible hydrodeoxygenation mechanism of phenol over noble metals, showing the synergy between support and metal nanoparticle.

and less formation of carbon compared to HDS catalysts.

Despite the good activity in HDO, noble-metal catalysts are discouraged for industrial scale use due to their high price and low availability. In addition, they are active also in hydrogenating aromatic rings, resulting in an excess consumption of hydrogen. They can also be poisoned by the low amount of sulphur in the bio-oil [36, 140, 153]. For these reasons, alternative catalysts also to noble metals are currently being designed and tested.

1.5.3   Alternative non-noble catalysts based on nickel

Other categories of catalysts were investigated in order to find an optimal solution, offering lower cost and hydrogen consumption than noble metals, and higher stability than HDS catalysts. Transition-metal phosphides, nitrides and carbides, Fe-based catalysts and nickel-based catalysts have been described in the literature [42]. Among them, nickel-based catalysts are an attractive and promising alternative [140, 154] thanks to their lower price, higher availability and potentially lower consumption of hydrogen with respect to noble metals.

The mechanism of this catalyst typology is analogous to the one described in Section 1.5.2. Nickel acts as an active centre for hydrogen adsorption, while the metal oxide support binds the oxygen functionality of the organic compound to the surface (Lewis acid) with a successive oxygen cleavage.

A number of studies have been published on nickel catalysts using model compounds, [41, 41, 97, 98, 113, 140, 155–162] while relatively few have involved real pyrolysis oils [113, 114, 116, 117, 163]. Yakovlev at al. [140] observed that in the conversion of anisole and bio-diesel, bimetallic Ni-Cu catalysts were more attractive than those containing nickel alone, due to the spill over effect enhanced by the presence of copper. Catalyst supports were found to have a role in HDO, with CeO_2 and Al_2O_3 being more effective in HDO of anisole (300 °C, 1 MPa).

Echeandia et al. [98] studied phenol conversion on Ni-W supported on active carbon in a fixed bed reactor (150-300 °C 1.5 MPa). Different W precursors were used for catalyst preparation. The catalyst prepared by phosphotungstic acid (HPW) was found to be more effective in HDO already at low temperature, and at 300 °C the conversion was 98% with selectivity circa 95% for cyclohexane. Benzene (<5%) was also observed from another reaction pathway involving deoxygenation of the aromatic ring without hydrogenation.

Zhao et al. [155] converted some phenolic monomers, like phenol, guaiacol,

syringol and similar compounds, over Raney nickel and Nafion/SiO$_2$ catalysts. Nickel is active as a hydrogenation catalyst, while Nafion acts as Brønsted acid for dehydration. The tests were carried out at 200 °C and 5 MPa, obtaining high conversion and selectivity for hydrocarbons.

Bykova et al. [156] tested in a batch reactor some nickel-based catalysts prepared by sol-gel methods at 320 °C and 17 MPa. The main products observed were cyclohexane, 1-methylcyclohexane-1,2-diol and cyclohexanone. The most active catalysts were supported on SiO$_2$ and SiO$_2$-ZrO$_2$.

Mortenson et al. [97] tested a total of 23 catalysts for phenol conversion at 275 °C and 10 MPa in a batch reactor. The catalysts belonged to different typologies, including oxide catalysts, methanol synthesis catalysts, reduced noble and non-noble metal catalysts, but significant HDO activity was recorded only by the last two categories. Among the noble metals, Ru was the most active, while among the non-noble metal catalysts Ni/ZrO$_2$ was found as most promising. HDO was proven to be influenced by the catalyst support, proving its role in the activation of the phenol and successive C-O cleavage.

Mortenson et al. [162] investigated also the influence of the active particle size of Ni/SiO$_2$ on the conversion of phenol at 275 °C and 10 MPa. The range of the particle size investigated was between 5-22 nm. Deoxygenation was observed only after previous hydrogenation of phenol, and the particle size affected the rate of HDO reaction steps. Bigger particles were more active for hydrogenation, and smaller particles for deoxygenation, demonstrating that the C-O cleavage probably occurred at step/corner sites, while hydrogenation was favoured on larger facets.

Bykova et al. [41] developed modified bimetallic NiCu/SiO$_2$–ZrO$_2$ adding P and Mo in order to increase their mechanical strength and their stability in acid media. The tests during guaiacol conversion at 320 °C and 17 MPa (initial hydrogen pressure) in an autoclave showed that phosphorus and molybdenum addition decreased the guaiacol conversion and deoxygenation degree, but the mechanical strength and the stability in the acidic medium were improved. Reduced tendency towards gas and coke formation was also observed.

Studies related to pyrolysis oil were mainly conducted at the University of Groningen, in collaboration with the Boreskov Institute of Catalysis. Ardiyanti at al. [113] tested bimetallic Ni-Cu catalysts proposed previously by Yakovlev et al. [140]. Different loadings and metal ratios were tested with pyrolysis in a batch reactor at 350 °C and 10 MPa H$_2$. Higher H/C ratio and low thermogravimetric residue was found for a loading of 16% Ni, 2% Cu on δ-alumina (chosen for its

higher thermal resistance and less acidic character in comparison to γ-alumina). Another study [114] focused on the influence of different supports for the bimetallic NiCu catalyst. The authors identified NiCu/TiO$_2$ as a catalyst that can improve the quality of the upgraded oil.

Novel bimetallic NiCu- and NiPd-based (Picula) catalysts [117] were tested in HDO of pyrolysis oil in an autoclave (1 h at 150 °C, 3 h at 350 °C, and 20 MPa initial pressure at 350 °C). They have high loadings of nickel (29–58 wt.%) and were prepared by sol–gel method using as supports SiO$_2$, La$_2$O$_3$, kaolin, ZrO$_2$, and combinations thereof. In this case the catalyst with the highest nickel loading (58 wt.% Ni) promoted with Pd (0.7 wt.%) was the most active, producing an upgraded oil with lower oxygen content, higher solubility in hydrocarbons, and less coke formation.

Yin et al. [163] tested the Picula catalyst (Ni 46%, Cu 5%) in a continuous reactor from 80 °C to 410 °C and 10-20 MPa. Upgraded oils with lower oxygen content (<13%) were found for 410 °C and a reactivity scale was identified: sugar derivatives reacted at temperatures <200 °C, lignin derivatives >300 °C and organic acids >350°C. Continuous operation over 40 h was demonstrated without serious problems of reactor clogging.

Nickel based catalysts can be a valid alternative, but more studies are necessary to understand this system, especially regarding the resistance to poisoning and their behaviour during long term operation.

1.5.4 Deactivation

Preventing catalyst deactivation in HDO is a big challenge, since different components present in pyrolysis oil can cause deactivation, like water, sulphur, potassium, calcium and chlorine. Some reactive organic molecules can also polymerise and deposit as coke on the catalyst surface [160].

In general, the deactivation of a catalyst can occur by chemical, mechanical and thermal means [153,164–166]. The most common deactivation causes in the context of pyrolysis oil hydrotreating are coke formation on the surface of the catalyst, deposition of alkali metals, adsorption of inorganic species like nitrogen or sulphur, sintering of the nanoparticles and leaching. Carbon deposition is reported as one of the main source of deactivation, which mechanically blocks access to the active sites. Elevated temperatures favour polymerisation reactions, therefore carbon formation is more observed with increasing temperature [33,164]. HDS conventional catalysts

tend to produce more carbon in comparison to noble metals, and in general supports that have more Lewis and Brønsted acid sites can form carbocations, resulting in polymerisation if the hydrogen pressure is too low [32, 42].

The stability of HDS conventional catalysts is compromised by the high oxygen content in the bio-oil, which results in formation of molybdenum oxide instead of the active sulphide form [167]. In order to prevent deactivation an additional sulphur source (co-feeding) is needed, but this can bring to production of organic compounds containing sulphur as products. The presence of water forms an inactive nickel sulphate layer that covers the active sulphide phase or nickel aluminate, and can convert the γ-alumina in boehmite. This leads to restructuring of the catalyst phase, blockage of the active site and consequently a decrease in activity.

Sulphur adsorption on the active metal surface can constitute a problem of deactivation for noble metals and nickel catalyst, but only few studies have been addressed to see the resistance of this catalyst to the relatively low sulphur content in pyrolysis oil [36, 160].

Concerning nickel catalyst deactivation, only a few studies in literature were reported and this subject should be deeply understood in order to evaluate the feasibility of these catalysts for the HDO process. Mortensen et al. [160] analysed the stability of Ni/ZrO_2 in the presence of sulphur, potassium and chlorine during hydrodeoxygenation of guaiacol. The catalyst exhibited deactivation in contact with even small amounts of sulphur forming bulk NiS. However, other studies regarding lignin hydrogenolysis [168,169] showed that this kind of deactivation might be prevented by high hydrogen pressure that shifts the equilibrium in favour of metallic nickel. Potassium seemed to have a role in the deoxygenation step, but was very marginal in hydrogenation. Chlorine decreased the activity of the catalyst by competitive adsorption on the active site, but the original activity was almost recovered when the chlorine source was removed from the stream.

In the studies of Ardiyanti et al. [113, 114, 117], the analysis of the spent catalysts after HDO of pyrolysis oil is reported and also preliminary tests about the regeneration feasibility [117]. The main sources of deactivation were coke deposition, leaching and sintering.

1.6 Motivation of the thesis

The depletion of crude oil makes the transition from a fossil-fuel based system to renewable resources more imminent. While heat and electric power can be generated

from several renewable energies in stationary plants, transport fuels and chemicals can currently be produced only by carbon-based sources and among the renewable resources mainly by biomass.

Biomass conversion has an increasing impact in scientific and industrial society and different methodologies have been developed in order to replace the products obtained by crude-oil. Petroleum is also a product of biomass transformation happening by intense heat and pressure over millions of years. Fast pyrolysis tries to accelerate this process, liquefying biomass on the scale of seconds. However, in comparison to crude oil, pyrolysis oil contains higher amounts of oxygen, which influences its properties negatively. Hydrodeoxygenation is an attractive upgrading method that reduces the oxygen content and produces more stable products with similar characteristics as crude-oil. Whereas fast pyrolysis technology is in an advanced state and ready for commercialisation, hydrodeoxygenation is still in its infancy. The main challenge is developing a HDO catalyst for conversion of a wide variety of compounds which remains stable over long operation times. Although several catalyst systems have been tested in literature, still no convincing catalyst has been developed for transferring this process to industrial scale. Current studies are addressed to develop alternatives to conventional HDS catalysts or those based on noble metals, and nickel-based catalysts offer good prospects.

As the investigation of nickel-based catalysts in the context of HDO started only circa 6-7 years ago [140], a lot of open questions are still present. The majority of studies have focused on HDO of model compounds, while HDO of pyrolysis oils is a topic that was investigated in relatively few works [113,114,116,117,163]. Hence, this thesis aims to study the HDO of pyrolysis oil over nickel-based catalysts. Different pyrolysis oils from fast and intermediate pyrolysis of wheat straw and beech wood were tested. The origin and therefore the different properties of the bio-oils can have an influence on the HDO reaction. Therefore, firstly an extensive characterisation of the oils is reported in Chapter 3. The main focus is addressed to pyrolysis oils derived from wheat straw instead of wood. This is a topic almost untouched in literature and it constitutes a challenge, since this type of pyrolysis oil normally has issues with phase stability and may contain more inorganic species, which could interfere in the upgrading process.

Different catalysts containing nickel were used with a light phase of pyrolysis oil from wheat straw in mild (Chapter 4) and deep hydrotreatment conditions (Chapter 5). The catalysts were selected on the basis of other studies in literature that reported good results with pyrolysis oil or model compounds. However, the

selected catalysts have not previously been compared in a consistent manner with pyrolysis oil. The catalysts chosen were characterised by different supports, active metal loadings and eventually promoters: Ni/Al_2O_3 [97], $NiCu/Al_2O_3$ [113,114,140], Ni/SiO_2 [97], Ni/ZrO_2 [97], NiW/AC (supported on activated carbon) [98] and Ni/TiO_2 [97]. The experiments were carried out in batch mode and the results were compared to those obtained over Ru/C used as a benchmark. The choice of the light phase of a pyrolysis oil was intended to better understand the reactivity of sugar derived components. This is a topic that has hardly been examined in literature, where the majority of the studies involve model compounds derived from lignin. Chapter 5 compares the conversion and selectivity of nickel catalysts towards selected model compounds in both pyrolysis oil and aqueous solution, in order to explain the different behaviours reported in literature.

In Chapter 6 deactivation of $NiCu/Al_2O_3$ is reported. The study was carried out in order to understand the effect of pyrolysis oil on the catalyst in terms of activity, selectivity and physical/chemical changes, and evaluate whether regeneration can restore the activity of the catalyst. This work is a preliminary study to test the suitability of $NiCu/Al_2O_3$ for long term operation, understanding which parameters influence the catalyst activity and how to prevent deactivation.

In the last part of the work (Chapter 7), a systematic variation of different parameters, including HDO temperature, pyrolysis temperature, biomass feedstock (wheat straw and beech wood) and catalyst type ($NiCu/Al_2O_3$ and Ru/C), was performed in order to define their influence on the composition of the HDO products. Only few studies in literature have reported systematic variations of these parameters [110, 170]. This experimental approach is important for understanding the reactivity of different compounds with respect to temperature and catalyst composition, in order to tune the upgraded oil composition to a more favourable one for the requested application.
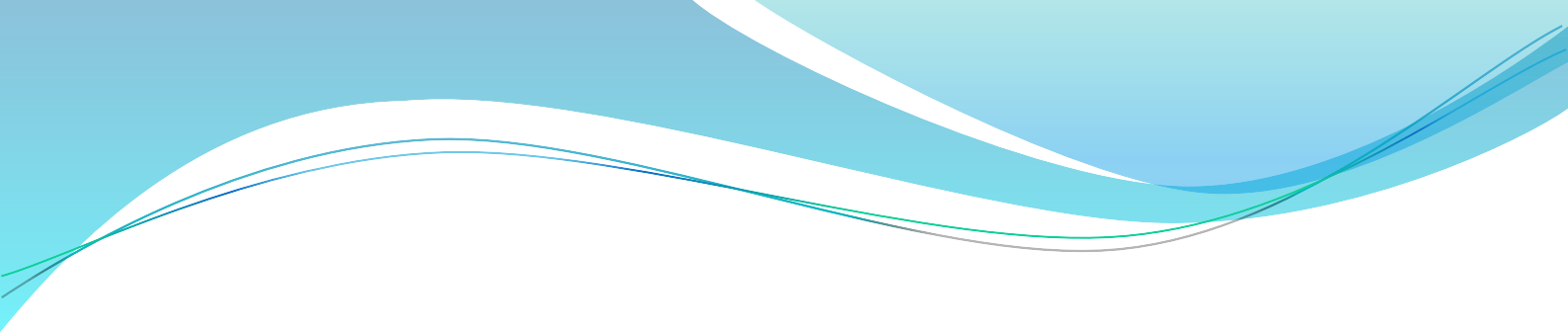
Chapter 2

Materials and methods

This chapter describes the materials, methods and procedures used for the experiments presented in this thesis. A description about the production of the pyrolysis oils will be given in the first section. In the second section, the preparation and characterisation of the catalysts before, after reaction and after regeneration are presented. In the third section the experimental setup, reaction conditions, product separation and mass balance are described. Finally, the analytical techniques used for characterisation of the bio-oil and the upgraded products are reported.

2.1   Pyrolysis oil production

Different bio-oils produced from fast and intermediate pyrolysis were used for the hydrotreatment. Fast pyrolysis oils from wheat straw were produced in the bioliq® pilot plant (500 kg/h, 2 MW$_{th}$) at the Karlsruhe Institute of Technology [10]. The wheat straw was previously ground and introduced in a twin-screw mixing reactor, where it was pyrolysed at 500 °C in the presence of hot sand as a heat exchanger. The pyrolytic vapours, after a residence time of few seconds, were condensed into two fractions: a water-rich fraction and the so-called bio-oil. Two pyrolysis oils from this plant were used: 1) an unstable bio-oil, which presented a spontaneous phase separation resulting in a "light phase" and "heavy phase" (described in Section 3.2); 2) a stable bio-oil (named bioliq bio-oil, Section 3.3). In the case of the stable oil, a pre-coat filtration was done in order to reduce the char content, using an apparatus from the company *J. Rettenmaier & Söhne GmbH* . The filtration was conducted at 0.6 MPa at 80 °C (not at higher temperature in order to avoid bio-oil polymerisation). The filter bed was 0.7 mm thick and composed of 125-250 µm char particles recycled from the pyrolysis process.

Intermediate pyrolysis oils were produced in STYX, a bench scale reactor developed in ITC/KIT (Institute of Technical Chemistry at the Karlsruhe Institute of Technology), previously described by Tomasi Morgano et al. [54]. The STYX is a screw reactor with integrated hot gas filtration (ceramic filter candles), which permitted elimination of char and minerals. The residence time of solids can vary in the range of 5–25 min. Three condensers quenched the vapours, obtaining an oily phase (bio-oil) and an aqueous phase. Four bio-oils from beech wood (Section 3.4) were produced at 350, 400, 450, 500 °C and a bio-oil from wheat straw (straw 450 °C bio-oil, Section 3.3) was produced at 450 °C.

2.2   Preparation and characterisation of the catalysts

Different nickel-based catalysts were screened in the hydrodeoxygenation reaction: NiCu/Al$_2$O$_3$, Ni/SiO$_2$, Ni/ZrO$_2$, NiW/AC and Ni/TiO$_2$ were prepared by wet impregnation and their activity was compared to that of commercial catalysts, such as Ru/C (Sigma Aldrich n. 206180, nominal loading 5%) and Ni/Al$_2$O$_3$ (C&CS METH 134, nominal loading 20%). In the following sections, preparation, characterisation, additional analysis of the spent catalyst and the regeneration

procedure will be described.

2.2.1 Preparation of the catalysts

Five nickel-based catalysts were prepared by wet impregnation of supports with aqueous solution of the precursors. The supports alumina (SA31145, mainly theta alumina, specific area 79.8 m^2/g), silica (SS61138, specific area 241 m^2/g), zirconia (SZ61152, tetragonal, specific area 126.9 m^2/g) and titania (ST61120, anatase, specific area 141 m^2/g) were supplied by Saint Gobain NorPro. Active carbon (AC) was purchased by Sigma Aldrich (Norit ROW 0.8 SUPRA, n.329428). The metal precursor salts used were $Ni(NO_3)_2 \cdot 6H_2O$ (Alfa Aesar n. A15540), $Cu(NO_3)_2 \cdot 2.5H_2O$ (Alfa Aesar n.12523) and sodium phosphotungstate hydrate (Aldrich n. 496626).

First the supports were milled to a fine powder (mean Waddel disk diameter less than 100 µm), then were mixed with the solution containing the metal precursors (weight ratio of support/solution circa 1:10). A rotary evaporator was used to remove water (50 °C, 0.005 MPa) and the resulting catalysts were dried overnight in an oven at 105 °C. The calcination was carried out in air at 500 °C (4 hours) for $NiCu/Al_2O_3$, Ni/SiO_2, Ni/ZrO_2 and Ni/TiO_2. The following reduction was performed at 500 °C in an atmosphere of 25% H_2 in N_2 (total flow 1.6 NL/min) for 4 hours. The preparation of NiW/AC was inspired by the one described by Echeandia et al. [98] with some variations: first the support was impregnated with the solution of the tungsten precursor (sodium phosphotungstate hydrate, pH 5), dried overnight, calcined under nitrogen at 400 °C, then impregnated again with the nickel solution, dried overnight and calcined again at 400 °C. The reduction was carried out at 500 °C with 25% H_2/N_2. The commercial Ni/Al_2O_3 was reduced at 500 °C for 4 hours under 50% H_2 atmosphere before use.

2.2.2 Regeneration of the catalysts

After the HDO reactions, the catalysts were regenerated in order to observe structural/chemical variations and in some cases changes in activity compared to the original catalysts (results reported in Chapter 6). Only catalysts with inorganic supports were regenerated. The spent catalysts recovered from the same reactions in the same conditions were calcined at 500 °C for 5 hours and reduced at 500 °C in the same conditions of the original catalyst (Section 2.2.1).

2.2.3 Basic catalyst characterisation

The catalyst metal content was determined by ICP-OES (Inductively Coupled Plasma - Optical Emission Spectrometry) using a Agilent 725 ICP-OES Spectrometer, after pre-digestion of the sample with HNO_3, HCl and H_2O_2 in a microwave oven (600 W, max 6 MPa, 240 °C, 45 min).

In order to determine the reduction temperature profile of the active metal, the temperature programmed reduction (TPR) was measured with an Autochem HP 2950 (Micrometrics) using a heating rate of 5 °C/min and 25% H_2 in Ar with a global flow of 30 ml/min.

The total specific surface area of the catalyst was determined by nitrogen physisorption with a Belsorp Mini II at 77 K and calculated by applying BET theory in the fitting range between 0.05-0.30 p/p_0 (12 points).

Powder X-Ray diffraction (XRD) was measured using an X'Pert PRO MPD instrument (PANalytical GmbH) equipped with a copper anode (Cu K_α 1.54060 Å). The XRD patterns were recorded for some samples in a 2θ range between 20° and 80° (30 min, step size 0.017°) and for others between 5° and 120° (1h, step size 0.017°). The average crystallite size was estimated using the Scherrer equation [171, 172] (shape factor used K=0.9) after correction of the instrumental line broadening and if necessary after subtracting the contribution of the support signal.

Leaching of the catalyst was monitored by analysing the aqueous phase by ICP-OES (Agilent 725 ICP-OES Spectrometer).

2.2.4 Electron Microscopy

In order to have an overview on the elements present on the catalyst, SEM-EDX (Scanning Electron Microscopy - Energy Dispersive X-ray spectroscopy) was employed. The FE-SEM (field emission-SEM) used was DSM 982 Gemini, Carl Zeiss Ltd. (Oberkocken, Germany) equipped with a secondary ion, backscattered and transmission detectors. The EDX unit constituted a Si(Li) X-ray detector (type INCA Penta FET; 30 mm^2 crystal size; Oxford Instrument UK). The approximate superficial concentration detected by SEM-EDX is reported as an average of ROIs (Region of Interest) of circa 1 mm^2.

Fresh $NiCu/Al_2O_3$ and used at 250 °C were analysed by TEM (Transmission Electron Microscopy) on a FEI Tecnai F20 ST TEM (operating voltage 200 kV, located in IAM/KIT), equipped with a field emission gun and EDAX EDS X-ray spectrometer (Si(Li) detecting unit, super ultrathin window, active area 30 mm^2,

resolution 135 eV (at 5.9 keV)). For TEM and STEM analysis, the catalysts were suspended in ethanol. A small droplet of the dispersed catalyst was deposited on an amorphous carbon-coated 200 mesh Al grids and eventually air dried.

Fresh $NiCu/Al_2O_3$ and used at 340 °C was analysed by TEM at INT/KIT. The powder samples of the catalysts were directly dispersed on molybdenum grids covered with holey carbon film. Morphology of the catalysts was characterised by high angle annular dark-field (HAADF) scanning transmission electron microscopy (STEM) and its composition information were acquired by single EDAX S-UTW EDX detector in FEI Titan 80-300 microscopy operating at 300 kV. Quantification analysis of EDX spectra and STEM-EDX spectrum imaging were based on standardless model of EDX Quant functions in TEM image & analysis (TIA 4.7 SP3 version) software.

2.2.5 Surface-sensitive methods for catalyst analysis

For the characterisation of the surface, XPS (X-ray photoelectron spectroscopy) was used. For this purpose, the catalyst powder was compressed into a pellet: circa 200 mg catalyst powder was pressed into a stainless steel grid (13 mm in diameter) at 0.5 MPa for 2 minutes with a hydraulic press and then mounted on a sample holder. The XPS measurements were performed using an Al K_α (non-monochromatic, 1486.68 eV) X-ray spectrophotometer with a VG Scienta R4000 electron energy analyser (located at IFG/KIT) . The instrument was calibrated with reference peaks of $Au4f_{7/2}$ (84.00 eV) and $Ag3d_{5/2}$ (368.26 eV). Surface composition and concentrations were determined after the subtraction of a Shirley background. A product of Gaussian and Lorentzian functions was used for fitting the peaks and the integrated area was divided by the Relative Sensitivity Factor (RSF) [173]. To eliminate the influence of surface charging, the binding energies were corrected assuming that C1s line of adventitious carbon is at 285 eV. An experiment to assess the exact position of peak Ni^0 nanoparticles, was performed with an in-situ reduction of the catalyst (500 °C for 1 hour at $5.0 \cdot 10^{-9}$ MPa).

For analysing deposits on the surface of the catalyst, ToF-SIMS (Time-of-Flight Secondary Ion Mass Spectrometry) was performed on a pellet prepared in the same way as for XPS. The spectrometer located at IFG/KIT, a TOF.SIMS5 instrument (ION-TOF GmbH, Münster, Germany), was equipped with a Bi cluster primary ion source and a reflectron type time-of-flight analyser. UHV base pressure was $<5 \cdot 10^{-9}$ mbar. For high mass resolution, the Bi source was operated in the "high

current bunched" mode providing short Bi^+ primary ion pulses at 25 keV energy, a lateral resolution of approx. 4 μm, and a target current of 0.8 pA. The primary ion beam was rastered across a 500×500 μm field of view on the sample, and 128 x 128 data points were recorded. Primary ion doses were kept below 1011 ions/cm^2 (static SIMS limit). For charge compensation an electron flood gun providing electrons of 21 eV was applied and the secondary ion reflectron tuned accordingly. Spectra were calibrated on the omnipresent C^-, C^{2-}, C^{3-}, or on the C^+, CH^+, $CH_2{}^+$, and $CH_3{}^+$ peaks. Based on these datasets the chemical assignments for characteristic secondary ions were determined. For depth profiling a dual beam analysis was performed in non-interlaced mode: the primary ion source was again operated in "high current bunched" mode with a scanned area of 300 x 300 μm (10 frames with 128 x 128 data points) and a sputter gun (operated with $O_2{}^+$ ions, 2 keV, scanned over a concentric field of 600×600 μm, target current 200 nA) was applied to erode the sample for 5 s followed by a 0.5 s pause. Thereby, the sputter ion dose density was >100 times higher than the Bi ion dose density.

2.2.6 X-Ray Absorption Spectroscopy

XAS (X-Ray Absorption Spectroscopy) was employed to determine the local structure of nickel (Ni K edge 8333 eV) and when possible of copper (Cu K edge 8988 eV). XANES (X-ray Absorption Near Edge Structure) and EXAFS (Extended X-ray Absorption Fine Structure) spectra were recorded at the XAS beamline of the ANKA synchrotron (Karlsruhe, Germany). For ex-situ measurements, a pellet was prepared by grinding and homogenising the catalyst with cellulose (in total 100 mg, dilution circa 1:4) and pressing it with a hydraulic press. The pellet was covered with Kapton tape. Nickel was measured in transmission and copper in fluorescence mode (due to its low concentration in comparison to nickel).

For *in-situ* measurements, a pre-reduced catalyst was diluted with alumina 1:2 (wt.%), sieved to obtain 100-200 μm grains and set as a packed bed in a quartz capillary with a diameter of 1.5 mm [174]. A flow of 5% H_2 in He (total flow 50 mL/min) was conducted through the capillary and it was heated at 5 °C/min using a hot air blower (Gas Blower GSB-1300, FMB Oxford [175]) until 500 °C. The reduction was followed during the heating ramp by XAS by measuring first the copper reduction and switching to nickel once the copper was completely reduced. This gave an indication of the reduction temperature of copper and nickel. Full EXAFS spectra were recorded once the sample was cooled down to

room temperature.

XANES spectra were analysed with the software Athena 0.8.054 (Ifeffit package [176]), by linear combination of NiO and Ni of a standard commercial catalyst. EXAFS spectra were analysed with Artemis 0.8.011 using FEFF 6.0 code for theoretical backscattering amplitudes and phases [177, 178]. Only the first-shell scattering paths were considered.

2.2.7   Analysis of carbonaceous deposits on the spent catalyst surface

Carbon deposition, sulphur and nitrogen content were mainly monitored by elemental analysis C, N, S of the spent catalysts measured on Elemental Vario el Cube. This method was not suitable for carbon-supported catalysts and in this case the difference between the weight of catalyst recovered after and before the reaction was reported in the case that the value was positive.

In order to gain information about the persistency of the carbon deposit, a Thermogravimetric Analysis (TGA, operated using Netzsch STA 409) was carried out under atmospheric pressure composed of 21% oxygen with the following program using circa 200 mg of sample: heating ramp 10 °C/min from 20 to 105 °C, stabilisation at 105 °C for 1 hour, heating ramp 10 °C/min from 105 to 1100 °C, temperature kept at 1100 °C for 1 hour.

The chemical nature of the carbon deposit was investigated by Attenuated Total Reflectance - Infrared Spectroscopy (ATR-IR), using a Varian 660-IR FT-IT spectrometer connected to an attenuated total reflection element (diamond). The catalyst powder was analysed directly without any pretreatment. The spectra were recorder with resolution of 1 cm^{-1} in the range 230-4000 cm^{-1}.

2.3   Reaction setup for mild and deep hydrotreatment

Following the synthesis and characterisation of the catalysts, the experimental setup and experimental procedures are presented in the next section. The recovery of the products, the hydrogen consumption as well the mass balance are also included.

2.3.1 Reactors for hydrotreatment

Mild hydrotreament experiments presented in Chapter 4 and in Chapter 6 were carried out using a 200 ml autoclave (Figure 2.1) built in the mechanical workshop of IKFT/KIT (Institute of Catalysis Research and Technology at the Karlsruhe Institute of Technology). It was built of 316Ti stainless steel and designed for a maximum temperature of 250 °C and pressure of 30 MPa. The heating system of this autoclave constisted of an aluminium mantle with four electrical cartridges (maximum heating power circa 5 °C/min). The stirrer was a magnetically coupled impeller (minipower Premex).

For deep hydrotreatment (Chapter 5 and 6) and the experiments presented in Chapter 7, a 200 ml autoclave made of Inconel alloy 625 was used (Figure 2.2). It was built in IKFT/KIT and designed for a maximum pressure of 36 MPa and a temperature of 400 °C. It was equipped with a magnetically coupled stirrer (torque 80 N·cm, Premex AG) and a gas injection stirrer, which facilitates the mass transfer of hydrogen in the liquid medium. The heating was performed using heating cartridges inserted in a brass mantle and the power supply was controlled by a self-made Labview program (Figure S1).
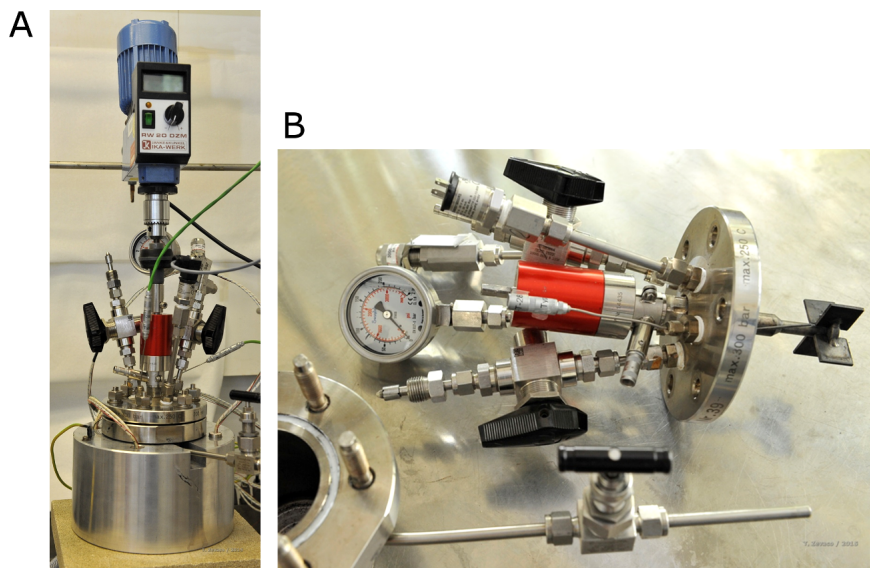
Figure 2.1: Autoclave used for mild hydrotreatment experiments (maximum temperature of 250 °C and pressure of 30 MPa). Reprinted from Ref. [179] according to the terms of Creative Commons Attribution License (CC BY).
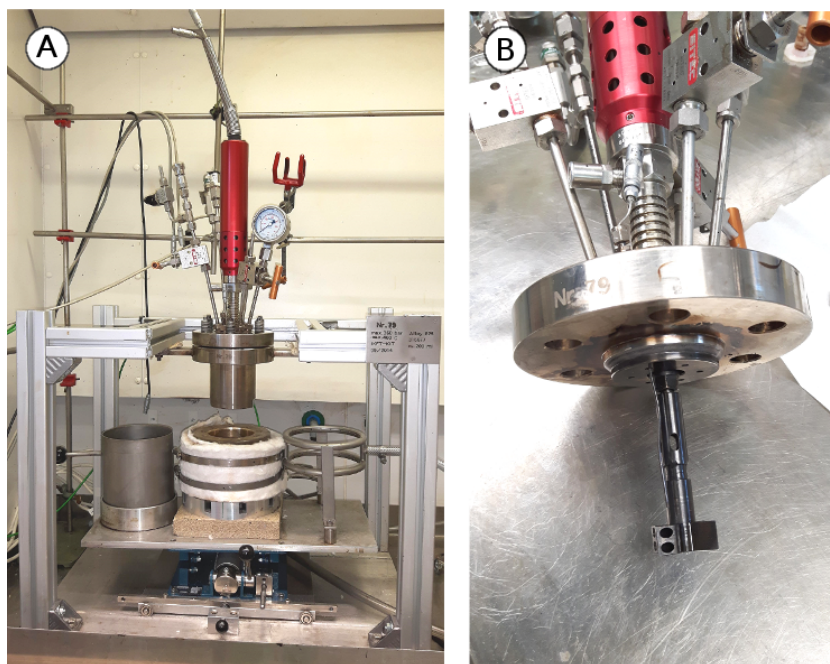
Figure 2.2: Autoclave used for deep hydrotreatment experiments (maximum temperature of 400 °C and pressure of 36 MPa).

2.3.2 Reaction conditions for the hydrotreatment

Independent of the autoclave used and the experiment done, the reactor was filled with 50 g of light phase or bio-oil and 2.5 g of a pre-reduced catalyst and purged with nitrogen before loading the hydrogen (6.0 Air liquid). In general a fine catalyst powder (mean Waddel disk diameter less than 100 µm) and the maximum speed rate of the impeller (1000 rpm) were used. Mass transfer and kinetic factors are difficult to accurately determine since pyrolysis oil contains many different components, each of them having its own hydrodeoxygenation/hydrogenation reaction mechanism with a different kinetic expression. However, minimising mass transfer, especially gas-liquid H_2 mass transfer (which play an important role), can be achieved using an adequate mixing, small catalyst grains and a stabilisation step (for example during the heating ramp or as an additional isothermal step) in order to favour hydrotreating over competitive reactions like polymerization [100]. Similar setups and reaction conditions to the one reported in this thesis were adopted previously in the literature [107, 112, 113]. The reaction time of each set of reactions was chosen in dependence of the hydrogen consumption of the bio-oil over the time (monitoring online the variation of hydrogen pressure). In each chapter the experiments presented were performed in different conditions, therefore a specific description

for each chapter will follow.

In Chapter 4, the light phase of the fast pyrolysis oil was used with different nickel-based catalysts, with Ru/C and without any catalyst (blank experiment). 8.0 MPa of hydrogen were inserted in the autoclave at room temperature. The heating ramp used was 5 °C/min and the stirrer was activated at 1000 rpm already during the heating ramp in order to stabilise the oil and avoid polymerisation at high temperature [34]. The mild hydrotreatment was carried out at 250 °C under autogenous pressure and the reaction was quenched in an ice bath after 4 hours at this temperature. Each experiment reported was repeated twice and was found to be reproducible. The results are reported as the average.

In Chapter 5 three kinds of experiments were carried out:

- light phase of the pyrolysis oil over different nickel-based catalysts and Ru/C: circa 50 g of pyrolysis oil and 2.5g of catalyst were inserted in the autoclave;

- light phase of pyrolysis oil and isotopically-marked platform molecules over NiCu/Al$_2$O$_3$ and Ru/C: circa 50 g of pyrolysis oil, 2.5 g of catalyst, 200 µg of phenol-d$_6$ (Aldrich, 176060) and 200 µg of D-glucose-^{13}C$_6$ (Deutero, 50302) were inserted in the autoclave;

- platform molecules in milliQ water over NiCu/Al$_2$O$_3$ or Ru/C: 50 g of a solution of 10 wt.% phenol (for synthesis, Merck, 8.22296.1000) and 2.5 g of catalyst were inserted in the autoclave. The same amount was used in case of a solution of 10 wt.% D-glucose monohydrate (for microbiology, Merck, 1.08342.2500). In order to have more information about the reactivity of D-glucose monohydrate, a single experiment with a concentration of 10 wt.% in pyrolysis oil was additionally carried out over NiCu/Al$_2$O$_3$ and Ru/C.

Once the reagents were inserted in the autoclave, the autoclave was closed and pressurized with hydrogen (6.0) until 8.0 MPa at room temperature. The stirrer was switched on at 1000 rpm and the heating ramp was started with a rate of 15 °C/min until 340 °C. The global reaction time, including the heating ramp, was 100 minutes. The reactor was quenched before in a flow of compressed air and subsequently in an ice/water bath. For each typology of experiment also a blank test (without catalyst) was run. Each experiment was repeated twice and the results are reported as an average.

In Chapter 6, the same experiments carried out with NiCu/Al$_2$O$_3$ in Chapter 4, 5 and 7 were performed with the regenerated catalyst using the same conditions.

In Chapter 7 different temperatures for the HDO reaction were used for beech 450 °C bio-oil and straw 450 °C bio-oil: 80, 150, 250, 350 °C. Two experiments were performed at 350 °C, with and without the stabilisation step at 150 °C. For the reaction at 80, 150 and 250 °C the reaction time was one hour at the final temperature. For the experiment at 350 °C the reaction temperature was kept for 2 hours (since the hydrogen consumption did not stop after 1 hour like at the other temperatures) and when used, the 150 °C stabilisation lasted 1 hour. The other beech-wood bio-oils produced by intermediate pyrolysis (350, 400, 500 °C) and the bioliq bio-oil were hydrotreated only at 350 °C (2 hours) with previous stabilisation step at 150 °C (1 hour). For the reactions presented in Chapter 7, NiCu/Al$_2$O$_3$ and Ru/C were used as catalysts. Once the reagents were inserted in the autoclave, hydrogen was pressurized to 14.0 MPa at room temperature. The stirrer was set at 1000 rpm and the reactor was heated until the desired temperature. Once the reaction was complete, the autoclave was quenched with compressed air and then with an ice/water bath. The experiments were repeated only once due to the restricted amount of pyrolysis oil.

2.3.3   Recovery of the products

After the reactor was quenched, an aliquot of gas was sampled and analysed by gas chromatography (details in Section 2.4.2). The liquid and solid products were collected from the reactor and centrifuged at 8000 rpm for 30 minutes (Thermo Scientific Heräus Biofuge Stratos, fixed angle rotor 26 n.75003014). The products were separated in an aqueous phase, an upgraded oil (in some experiments two organic phases were present) and the catalyst together with eventual carbonaceous solids formed. The aqueous and oil phases were separated and weighted. The residue in the reactor (usually consisting of catalyst, solid and tar-like components) was collected by washing the reactor wall with acetone. This fraction, together with the solid fraction from centrifugation, was washed with acetone and filtered with a Whatman filter (Grade 589/3 blue ribbon).

In general, the filtrate was dried under vacuum and only in Chapter 4 it was dried overnight at 105 °C and then weighed. The carbon content of the solids formed was determined by elemental analysis of the spent catalyst. Only in Chapter 4 in the case of Ru/C, NiW/AC and the blank experiment, it was not possible to separate the solid from the oil, therefore the fraction soluble in acetone was analysed after acetone evaporation with the same techniques used for the oil.

2.3.4 Calculation of the hydrogen consumption and gas production

The hydrogen consumption (indicated as $molH_{2c}$ in eq. 2.1) was determined from the difference of the number of hydrogen moles before ($molH_{2i}$) and after the reaction ($molH_{2f}$) at room temperature. The starting moles of hydrogen and the final total moles of gas (mol_{TOT}) were calculated using the Soave-Redlich-Kwong equation [180, 181] for real gases. The ($molH_{2f}$)was calculated multiplying mol_{TOT} by the hydrogen fraction in the gas (C_{H2}) determined by GC (Section 2.4.2). Generally, the volume of the gas phase before and after the reaction was considered unchanged. The cubic equation for the variable moles obtained by the Soave-Redlich-Kwong equation was solved by iterative method. Often in this work the hydrogen consumption is reported as NL per kg of pyrolysis oil (NL/kg), calculated by conversion of mol in NL.

$$molH_{2c} = molH_{2i} - molH_{2f} = molH_{2i} - mol_{TOT} \cdot C_{H2} \tag{2.1}$$

For estimation of the hydrogen consumption during the reactions, the following assumption and simplifications were made. In the case of the light phase, its partial pressure was well approximated by the Clausius-Clapeyron equation calculated for water (Figure S2). The change of the gas volume, the hydrogen solubility [182] and the production of other gases were considered negligible. Therefore the partial pressure of hydrogen was calculated subtracting the partial pressure of the light phase at each temperature from the total pressure. The moles of hydrogen in the reactor over time were calculated by the Soave-Redlich-Kwong equation.

For the estimation of each gas produced (mol_i), the global amount of moles contained at the end of the reaction (mol_{TOT}) was multiplied for component fraction (C_i) measured by GC (eq. 2.2).

$$mol_i = mol_{TOT} \cdot C_i \tag{2.2}$$

2.3.5 Calculation of the mass balance, elemental composition and Higher Heating Value

In Chapter 4, the mass balance was calculated by weighing each phases and the losses were usually below 10%.

In the experiments reported in the other chapters, the losses of the liquid products on the reactor wall and on the catalyst were in the range of 10-20 wt%. In this case, the mass balance of the liquid products was calculated using the elemental composition of each phase and the principle that the mass of carbon and oxygen should be conserved during the reaction.

$$
\begin{cases}
TotC = \dfrac{\%wp \cdot C_w + \%oil \cdot C_{oil}}{100} \\
TotO = \dfrac{\%wp \cdot O_w + \%oil \cdot O_{oil}}{100}
\end{cases}
\tag{2.3}
$$

In the equation system 2.3, *Tot C* and *Tot O* are the quantity of carbon and oxygen theoretically recovered in the upgraded oil and aqueous phase. These quantities were calculated subtracting the carbon and oxygen contained in the gas and solids from the amount of the feed. The mass and elemental composition of the gas phase were calculated as described in Section 2.3.4. The carbon present in the solid was determined by elemental analysis (Section 2.2.7), while the oxygen was considered negligible. *%wp* and *%oil* are the quantity (wt.%) of aqueous phase and upgraded oil respectively produced from the reaction. C_w and C_{oil} are the carbon percentage measured by elemental analysis of the aqueous and the oil phase. O_w, O_{oil} is the analogous oxygen percentage. Solving the following system for *%wp* and *%oil* permits calculation of the mass balance minimizing the losses and giving a more precise result. This permitted closing the mass balance with less than 3% error, but it was not possible to use it when two organic phases and an aqueous phase were formed.

The Higher Heating Value (HHV) of bio-oils and upgraded oils was calculated with Channiwala's equation (eq.2.4, [183]).

$$
HHV(MJ/kg) = 0.3491C + 1.1783H - 0.1034O - 0.0151N + 0.1005S - 0.0211ash
\tag{2.4}
$$

2.4 Characterisation of the bio-oils and the upgraded products

Hydrotreatment of pyrolysis oil formed several product phases: a gas phase, an upgraded oil, an aqueous phase and solids (not separable from the catalyst). Different analytical techniques were used in order to determine the characteristics

of the bio-oils and upgraded products. Herein a short description of the techniques and the methods used are reported.

2.4.1 Elemental composition of bio-oils and upgraded products

The water content was determined by Karl Fischer titration (titration system Titrando 841, Metrohm). HYDRANAL-Methanol dry and HYDRANAL-Composite 5 (Sigma Aldrich) were used as solvent and reagent for the titration.

Elemental analysis C, H, N of the bio-oils, upgraded oils and aqueous phases were measured by the elemental analyser CHN628 (Leco). Oxygen was calculated by the difference. The results of elemental analysis presented in Chapter 4 were provided by an external institute (FM-VEA, KIT) following the method DIN51721 for carbon and hydrogen determination and DIN51722 for nitrogen. Also in this case the oxygen content was calculated by difference.

In the case of the light phase of the fast pyrolysis oil (Section 3.2), since nitrogen was under the detection limit of the elemental analysis, the TNb (Total Nitrogen bound) was measured with a Dimatec 2000 (Dimatec). The sulphur and the metal content were determined by ICP-OES (Agilent 725 Inductively Coupled Plasma Optical Emission Spectrometer).

2.4.2 Analysis of the gas phase

The gas phase was analysed by gas chromatography using a 7890A Agilent gas chromatograph equipped with two columns (Restek 57096 Hayesep Q and Resteck Molsieve 5A) and connected to a TCD and an FID detector. 100 µl of the gas were injected (injector temperature 250 °C) and a split ratio 28:1 was used (carrier gas helium). The oven temperature program for the analysis was: 50 °C for 10 min, heating rate 3 °C/min until 90 °C, 20 °C/min until 150 °C (temperature held for 16 min), 50 °C/min until 230 °C, 10 min at 230 °C. A system of switching valves between the two columns during the measurement and a catalyst for the conversion of CO and CO_2 to methane were used.

In Chapter 4, the composition of the gas was characterised using an analogous system constituted by a 6890 Agilent gas chromatograph equipped with the same columns and TCD and FID detectors, but no catalyst for the conversion of CO and CO_2.

2.4.3 Analysis of bio-oil and upgraded products by gas chromatography

The liquid products were analysed by different gas chromatography techniques for qualitative and quantitative measurements. Helium was used as carrier gas.

A gas chromatograph HP 5890 with a column Type Rxi-5Sil MS (0.25 µm x 0.25 mm x 30 m) and a FID detector was used for quantification of mainly phenol derivative compounds. The samples were diluted or extracted in ethylacetate, dependent on their miscibility with this solvent. An external calibration was used for quantification of specific components. The injection volume was 1 µl (split ratio 1:30, injector temperature 275 °C). The following program for the GC oven was used: 35 °C for 3 min, heating rate 6 °C/min until 180 °C, heating ramp 30 °C/min from 180 °C to 280 °C and 20 min at 280 °C.

For the quantification of acids, alcohols, ketones and cyclohexane, a gas chromatograph HP 7980A equipped with a capillary column Stabilwax-DA (Resteck, 0.25µm x 0.25mm x 30m) and a FID detector was used. The samples were generally diluted 1:10 or 1:20 (depending on the analyte concentration) in methanol and then filtered with 200 µm PTFE filters. External calibration was used for the specific components. The injection volume was 1 µl (injection temperature 250 °C) and a split ratio of 10:1 was used. The following program of the GC oven was used: starting temperature 40 °C, heating rate 8 °C/min until 250 °C and 10 min at 250 °C. Helium was used as carrier gas.

For qualitative analysis, a GC-MS (HP G1800A, GCD system) was employed also with a Stabilwax column (same characteristic as that for GC-FID). Methanol was used as solvent for dilution (1:10 or 1:20) of the samples and 1 µl volume was injected with a split ratio 20:1 (injector temperature 250 °C). The following heating program for the GC oven was used: 5 min at 40 °C, heating rate 8 °C/min until 250 °C, 10 min at 250 °C.

Only the qualitative results in Chapter 4 were obtained using the GC-MS (Agilent 6890 Network Gas Chromatograph) equipped with the column Type DB5 0.25 (µm x 0.25 mm x 30 m, Agilent 5873 Mass Selective detector). The injection temperature was 305 °C and the injection volume 1 µl (split ratio 1:15). The following oven program was used: 40 °C for 5 min, heating rate 20 °C/min until 300 °C and 20 min at 300 °C.

Selected samples were sent to the Institute of Wood Research (Thünen Institute) in Hamburg for GC-MS/FID analysis. The method used is reported by D. Meier and

M. Windt [67] and it can provide the quantification of more than 100 compounds.

2.4.4 Nuclear Magnetic Resonance Spectroscopy

^{1}H-NMR analysis was performed in a Bruker Biospin spectrometer with ^{1}H frequency 250 MHz (5.47 T magnet). Circa 100 mg of the samples were dissolved in 1 ml of CD_3OD containing as internal standard TMSP-d$_4$ (sodium 3-trimethylsilyl-2,2',3,3-tetradeutero-propionate, circa 2 g/L). Afterwards the samples were centrifugated and measured at 25 °C. ^{1}H-NMR data processing were performed using MestReNova (version 9.0). ^{1}H-NMR spectra were measured with the following parameters: 90° pulse program (4.95 µs), acquisition time 10 s, relaxation delay 1.0 s, number of scans 24, spectral width 3255.2 Hz and time domain 32k. The use of an internal standard permitted to convert the integrated signal in moles of protons [184]. By this, it was possible to compare samples with different hydrogen contents. The spectra were integrated in different regions typical for specific functional groups [185], as reported in Table 2.1.

Table 2.1: ^{1}H-NMR regions of integration and assignment of the protons to specific functional groups.

Integration range of ^{1}H-NMR spectra	Proton assignment
10.1-9.5	Aldehydes
8.5-6.0	(Hetero-)aromatic
6.0-4.3	Carbohydrates, water, O-H exchanging groups
4.3-3.0	Alcohols, ethers, alkenes
3.0-1.5	α-proton to carboxylic acid or keto-group, α-proton to unsaturated groups
1.5-0.5	Alkanes

^{13}C-NMR spectra of the bio-oil and upgraded products were acquired using pulse width of 15.6 µs, aquisition time 1.0 s, time delay 2.5 s, number of scan 14000, spectral width 16340 Hz and time domain 16k.

2.4.5 Solvent fractionation

Solvent fractionation is a method often used in literature to gain basic information about the nature of a complex matrix like bio-oil. Extracting the bio-oils in different solvents permitted separating compounds with characteristic polarity into several
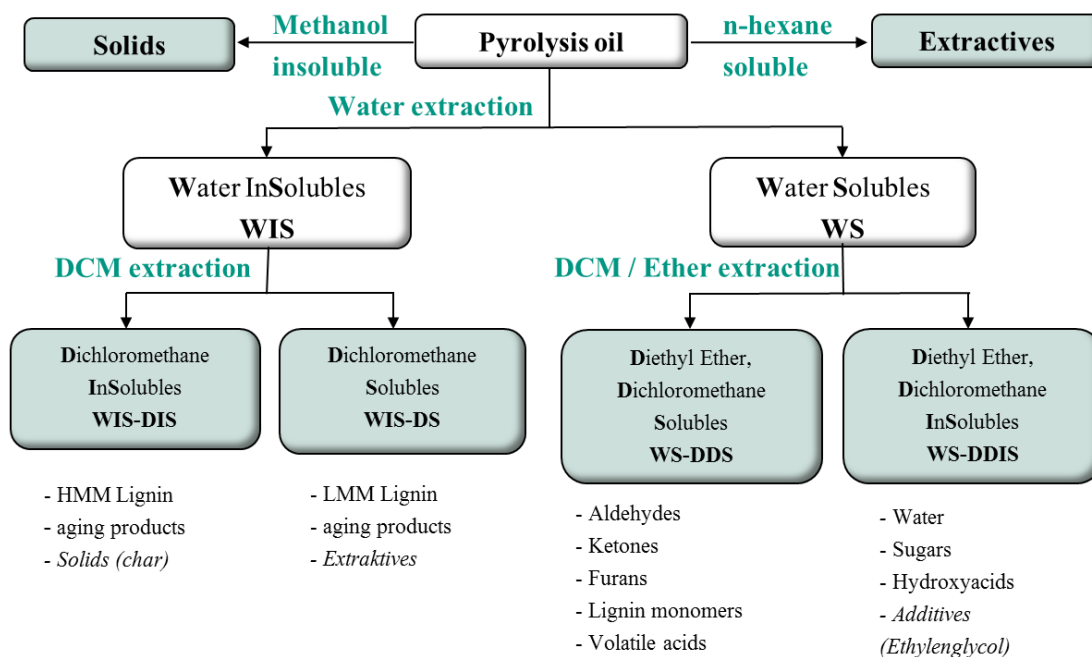
Figure 2.3: Solvent fractionation scheme of bio-oils. In the scheme, HMM indicates High Molecular Mass (circa 1050 Da), while LMM Low Molecular Mass (circa 400 Da) [186]. Reprinted from Ref. [179] according to the terms of Creative Commons Attribution License (CC BY).

classes, which are associated to the degradation of specific building blocks of the biomass. The procedure adopted took inspiration from Oasmaa et al. [66], but some modifications were done. The scheme of the extraction is illustrated in Figure 2.3.

The first step of the separation consists of pyrolytic lignin precipitation. This was performed by mixing with an Ultraturax stirrer of the bio-oil and cold water (circa 1 °C) in a proportion 1:10. The precipitate was filtrated, freeze-dried for 24 hours and weighed (WIS= Water InSoluble).

The WIS fraction was solubilized in dichloromethane (1:7 in weight), sonicated for 15 minutes and filtrated. The solids obtained by the filtration were weighed and it constitutes the WIS-DIS (Water InSoluble - Dichloromethane InSoluble). The WIS-DS (Water InSoluble - Dichloromethane Soluble) was calculated by the difference between WIS and WIS-DIS.

The aqueous solution (WS= Water soluble) obtained from lignin precipitation was extracted in diethyl ether (1:1 in weight) and subsequently in dichloromethane (1:1 in weight). The aqueous phase obtained was dried at 40 °C and 50 mbar

by rotary evaporator, dried over night at 40 °C and weighed (WS-DDIS= Water Soluble- Diethyl ether/ Dichloromethane InSoluble). The class WS-DDS (Water Soluble - Diethyl ether/ Dichloromethane Soluble) was calculated by the difference between WS and WS-DDIS.

After the bio-oil was diluted 1:5 with ethylene glycol to decrease the viscosity, an extraction with n-hexane (ratio n-hexane/bio-oil 10:3) was repeated three times. The n-hexane present in the extracted fraction was evaporated and the residue weighed (extractives). The solids were determined solubilising the bio-oil in methanol (1:3), filtering the solution and weighing the residue.

The main components for each class are illustrated in Figure 2.3 and deeply described by Oasmaa et al. [63, 66].

2.4.6 Supplementary techniques

In order to gain insight about the molecular weight of the components in the bio-oil, gel permeation chromatography was performed in a Column-Thermostate T 6300 from Merck provided with a pre-column PSS SDV 5 µ8 x 50 mm, two columns PSS SDV 5µ1000A 8 x 300 mm and PSS SDV 5µ100A 8 x 300mm and a RI-Detector L-7490 from Merck. 10 mg of the sample were dissolved in 5 ml of THF with internal standard toluene.

A density meter DMA 450 M from Anton Paar was used for density determination, while the pH was measured with a 691 pH Meter (Metrohm).

Anion chromatography was used for the determination of chlorides, sulphates and phosphates. The device used was from Metrohm, equipped with Suppressor 753, Interface 830, Separationscenter 820. The column Was Metrosep Dual2 Fa. Methohm and the eluent consisted of 381 mg Na_2CO_3, 337 mg $NaHCO_3$, 300 ml Acetonitril in 2 liter water.

In order to determine the coking tendency of the upgraded oil [113], a TGA analysis was performed with a Netzsch STA 409. The measurement was performed using 200 mg of the sample under nitrogen atmosphere with a heating ramp of 10 °C/min from 30 °C to 900 °C (30 min at this temperature).

Chapter 3

Characterisation of bio-oils

This chapter gives an overview of the pyrolysis oils used in this thesis for hydrotreatment. Pyrolysis feedstock, pyrolysis temperature, vapour residence time and reactor type influence the bio-oil composition, which in turn will affect the performance of the hydrotreatment. Herein different pyrolysis oils were produced from wheat straw and beech wood, by fast and intermediate pyrolysis. The oils were characterised and compared using elemental analysis, Karl Fischer titration, solvent fractionation, gas chromatography and ^{1}H-NMR spectroscopy. Bio-oil produced from beech wood was found to be more stable and easier to handle than that of wheat straw. Intermediate pyrolysis oils exhibited molecules with lower molecular weight due to higher degree of pyrolytic fragmentation in comparison to fast pyrolysis oils. The pyrolysis temperature influenced the composition of the bio-oil, resulting in oil with lower oxygen content and higher fragmentation at higher temperatures, but at the expense of oil yield. For hydrotreatment it is fundamental to avoid solids and minerals in the bio-oil. In this regard hot vapour filtration downstream to the pyrolysis process presented a good solution.

3.1   Introduction

Different parameters affect the yield and quality of bio-oil produced during pyrolysis of biomass [31]. The feedstock is an important parameter [3, 37, 53] and the main distinction lies between woody biomass and non-woody biomass (grass-like) [187, 188]. These two categories contain a different percentage of cellulose, hemicellulose and lignin, which have different reactivity during pyrolysis [48]. More lignin, with higher percentage of synapsyl and conyferyl alcohols as building blocks, is present in the hard wood, conferring the typically hard and less flexible structure in comparison to grass [189]. Non-woody biomass contains more cellulose and hemicellulose, and in addition is characterised by a higher content of minerals [190], especially alkali metals, which permit the plant to grow rapidly. However, alkali metals, in particular potassium and sodium, are active during the pyrolysis, catalyzing secondary cracking of the vapours and decreasing both the yield and quality of the oil [31, 191]. Hence, this kind of bio-oil contains generally more fragmented molecules (e.g. usually hydroxypropanone and other aldehydes instead of levoglucosan [192]) and it suffers from phase instability. These are also the main reasons why non-woody biomass remains an open challenge in pyrolysis process.

Pyrolysis processes are mainly distinguished between fast, intermediate and slow pyrolysis [31, 55], with the type affecting the yield and quality of the oil produced. Since slow pyrolysis is aimed at char production, only fast and intermediate pyrolysis are considered for bio-oil. The yield of liquid products is generally higher for fast pyrolysis, whereas intermediate pyrolysis can be a system easier to control [55]. A further possibility for subsequent processing of pyrolysis oil is hot-vapour filtration [31]. In this case, before the quench, the pyrolysis vapours are filtrated, eliminating solids, heavy tar substances and minerals and providing an oil with very low or negligible solids and metal content. This is an advantage for the catalyst during subsequent hydroprocessing, avoiding the risk of fouling the catalyst surface by mineral deposition or clogging of the reactor due to char.

This chapter describes the characteristics of the various pyrolysis oils used in the hydrotreatment throughout this thesis. The main focus of this thesis lies on pyrolysis oil produced by wheat straw. The following sections report the main characteristics of the wheat straw bio-oils used: an unstable fast pyrolysis oil (light and heavy phase, Section 3.2), a bio-oil from intermediate pyrolysis followed by hot-vapour filtration (straw 450 °C bio-oil, Section 3.3), and a stable bio-oil from fast pyrolysis (bioliq bio-oil, Section 3.3). Furthermore, four beech wood bio-oils

produced from intermediate pyrolysis at different temperatures and subsequent hot vapour filtration are described in Section 3.4 and used for investigating the influence of pyrolysis temperature in HDO (Chapter 7).

3.2 Bio-oil from fast pyrolysis of wheat straw: characterisation of the light and heavy phase

The investigated bio-oil was produced from wheat straw in the bioliq® pilot plant at KIT (2011, week 48). Immediately after production, it was a homogenous single phase, but after some weeks a natural phase separation occurred, resulting in a light phase constituting approximatively 25 wt.% of the original mass and a heavy phase around 75 wt.% (Figure 3.1). This phenomenon is common in the case of pyrolysis oil produced by straw, especially when the water content and the char/ash content exceeds a determined amount [186, 193]. The light phase constitutes a homogenous phase, while the heavy phase is a complex multiphase system including an aqueous phase, tar-like substances and solids. The solid content of the heavy phase was too high for filtering by conventional laboratory methods. This presented a disadvantage for hydrotreatment, since the presence of char (together with the minerals contained in it) can result in production of additional coke and can create problems during the reaction and product separation. A preliminary hydrotreatment experiment demonstrated that the heavy phase was not a suitable feed for upgrading, generating mainly solids as product. For this reason, only the hydrotreatment of the light phase was carried out, although the characterisation of both fractions is presented here in order to better understand the phase separation process.

The main physical characteristics and composition of the two phases of the bio-oil are reported in Table 3.1. The light phase had a higher water content, which limited

Figure 3.1: Light phase (left) and heavy phase (right) of a fast pyrolysis oil from wheat straw.

the recovery of organic compounds in this fraction (carbon content 20.7%). The oxygen in the organic molecules (dry basis) was 40.0 wt.%, while the content of heteroatoms like N and S was relatively low, agreeing well with the values reported for other pyrolysis oils in literature [32]. Potassium was the main metal detected in solution with a concentration of 1.2 wt.%. The heavy phase contained less water and more carbon (Table 3.1), characteristics that are preferred for bio-oil applications. However, its biggest limitation especially for HDO was the high amount of solids (15.2%), which increases the viscosity, causing technical difficulties for processing this phase. Heteroatoms like N and S were present in higher concentrations in comparison to the light phase, raising the risk of poisoning the catalysts.

Table 3.1: Physical properties and chemical composition of the light phase and the heavy phase of a bio-oil produced by fast pyrolysis of wheat straw.

Property	Light phase	Heavy phase
Density (kg/l)	1.11	1.13
pH	4	-
Water content (wt.%)	56.7	14.4
Elemental composition, wet basis; dry basis (wt.%)		
C	20.7 ; 47.7	58.0 ; 67.7
H	9.5 ; 7.4	7.0 ; 6.3
O	67.8 ; 40.0	33.8 ; 24.4
N	0.3 ; 0.7	1.2 ; 1.4
S	0.05 ; 0.12	0.10 ; 0.12
Solids (wt.%)	0.3	15.2
Chloride (wt.%)	0.27	n.d.
Metals (wt.%)	1.72	1.83
Higher heating value (HHV) wet basis; dry basis (MJ/kg)	9.2 ; 21.2	24.4 ; 28.5

According to solvent fractionation (Chapter 2.4.5), the spontaneous phase separation induced the repartition of the sugar derivatives and low molecular mass compounds in the light phase, and the pyrolytic lignin and higher molecular weight compounds in the heavy phase (Figure 3.2, and see schema in Figure 2.3). In some cases, natural or induced phase separation could constitute an advantage in hydrotreatment, since two main typologies of compounds are isolated and can be treated in different conditions, which are optimal for each class of compounds [80]. Therefore, the light phase constituted an ideal system to investigate the reactivity of sugar-derived components during the hydrotreatment. The heavy phase, due to the high content of solids, would rather be more suitable for other types of processing
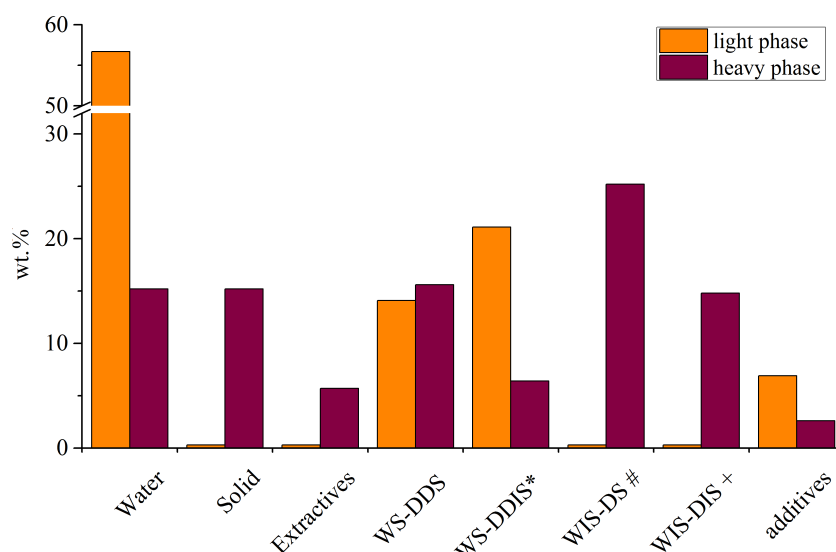
Figure 3.2: Solvent fractionation of the light and heavy phase of the fast pyrolysis oil from wheat straw. Classes: WS-DDS= Water soluble- Dichloromethane diethylether soluble; WSDDIS*= Water soluble Dichloromethane diethylether insoluble without water; WIS-DS#= Water insoluble-dichloromethane soluble without extractives; WIS-DIS+= Water insoluble-dichloromethane insoluble without solids (see Section 2.4.5 for details about the classes).

Table 3.2: Classes of compounds detected by GC-MS/FID present in the light and heavy phase of a fast pyrolysis oil from wheat straw (measurements performed at the Thünen Institut).

	Light phase (wt.%)	Heavy phase (wt.%)
Water	56.1	14.4
Acids	6.07	4.13
Non-aromatic ketones	7.17	5.93
Non-aromatic alcohols	7.82	2.71
Lignin derived phenols	0.27	1.76
Guaiacol (methoxy-phenols)	0.37	2.02
Syringol (dimethoxy-phenols)	0.31	1.5
Furans	0.72	0.95
Sugars (anhydro-)	2.78	0.93
Non-aromatic esters	0.45	0.28
Non-aromatic aldehydes	0.30	0.17
Unidentified compounds	17.64	65.22

like gasification, as designed in the bioliq plant [10].

In order to characterise more precisely the compounds contained in the light and

heavy phase, the samples were analysed at the Thünen Institute in Hamburg by GC-MS/FID (see parameters in Chapter 2.4.3). The main classes of compounds present are reported in Table 3.2.

About 70 molecules were identified with a concentration larger than 0.01 wt.%. However a significant percentage of the compounds was not detected (Table 3.2), a fact that reflects the high complexity of these oils and the low volatility of higher molecular compounds. In Table 3.3, a list of the most representative compounds is shown. Both fractions contained a significant percentage of acids (mainly acetic acid) and non-aromatic ketones (predominantly hydroxypropanone). The light phase had a higher percentage of ethylene glycol, which was an additive used during the pyrolysis process in the bioliq® plant. Levoglucosan, furfural and cyclopentanones, as representatives of the sugar fraction, were more concentrated in the light phase. On the other hand, the heavy fraction had a higher percentage of phenol, guaiacol and syringol derivatives, produced by thermal decomposition of lignin.

In order to more accurately determine the specific nature of the components present, the samples were further analysed by ^{1}H-NMR. ^{1}H-NMR spectra integration provides information about the chemical makeup of protons in the bio-oil fractions (Figure 3.3). Apart from the main signal due to water (6.0-4.3 ppm), protons alpha to alcohols or ether/esteric bonds (4.3-3.0 ppm) and to carboxylic, carbonyl and unsaturated groups (3.0-1.5 ppm) were predominant in the light phase. On the other hand, the heavy phase had a main signal in the region between 3.0-1.5 ppm, but the contribution of protons located on aromatics (8.5-6.0 ppm) and alkanes (1.5-0.5 ppm) was relatively high.
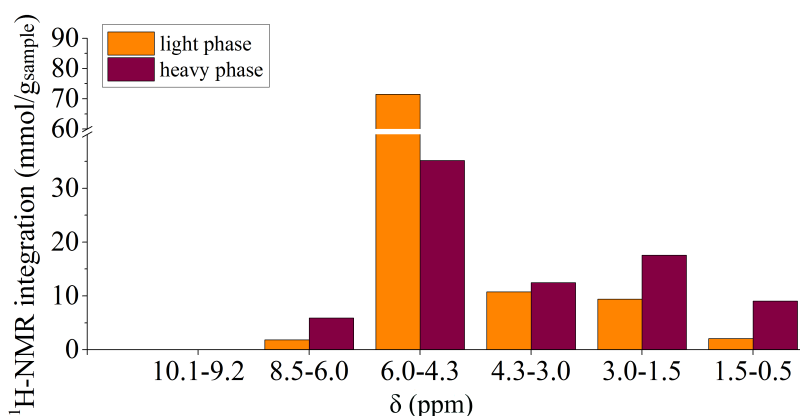
Figure 3.3: ^{1}H-NMR spectra integration of the light phase and the heavy phase of a fast pyrolysis oil from straw. The assignment of protons to the specific classes of compounds is reported in Table 2.1.

Table 3.3: Main components detected by GC-MS/FID in the light and heavy phase of a fast pyrolysis oil from wheat straw.

	Light phase (wt.%)	Heavy phase (wt.%)
Acetic acid	4.92	3.02
Propionic acid	1.15	1.11
Acetic acid 2-hydroxyethyl ester	0.41	0.28
Ethylene glycol	7.78	2.71
Acetaldehyde, hydroxy-	0.3	0.17
Acetol (Hydroxypropanone)	5.31	2.76
Butanone, 1-hydroxy-2-	0.67	0.02
Cyclopenten-1-one, 2-	0.13	0.26
Cyclopenten-1-one, 2-methyl-2-	0.05	0.17
Cyclopenten-1-one, 3-methyl-2-	0.08	0.2
Cyclopenten-3-one, 2-hydroxy-1-methyl-1-	0.53	0.74
Furfuryl alcohol, 2-	0.04	0.09
Furanone, 2(5H)-	0.10	0.13
Furaldehyde, 2-	0.05	0.10
Butyrolactone, γ-	0.18	0.22
Phenol	0.11	0.41
Cresol, o-	0.04	0.31
Cresol, p-	0.03	0.16
Cresol, m-	0.03	0.16
Phenol, 2,5-dimethyl-	0.02	0.07
Phenol, 2,4-dimethyl-	n.d.	0.05
Phenol, 2-ethyl-	n.d.	0.06
Phenol, 3-ethyl-	0.02	0.06
Phenol, 4-ethyl-	0.02	0.19
Guaiacol	0.13	0.45
Guaiacol, 4-methyl-	0.03	0.14
Guaiacol, 4-ethyl-	0.03	0.18
Guaiacol, 4-vinyl-	n.d.	0.17
Guaiacol, 4-allyl- (Eugenol)	n.d.	0.07
Guaiacol, 4-propenyl- cis (Isoeugenol)	n.d.	0.11
Guaiacol, 4-propenyl-(trans) (Isoeugenol)	n.d.	0.39
Vanillin	0.08	0.17
Syringol	0.14	0.43
Syringol, 4-methyl-	0.05	0.12
Syringaldehyde	0.03	0.13
Anhydro-β-D-arabinofuranose, 1,5-	0.20	0.11
Anhydro-β-D-xylofuranose, 1,5-	0.20	n.d.
Anhydro-β-D-glucopyranose, 1,6- (Levoglucosan)	1.61	0.59

3.3 One-phase pyrolysis oils from wheat straw

The production of one-phase pyrolysis oil from straw remains a challenge in bio-fuel research [193,194]. In this section, two bio-oils produced from the same wheat straw as feedstock are characterised: one from fast pyrolysis at 500 °C in the bioliq® plant (named as "bioliq bio-oil") and the other from intermediate pyrolysis at 450 °C in ITC/KIT (named "straw 450 °C bio-oil"). Downstream to the intermediate pyrolysis process, hot vapour filters were located, permitting a bio-oil with lower amount of minerals and tar-like substances to be recovered. The bioliq bio-oil was produced in November 2015, while the straw 450 °C bio-oil in June 2016. Both pyrolysis oils were analysed and hydroprocessed when they were one phase. Currently (October 2016) the bioliq bio-oil has still no problem in stability, whereas straw 450 °C bio-oil formed a small amount of a separated aqueous phase.

Also when it was one phase, the straw 450 °C bio-oil showed a tendency to separate if centrifuged (8000 rpm, 30 min, same condition for the separation of HDO products). The separation resulted in the formation of two phases, similar to the ones described in Section 3.2: the light fraction consisted of 25 wt.% of the original mass with a water content of 60.6% and the heavy phase was 75 wt.% with a water content of 14.4%.

Since the bioliq® process is designed for gasification of slurries, the issue relative to this bio-oil was the solid content (6.3%), which imposes limitations to the hydrotreatment process. Since the amount of solids present was lower compared to the heavy phase reported in Section 3.2, the bio-oil was filtered by pre-coat

Table 3.4: Physical properties and chemical composition of straw 450 °C bio-oil (produced by intermediate pyrolysis of wheat straw) and of bioliq bio-oil (produced by fast pyrolysis of wheat straw in the bioliq plant).

Property	Straw 450 °C	bioliq
pH	3.8	3.7
Water content (wt.%)	23.7	11.9
Elemental composition, wet basis; dry basis (wt.%)		
C	49.7 ; 65.1	55.2 ; 62.7
H	8.5 ; 7.6	7.4 ; 6.9
O	40.6 ; 25.6	37.4 ; 30.4
N	1.2 ; 1.5	1.0; 1.1
S	0.3 ; 0.4	0.1; 0.1
Higher heating value (HHV) wet basis; dry basis (MJ/kg)	22.2 ; 29.1	23.7 ; 26.9

filtration. This permitted reducing the solid content to 0.8%, but as counterpart the sample was contaminated with ethylene glycol used to prepare the filter (21.4%). Apart the dilution with ethylene glycol, the sample showed analogous composition of the original oil according to GC and ^{1}H-NMR.

In Table 3.4, the characteristics of the straw 450 °C and bioliq bio-oils are reported. The pH was similar between them and also comparable with the wheat-straw bio-oil in Section 3.2, but in generally higher in comparison to the ones from beech wood (Section 3.4). The water content was higher for the straw 450 °C bio-oil, but this bio-oil contained less oxygen on dry basis. Both bio-oils
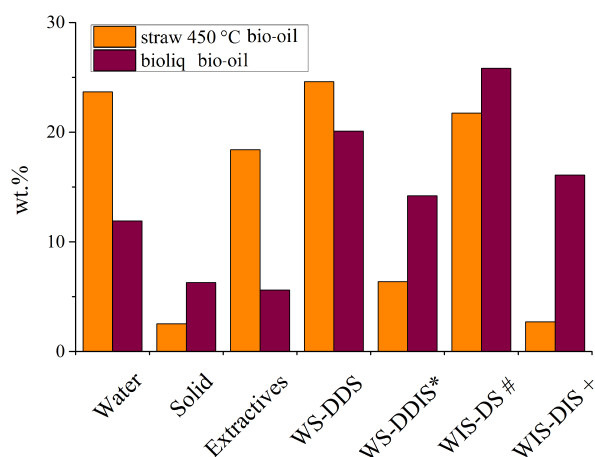
Figure 3.4: Solvent fractionation of straw 450 °C bio-oil (produced by intermediate pyrolysis of wheat straw) and of bioliq bio-oil (produced by fast pyrolysis of wheat straw in the bioliq plant), (class details in Figure 2.3, abbreviations listed in Figure 3.2).
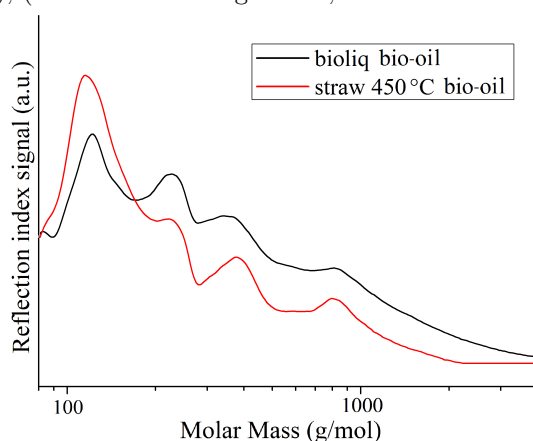
Figure 3.5: Gel permeation chromatography of straw 450 °C bio-oil (produced by intermediate pyrolysis of wheat straw) and of bioliq bio-oil (produced by fast pyrolysis of wheat straw in the bioliq plant).

55

contained a relatively high content of heteroatoms, such as N and S, which can cause deactivation of HDO catalysts.

The solvent fractionation (Figure 3.4) shows that the two bio-oils were quite different in composition. The straw 450 °C bio-oil had a lower content of the fraction containing pyrolytic lignin (WIS), especially that with high molecular weight (WIS-DIS), indicating that higher residence time and the hot-vapour filtration eliminated this fraction. In the same way, the sugar derivatives (WS-DDIS) were less concentrated in the intermediate pyrolysis oil, a fact explained also by the higher
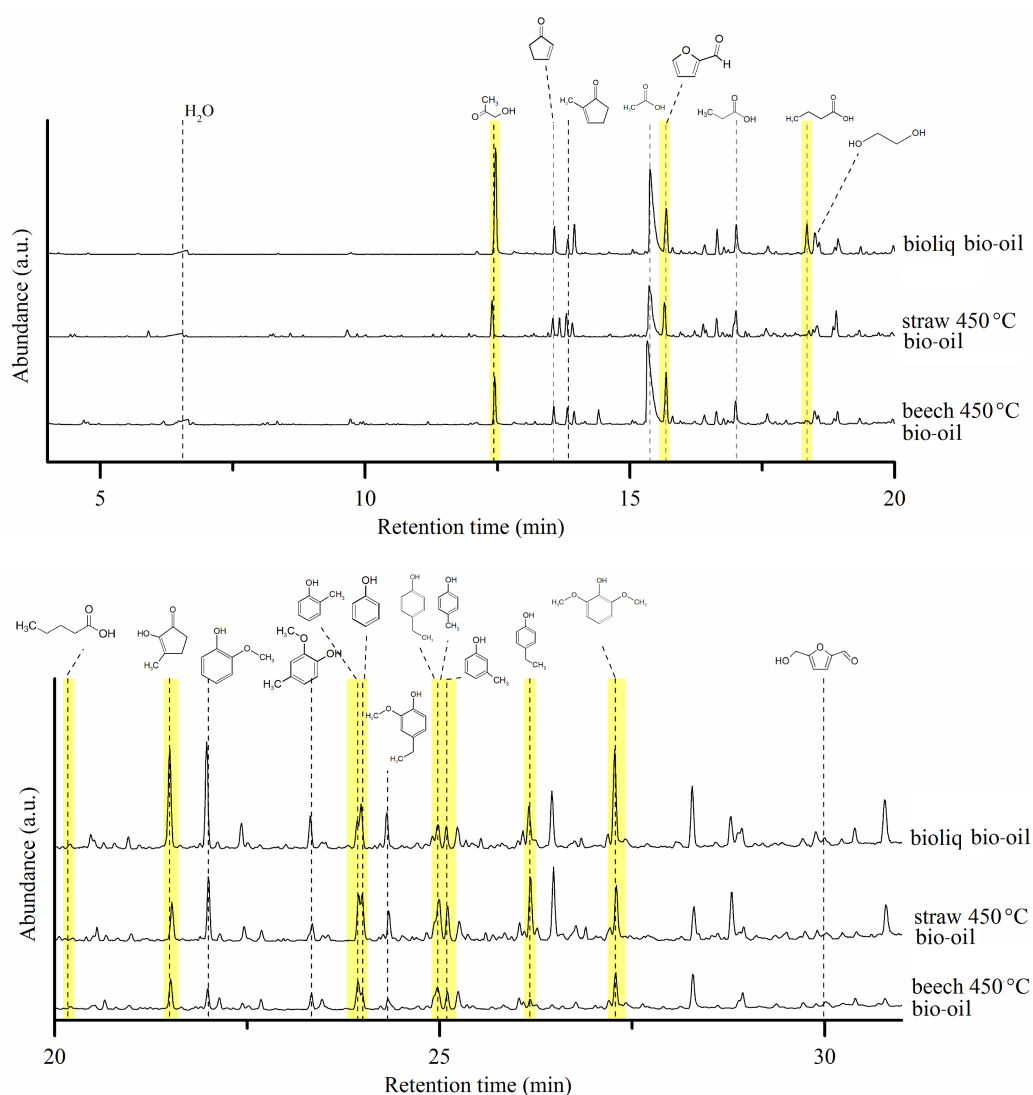
Figure 3.6: GC-MS of straw 450 °C bio-oil (produced by intermediate pyrolysis of wheat straw) and of bioliq bio-oil (produced by fast pyrolysis of wheat straw in the bioliq plant), in comparison to beech 450 °C bio-oil.

degree of decomposition over a prolonged time. On the other hand, the intermediate bio-oil contained more monomeric compounds, like furans and phenols (WS-DDS) and extractives. The high amount of extractives is difficult to explain, but this could be justified by the presence of compounds that are less polar and therefore more soluble in n-hexane (long chain molecules C_{14}-C_{20} with different functionalities were detected by GC-MS). This could also have influenced the polarity of straw 450 °C bio-oil, which in fact was not completely soluble in methanol (see solids content, Figure 3.4), but in acetone.

GPC (Figure 3.5) shows for the two bio-oils the same peaks at 120, 230, 380 and 780 g/mol approximately, but straw 450 °C bio-oil had a lower content of high molecular compounds in comparison to bioliq bio-oil. This fits well with the solvent fractionation results.

Similar compounds were detected by GC-MS in the two bio-oils (Figure 3.6). Analogous compounds were also detected in the pyrolysis oil from beech wood (450 °C, ITC/KIT, section 3.4). The production of acetic acids was more accentuated in the bioliq bio-oil, as well for cyclopentenones and methoxy-phenols, indicating that the shorter residence time prevents an excessive fragmentation. Alkyl-phenols were more concentrated in the intermediate pyrolysis bio-oil, meaning that longer exposure time can cause rearrangement and alkylation of aromatic ring. Note that GC-MS does not give information on high molecular weight compounds.

The integration of ^{1}H-NMR signals of the bioliq and straw 450 °C bio-oils are reported in Figure 3.7. The straw 450 °C bio-oil was found to contain more water (6.0-4.3 ppm), alkane groups (1.5-0.5 ppm) and aromatic protons (8.5-6.0 ppm).
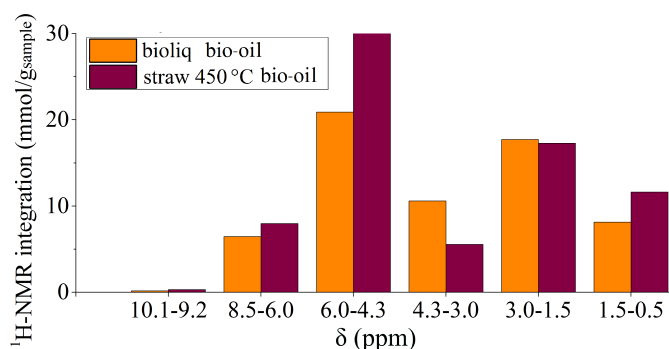
Figure 3.7: ^{1}H-NMR spectra integration of straw 450 °C bio-oil (produced by intermediate pyrolysis of wheat straw) and of bioliq bio-oil (produced by fast pyrolysis of wheat straw in the bioliq plant). The assignment of protons to the specific classes of compounds reported in Table 2.1.

Alcohols/etheric bonds were more concentrated (4.3-3.0 ppm) in the bioliq bio-oil. This observation is in line with previous results obtained by GC-MS, elemental composition and Karl Fischer titration.

3.4 Characterisation of bio-oils produced from beech wood

Four bio-oils were produced by intermediate pyrolysis followed by hot vapour filtration (Section 2.1) of beech wood at different pyrolysis temperatures: 350, 400, 450 and 500 °C. The experiments were carried out at ITC/KIT. The main properties of the bio-oils are reported in Table 3.5, name "beech xxx °C bio-oil", where xxx indicates the pyrolysis temperature used. Their characteristics varied gradually with the temperature. For example the pH increased with higher pyrolysis temperature, while the water content decreased. The higher content of water for lower temperatures was attributed to a different equilibrium established in the condensation of the vapours (mass balance not reported in this work). In fact, the aqueous phase contained less water at lower temperatures and more carbon was recovered in this phase.

The use of a higher temperature (500 °C) promoted the formation of a bio-oil with high carbon content and the lowest oxygen content on dry basis. However,

Table 3.5: Physical properties and chemical composition of four bio-oils produced by intermediate pyrolysis of beech wood at different pyrolysis temperatures.

	Beech 350 °C	Beech 400 °C	Beech 450 °C	Beech 500 °C
pH	2.5	2.6	2.7	3.0
Water content (wt.%)	17.8	14.6	12.4	11.5
Elemental composition, wet basis; dry basis (wt.%)				
C	49.3 ; 60.0	52.2 ; 61.1	55.4 ; 63.2	58.9 ; 66.6
H	7.7 ; 7.0	7.6 ; 7.0	7.1 ; 6.5	7.2 ; 6.7
O	43.0 ; 33.1	40.2 ; 31.9	37.5 ; 30.2	33.9 ; 26.8
N	<0.3	<0.3	<0.3	<0.3
S	<0.005	<0.005	<0.005	<0.005
Higher heating value (HHV) wet basis; dry basis (MJ/kg)	21.1 ; 25.7	22.5 ; 26.3	23.4 ; 26.7	25.1 ; 28.4
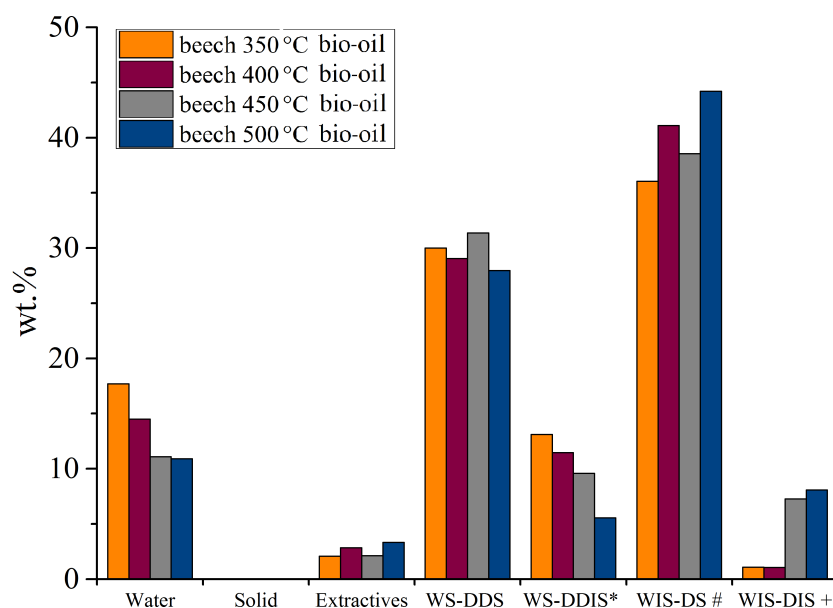
Figure 3.8: Solvent fractionation of four bio-oils produced by intermediate pyrolysis of beech wood at different pyrolysis temperatures (class details in Figure 2.3, abbreviations listed in Figure 3.2).

higher temperatures favour fragmentation reactions that form more gases at the expense of the liquid product yield. For this reason, the hydrotreatment study will focus more on beech 450 °C bio-oil, since it constituted a good compromise between the oxygen content and the bio-oil yield. An important feature of these bio-oils was the low amount of heteroatoms like nitrogen and sulphur, and the absence of solids, which make these bio-oils especially suitable for hydroprocessing (Table 3.5).
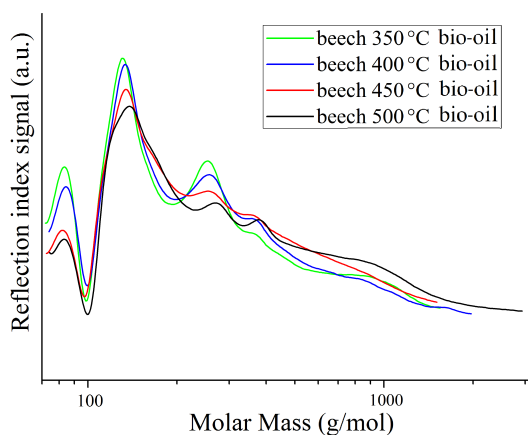
Figure 3.9: Gel permeation chromatography of four bio-oils produced by intermediate pyrolysis of beech wood at different pyrolysis temperatures.

Solvent fractionation (Figure 3.8) showed that the content of sugar derivatives (WS-DDIS) decreased with increasing pyrolysis temperature. On the contrary the non-soluble fraction in water (WIS-DS and WIS-DIS), constituted mainly of pyrolytic lignin, increased. Since the degradation temperature of lignin is higher in comparison to hemicellulose and cellulose [48], more pyrolytic lignin (LMM and HMM) was released at higher temperature. At the same time sugar-derived components can undergo further degradation forming low molecular weight compounds. The main fraction of all beech bio-oils produced by intermediate pyrolysis was WIS-DS#, containing mainly pyrolytic lignin with low molecular
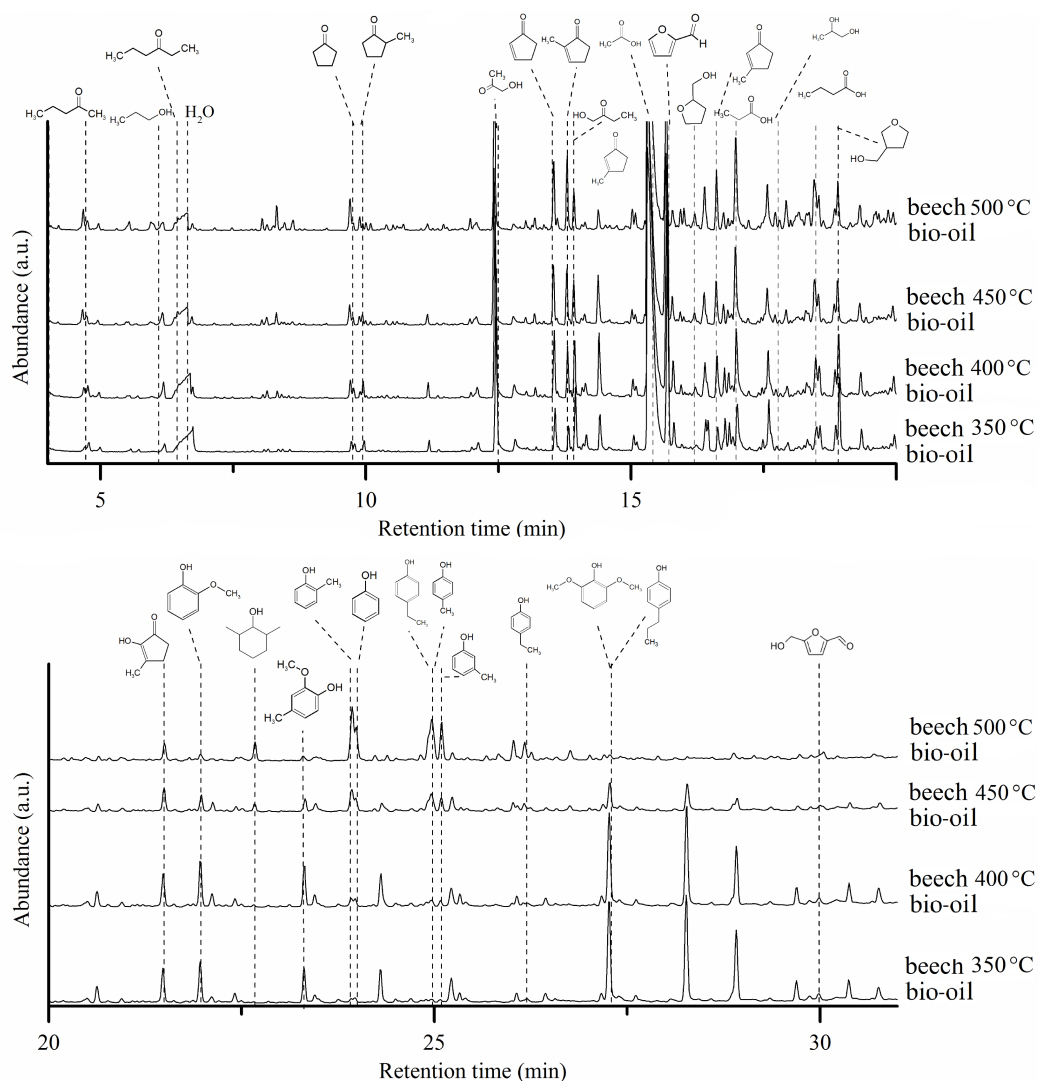
Figure 3.10: GC-MS of four bio-oils produced by intermediate pyrolysis of beech wood at different pyrolysis temperatures.

weight. High molecular weight lignin derivatives appeared only for higher temperatures (450 and 500 °C), as a result of further decomposition of components that otherwise would be recovered as char.

Gel permeation chromatography (Figure 3.9) was used to monitor the molecular mass distribution of each bio-oil. Peaks observed at 130, 250, 370 g/mol can be attributed to monomers, dimers and trimers of phenols derivatives, respectively (for example the molecular mass of guaiacol is 124 g/mol). Higher pyrolysis temperatures favoured higher molecular weight compounds, as also observed by solvent fractionation.

Gas chromatography coupled with a mass detector (Figure 3.10) shows similar low molecular weight compounds contained in all bio-oils. In general, beech 350 °C - beech 400 °C and beech 450 °C - beech 500 °C bio-oils were more similar between them, respectively. The main differences observed concerned the aromatics. Higher temperature caused higher fragmentation, producing more aromatic rings with less or shorter-chain substitutions. For instance, higher amounts of phenol were detected at higher temperature instead of guaiacol and syringol, because at higher temperature demethoxylation/demethylation processes are enhanced. In addition, alkyl-phenols were detected in higher concentration at higher temperatures, indicating alkylation of the aromatic ring (probably due to radical rearrangement) or a different kind of fragmentation pathway [195, 196]. At the retention time 28-30 min, not unequivocal identified molecules constituted by a phenolic unit with substitutions (molecular mass between 160-200 g/mol) were detected with relatively high concentration for low temperatures, but they disappeared at 500 °C, confirming higher levels of fragmentation. At the retention time between 8 and 9 min, aromatic compounds without heteroatoms were detected
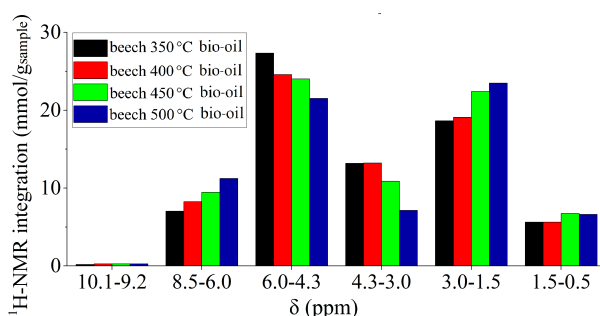
Figure 3.11: ^{1}H-NMR spectra integration of four bio-oils produced by intermediate pyrolysis of beech wood at different pyrolysis temperatures. The assignment of protons to the specific classes of compounds reported in Table 2.1.

in higher concentration for higher temperatures. They have the structure of xylene, easily identifiable by the tropilium ion (m/z =91), but the retention time of each isomer was not assigned.

Trends dependent on the pyrolysis temperature were also observed by ^{1}H-NMR (Figure 3.11). Aromatic protons (8.5-6.0 ppm) had a higher signal with increasing temperature, as well as the protons alpha to carboxylic/carbonylic/unsaturated groups (3.0-1.5 ppm). Those related to alcohols and ethers (4.3-3.0 ppm) decreased with temperature, probably as contribution of the methoxylation/methylation reactions, as also observed by GC. The concentration of the protons belonging to alkane groups was similar for 350-400 °C and 450-500 °C.

3.5 Conclusions

In this chapter an overview of the different pyrolysis oils used for hydrotreatment was presented. A big challenge is the production of a stable pyrolysis oil from non-woody biomass, e.g. low value agricultural residues. Wheat straw has a high availability, but it is generally converted in pyrolysis oils with low phase stability. In the first section of this chapter, a bio-oil from fast pyrolysis of wheat straw was thoroughly characterised. The spontaneous phase separation resulted in the formation of a light phase (containing mainly water, sugar derived components and other low molecular weight molecules) and a heavy phase (tar-like, viscous and with high solid content). In general, phase separation does not constitute a problem for hydrotreatment, but this behaviour could lead to a new strategy to process different classes of compounds under distinct conditions. However, the solid content in the heavy phase was a limitation for HDO and this phase should be employed in other applications where solids are not a problem, e.g. gasification.

In recent years, the bioliq® technology was improved and recent bio-oils show no phase separation, but still contain solids. The one-phase bio-oil produced in the bioliq® plant by wheat straw (bioliq bio-oil) contained originally 6.3% solids, which were reduced to 0.8% after pre-coat filtration. This oil was compared with one produced from the same feedstock, but using intermediate pyrolysis (straw 450 °C bio-oil). The straw 450 °C bio-oil contained more water, more pyrolytic lignin with lower molecular weight and less components derived from sugar decomposition in comparison to the fast pyrolysis oil. Intermediate pyrolysis has a longer residence time in the pyrolysis reactor and therefore more fragmentation reactions take place. The main advantage of working with the intermediate pyrolysis facility was the hot

vapour filtration applied downstream, which permitted the elimination of minerals, tar components and solids.

Intermediate pyrolysis was applied also to beech wood and a screening of different pyrolysis temperatures was conducted. In general, the quality and the stability of beech wood oils were much superior compared to straw. Even after centrifugation the beech-wood bio-oils presented phase stability. Beech wood pyrolysis oil has the advantage of low sulphur and nitrogen content (in contrast to the bio-oil from straw), which is preferable if the oil is going to be treated by HDO.

Regarding the influence of the pyrolysis temperature on the quality of the oil, a higher temperature promoted a higher fragmentation, decreased the water and oxygen content. According to the solvent fractionation, higher temperatures increased the lignin derived compounds to the detriment of sugar fraction, since lignin has higher decomposition temperature than cellulose and hemicellulose. As disadvantage, a higher pyrolysis temperature favours also the formation of more gaseous products, lowering the bio-oil yield. A good compromise was found carrying out the intermediate pyrolysis of beech wood at 450 °C.

Chapter 4

Mild hydrotreatment of the light fraction of fast pyrolysis oil

The chapter deals with hydrotreatment at 250 °C of the light phase of the fast pyrolyis oil produced in the bioliq® plant. Several nickel-based catalysts with different metal loadings and supports were tested and compared with Ru/C as benchmark catalyst. Similar activity was recorded for all nickel-based catalysts, with slightly higher hydrogen consumption for $NiCu/Al_2O_3$. The main products consisted of an aqueous phase and an upgraded oil with a higher density. Although the upgraded oil yield was less than 20%, the main organic components were recovered in this phase. The oxygen content decreased from 40% in the original feed to 20-26% in the upgraded oil, as a result of the hydrodeoxygenation and partitioning of the components into two phases. GC-MS and ^{1}H-NMR were powerful methods to monitor the reactivity of some molecules and of their functional groups. The valorization of the light phase of the pyrolysis oil by HDO was demonstrated to be possible, obtaining an upgraded oil with lower oxygen content from a non-valuable fraction containing mainly sugar derivatives.

4.1   Introduction

Hydrodeoxygenation (HDO) is an upgrading method for bio-oils that has attracted much attention in the last decades (Chapter 1.4). Much more focus has been addressed to deep hydrodeoxygenation compared to mild hydrotreatment, because it can reach higher level of deoxygenation and it produces an oil with higher quality. However, with the new concept of integrating bio-oils in an existing crude-oil refinery, mild hydrotreatment has been reconsidered since it can produce an oil that, despite the higher oxygen content, is compatible with crude-oil and it can be co-processed [33, 34, 38, 197, 198]. This permits to lower the cost and the energy of HDO, since less hydrogen, lower temperature and pressure are required.

Another concept, which is presented in literature and which could simplify the HDO process, is to induce a phase separation of the bio-oil and separately upgrade the light and heavy fractions [80]. This would result in the partition of the sugar and the lignin derivatives into two phases. As they have different reactivities, their separation would allow optimisation of the hydroprocessing using more adequate conditions. Since in the case of this study the phase separation happened spontaneously (Section 3.2), the light phase of a fast pyrolysis oil produced from wheat straw was used for the mild hydrotreatment. The advantage of using this fraction with respect to a bio-oil is also the possibility to limit the attention to the reactivity of some special classes of compounds, like sugars derivatives, lignin derived monomers, furans, ketones, aldehydes and acids. In comparison to model compounds typically studied in literature, it represents a more realistic example, and compared to the whole bio-oil it is a system that is more easily understandable.

Stability and economical viability are characteristics demanded for HDO catalysts. So far no optimal solutions have been found and research has been addressed to find alternatives to conventional hydrodesulfurization catalysts and noble metals [3, 32]. For this purpose, alternative nickel-based catalysts were the focus of this thesis. Various supports and eventually promoters, which demonstrate an improvement in conversion, were chosen: NiW/AC [98], NiCu/Al$_2$O$_3$ [113, 114, 140], Ni/ZrO$_2$ [97], Ni/SiO$_2$ [97], Ni/TiO$_2$ [97], Ni/Al$_2$O$_3$ [97] were tested in mild HDO conditions at 250 °C in a 200 ml batch reactor. As a benchmark, a Ru/C catalyst was used in the same conditions, in order to compare the activity of nickel catalysts to a system well-studied in literature.

Analysis of the bio-oils and upgraded products is complex and many works in literature focussed on implementing new methods and defined new standard

procedures [66]. In this work, besides more standard techniques like elemental analysis and Karl Fischer titration, quantitative ^{1}H-NMR analysis applied to bio-oils was introduced for the first time and gas chromatography was used for identifying reaction pathways.

4.2 Characterisation of the catalysts

Various nickel-based catalyst with different loadings and supports were tested (Section 2.2.1). Their basic structural properties are reported in Table 4.1.

X-ray diffraction (Figure 4.1) showed no reflections of the active metal for the catalysts with loading less than 6%, indicating amorphous phases or a high dispersion of the nickel particles. The estimation of the average crystallite size was estimated using the Scherrer equation (Table 4.1): for $NiCu/Al_2O_3$ 8 nm, for Ni/Al_2O_3 15 nm and for Ni/SiO_2 20 nm. For the NiW/AC only the tungsten oxide reflections were observed, but they were not easily assigned, probably due to the presence of intermediate tungsten oxide (reported previously in other studies [199]) and not only of WO_2 or WO_3.

The TPR profile (Figure 4.2) showed that nickel was mostly reduced below 500 °C, the temperature chosen for catalysts reduction. Only NiW/AC showed other peaks above 500 °C. The peaks at 410 and 520 °C were attributed to nickel, the one at 630 °C to the active charcoal (catalyst support) and at 780 °C to tungsten. The addition of copper, like for $NiCu/Al_2O_3$, decreased the reduction temperature of nickel, as demonstrated by Ardiyanti et al. [113] and Wu et al. [200].

Table 4.1: Composition and physical characteristics of the HDO catalysts tested. Reproduced from [179] according to the terms of Creative Commons Attribution License (CC BY).

Name	Loading active metal (wt.%)	Support	BET surface (m^2/g)	Scherrer eq. average crystallite size (nm)
Ru/C	Ru 5*	active carbon	870	n.d.
Ni/Al$_2$O$_3$	Ni 20*	alumina	76	15
NiCu/Al$_2$O$_3$	Ni 17.8; Cu 2.1	alumina	66	8
Ni/SiO$_2$	Ni 22.0	silica	170	20
Ni/ZrO$_2$	Ni 5.8	zirconia	110	n.d.
NiW/AC	Ni 3.2; W 7.8	active carbon	1110	n.d.
Ni/TiO$_2$	Ni 5.8	titania	86	n.d.

*nominal loading of the commercial catalysts
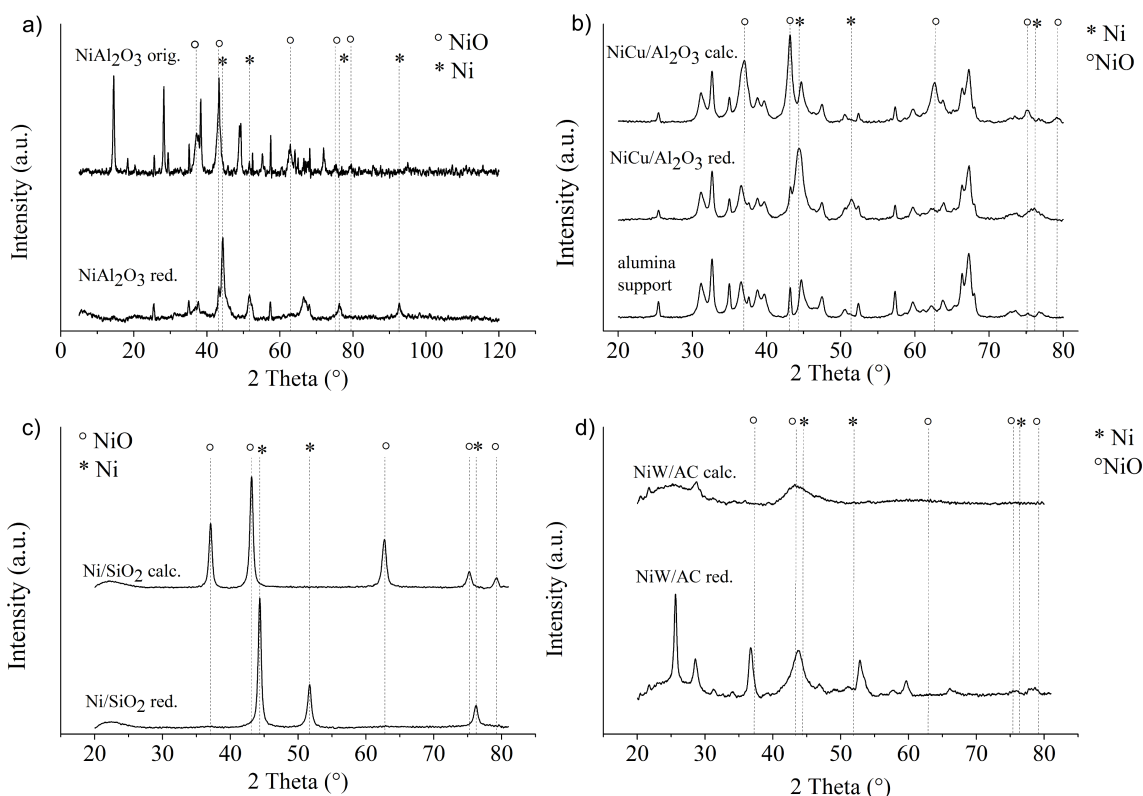
Figure 4.1: XRD patterns of Ni/Al$_2$O$_3$ (a), NiCu/Al$_2$O$_3$ (b), Ni/SiO$_2$ (c) and NiW/AC (d) (orig.= as received, calc.=calcined, red.=reduced). Reproduced from Ref. [179] according to the terms of Creative Commons Attribution License (CC BY).
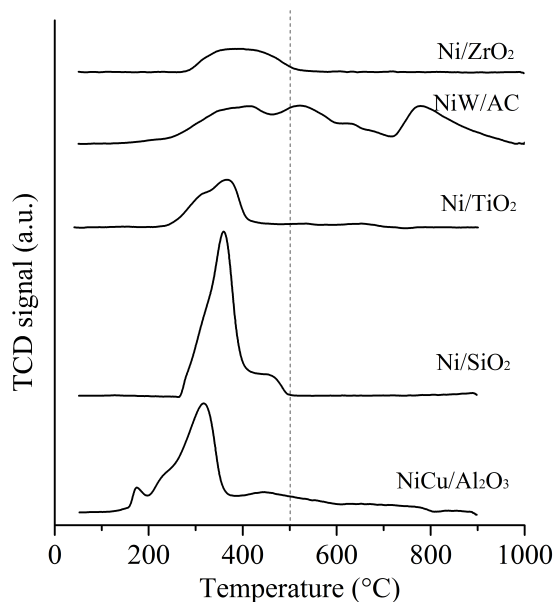
Figure 4.2: Temperature programmed reduction (TPR) of the nickel-based catalysts used in this study (the dashed line shows the reduction temperature used for activating the catalysts). Reproduced from Ref. [179] according to the terms of Creative Commons Attribution License (CC BY).

4.3   Hydrogen consumption and mass balance

The hydrogen consumption during HDO over the nickel catalysts was similar (Figure 4.3a). $NiCu/Al_2O_3$ had a slightly higher activity, but it was still lower than Ru/C. A hydrogen consumption of 102 NL/kg_{po} reported by Venderbosch et al. [33] using a continuous reactor at 225°C and Ru/C was similar to that observed in this work. For $NiCu/Al_2O_3$, only a study from Ardiyanti et al. [114] is available for comparison and it reported a value of 146 NL/kg_{po} at 350°C , hardly comparable due to the different temperature.

In figure 4.3b, an estimation of the hydrogen consumption (see Section 2.3.4) as function of the reaction time is shown. The hydrogen moles inserted in the autoclave decreased mainly in the first two hours, while the consumption continued only slowly for the remaining time. For the hydrogen consumption profile of the blank experiment (without catalyst), a negative trend was observed at the beginning, which could be due to the production of other gases.

The mild hydrotreatment reaction formed four phases: an upgraded oil (with higher density than water), an aqueous phase, gases and solids (Figure 4.4). The upgraded oil yield was between 7-15 wt.% of the light phase weight employed,
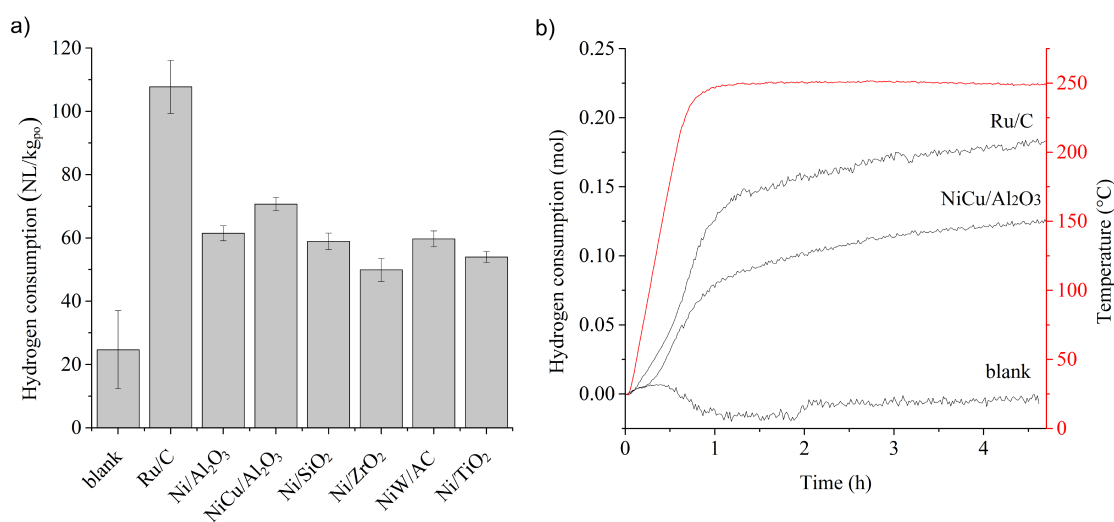
Figure 4.3: a) Hydrogen consumption (NL/kg_{po}= normal liter per kilogram of bio-oil light phase) for the mild hydrotreatment of the light phase over different catalysts (250 °C, 8.0 MPa hydrogen at room temperature); b) estimation of the hydrogen consumption over the time during the mild hydrotreatment of 50 g of the bio-oil light phase (250 °C, 8.0 MPa hydrogen at room temperature). Reproduced from Ref. [179] according to the terms of Creative Commons Attribution License (CC BY).

while the aqueous phase between 75-83 wt.%. Despite the aqueous phase being predominant, it contained mostly water (70.2 $\pm$ 1.7 wt.%) and it is considered a by-product. The energy and the carbon recovery was concentrated mainly in the upgraded oil, which contained only 8.8 $\pm$ 0.9 wt.% of water. The amount of gases and solids was negligible. The solids content was in general less than 3 wt.% and their formation was more pronounced over carbon based catalysts. The recovery losses were in the range of 5-10%.
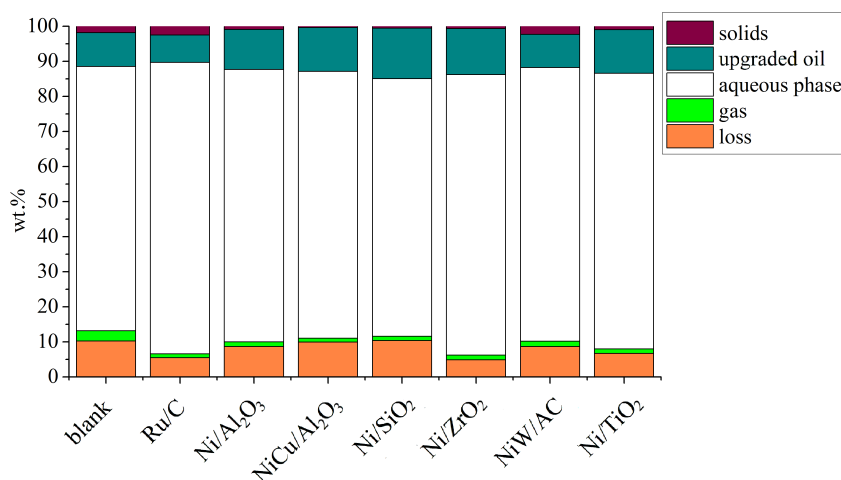
Figure 4.4: Mass balance of the products after mild hydrotreatment (250 °C, 8.0 MPa hydrogen at room temperature). Reproduced from Ref. [179] according to the terms of Creative Commons Attribution License (CC BY).

4.4   Carbon, oxygen and hydrogen distribution

The target of a hydrotreatment experiment is to eliminate oxygen from the organic molecules while minimising the loss in carbon. Since four phases are produced, the organic molecules of the products (therefore the elements contained in them) are redistributed. In this section, the distribution of elements in the different phases is analysed, in order to monitor the carbon recovery.

100 g of the original feed contain 20.7 g carbon, 67.8 g oxygen and 9.5 g hydrogen. Figure 4.5a shows that the carbon was recovered mainly between the aqueous phase and upgraded oil. For the blank test and for the nickel-based catalysts circa half of the carbon recovered was present in the upgraded oil, while in case of Ru/C more carbon remained in the aqueous phase, due to the higher hydrogenation activity that produced more alcohols. As the upgraded oil constituted only 7-15 wt.% of
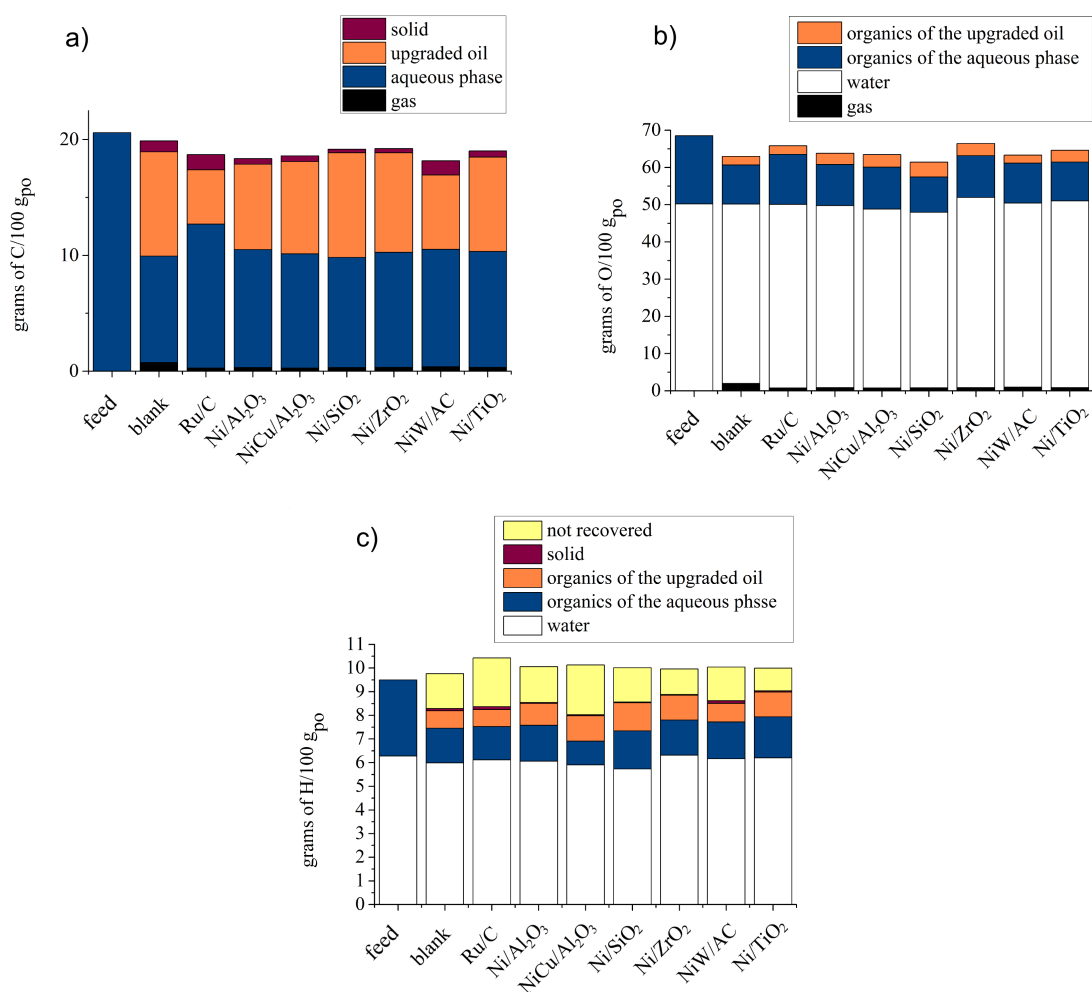
Figure 4.5: Carbon (a), Oxygen (b) and Hydrogen (c) distribution on the product phases after mild hydrotreatment (250 °C, 8.0 MPa hydrogen at room temperature). Reproduced from Ref. [179] according to the terms of Creative Commons Attribution License (CC BY).

the products, this represents a densification of the organic molecules in this phase, therefore a densification in energy and valorisation.

Oxygen was mainly distributed in the aqueous phase (Figure 4.5b) mostly in form of water with only a lower percentage bonded to organic molecules. The oxygen content on dry basis in the aqueous phase was in average 50 ± 3 wt.% and in the upgraded oil in the range of 20-26%. This demonstrated that the decrease of the oxygen content in the upgraded oil is due to a combination of the hydrodeoxygenation reaction and preferable repartition of oxygen-rich compounds in the aqueous phase.

The hydrogen amount increased after the hydrotreatment reaction (Figure 4.5c), but the change was relatively small in comparison to the starting value (less than 10%) . Hydrogen was mainly present in form of water in the aqueous phase and bound in the organic molecules in the upgraded oil.

4.5 Gas composition

The amount of gases produced during the reaction was less than 2%. The main gas produced was CO_2 (Figure 4.6), which was probably generated by decarboxylation of organic acids. CO_2 production was more pronounced for the blank experiment, where cracking reactions seemed to be favoured, while Ru/C produced a wider variety of gases, like methane, propane, etc.
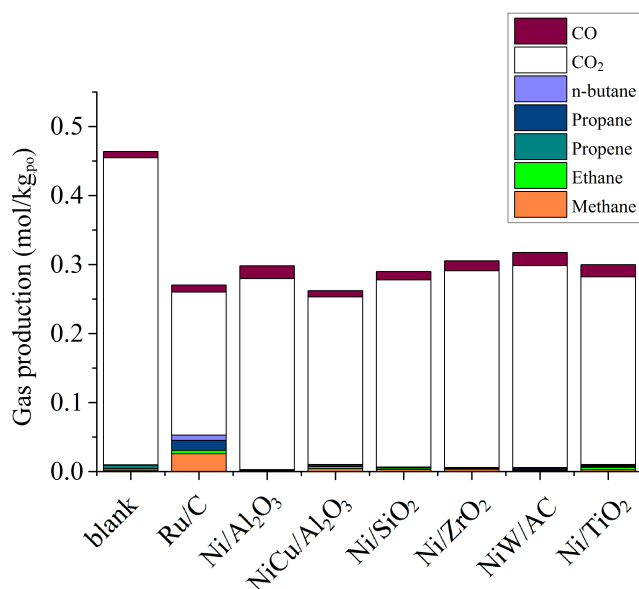
Figure 4.6: Gas production during the mild hydrotreatment over different catalysts (250 °C, 8.0 MPa hydrogen at room temperature). Reproduced from Ref. [179] according to the terms of Creative Commons Attribution License (CC BY).

4.6 Characterisation of the liquid products

The van Krevelen plot shows the composition of the feed and the upgraded oils (Figure 4.7). The oxygen content decreased in the upgraded oils, reaching a concentration of 20-26% instead of 40% in the feed. Among the catalyst, Ru/C

produced an upgraded oil with the highest H/C ratio, while O/C was slightly higher in comparison to the other nickel-based catalysts. The blank experiment reached a more extensive level of deoxygenation, but the H/C ratio remained low, a parameter that also determines the quality of the oil. In fact the upgraded oil from the blank experiment was much more viscous and tar-like compared to the others produced. The upgraded oils produced by hydrotreatment over nickel catalysts showed similar H/C and O/C ratios (considering the error bars), as could be expected by the hydrogen consumption values. The HHV of the upgraded oils was on average 31 ± 1 MJ/kg on dry basis, and considering that the HHV of the feed was 9.2 MJ/kg, the hydrotreatment process succeeded in densifying the energy content in one phase.
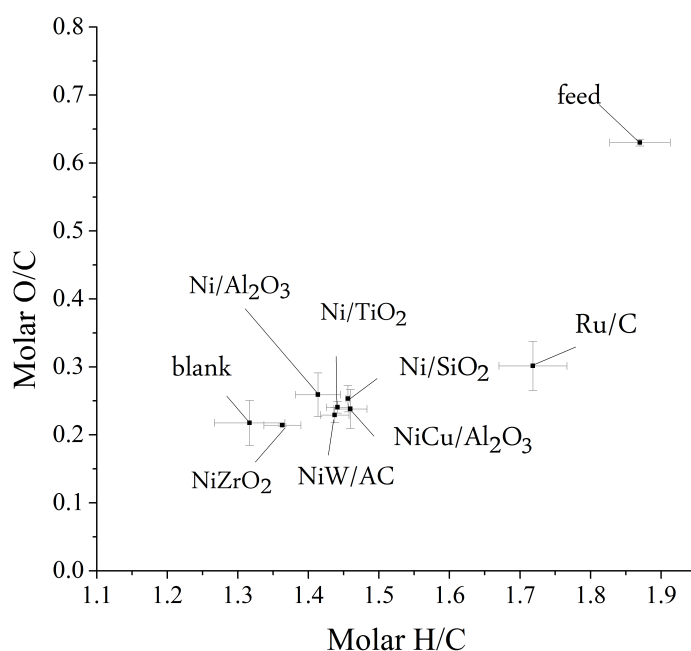
Figure 4.7: Van Krevelen plot of the upgraded oils (dry basis) produced at 250 °C and 8.0 MPa hydrogen at room temperature. Reproduced from Ref. [179] according to the terms of Creative Commons Attribution License (CC BY).

GC-MS/FID permitted identification and quantification of a percentage of the compounds present in the bio-oil. The compounds detected by GC are restricted to the volatile molecules, which are generally 20-30% of the upgraded oil mass. Gas chromatography permitted determination of the reactivity of some representative

Table 4.2: Concentration of some representative compounds in the aqueous phases and upgraded oil (hydrotreatment of the light phase at 250 °C, 8.0 MPa H_2 room temperature) evalutated by GC-MS/FID (Thunen Institute). The value are reported in wt.%.

	light phase	blank aqueous phase	blank upgraded oil[a]	Ru/C aqueous phase	Ru/C upgraded oil[a]	NiCu/Al$_2$O$_3$ aqueous phase	NiCu/Al$_2$O$_3$ upgraded oil[b]
water	55.62	71.54	5.13	65.45	10.1	69.35	8.66
NONAROMATIC COMPOUNDS	21.8	12.15	12.14	14.55	26.9	11.72	17.54
Acids	6.07	8.16	5.54	5.60	8.68	6.56	7.16
Nonaromatic Esters	n.d.	n.d.	0.77	n.d.	1.21	n.d.	0
Nonaromatic Alcohols	7.82	3.04	2.86	8.88	16.90	3.98	1.25
Nonaromatic Alcohols without Ethylenglycol	0.04	0.60	n.d.	6.40	4.04	1.61	0.61
Nonaromatic Aldehydes	0.30	n.d.	n.d.	n.d.	n.d.	n.d.	n.d.
Nonaromatic Ketones	7.17	0.95	2.98	0.06	0.11	1.18	8.75
Hydrocarbons	n.d.	n.d.	n.d.	n.d.	n.d.	n.d.	0.38
HETEROCYCLIC COMPOUNDS	0.78	0.64	0.32	1.22	1.65	0.82	1.87
Furans	0.72	0.63	0.32	1.05	1.65	0.81	1.79
Pyrans	0.06	0.01	n.d.	0.17	n.d.	0.01	n.d.
CARBOHYDRATES	2.78	0.19	n.d.	0.1	n.d.	0.09	n.d.
Sugars	2.78	0.19	n.d.	0.10	n.d.	0.09	n.d.
AROMATIC COMPOUNDS	0.97	0.24	3.79	0.26	6.73	0.20	4.42
Benzenes	0.01	n.d.	0.06	n.d.	0.19	n.d.	0.06
Lignin derived Phenols	0.27	0.08	1.89	0.12	3.67	0.07	2.53
Guaiacols (Methoxy phenols)	0.37	0.08	1.06	0.08	1.66	0.07	1.11
Syringols (Dimethoxy phenols)	0.31	0.07	0.73	0.06	1.21	0.05	0.68
OTHER ORGANIC COMPOUNDS	0.21	3.46	0.12	3.05	0.47	3.98	0.90
Total compounds detected	26.55	16.68	16.37	19.18	35.75	16.81	24.73

[a] oil recovered from acetone wash

[b] oil without treatment

n.d.= not detected

classes of compounds, like phenol, furfural, cyclopentanone and their derivatives. In general, the nickel catalysts exhibited similar activity, selectivity and conversion, therefore in the following text, only the results of NiCu/Al$_2$O$_3$ will be presented.

The aromatic compounds tended to accumulate in the upgraded oil (Table 4.2) rather than the aqueous one. Their concentrations decreased in the aqueous phase after the reaction, also in the blank experiment. Combining the concentration calculated by the GC-MS/FID and the mass balance, on average only 50% of

the original syringol and 60% of guaiacol were recovered after the hydrotreatment, suggesting that they could be partially converted. Phenol was recovered in different percentages depending on the catalyst: 66% over blank, 78% over Ru/C, 91% over NiCu/Al$_2$O$_3$. The concentration of phenol depends on different reaction paths, since it can be formed and produced at the same time during hydrodeoxygenation reaction. It can be produced by demethoxylation of guaiacol and syringol or from the decomposition of pyrolytic lignin, and it can be consumed if it is hydrodeoxygenated or it undergoes other side-reactions (like polymerisation and char production).

Over Ru/C, phenol was partially converted to cyclohexanol (Figure 4.8), exhibiting therefore more hydrogenation activity at 250 °C rather than
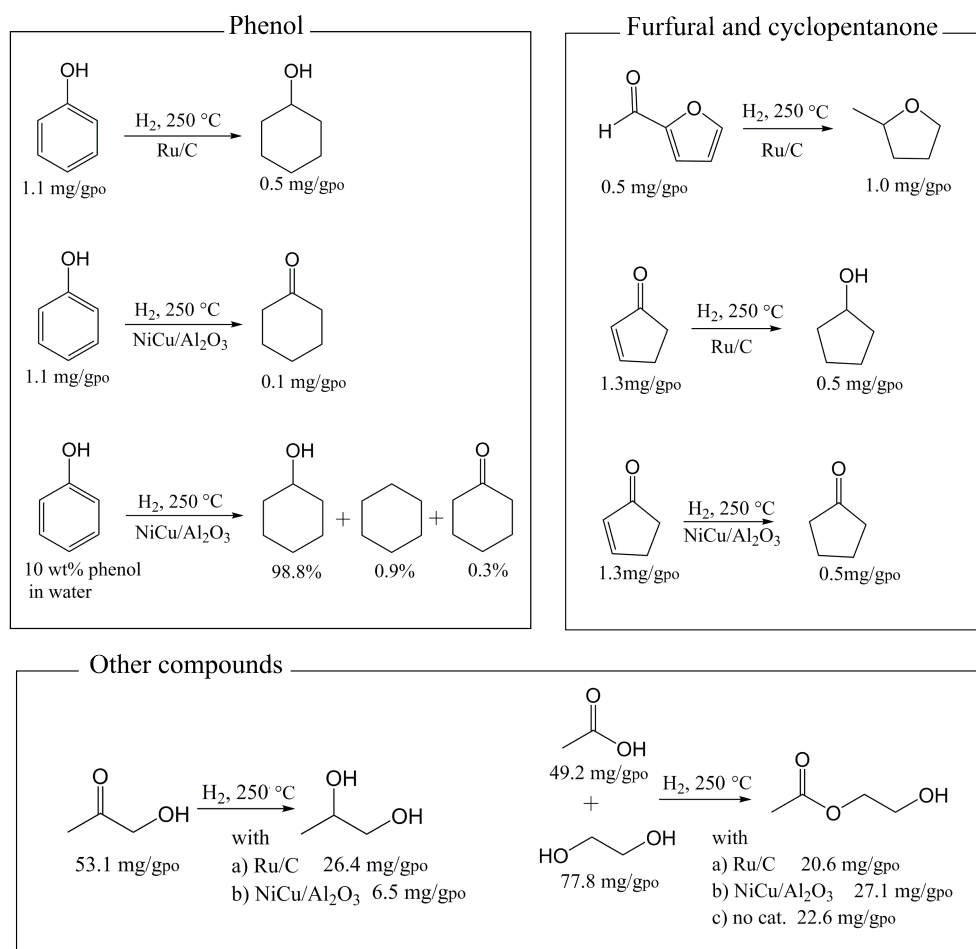
Figure 4.8: Main reactions observed over different catalysts during mild hydrotreatment (250 °C, 8.0 MPa hydrogen at room temperature). Reproduced from Ref. [179] according to the terms of Creative Commons Attribution License (CC BY).

hydrodeoxygenation. Over $NiCu/Al_2O_3$, only a small percentage of cyclohexanone was detected, showing that this catalyst was not particularly active for phenol conversion. In general, nickel catalysts were found to have a selectivity for the production of ketones, in fact a variety of aliphatic ketones (homologous of cyclopentanone, cyclohexanone, pentanone and hexanone) were detected. Therefore nickel was able to hydrogenate olefins, but not ketones to alcohols. This behaviour was not expected for a nickel catalyst, since as reported in literature [201], phenol should be converted mainly to cyclohexanol. This behaviour known in literature was also confirmed by an experiment using phenol in aqueous solution over $NiCu/Al_2O_3$. Also in this case phenol was converted mainly to cyclohexanol (Figure 4.8). This is an indication that the pyrolysis oil environment had strong influence on the conversion and the selectivity of the reactions. This topic will be dealt with more thoroughly in Chapter 5.

At 250 °C, complete hydrodeoxygenation of aromatic compounds was not observed, but the mechanism proposed by Mortensen et al. [97] and Bykova et al. [158], which supposed the hydrogenation of the aromatic ring before deoxygenation, explains the production of intermediate products like cyclohexanol over Ru/C and cyclohexanone over $NiCu/Al_2O_3$.

Another class of interest is the furfural and cyclopentanone-related compounds. Furfural was present in the light phase in a concentration of 0.05 wt.% and was completely converted after the reaction in the blank experiment and over all the catalysts. 2-methyl-tetrahydrofuran was identified in the aqueous phase produced over Ru/C in a concentration of 0.12 wt.%, indicating that Ru/C hydrogenated the unsaturated bonds and deoxygenated the aldehyde group, as also observed by Elliott et al. [101, 102]. Since the concentration was higher than the one obtained from furfural, this suggested that furfural or analogous molecules could be produced from other molecules, like sugar derivatives. Other analogous compounds, which could be derived from hydrogenation and hydrodeoxygenation, like 2-methanol-tetrahydrofuran, furan-2-(3H)-one and 2,5-methyl-tetrahydrofuran were detected in the aqueous phase after reaction with Ru/C. In contrast, no significant amount of these compounds were detected over $NiCu/Al_2O_3$. This indicates that probably nickel catalysts favoured other reaction paths, like ring opening as documented by Sitthisa and Resasco [202] or Piancatelli rearrengment [203, 204] (formation of hydroxycyclopentenone derivatives from 2-furylcarbinols under acid-catalysis conditions).

Cyclopentanone and 2-methylcyclopentanone were detected in higher

concentration for nickel catalysts. They were identified as products of selective hydrogenation of cyclopentenone compounds: 2-cyclopenten-1-one (0.13%) and 2-methyl-2-cyclopenten-1-one (0.05%) were present in the light phase, while 2 methyl-2-cyclopenten-1-one was produced during the reaction favoured by the acid environment or thermally as demostrated in the blank experiment. Cyclopentenone was mainly not converted in the blank experiment, while over Ru/C mainly cyclopentanol and analogues were formed, favouring the hydrogenation of ketones to alcohols as observed previously.

Hydroxypropanone is one of the main components of the light phase (5.31 wt.%). It is formed by the thermal degradation of cellulose and hemicellulose during pyrolysis [205]. After the mild hydrotreatment it was completely converted, partially to 1,2-propandiol (the concentration in the aqueous phase was 3.17 wt.% for Ru/C and 0.83 wt.% for NiCu/Al$_2$O$_3$). Esterification reactions also took place, for example, 2-hydroxyethyl acetate was formed from ethylene glycol and acetic acid.

In Table 4.2, an overview of the concentration of different classes of compounds is reported. The products obtained over Ru/C had the lowest acid concentration, while the ones of the blank experiment the highest. Eliminating the contribution of ethylene glycol (used as an additive of the pyrolysis process), it was demonstrated that Ru/C produced the highest quantity of alcohols, followed by the NiCu/Al$_2$O$_3$ catalyst, while the blank showed almost no production. On the other hand, NiCu/Al$_2$O$_3$ had a high production of ketones. Sugar derivatives like levoglucosan were completely converted, but specific products associable to them were not identified. As expected for the polarity, the repartition of aromatic compounds and ketones in the upgraded oil, and of alcohols and acids in the aqueous phase was observed in Table 4.2.

In conclusion, nickel-based catalysts showed a similar behaviour independent from the support type, as observed by the gas chromatography and the van Krevelen plot. This could be explained since mainly hydrogenation reactions were detected instead of hydrodeoxygenation. The role of the support in the mechanism should be more pronounced at higher temperature where HDO reactions are favoured.

4.7 ^{1}H-NMR analysis of the upgraded products

^{1}H-NMR spectroscopy is another possible and complementary method to follow the conversion of certain functional groups. The ^{1}H-NMR spectra of bio-oils and related upgraded products are complex, showing overlapping peaks which look like
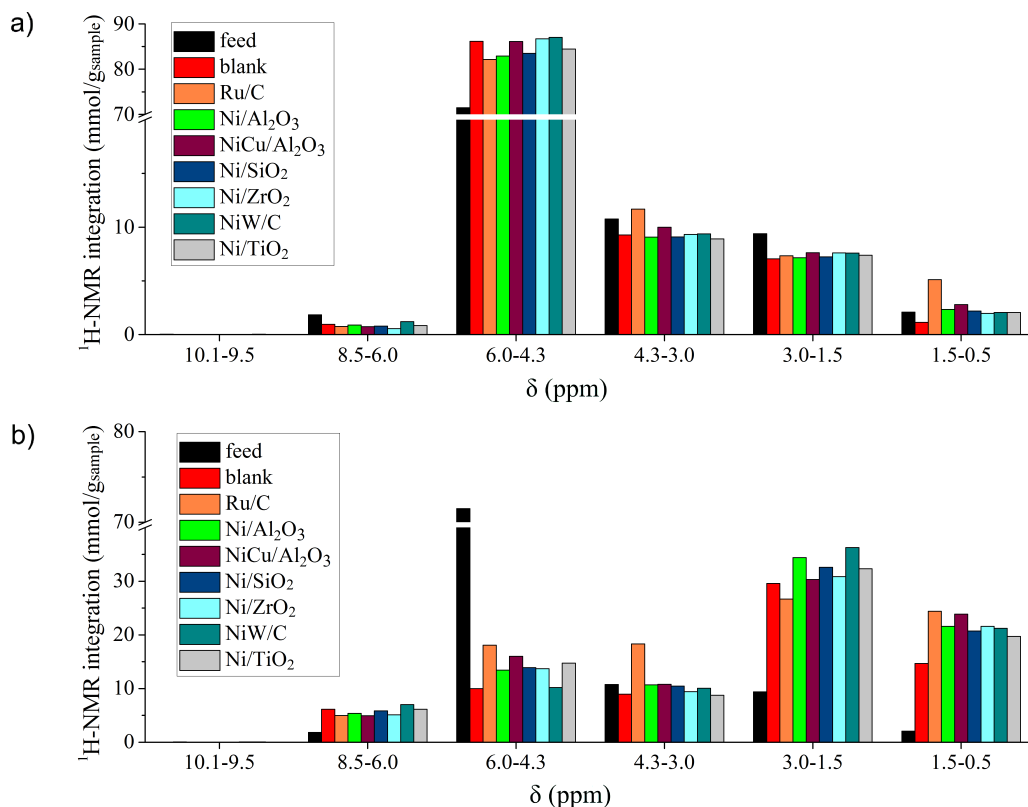
Figure 4.9: Integration of the different regions of the ^{1}H-NMR spectra of the aqueous phase (a) and the upgraded oil (b) produced from the mild hydrotreatment (250°C, 8.0 MPa hydrogen at room temperature). The assignment of protons to the specific classes of compounds is reported in Table 2.1. Reproduced from Ref. [179] according to the terms of Creative Commons Attribution License (CC BY).

broad bands. For this reason it is not possible to identify compounds with a concentration less than 0.5% by ^{1}H-NMR. The main peaks that were assigned in the upgraded products belonged to acetic acid (2.00 ppm), hydroxypropanone (2.12 and 4.26 ppm), ethylene glycol (3.61 ppm) and water (4.8 ppm). However, a rough assignment of the signals in different classes of compounds is possible, as reported in literature [185] and the comparison among different samples with different hydrogen content was facilitated by the introduction of an internal standard (TMSP) and by using quantitative ^{1}H-NMR.

The aqueous phases (Figure 4.9a) had a high amount of water (circa 70% in the aqueous phase and 56.7% in the feed by Karl Fischer titration), therefore the spectral region between 6.0 and 4.3 ppm had the highest intensity. After mild hydrotreatment, the concentration of protons in the aromatic region (8.5-6.0 ppm)

and protons in α-position to carboxylic acids, ketones and unsaturated groups (3.0-1.5 ppm) decreased. Protons α to alcohol/ether groups (4.3-3.0 ppm) decreased for all the nickel catalysts, but not for Ru/C, as confirmed by gas chromatography. The ^{1}H-NMR signal related to aliphatic groups (1.5-0.5 ppm) was significantly higher for Ru/C, as result of an efficient hydrogenation. The results among the nickel catalysts were similar, whereas the blank experiment led to lower ^{1}H-NMR signal.

The ^{1}H-NMR spectra integration of the upgraded oils are reported in Figure 4.9b. A different distribution of the protons was observed comparing the aqueous phase and feed. An increase was observed in the concentration of aliphatic protons (1.5-0.5 ppm), of protons in the region 3.0-1.5 ppm and of aromatic protons (8.5-6.0 ppm), indicating that the upgraded oils were composed of more apolar compounds. The protons between 4.3-3.0 ppm had similar concentration to the feed for the experiments carried out with nickel catalysts, while for Ru/C this value was higher, as observed also in the aqueous phase. The contribution in the region 6.0-4.3 ppm was lower in comparison to the aqueous phase, since the water content in the upgraded oil was on average only 8.8%.

The millimoles of protons calculated from the integration of the whole spectrum were quite in agreement with the hydrogen content determined by elemental analysis (less than 10% difference from the value of elemental analysis).

4.8 Conclusions

In this chapter, the upgrading of the light phase of fast pyrolysis oil from wheat straw was carried out over various nickel catalysts in mild hydrotreatment conditions (250°C, 80 bar H_2 at room temperature). The hydrotreatment was demonstrated to be successful in converting a non-valuable fraction (containing mainly sugar derivatives) into an upgraded oil with lower oxygen content (20-26% in comparison to 40% of the feed) and concentrating most of its energy and carbon content in a smaller volume.

All the used nickel catalysts showed similar activity, with slightly higher hydrogen consumption for NiCu/Al_2O_3. In comparison, Ru/C (used as a benchmark) had higher hydrogen consumption and the respective upgraded oil was more hydrogenated. However, the deoxygenation degree reached was slightly higher for the nickel-based catalyst. This result, together with the cheaper price and higher availability, can make nickel catalysts an attractive alternative to noble metals.

GC-MS/FID was a powerful technique for identifying some reaction trends.

Nickel catalysts were active in the hydrogenation of olefins, but not of ketones (which were the main products), while Ru/C showed a different selectivity that resulted in the formation of alcohols. Phenol components were mainly not converted in the bio-oil, but it was demonstrated that when phenol was treated in the same condition in an aqueous solution over NiCu/Al$_2$O$_3$, it was quantitatively converted to cyclohexanol. This is a first indication of how the reactivity differ in two different reaction environments. This topic will be discussed further in Chapter 5.

Complementary results in the analysis of bio-oils were obtained by the use of quantitative ^{1}H-NMR spectroscopy, which was introduced for the first time in the bio-oil analysis context. This technique permitted an overview of all the functional groups contained in the bio-oil (while GC can analyse only a relatively volatile fraction of the oil) and it allowed calculating the concentration of protons related to a specific group.

In Chapter 5, further research will be addressed to higher HDO temperature in order to gain higher deoxygenation degree and to understand the different reactivity of model compounds in comparison to bio-oil.

Chapter 5

Deep Hydrodeoxygenation of the light fraction of pyrolysis oil: a study of the reactivity of platform molecules

In this chapter, the activity of different nickel-based catalysts was screened during deep hydrotreatment (340 °C, 8.0 MPa H_2 at room temperature) of the light phase of a pyrolysis oil from wheat straw. The highest activity in terms of hydrogen consumption was associated to $NiCu/Al_2O_3$, but was still inferior in comparison to Ru/C used as benchmark. Nickel catalysts produced upgraded oils containing significant amount of ketones, while Ru/C mainly alcohols and hydrocarbons. The reactivity of platform molecules was investigated in aqueous solution and in the pyrolysis oil in order to understand the different behaviour in the two media. For this target isotopically-labelled phenol and D-glucose were employed. Phenol was found to be resistant to HDO in pyrolysis oil, while in aqueous solution it was converted mainly to cyclohexane over $NiCu/Al_2O_3$ and to methane over Ru/C. D-glucose in aqueous solution was converted to methane in presence of Ru/C and $NiCu/Al_2O_3$, while in pyrolysis oil a complex mixture of products was formed, which were recovered mainly in the upgraded oil phase. Analysis of the spent catalysts showed chemical and physical modifications (like deposition of inorganic and organic material and formation of Ni_3S_2) that can partially explain the different reactivities in the two media.

5.1   Introduction

Deep hydrotreatment has been widely investigated as a method to reduce the oxygen content of bio-oils. However, a lot of studies have addressed the reactivity of model compounds in different solvents [42, 118] or the characterisation of the main properties of the upgraded products [32, 33, 36, 113, 114, 117, 206], without focussing on the reactivity of platform molecules in the pyrolysis oil.

The higher amount of studies related to model compounds rather than pyrolysis oils can be easily explained by the difficulties faced in evaluating the performance of a catalyst in a complex mixture. In addition, no standard pyrolysis oil exists, since the composition of bio-oils varies depending on different parameters (described in Chapter 3), making it complicated to compare different studies. However, it is important to investigate the reactivity of some platform molecules, not only in pure solvents, but also in pyrolysis oil, since their conversion and selectivity could be influenced by several factors. For example, the polarity of the medium of the reaction [207], the competitive adsorption of different species on the catalyst surface [208,209] the eventuality of faster parallel reactions [100,208,210] and a simultaneous deactivation of the catalyst [160,164,211] (more likely in the pyrolysis oil) can drive the reaction to the formation of different products.

The present work aimed to compare and integrate the HDO study of pyrolysis-oil with model compounds, using nickel-based catalysts and Ru/C (as a benchmark). The light phase of a pyrolysis oil (Section 3.2) was used for these reactions, because it is simpler to characterise in comparison to the whole pyrolysis oil. This allowed focusing on the reactivity of polar low molecular-weight compounds and sugar derivatives, which have not been so well investigated in the literature so far. In the first part of this chapter, a screening of the different nickel-based catalysts in deep hydrotreatment conditions (340 °C, 8.0 MPa H_2 at room temperature) is reported in comparison to Ru/C (Section 5.2-5.6). These experiments are analogous to those conducted in mild hydrotreatment conditions (250 °C, 8.0 MPa H_2 at room temperature) described in Chapter 4, with the difference that using higher HDO temperature higher deoxygenation degree are expected. Successively, the reactivity of platform molecules over NiCu/Al_2O_3 and Ru/C in water and in the pyrolysis oil is discussed (Section 5.7-5.8). The choice of using water for the model compounds and not other organic solvents, which could favour more HDO [206], was justified because water is the main component in pyrolysis oil. As platform molecules, phenol was chosen as the representative for the lignin fraction and D-glucose for the cellulose.

Phenol has gained a lot of attention in HDO studies [97] since it is one of the most HDO resistant components in pyrolysis oil. During hydrotreatment, phenol can be converted to cyclohexane, but it can also be produced by demethoxylation of guaiacol and syringol or through other pathways from lignin derivative compounds. Therefore if phenol is still detected in the upgraded products, it is difficult to establish if it reacts or not.

D-glucose was chosen since it is the building block of cellulose and only few studies regard its reactivity. The sugar derivatives of pyrolysis oil represent a big challenge in terms of characterising and understanding its reactivity. Few studies have been addressed to this fraction [80, 111, 208, 212] and usually they were carried out at lower temperature, with a complex mixture mainly consisting of alcohols and polyols as main products.

By adding isotopically-marked compounds in the pyrolysis oil, like phenol-d_6 and glucose-$^{13}C_6$, it was possible to monitor and compare their reactivity in aqueous medium and in pyrolysis oil.

5.2 Hydrogen consumption and mass balance

The main hydrogen consumption took place during the heating ramp, while once the temperature 340 °C was reached only small variations of pressure were recorded. For this reason the reaction time was restricted to 100 min. The autogenous pressure reached at the final temperature in the autoclave was variable and dependent on the catalyst used. For the blank experiment, the maximum pressure reached was 31 MPa, while for Ru/C and NiCu/Al$_2$O$_3$ 23 MPa and 25 MPa were recorded respectively.

As reported in Chapter 4, for similar experiments at 250 °C, the highest hydrogen consumption at 340 °C was observed over Ru/C (Figure 5.1). Among the Ni-based catalysts, NiCu/Al$_2$O$_3$ had slightly higher activity. The low percentage of copper seemed to enhance the hydrogenation/hydrodeoxygenation activity of the catalyst, probably due to the spillover of hydrogen [117, 213].

In all cases, four products were formed in similar amounts (Table 5.1): an upgraded oil, an aqueous phase (highest mass yield), gases and solids. The upgraded oil was only a small percentage in mass in comparison to the feed, but contained only a low percentage of water (3-10% depending on the experiment) and high concentration of organics (further analysis in Section 5.5). The aqueous phase consisted of 80 ± 1% water and only few organic compounds, representing therefore

83
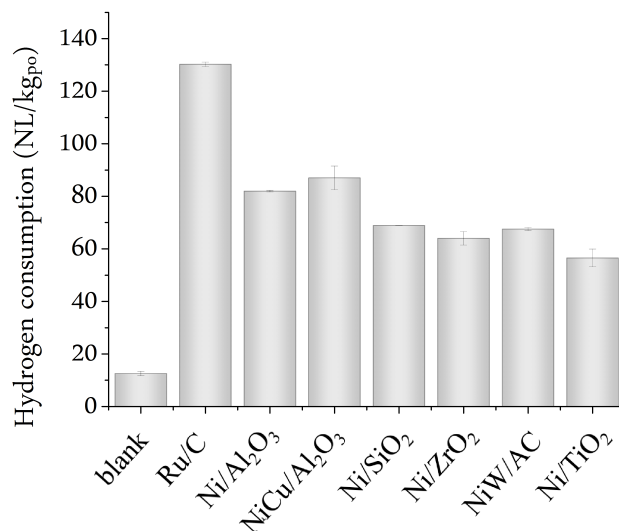
Figure 5.1: Hydrogen consumption during HDO of the light fraction of pyrolysis oil over different catalysts (340 °C, 8.0 MPa of hydrogen at room temperature).

a low quality product. The solid and gas formation were negligible compared to the liquid products. Some losses were found in all cases (circa 3%, note additional hydrogen that is incorporated) and are due partially to the mineral content and to the error propagation in the calculation of the mass balance using the experimental data of the elemental analysis and Karl Fischer titration.

A similar study [113] reported a hydrogen consumption of 146 NL/kg$_{po}$ for a

Table 5.1: Mass balance (in weight percent with respect to the feed) of the products of the HDO reaction over different catalysts (340 °C, 8.0 MPa of hydrogen at room temperature).

	Upgraded oil (wt.%)	Aqueous phase (wt.%)	Gas (wt.%)	Solid (wt.%)	Loss (wt.%)
blank	17.4 ± 0.5	75.6 ± 0.5	4.9 ± 0.3	n.d.	2.3 ± 0.6
Ru/C	17.4 ± 0.1	78.0 ± 0.3	3.5 ± 0.1	n.d.	2.3 ± 0.1
Ni/Al$_2$O$_3$	17.6 ± 0.2	76.2 ± 0.6	3.4 ± 0.1	0.2 ± 0.1	3.3 ± 0.5
NiCu/Al$_2$O$_3$	17.9 ± 0.2	78 ± 2	3.1 ± 0.3	0.1 ± 0.1	2 ± 1
Ni/SiO$_2$	17.6 ± 0.8	76 ± 1	3.5 ± 0.2	0.3 ± 0.1	2.9 ± 0.0
Ni/ZrO$_2$	17.6 ± 0.5	76.5 ± 0.1	3.6 ± 0.2	0.3 ± 0.1	2.5 ± 0.2
NiW/AC	18.2 ± 0.1	76.0 ± 0.5	3.7 ± 0.4	n.d.	2.7 ± 0.1
Ni/TiO$_2$	16.8 ± 0.2	76.8 ± 0.1	3.9 ± 0.1	0.2 ± 0.1	2.7 ± 0.1

NiCu/Al$_2$O$_3$ and 272 NL/kg$_{po}$ for a Ru/C catalyst. Considering that the bio-oil described in literature had only 23.9% of water (organic components 76.1%), while the light phase hydrotreated in this study had 56.7% of water (organic components 43.3%), the results of both studies are quite similar considering the dry bio-oil.

Although the setup and reaction time here and in the previous study (Chapter 4) at 250 °C were different, only qualitative conclusions can be derived. The hydrogen consumption was higher for 340 °C, but the values were still comparable at 250 °C. For example, the uptake of hydrogen at 340 °C was for Ru/C 21% higher than at 250 °C, for NiCu/Al$_2$O$_3$ 23%, for Ni/Al$_2$O$_3$ 33%, Ni/ZrO$_2$ 28%, for Ni/SiO$_2$ 17%, for NiW/AC 13% and Ni/TiO$_2$ 5%. The consumption of hydrogen for bio-oil upgrading is known not to be a linear function of the temperature [33]. Hydrogenation already occurs at mild conditions, whereas deoxygenation is favoured at higher temperatures and it requires less hydrogen consumption. For example for 1 mol of phenol, 3 mol H$_2$ are consumed for hydrogenation of the aromatic ring and 1 mol H$_2$ for the last HDO step. This could explain why the hydrogen consumption at 340 °C was only slightly higher than at 250 °C.

5.3 Tracking the fate of carbon, hydrogen and oxygen in the product phases

In 100 g of the original light phase of the pyrolysis oil, there is 20.7 g of carbon, 9.5 g hydrogen, 67.8 g oxygen and the remaining percentage of minerals. After the HDO reaction, the elemental components were redistributed in four phases. Notably, most of the carbon (circa 60%) was recovered in the upgraded oil (Figure 5.2). Only 33% remained in the aqueous phase and 6% in the gas. Hence, the hydrotreatment allowed concentrating the majority of the carbon in a smaller volume, even more of what observed at mild conditions (Section 4.4). The feed used was a low-quality fraction with a high water content, a lot of sugar derivatives (21.1% WS-DDIS, see Chapter 4), and low heating value (HHV 9.2 MJ/kg) and it was converted to an upgraded oil with a HHV of 35-37 MJ/kg. The valorization of sugar derivatives by hydrotreatment has only recently attracted attention, and only few studies [80, 206, 212] about the reactivity of this fraction have been carried out.

The majority of the oxygen was present in the aqueous phase and circa 87-89% in form of water. The upgraded oil contained 13 ± 1% oxygen in dry basis, in accordance with other similar studies [113, 114]. As shown in table 5.2, Ru/C
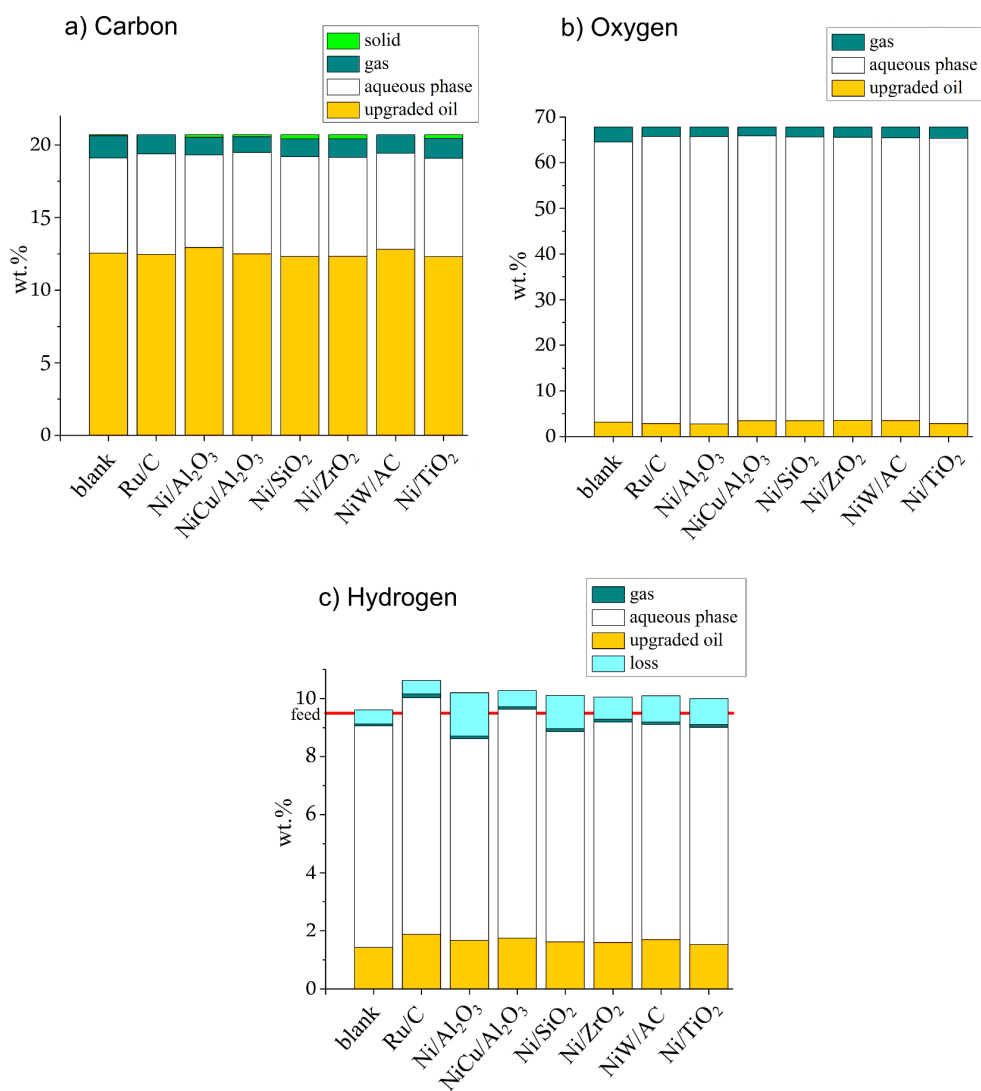
Figure 5.2: Distribution of carbon (a), oxygen (b) and hydrogen (c) in different phases after HDO (340 °C, 8.0 MPa of hydrogen at room temperature).

produced the highest amount of water, in agreement with its higher activity in HDO and hydrogenation compared to the other catalysts. It should be noted that the effective water production was less than the value calculated by the hydrogen consumption, indicating that hydrogenation also occurred. The blank experiment also showed water production, due to dehydration reactions favoured thermally or by the acid environment. Experiments with nickel-based catalysts resulted in a slightly higher water production in comparison to the blank experiment. However, in all cases water produced derived from the combination of thermal/acidic dehydration and HDO.

The global hydrogen amount increased during the reaction compared to the feed (Figure 5.2). The hydrogen mass balance could not be perfectly closed, with an average error of 8% with respect to the theoretical value. This is again due to the propagation of errors in elemental analysis and in Karl Fischer titration. Similar to oxygen, the main quantity of hydrogen was bound as water in the aqueous phase and the remaining fraction mainly to the upgraded oil, which resulted more hydrogenated after the use of a catalyst.

Table 5.2: Production of water related to 100 g of the light phase of pyrolysis oil compared to the H_2 consumption (hydrotreatment 340 °C, 8.0 MPa of hydrogen at room temperature).

Catalyst	Water production (g)	Hydrogen consumed (g)	Maximum ammount of water generated by H_2 (g)
blank	5.2	0.10	0.9
Ru/C	7.2	1.07	9.6
Ni/Al$_2$O$_3$	5.7	0.67	6.1
NiCu/Al$_2$O$_3$	5.6	0.72	6.5
Ni/SiO$_2$	5.5	0.57	5.1
Ni/ZrO$_2$	5.5	0.53	4.7
NiW/AC	5.7	0.55	5.0
Ni/TiO$_2$	5.6	0.46	4.2

5.4   Analysis of the gaseous products

The amount of gas produced at 340 °C was on average three times higher than the experiments at 250 °C (Chapter 4). The main gas detected was CO_2, but the amount of other gases, especially methane, ethane and propane was significant as result of the higher cracking activity at high temperature (Figure 5.3).

The blank experiment (without catalyst) had the highest tendency towards cracking. Over Ru/C and NiCu/Al$_2$O$_3$, unsaturated molecules like ethene and propene were lower, probably due to the high hydrogenation activity, which converted them to ethane and propane. NiCu/Al$_2$O$_3$ had a slightly lower gas production in comparison to the other catalysts. For nickel-based catalysts the quantity of CO_2 seems inversely proportional to the hydrogen consumption, but no higher production of methane was detected, excluding that the extra hydrogen consumption converted CO_2 to CH_4. Methanation of CO_2 was demonstrated by a previous study [214] to be prevented in presence of pyrolysis oil over Ni/Al$_2$O$_3$.
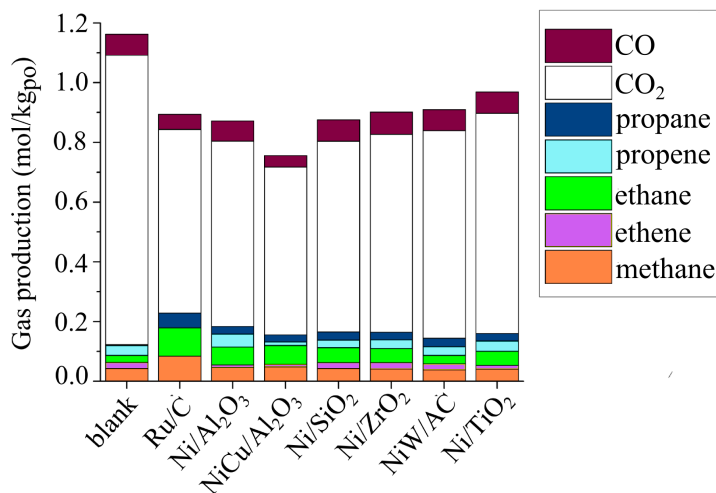
Figure 5.3: Gases produced during hydrotreatment over different catalysts (340 °C, 8.0 MPa of hydrogen at room temperature).

Therefore methane can be associated more to demethoxylation or demethylation of some compounds, which can take place also without a catalyst, since methane was detected also in the blank experiment. CO_2 can be produced from decarboxylation, but it could not be excluded that redox reactions among organic molecules and with water took place.

5.5 Characterisation of the liquid products

The van Krevelen plot of the upgraded oils is reported in Figure 5.4.

The level of deoxygenation reached was similar for each experiment (68 ± 2%), also for the blank experiment. On the other hand, the H/C ratio changed considerably, determining the quality of the oil. The upgraded oil produced in the blank experiment had a low H/C ratio, resulting in a very viscous oil with a density higher than water. On the contrary, the upgraded oils obtained using a catalyst had a lower density than the aqueous phase and a viscosity that was apparently lower for higher H/C ratio. The highest H/C ratio was attributed to Ru/C, then to $NiCu/Al_2O_3$, in agreement with the hydrogen consumption. The other catalysts produced upgraded oils that were comparable in composition according to the van Krevelen plot and the GC-MS results.

The most significant differences in the chemical composition of the upgraded oils were detected among the blank experiment, Ru/C and $NiCu/Al_2O_3$ (chosen as

88
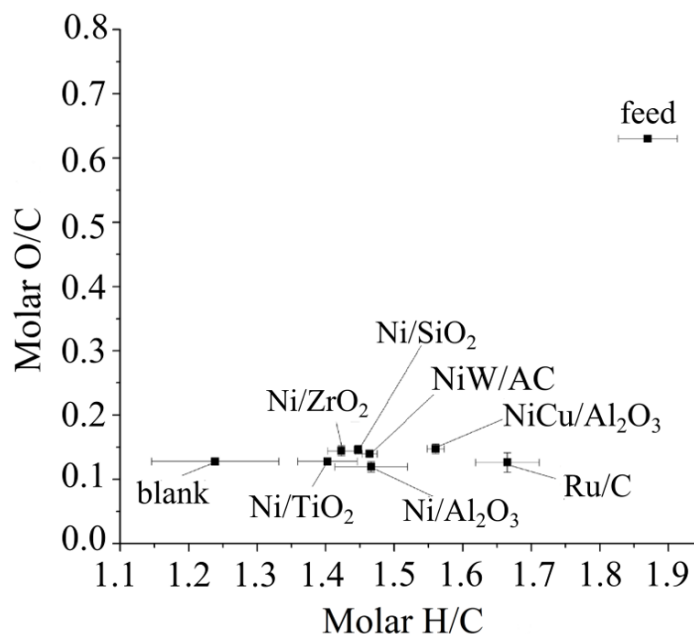
Figure 5.4: Van Krevelen plot of the upgraded oils after hydrotreatment over different catalysts (340 °C, 8.0 MPa of hydrogen at room temperature).

the representative of the nickel-based catalysts). The chromatograms recorded by GC-MS are reported in Figure 5.5 and are divided in 3 regions where the following components are mainly present: a) hydrocarbons; b) cyclic ketones and acids; c) phenolic derivatives. At the retention time of 3.3-10 min (not shown), only few and unidentified components were detected.

Ru/C had the highest production of hydrocarbons, mainly as methylcyclopentane and cyclohexane, which were identified as HDO products of the sugar derivatives and lignin fraction respectively. Some cyclohexane was formed, probably as product of the hydrogenation and hydrodeoxygenation of phenol. A possible pathway is reported in Figure 5.6a (also confirmed by other studies [97]). Methylcyclopentane could be formed from the hydrogenation and hydrodeoxygenation of 2-methylcyclopent-2-enone (Figure 5.6b). This compound was not present in the feed, but its formation from sugar derivatives was favoured by the acid environment and the temperature. Specifically it can be derived from the rearrangement of furfural-like compounds [36, 179, 206, 215, 216] or anhydro-sugars like levoglucosan. Isomerization of cyclohexane to methylcyclopentane could take place during the dehydration of cyclohexanol under acid conditions and in the presence of a catalyst [217], but it seemed negligible in this study.

89
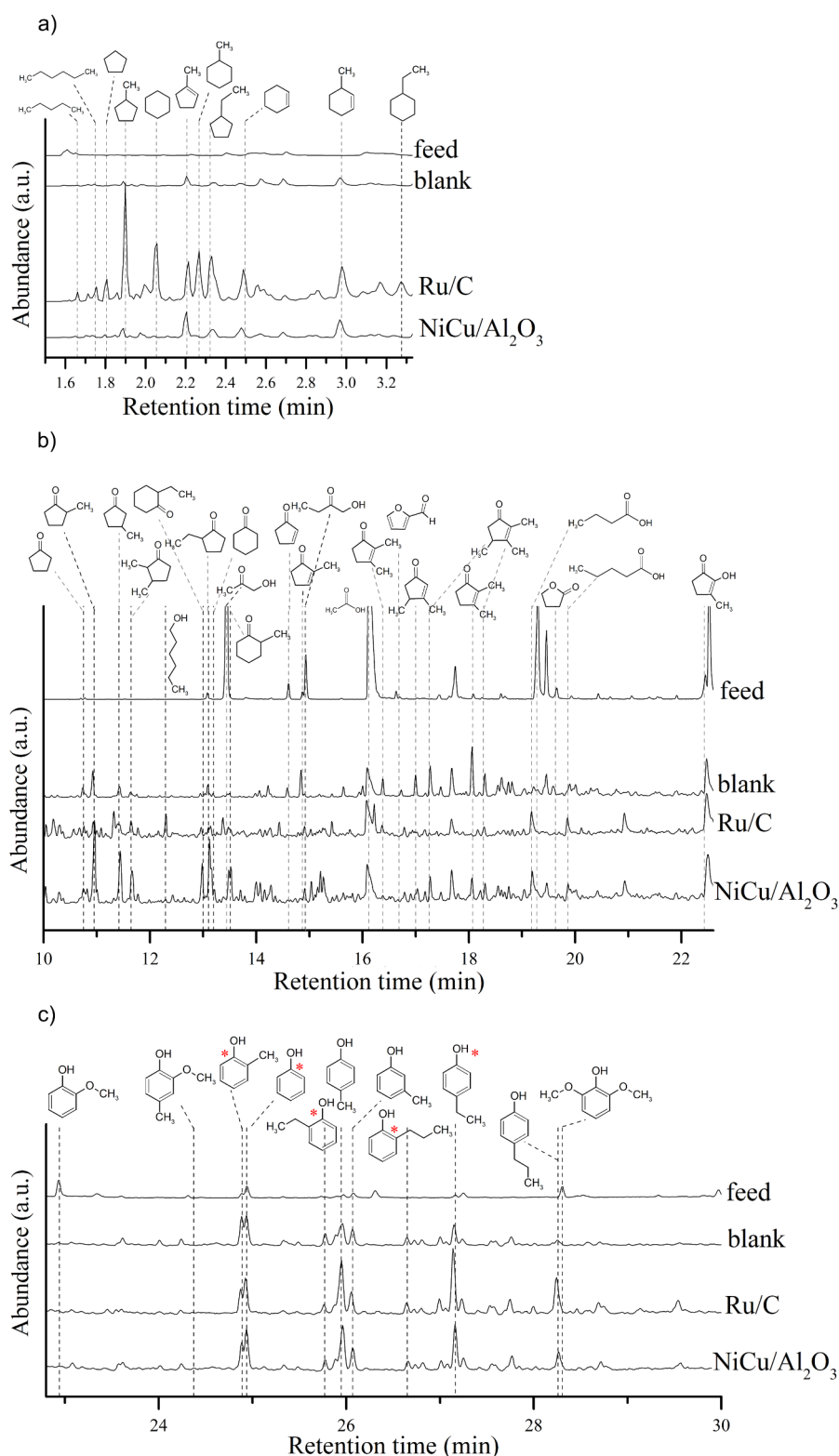
Figure 5.5: Chromatograms (GC-MS) of the upgraded oils (hydrotreatment of the light phase of the pyrolysis oil at 340 °C, 8.0 MPa of hydrogen at room temperature) over different catalysts compared to the feed. The isotopically-marked products derived from phenol-d_6 are indicated with red "*".

Table 5.3: Concentration in weight percent (wt.%) of some representative components in the aqueous phase and in the upgraded oils (hydrotreatment at 340 °C, 8.0 MPa of hydrogen at room temperature).

	light phase of p.o.	blank		Ru/C		NiCu/Al$_2$O$_3$	
		upgraded oil	aqueous phase	upgraded oil	aqueous phase	upgraded oil	aqueous phase
cyclopentanone*	n.d.	0.13	0.03	n.d.	n.d.	0.34	0.04
2methyl-cyclopentanone°	n.d.	0.39	0.03	0.08	n.d.	1.41	0.10
phenol*	0.11	0.80	0.04	0.69	0.05	0.60	0.04
cyclohexanone°	n.d.	n.d.	n.d.	n.d.	n.d.	0.50	n.d.
cyclohexane°	n.d.	n.d.	n.d.	0.05	n.d.	n.d.	n.d.
o-cresol°	0.04	0.39	n.d.	0.49	n.d.	0.31	n.d.
4-ethylphenol°	0.02	0.41	n.d.	0.73	n.d.	0.64	n.d.
acetic acid*	4.90	3.49	6.38	3.80	5.24	4.40	5.54
ethylene glycol*	7.80	n.d.	5.35	n.d.	1.54	1.02	4.75

°analysed by GC equipped with column Type Rxi®5Sil MS (0.25μm x 0.25mm x 30m);

*analysed by GC equipped with column Stabilwax (0.25μm x 0.25mm x 30m).

NiCu/Al$_2$O$_3$ was not active at 340 °C for the production of hydrocarbons (similar results were reported in previous studies [113, 114]). On the other hand, the experiments over nickel catalysts showed a higher production of cyclic ketones (Figure 5.5b) as also observed by Ardiyanti et al. [113, 114]. Over NiCu/Al$_2$O$_3$ some cyclohexanone was detected from phenol conversion instead of cyclohexane over Ru/C (Table 5.3). Note that in both cases a lot of phenol was not converted. With analogies, cyclopentanone and 2-methylcyclopentanone were the main products from the sugar derivatives over NiCu/Al$_2$O$_3$, instead of cyclopentane
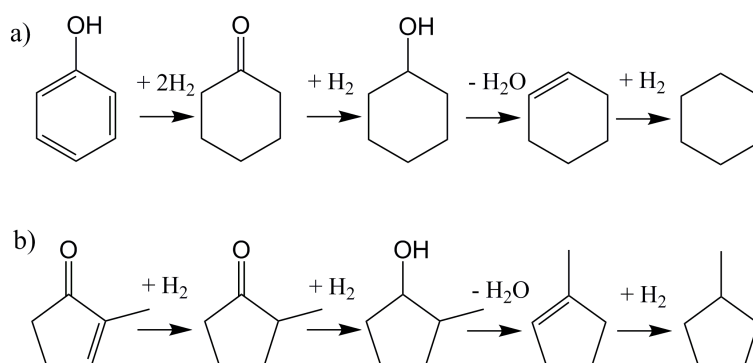
Figure 5.6: Suggested mechanism of hydrodeoxygenation of phenol (a) and 2-methylcyclopentenone (b).

and methylcyclopentane as observed over Ru/C. It seems that nickel catalysts followed the same mechanism reported in Figure 5.6, but since they were less active the reaction stopped at the ketone products, whereas Ru/C allowed further hydrogenation/ hydrodeoxygenation.

Concerning the phenol derivatives, in all experiments guaiacol and syringol were completely converted and no methoxy-groups or other alkoxy-groups bonded to an aromatic unit were detected in the products. Phenolic aromatic rings substituted with alkyl groups and also phenol were still detected, demonstrating a lower activity toward the HDO of the phenolic hydroxyl group (Figure 5.5c). As reported in the literature [97,156,159], phenol has a lower reactivity to HDO in comparison to anisol, which explains the resistance of phenolic compounds in the products to HDO.

The aqueous phase of each experiment contained few components, and mainly acids (especially acetic acid) and alcohols (mainly ethylene glycol) were identified (Table 5.3). For example, in the case of $NiCu/Al_2O_3$ and Ru/C acetic acid, methyl acetate (esterification product), ethanol, propionic acid, 1,2-ethanediol monoacetate (esterification product), and phenol were detected (propanol only for Ru/C). For the blank experiment, acetic acid, acetone, methyl acetate, ethanol, 3-methylcyclopent-2enone were detected, but various components could not be identified.

The content of acetic acid was still high also in the upgraded oil (Table 5.3), but the use of a catalyst slightly reduced this value. Ethylene glycol was recovered mainly in the aqueous phase, but it was partially converted, especially over Ru/C (esterification or ethane formation).

5.6 Additional information about the upgraded products by quantitative ^{1}H-NMR spectroscopy

Quantitative ^{1}H-NMR can give more complete information than GC about the functional groups present in the products, since each proton present in solution has the same impact and the signal is not dependent by the volatility of the substance. As reported in Figure 5.7, the aromatic groups (8.5-6.0 ppm) were strongly concentrated in the upgraded oil, while the aqueous phase was almost free of aromatics. Water and proton-exchange groups (6.0-4.3 ppm), was the main component in the aqueous phase, whereas its concentration was relatively low in the upgraded oil. Aldehydes (10.1-9.5 ppm) were present in lower amount in the

feed and they were completely hydrogenated after the upgrading. Alcohols (or ether groups, 4.3-3.0 ppm) had a similar concentration between the aqueous and oil phase, while the concentration of alpha protons to carboxylic acid, ketones and unsaturated groups (3.0-1.5 ppm) was higher for the upgraded oils. The protons of alkane groups (1.5-0.5 ppm) were more concentrated in the upgraded oils, and Ru/C had the highest signal, confirming the higher hydrogenation/hydrodeoxygenation activity monitored also by GC.
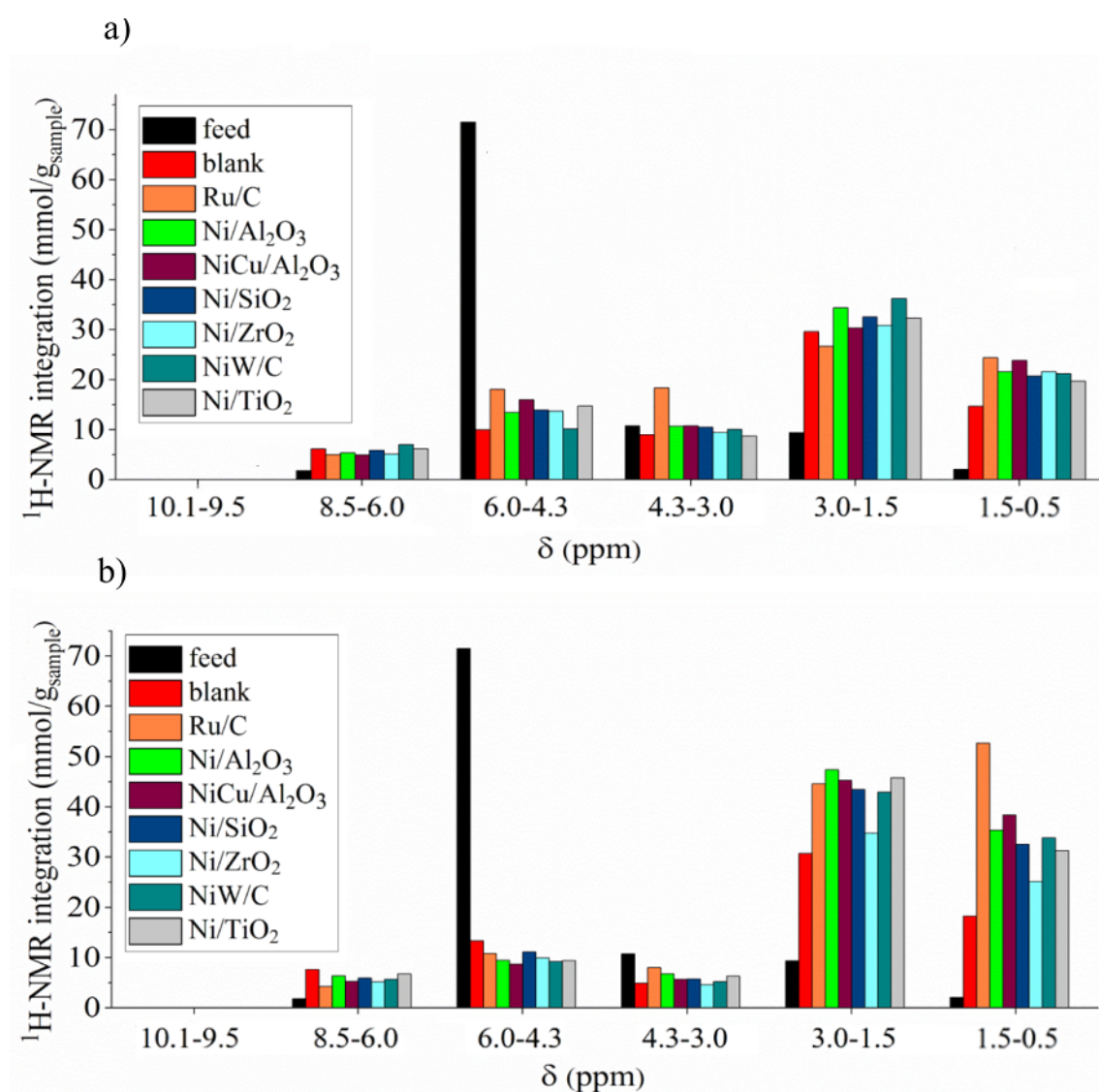
Figure 5.7: ^{1}H-NMR integration of the spectra of the upgraded oil (a) and the aqueous phase (b) in specific chemical-shift range (hydrotreatment at 340 °C, 8.0 MPa of hydrogen at room temperature). The assignment of protons to the specific classes of compounds is reported in Table 2.1.

The oil upgraded with Ru/C had also a slightly lower concentration of protons in the aromatic region, indicating again that Ru/C is more active in hydrogenation of the aromatic ring than the nickel catalysts. Comparing all catalysts used, only the upgraded oil over Ni/ZrO$_2$ had a lower concentration in protons, probably due to incomplete solubility in methanol, since the hydrogen content determined by elemental analysis was comparable to the other oils.

5.7 Reactivity of phenol in aqueous solution and in the pyrolysis oil

The reactivity of phenol was first investigated using an aqueous solution 10 wt.% of phenol and successively pyrolysis oil with the addition of phenol-d$_6$ (concentration 0.4%), which is easily traceable by GC-MS. The use of Ru/C for the aqueous solution of phenol resulted in its complete conversion with high selectivity to methane (70% of the carbon recovery, Table 5.4). The combination of the temperature, high pressure of hydrogen and the presence of Ru/C promoted the hydrocracking of cyclohexane [206]. Using NiCu/Al$_2$O$_3$, the reaction formed mainly cyclohexane (100% conversion, selectivity 85%) and cyclohexanol (selectivity 15%, concentration 13.1 g/kg in aqueous phase, 50.5 g/kg in the cyclohexane phase) and traces of benzene (0.2 g/kg in the cyclohexane phase).

Regarding pyrolysis oil, a comparison between the experiments performed with and without phenol-d$_6$ was performed. Low conversion of phenol-d$_6$ was observed when it was treated at 340 °C in pyrolysis oil. For the experiment with unmarked phenol an average (for the blank experiment, Ru/C and NiCu/Al$_2$O$_3$) of 150 ± 10% of the original amount was recovered, probably because additional phenol was produced from guaiacol and syringol. This was plausible since these molecules were not longer detected after the experiment. Also in other studies [113,114,206], phenol or the phenolic derivatives increased after hydrotreatment.

In the case of deuterated phenol, an average of 74 ± 2% was recovered in the blank experiment, for the NiCu/Al$_2$O$_3$ and Ru/C, demonstrating that it reacted in all cases only partially. Measuring the mass spectra, it was observed that the unreacted isotopically-marked phenol was not completely inert. This was also demonstrated by an additional experiment with phenol-d$_6$ and water: at 340 °C phenol can exchange protons in the aromatic ring with the external solvent, as an effect of the temperature and the acidic medium (independent from the presence of

a catalyst).

In Figure 5.8a, the mass spectra of the marked phenol before and after reaction are shown. Before the reaction, only 5 deuterium atoms were detected by GC-MS because of the quick H/D exchange of the hydroxyl group with the pyrolysis oil. An average of three deuterium atoms were exchanged, which could be identified by ^{1}H-NMR. The chemical shifts 6.79 and 6.82 ppm were recorded after the experiment with phenol-d_6 in water. In the upgraded oil the signals were a bit shifted and they overlapped. The peak integration (2:1 ratio) suggested that deuterium atoms in the more shielded positions exchanged thermally with the protons in the medium (Figure 5.8b). The deuterium atoms in ortho- and para-positions are bonded to more electronegative carbons for inductive and mesomeric effect. The mechanism of proton exchange is suggested in Figure 5.8c. The exchange is supposed to happen through a proton addition and elimination of deuterium, creating a carbocation as intermediate.

Note that this kind of carbocation can potentially initiate polymerization reactions [153], but in this case most of the phenol was recovered. The product cyclohexane was observed only for Ru/C and in the case of adding phenol-d_6, a slightly higher concentration of cyclohexane (1.1 g/kg of upgraded oil vs. 0.5 g/kg) was detected. 1.1 g/kg is still a small amount since it is circa 5% of the starting deuterated phenol. In an additional study about phenol-d_6 in water over

Table 5.4: Gaseous products (mol) formed during the hydrotreatment of phenol over Ru/C and of D-glucose in the blank experiment, over Ru/C and NiCu/Al$_2$O$_3$ in 50 g water (340 °C, 8.0 MPa hydrogen at room temperature).

Compound	5g phenol (0.319 mol C)	5g D-glucose monohydrate (0.151 mol C)	5g D-glucose monohydrate (0.151 mol C)	5g D-glucose monohydrate (0.151 mol C)
Catalyst	Ru/C	blank	Ru/C	NiCu/Al$_2$O$_3$
Methane	0.223	-	0.136	0.099
Ethane	0.002	-	0.001	0.005
Propane	0.001	-	0.001	0.003
CO$_2$	0.019	0.013	<0.001	0.001
CO	0.008	0.003	0.006	0.005
Ethene	-	0.003	-	-
Propene	-	0.001	-	-
Total mol recovered	0.253	0.020	0.144	0.113

NiCu/Al$_2$O$_3$, it was observed that the cyclohexanol produced tends to exchange all the deuterium during the hydrogenation, making it difficult to discriminate it from other HDO products by GC-MS.
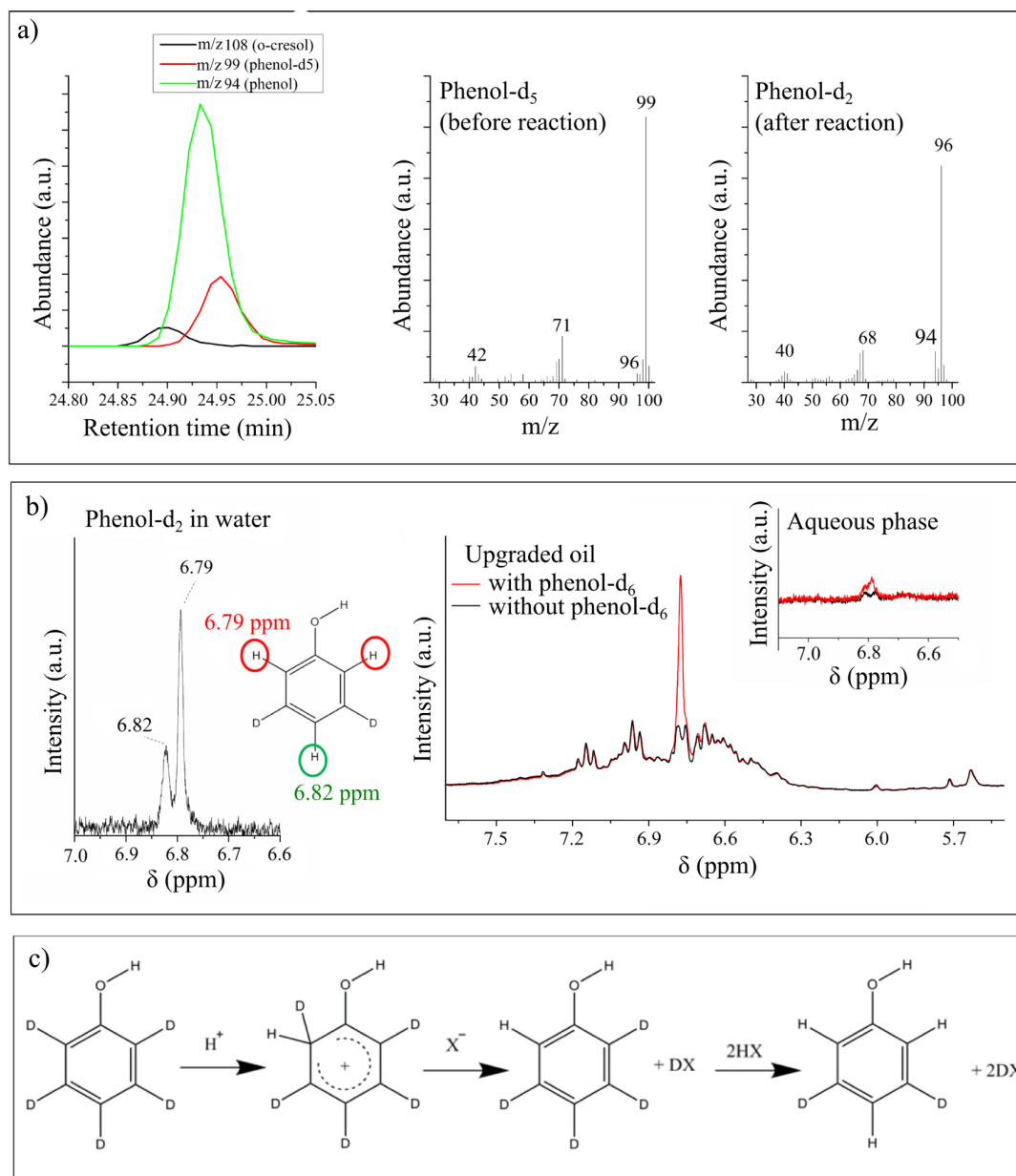
Figure 5.8: Reactivity of phenol-d$_6$. a) Chromatogram (GC-MS) of phenol-d$_5$ and phenol-d$_2$ with relative mass spectra. b) Comparison of ^{1}H-NMR spectra between the upgraded oils (also the aqueous phase) of the blank experiment with and without adding phenol-d$_6$. Thermal/acidic exchange of deuterium atoms in ortho and para positions of phenol-d$_6$. c) Mechanism of exchange of deuterium exchange of phenol-d$_5$.

A phenomenon that was limited to a small percentage, but that is still interesting, is the presence (detected by GC-MS) of a small amount of alkyl-phenol that contained 2 m/z units more (2 deuterium atoms that remain in the phenol ring). For example 2-methyl-phenol, 2-ethyl-phenol, 4-ethyl-phenol and 2-propyl-phenol (Figure 5.5c, marked by *) have a small component in which the molecular weight exceeded the expected molecular weight by 2 mass units. This may indicate that in pyrolysis oil, C-alkylation between phenol and an alcohol was favoured in para- and ortho-positions by the acidic environment [218, 219]. This observation is not dependent on the catalyst since it is also monitored in the blank experiment, but it was enhanced by the acid environment.

5.8 Reactivity of glucose in aqueous solution and in the pyrolysis oil

The reactivity of D-glucose was first investigated in aqueous solution 10 wt.% without catalyst, over Ru/C and NiCu/Al$_2$O$_3$. In the experiment without catalyst at 340 °C, no consumption of hydrogen was detected and the main product was coke (82.5 % of the mol of carbon), while the rest was gas (Table 5.4). The decomposition of glucose happened already in the heating ramp as already reported in the literature [220, 221]. The profile of decomposition was described qualitatively in Figure S3. Glucose was completely converted at 250 °C, forming mainly coke and other compounds detected in the liquid phase, such as hydroxymethylfurfural, furfural, acetic acid, formic acid, hydroxypropanone, glycolaldehyde and dihydroxyacetone. The amount of carbon still detected in the liquid after the heating ramp at 250 °C was 38.5% of the starting carbon moles. The rest was mainly converted into solid components.

In the case of Ru/C in aqueous solution, the glucose was gasified (carbon recovery in the gas of 96.7% mol), mainly into methane (Table 5.4) resulting from hydrocracking [222], that seemed to be particularly favoured at this temperature and over this catalyst. NiCu/Al$_2$O$_3$ had the same effect: 81,9% of C was recovered as gas (mainly methane, Table 5.4), 5.1% in the liquid and 0.7% in the solid (total recovery 87.7%). Where a catalyst was used, the first consumption of hydrogen happened already at low temperature (Figure S4), with a maximum consumption rate of hydrogen for Ru/C at 85 °C and for NiCu/Al$_2$O$_3$ at 130 °C. Glucose was converted at this temperature selectively to sorbitol over both catalysts as proven
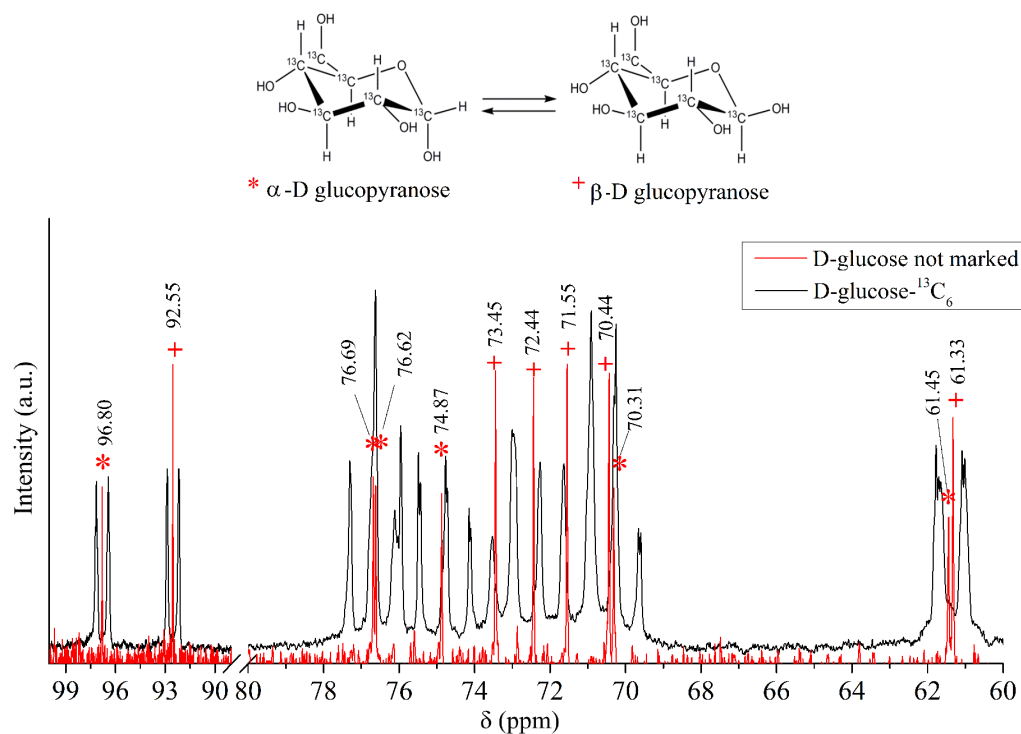
Figure 5.9: Comparison of the ^{13}C-NMR signal for D-glucose with natural isotopic composition and D-glucose-[13]C$_6$. The specific assignment of the D-glucose signal is reported by Pomin [223].

experimentally by NMR.

The reactivity of D-glucose in pyrolysis oil was further studied by adding glucose-[13]C$_6$ in pyrolysis oil (concentration 0.4%) and monitoring it by ^{13}C-NMR. Glucose-[13]C$_6$ has a typical coupling signal ([1]J$_{C,C}$ circa 170-180 Hz, Figure 5.9) that permits differentiation of the signal originated by its conversion products from all other compounds present in the pyrolysis oil (provided that the decomposition product has a direct [13]C-^{13}C bond).

After the HDO reaction in pyrolysis oil, the glucose-[13]C$_6$ was completely converted, but no signals with the specific coupling were detected clearly in the liquid products (Figure S5). No significant differences were recorded in the spectra or by elemental analysis of the products of the experiment without glucose-[13]C$_6$. The mass spectra of the gases did not show any detectable concentrations of isotopic species, as well as no peak shift in ATR-FTIR spectra of the spent catalysts indicated the deposit of carbonaceous species derived from the marked D-glucose. This suggests that D-glucose formed different and unspecified products with concentrations below

Table 5.5: Main differences between the hydrotreatment experiments with and without addition of glucose (10 wt.% in pyrolysis oil, at 340 °C, 8.0 MPa of hydrogen at room temperature).

	Ru/C without glucose	Ru/C with glucose	NiCu/Al$_2$O$_3$ without glucose	NiCu/Al$_2$O$_3$ with glucose
Hydrogen consumption (mol H$_2$/100g p.o; NL/kg)	0.535 mol/100g p.o.; 130 NL/kg p.o.	0.620 mol/100g p.o.; 151 NL/kg p.o.	0.357 mol/100g p.o.; 87 NL/kg p.o.	0.414 mol/100g p.o.; 101 NL/kg p.o.
Elemental composition (dry basis, wt.%)				
C content	75.7	76.0	74.9	76.0
H content	10.5	10.0	9.7	9.6
O content	12.7	12.9	14.3	13.4
N content	1.1	1.0	1.1	1.1
Mass balance*				
Upgraded oil (wt.%)	17.4	21.5	18.1	22.7
Aqueous phase (wt.%)	78.0	82.8	77.1	81.5
Gas (wt.%)	3.5	4.0	3.1	4.1
Solids (wt.%)	n.r.	n.r.	0.15	0.21
Losses (wt.%)	1.2	2.8	1.7	2.7
Water production for 100g p.o. (g)	7.2	11.3	5.6	10.3
CO$_2$ production (mmol for 100 g of p.o.)	61	87	56	85
Cyclohexane production (g/L in upgraded oil)	0.5	3.4	n.d.	n.d

* normalised to 100 g bio-oil;

n.r. = value not possible to determine by catalyst recovery.

the detection limit of each technique used.

The decomposition of glucose in pyrolysis oil during the heating ramp (Figure S6) was detected using the autoclave with a sampling valve. Glucose-^{13}C$_6$ was monitored until a temperature of 150 °C, when the pyrolysis oil was only one phase. At the next sampling point at 180 °C, the pyrolysis oil separated in two phases and glucose was neither detected in the oil phase nor in the aqueous phase.

An alternative experiment was carried out in order to understand the behavior of glucose during hydrotreatment with a catalyst. A higher amount of natural D-glucose monohydrate (10 wt.%) was added to the pyrolysis oil. This higher

Table 5.6: Elemental mass balance of the hydrotreatment experiments with and without addition of glucose (10 wt.% in pyrolysis oil, at 340 °C, 8.0 MPa at room temperature). The results are reported in g per 100 g of light phase (mass balance closure for light phase with glucose 111 g).

	Ru/C without glucose	Ru/C with glucose	NiCu/Al$_2$O$_3$ without glucose	NiCu/Al$_2$O$_3$ with glucose
Carbon in upgraded oil (g)	12.5	15.9	12.5	15.7
Carbon in aqueous phase (g)	6.9	7.0	7.0	7.2
Carbon in gas (g)	1.3	1.4	1.0	1.4
Oxygen in upgraded oil (g)	2.8	3.2	3.5	4.6
Oxygen in aqueous phase (g)	62.9	67.7	62.4	66.3
Oxygen in gas (g)	2.0	2.6	1.9	2.6
Hydrogen in upgraded oil (g)	1.9	2.2	1.8	2.2
Hydrogen in aqueous phase (g)	8.2	8.1	7.9	7.9
Hydrogen in gas (g)	0.1	0.1	0.1	0.1
Total water (g)	63.7	67.8	62.1	66.8

amount could modify a bit the matrix and the reactivity of the system, therefore it was not so optimal as using an isotopically-marked substance, but can give more information in case glucose forms different products in small concentrations.

Normalizing the hydrogen consumption for 100 g of pyrolysis oil gave a clear indication about the contribution of the hydrogen consumed by glucose. The hydrogen consumption was higher for the experiment with glucose (Table 5.5): for Ru/C an extra quantity of hydrogen was required equivalent to 1.5 mol H$_2$/mol glucose, while for NiCu/Al$_2$O$_3$ to 1.0 mol H$_2$/mol glucose. The extra hydrogen was required during the heating ramp over 200 °C with a maximum hydrogen consumption rate at 210 °C (Figure S7). As demonstrated before, the acid environment of the pyrolysis oil caused complete conversion of glucose under 180 °C, therefore the hydrogen consumption should be attributed to other species generated from glucose decomposition (probably from dehydration reactions). Since the catalysts are mainly active for hydrogenation reactions in the range of 200-230 °C, probably hydrogenation of unsaturated groups was more probable (for example furfural or hydroxymethylfurfural) than hydrodeoxygenation.

The elemental composition of the upgraded oil was not significantly affected by the presence of glucose (Table 5.5), suggesting that the products formed by glucose have a similar composition to the upgraded oil. In order to highlight any differences,
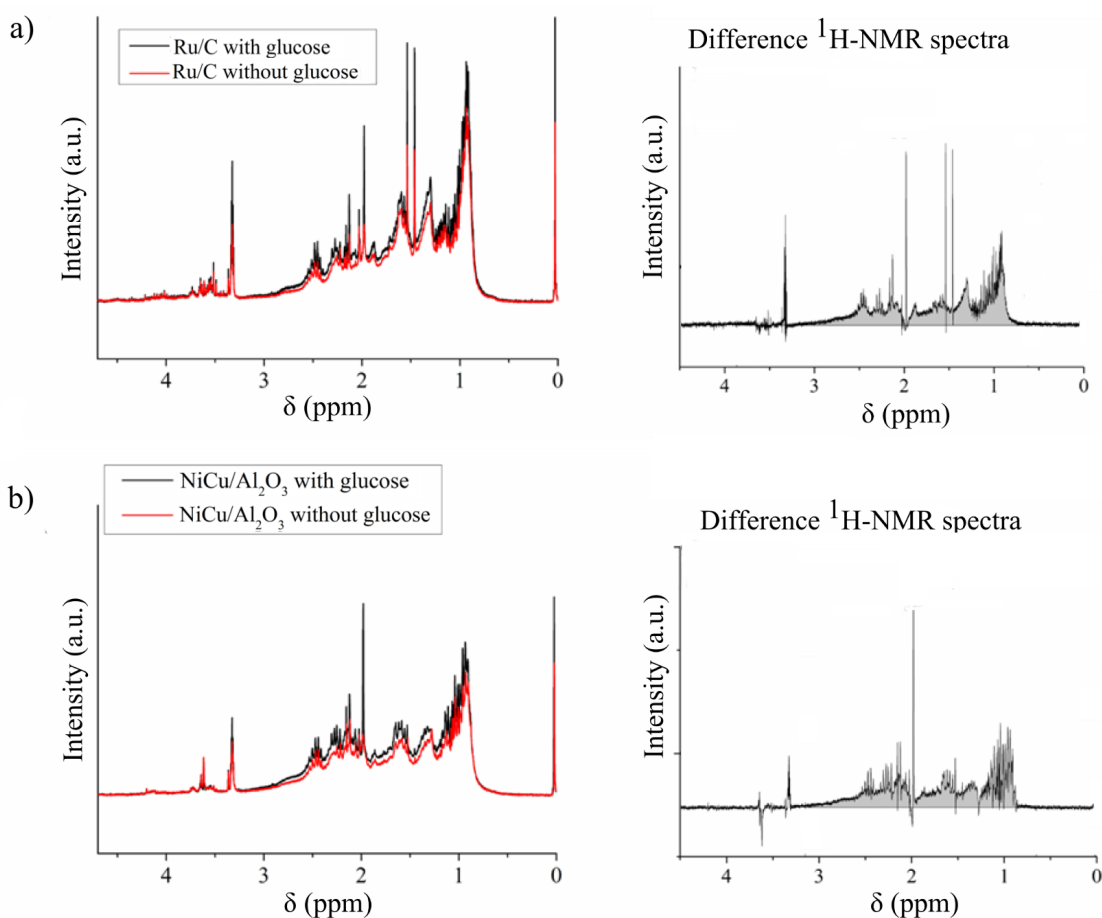
Figure 5.10: Comparison of ^{1}H-NMR spectra of the hydrotreatment experiments over Ru/C (a) and NiCu/Al$_2$O$_3$ (b) with and without addition of glucose (10 wt.% in pyrolysis oil, at 340 °C, 8.0 MPa hydrogen at room temperature): on the left comparison of the spectra normalized by the pyrolysis oil amount; on the right difference of the signal between the two spectra.

the mass balance was normalized for 100 g of pyrolysis oil, with the result that the balance for pyrolysis oil with D-glucose amounted to 111 g.

Comparing the experiments with and without glucose, an increase in the aqueous phase and in the upgraded oil was mainly observed. The increase in the aqueous phase was almost justified by an extra production of water (Table 5.5) and only few organic compounds that were soluble in water (see carbon mass balance in Table 5.6). For 1 mol of glucose an extra production of 4.0 mol water was associated for Ru/C and 4.6 mol for NiCu/Al$_2$O$_3$ (1 mol of water derives from the feedstock since we used glucose monohydrate, so effectively 3.0 mol and 3.6 mol). Therefore D-glucose produced molecules with a lower amount of oxygen, as also observed in

the oxygen mass balance (Table 5.6). Oxygen from glucose was mainly distributed in the aqueous phase in form of the water. The errors associated to the hydrogen mass balance are usually bigger than for carbon and oxygen, therefore no specific observations could be done. The quantity of the gases was slightly higher when glucose was used, and the main contribution was due to extra production of CO_2 (circa 0.5 mol CO_2 per mol of glucose). The solid formation was difficult to monitor with Ru/C, since the amount of catalyst before the reaction and after recovery was similar. For $NiCu/Al_2O_3$ a slightly higher amount of carbon was detected on the surface of the catalyst, but this quantity was not significant (Table 5.5).

In conclusion, D-glucose was converted to different components that were mainly distributed in the upgraded oil. De facto the carbon recovery of glucose was for Ru/C 85.0% in the upgraded oil, 7.7% in the gas, 2.5% in the aqueous phase; for $NiCu/Al_2O_3$ 80.0% in the upgraded oil, 8.6% in the gas, 5.0% in the aqueous phase.

By normalizing the two ^{1}H-NMR spectra of the experiments with and without glucose per 100 g of pyrolysis oil, this difference represents the signal from the glucose products. In Figure 5.10, the two spectra and the result of their subtraction
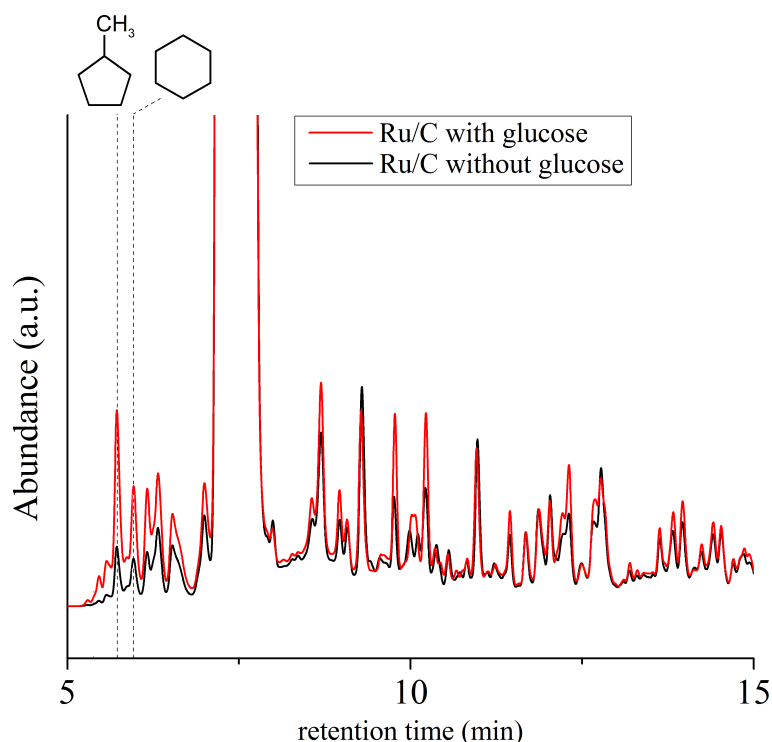
Figure 5.11: Comparison of the chromatograms (GC-MS) of upgraded oils from the hydrotreatment experiments over Ru/C with and without addition of glucose (10 wt.% in pyrolysis oil, at 340 °C, 8.0 MPa of hydrogen at room temperature).

are reported in the case of Ru/C and NiCu/Al$_2$O$_3$. No contributions came from the aromatic region and neither from the alcohols (the only peak shown at 3.3 ppm is due to the deuterated solvent). The main contribution seems to belong to the alkane region (0.5-1.5 ppm, more intense for Ru/C) and to the alpha protons to carboxylic, ketones and unsaturated groups (1.5-3.0 ppm). This is in agreement with the elemental mass balance, affirming that glucose products should have a lower content of oxygen.

In Figure 5.11, the GC-FID chromatograms are reported. The same components are present, but their concentrations are slightly different. The first region of the chromatogram (5-7 min) was characterised by alkanes and alkenes. Ru/C had the ability to produce more hydrocarbons and among them we identified cyclohexane and methylcyclopentane. Cyclohexane was calibrated and the amount detected for Ru/C upgraded oil was 3.4 g/l for the experiment with glucose and 0.5 g/l for the experiment without it (Table 5.5). The extra amount formed can be attributed to glucose, but this represents only 1.4% of the carbon mols of the initial glucose. The low concentrations and vast range of products explain the difficulties in monitoring differences in ^{13}C-NMR. In the region between 8-15 min, other peaks with a higher intensity for Ru/C were detected, but not identified. In the case of NiCu/Al$_2$O$_3$, the chromatograms were similar and no significant differences were detected, indicating that no hydrocarbons were formed and that probably the glucose formed products with higher molecular weight not detectable by GC.

5.9 Conclusions

This chapter described deep HDO at 340 °C of the light phase of pyrolysis oil and platform molecules over alternative nickel-based catalysts and Ru/C. An upgraded oil with a density lower than the aqueous phase and a HHV of 35-37 MJ/kg was produced from the light phase of pyrolysis oil. This demonstrated that it is possible to valorize also a low-value feed containing a large percentage of water (56.7%) and sugar derivatives (21.1%) and obtain an upgraded oil with 13 ± 1% oxygen and a carbon recovery of 60%. Ruthenium was more reactive than nickel at 340 °C, as also observed for mild hydrotreatment at 250 °C. Over ruthenium, hydrocarbons were also generated, mainly cyclohexane (from lignin derivatives) and methylcyclopentane (from cellulose derivatives). NiCu/Al$_2$O$_3$ was the most active among the nickel-based catalysts, but no hydrocarbons were detected and the main products were cycloketones.

Phenolic compounds were resistant to HDO when monitored in the pyrolysis oil. They exhibited only a tendency to exchange the protons in ortho- and para-positions of the aromatic ring with the medium as a result of a thermal/acid phenomenon. On the contrary, phenol was completely converted when studied in aqueous solution, forming mainly methane in the case of Ru/C and cyclohexane in the case of NiCu/Al$_2$O$_3$.

D-glucose was a more complex case of study, since it decomposes at higher temperature. As a platform molecule in water over Ru/C and NiCu/Al$_2$O$_3$, it was converted at low temperature to sorbitol and at 340 °C mainly to methane. In pyrolysis oil, it decomposed before being hydrogenated and as a result of dehydration and hydrogenation, a complex mixture of compounds were produced and recovered in the upgraded oil.

The significant changes detected in the catalyst after reaction (showed in Chapter 6) can explain the different behavior of platform molecules in the two different media. However, other factors should also be taken into consideration, like the polarity of the medium and the competitive adsorption of different species on the catalyst surface. Leaching of the biomass before pyrolysis to remove inorganics could help to solve the contamination of the catalyst, despite this process being more difficult to scale up for industrial applications. Another more practical solution to reduce the content of inorganics in the pyrolysis oil could be hot vapour filtration during the fast pyrolysis process, as further mentioned in Chapter 7.

Chapter 6

Selectivity, stability and deactivation of NiCu/Al$_2$O$_3$ and other nickel-based catalysts during hydrotreatment of pyrolysis oils

This chapter aims to identify which factors play a role in the activity, selectivity and deactivation of Ni-catalysts during hydrotreatment. Previous HDO studies of phenol demonstrated that different products were formed when using water or pyrolysis oil as a reaction medium (Sections 5.7). Characterisation of the spent catalysts after reaction with pyrolysis oil showed deposition of alkali metals and sulphur on the surface. Coke was also monitored, but it could be easily removed during the regeneration. HDO experiments with the regenerated NiCu/Al$_2$O$_3$ and different pyrolysis oils (with and without alkali metals) indicated that the main influence on activity and selectivity was associated to the adsorption of sulphur and formation of Ni$_3$S$_2$ on nickel nanoparticles. For this reason phenols and other aromatic compounds were not converted significantly in pyrolysis oil over nickel-based catalysts and the HDO reactions of many other compounds ended at the stage of ketones. Despite the sulphur deposition, the upgraded oil produced over Ni-catalysts had higher quality compared to the original feed, containing a lower oxygen percentage and having low tendency to coking with temperature. Catalyst sintering were only observed if the sulphur concentration in the pyrolysis oil was too high (0.3%).

6.1   Introduction

The development of novel catalysts for hydrodeoxygenation (HDO) of pyrolysis oils
is a critical point for using this process for fuels and chemicals production from
renewable resources such as biomass. Stability, selectivity and preferably economic
viability are prerequisites for an appropriate HDO catalyst [38, 39, 153, 165]. The
activity of nickel-based catalysts has been investigated in the literature with model
compounds [97, 98, 155–157, 224, 225] and pyrolysis oil [113, 114, 117, 140] in order to
evaluate their feasibility for HDO and interesting prospects were found. However,
only few studies have addressed catalyst stability and the influence that some
components of pyrolysis oil could have on their activity [113, 116, 117, 160].

Upgraded oils produced over a nickel catalyst retain a lot of phenolic compounds
and ketones [113, 116, 117, 179], which according to the model compound studies
[97] should be easily converted. This stimulated the interest to understand why
under similar reaction conditions different products were formed in the case of model
compounds and pyrolysis oil.

Some of the components present in pyrolysis oils are potential poisons, which
may cause deactivation of the catalyst [160]. These include sulphur, potassium,
calcium, chlorine and some organic molecules, which could polymerize and block
the catalyst surface by coke deposition. Mortensen et al. [160] investigated the
influence of sulphur, potassium and chlorine on the activity of the catalyst during
HDO of guaiacol. The work reported complete deactivation of Ni/ZrO_2 catalyst by
the formation of bulk NiS. Potassium seemed not to influence the hydrogenation,
but it affected the deoxygenation. Chlorine decreased the activity of the catalyst
by competitive adsorption on the active site, which was reversible when chlorine
was removed from the feed. Analysis of the spent nickel catalysts after HDO of
pyrolysis oil and first catalyst regeneration strategies were reported by Ardiyanti et
al.[113, 114, 117]. Coke deposition, leaching and sintering were identified as main
sources of deactivation.

This work aims to investigate the influence of different components in pyrolysis
oil on the activity, selectivity and deactivation of nickel-based catalysts. For this
purpose, $NiCu/Al_2O_3$ was tested with three different pyrolysis oils: a light phase of
pyrolysis oil from straw (Section 6.2) and two pyrolysis oils filtrated by hot vapour
filtration (one from beech wood and one from wheat straw, Section 6.7). The
light phase contained different minerals, while the only possible inorganic sources
of poisoning for the other two pyrolysis oils was sulphur (see composition of the

pyrolysis oil in Chapter 3). In Section 6.6 the effect of the light phase of pyrolysis oil at 250 and 340 °C was also investigated with other nickel-based catalysts. By comparing experiments under different conditions (mild and deep hydrotreatment), with different bio-oils and with the regenerated catalysts, we could gain insights into the role of the pyrolysis oil components on the activity and selectivity of the catalyst and explain the different behavior with respect to model compounds.

6.2 Reactivity of the regenerated catalyst in comparison to the fresh catalyst

In order to monitor the effect of pyrolysis oil on the catalyst activity and selectivity, HDO experiments at 250 and 340 °C were repeated using a regenerated catalyst employed previously with the bio-oil. In this context, $NiCu/Al_2O_3$ (Ni 17.8%, Cu 2.1%) used in HDO of the light phase (described in Section 3.2) was regenerated according to the procedure in Section 2.2.2 and used again with this pyrolysis oil fraction under same conditions. Additionally, in order to monitor the effect on a single component, the regenerated $NiCu/Al_2O_3$ was tested in the conversion of an aqueous solution of 10% phenol. The HDO reactions over the fresh and the spent catalysts were compared for the light phase and for phenol in water respectively.

In the case of the light phase of pyrolysis oil, the regenerated $NiCu/Al_2O_3$ exhibited activity only slightly inferior to the fresh catalyst. De facto, the hydrogen consumption at 250 °C and 340 °C of the regenerated catalyst was 87% and 84% of the fresh one respectively (Table 6.1). At 250 °C both upgraded oils were denser than the aqueous phase, while at 340 °C they were lighter and less viscous. At the same temperature, the mass balance and elemental analysis of the products were similar. The main difference between the mass balances at 250 °C was justified by a different repartition of the compounds between the upgraded oil and the aqueous phase, with a higher carbon recovery in the aqueous phase for the fresh catalyst. The elemental composition of the products was comparable, with a slightly higher amount of oxygen in the experiments with regenerated catalyst. The level of deoxygenation of the upgraded oil was slightly inferior in the case of the regenerated catalyst, but still comparable. The gas production was superior over the regenerated catalyst, indicating that in this case probably cracking reactions were more favoured (Table 6.1).

The similarity between the products was proven also by ^{1}H-NMR and GC-MS.

Table 6.1: Mass balance and composition of the upgraded products from hydrotreatment of the light phase of pyrolysis oil (Section 3.2) over fresh and regenerated NiCu/Al₂O₃ at 250 and 340 °C (8.0 MPa H₂ at room temperature).

	250 °C fresh	250 °C regenerated	340 °C fresh	340 °C regenerated
Hydrogen consumption (NL/kg)	71	62	87	73
Mass balance				
Upgraded oil (wt.%)	12.7	16.5	17.9	17.9
Aqueous phase (wt.%)	84.2	80.0	78.0	76.8
Gas (wt.%)	1.2	1.7	3.1	3.2
Solids (wt.%)	0.5	0.5	0.1	0.1
Losses (wt.%)	1.4	1.4	1.5	2.0
Upgraded oil (dry basis; wet basis)				
C (wt.%)	71.4 ; 63.0	70.5 ; 61.7	74.9 ; 69.8	73.2 ; 71.5
H (wt.%)	9.3 ; 9.5	9.2 ; 9.4	9.7 ; 9.8	9.5 ; 9.5
O (wt.%)	18.2 ; 26.6	19.3 ; 28.0	14.3 ; 19.4	16.2 ; 17.9
N (wt.%)	1.0 ; 0.9	1.0 ; 0.9	1.1 ; 1.0	1.1 ; 1.1
H₂O (wt.%)	11.8	12.5	6.8	2.3
D.O.D (%)	54	51	64	59
HHV (MJ/kg)	34	33	36	35
Aqueous phase (dry basis; wet basis)				
C (wt.%)	46.2 ; 14.1	44.1 ; 12.0	44.9 ; 9.0	43.1 ; 8.8
H (wt.%)	9.0 ; 10.5	8.9 ; 10.5	6.0 ; 10.1	5.0 ; 9.9
O (wt.%)	44.8 ; 75.4	47.0 ; 77.5	49.1 ; 80.9	51.8 ; 81.3
H₂O (wt.%)	69.5	72.8	80.0	79.7
Gas composition				
CO₂ (mol/kg)	0.262	0.340	0.563	0.649
CO (mol/kg)	0.010	0.018	0.039	0.026
methane (mol/kg)	0.005	0.004	0.048	0.02
ethane (mol/kg)	0.003	0.001	0.062	0.045
propane (mol/kg)	0.003	0.002	0.012	0.020

In general more differences in the upgraded product composition were detected for 250 °C than for 340 °C. The ¹H-NMR spectra integration shows that more alkane groups (0.5-1.5 ppm) were produced by the fresh catalyst (Figure 6.1). The aromatic protons (6.0-8.5 ppm) were similar in both cases, demonstrating that this fraction was not affected by the recycle of the catalyst and suggesting that the deactivation for these compounds could have already happened in the fresh catalyst during operation. The products generated over the regenerated catalyst at 250 °C had
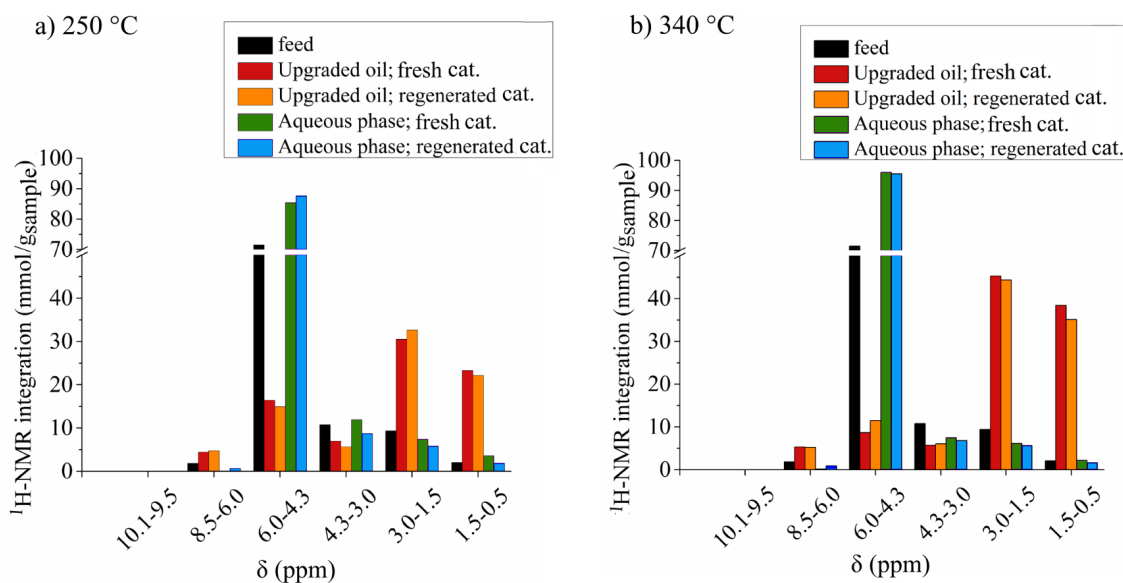
Figure 6.1: Integration of ^{1}H-NMR spectra of upgraded oil and aqueous phase produced from hydrotreatment of the light phase of pyrolysis oil (Section 3.2) over fresh and regenerated NiCu/Al$_2$O$_3$ at 250 and 340 °C (8.0 MPa H$_2$ at room temperature). The assignment of protons to the specific classes of compounds is reported in Table 2.1.

a higher signal of protons alpha to carboxylic/carbonylic groups and unsaturated compounds (1.5-3.0 ppm). This was supported also by GC-MS, which showed higher production of acids, while at 340 °C no significant difference was reported. Protons alpha to alcohol or etheric/esteric groups (3.0-4.3 ppm) had a low signal: at 250 °C the proton concentration was higher for the fresh catalyst, while it was comparable at 340 °C.

The results obtained by ^{1}H-NMR were confirmed also by GC-MS (chromatogram reported in Figure S8 and S9), proving that the composition of the upgraded oils obtained for the fresh and regenerated catalysts was similar (more differences were observed for 250 °C than 340 °C). All aromatic compounds had similar concentrations, except for phenol at 250 °C, where the regenerated catalyst showed less conversion. The phenol concentration in the upgraded oil was 0.7 wt.% for the fresh, 1.2 wt.% for the regenerated, while at 340 °C it was 0.6 wt.% for both oils. Similarities between the upgraded oil components at 250 °C and 340 °C were also found, with cycloketones and phenolic derivatives detected as main products. One of the main differences observed by GC-MS was the conversion of methoxy-phenols (like guaiacol and syringol) and the formation of alkoxy-phenols at higher temperature.

In the case of phenol in aqueous solution (10 wt.%), the fresh NiCu/Al$_2$O$_3$
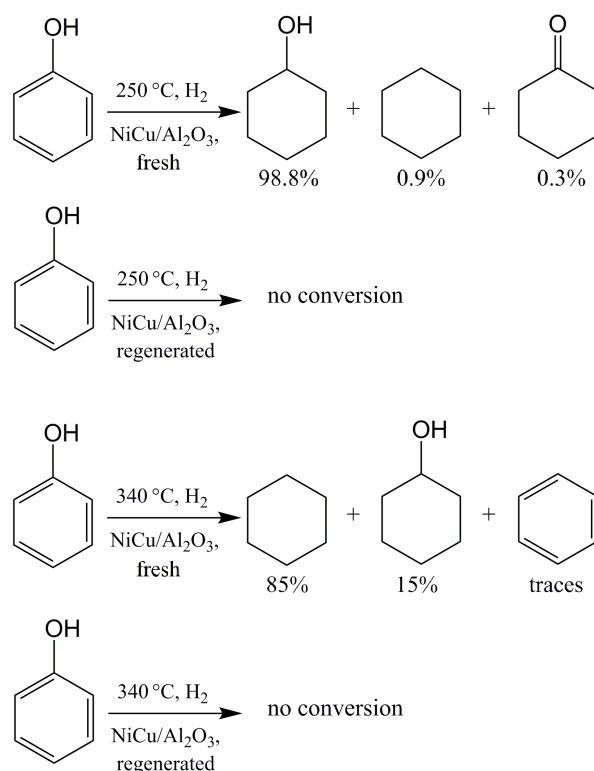
Figure 6.2: Conversion of 10 wt.% phenol in water over the fresh and regenerated NiCu/Al$_2$O$_3$ (250, 340 °C 8.0 MPa H$_2$ at room temperature).

was able to convert it completely, obtaining mainly cyclohexanol at 250 °C and cyclohexane at 340 °C (Figure 6.2). Interestingly, the regenerated catalyst (used previously with pyrolysis oil) could no longer convert phenol in aqueous solution (Figure 6.2), indicating that its preceding use with the pyrolysis fraction caused permanent deactivation, inhibiting the phenol conversion.

Actually, also during the use of the fresh and regenerated NiCu/Al$_2$O$_3$ with the light phase of pyrolysis oil, phenol was not significantly converted, showing analogies to the studies with model compounds. This behaviour suggested that pyrolysis oil affected immediately the activity and the selectivity of the fresh and regenerated catalyst, driving to the production of cycloketones and preserving phenol derivatives from hydrogenation and HDO. However, despite the deactivation, the upgraded oils obtained from the light phase had a higher quality in comparison to the feed, and a lower level of oxygen: 18.2 and 19.3 % at 250 °C and 14.3 and 16.2 % at 340 °C (dry basis, Table 6.1) respectively for fresh and regenerated catalysts (the feed had 40.0 wt% oxygen content). Ardiyanti et al. [113, 114, 117] worked also with nickel-based catalysts applied to pyrolysis oils and the upgraded oils contained also a significant

percentage of ketones and phenolic compounds, but no explanation to this behaviour was reported.

An advantage that can derive from having a catalyst selective for the production of phenols and ketones would be the possibility to produce fine chemicals (instead of fuels) and employ less hydrogen. This would result in products with higher economic value by investing less energy during their production. Considering the TGA analysis of the upgraded oils for determining their tendency to coking (residue at 900 °C, Section 2.4.6), the oil produced at 250 °C had a residue of 11.9% and the one produced at 340 °C of 3.0%. For this last temperature, probably fractionated distillation could be considered for separating the component classes. Therefore a catalyst that could stabilize pyrolysis oil and be selective for production of phenol derivatives and ketones could be the starting point for developing a process for chemicals production instead of fuels.

6.3   Cause of deactivation related to the light phase of the pyrolysis oil

The experiments illustrated in Section 6.2 were carried out using the light phase of the pyrolysis oil described in Section 3.2.

Table 6.2: Concentration of elements and water contained in the light phase of a pyrolysis oil produced from wheat straw.

Element or compounds	Concentration (wt.%)
C	20.7
H	9.5
O	67.8
H_2O	56.7
S	0.05
Cl	0.27
N	0.3
Ca	0.22
Fe	0.13
K	1.17
Mg	0.08
Na	0.002
P	0.06
Si	0.005

This contained mainly water and organic compounds derived principally from the cellulose and hemicellulose fraction of wheat straw. Beside these, minerals and other inorganic elements were also present in small amounts (Table 6.2).

Different processes of deactivation can occur during the hydrotreatment of the light phase. The low pH (pH=4) and the complex mixture of molecules with different oxygen-containing functional groups (especially alcohols, acids, phenols, aldehyde) can favour polymerization and produce undesired coke deposits on the surface of the catalyst, blocking the active sites [153]. Water (56.7 wt%) can also cause sintering or oxidation of the active metals and phase change of the support (e.g. for alumina).

Minerals and other inorganic elements can negatively influence the activity of the catalyst. Potassium and calcium have higher concentration in comparison to the other inorganics (Table 6.2) and their role in catalyst deactivation is usually associated to unselective covering and blockage of the active sites [153]. Chlorine can promote sintering of the active metal and competitive adsorption on the active site [160].

The concentration of sulphur is relatively low, but still enough to completely deactivate the catalyst since sulphur can bind nickel in an irreversible way [153]. Circa half of the concentration of sulphur is connected to the presence of sulphate (0.087% sulphates, 0.029% sulphur). Phosphorus is present mainly as phosphate in a concentration of 0.066 wt%.

6.4 Characterisation of the active metals in the fresh, spent and regenerated catalysts

The combination of multiple techniques, like XRD, XAS, XPS and STEM-EDX, permitted definition of the catalyst structure before, after the HDO of the light phase of the bio-oil at 250 and 340 °C, and after regeneration. Analysing the differences among NiCu/Al$_2$O$_3$ in these stages can give insights on the deactivation source, which blocks the conversion of aromatics (e.g. phenol) and induces ketone production.

XRD gave information about the crystal structure of the catalyst. As shown in Figure 6.3, the catalyst before the reaction (NiCu/Al$_2$O$_3$ red.) had reflections only corresponding to metallic Ni. These were slightly shifted (44.25° versus 44.51° for the reflection (111)) to lower angles in comparison to pure metallic nickel (Vergard's law), indicating that copper was integrated in the lattice of nickel forming an alloy.
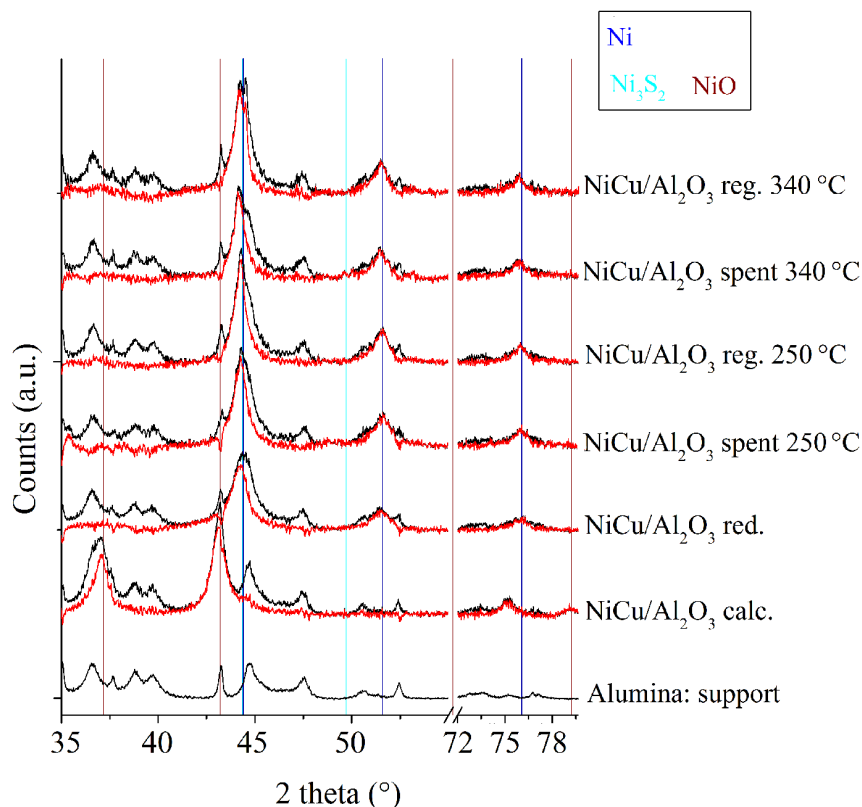
Figure 6.3: XRD pattern of NiCu/Al$_2$O$_3$ (Ni 17.8%, Cu 2.1%) during the preparation and after the reaction and regeneration. In black, the XRD pattern as recorded, in red after subtraction of the alumina support signal. Abbreviations: calc.= calcined, red.= reduced (fresh), reg.=regenerated.

Nickel oxide reflections were not observed in the reduced catalyst, but only in the calcined one.

Also in the spent and the regenerated catalyst, only metallic Ni reflections were detected. Applying the Scherrer equation for the reflection Ni (111), the average crystallite size of the nickel particles in the fresh catalyst was estimated as 8 nm. This value slightly increased to 10 nm after the reaction at 250 °C and to 12 nm at 340 °C. The regeneration influenced also the average crystallite size, obtaining the value of 14 nm for the regenerated catalyst used at 250 °C and the separation in two reflections for the one at 340 °C. In this last case, the reflection at 44.21° was still attributed to nickel-copper alloy and the new smaller one formed at 44.52° to pure metallic nickel. Therefore a tendency for the two metals to separate seemed to take place at higher temperatures, supported also by STEM-EDX (shown later in

this Section). Only in the spent catalyst at 340 °C small typical reflections of Ni$_3$S$_2$ at 49.86° and 50.26° were observed, but they disappeared once the catalyst was regenerated. A hypothesis that could explain the nickel-copper separation is that once Ni$_3$S$_2$ is formed, nickel does not recombine with copper after the regeneration, but remains segregated.
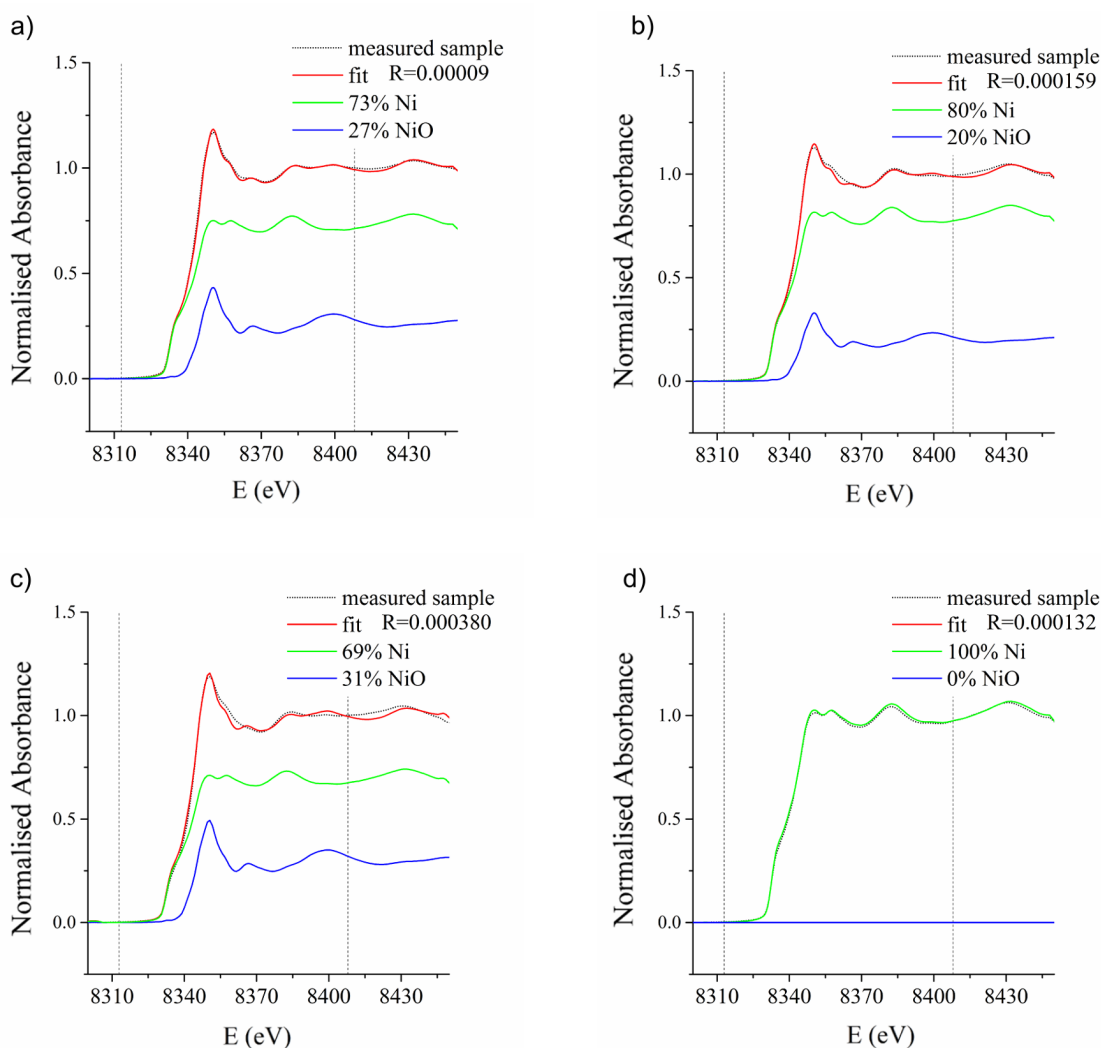
Figure 6.4: Ni-K edge X-ray absorption spectra of the fresh (a), 250 °C-spent (b), 340 °C-spent(c) and 250 °C-regenerated (d) NiCu/Al$_2$O$_3$ catalyst. The catalyst in (a), (b) and (c) was measured *ex-situ* as pellet; in (d) it was measured *in situ* in a capillary after reduction at 500 °C.

Since XRD only gives information about the crystalline component, XAS was employed in order to gain further insight on the structure and oxidation state of the catalyst, including also the amorphous part. The fit of the XANES spectra of the

Table 6.3: Local structural parameters refined from EXAFS spectra for nickel and copper atoms in the fresh $NiCu/Al_2O_3$ catalyst.

Sample	Edge	Atom	N	r(Å)	$\sigma^2 \cdot 10^{-3}(\text{Å}^2)$	$\rho(\%)$
Fresh	Ni K	O	2.0 ± 0.5^f	2.04 ± 0.02^f	4.5 ± 2.2^c	1.5
		Ni	8.2 ± 1.5^f	2.50 ± 0.01^f	7.1 ± 1.5^f	
Ni foil	Ni K	Ni	12^c	2.48^{*f}	5.9 ± 0.1^f	1.5
NiO	Ni K	O	6^c	2.08 ± 0.01^f	3.8 ± 1.5^f	1.2
Fresh	Cu K	O	1.4 ± 0.3^f	1.90 ± 0.03^f	7.1 ± 3.9^f	1.9
		Cu	5.9 ± 1.2^f	2.49 ± 0.01^f	9.3 ± 1.9^f	
Cu foil	Cu K	Cu	12c	2.54 ± 0.01^f	8.7 ± 0.5^f	0.3
CuO	Cu K	O	4^c	1.96 ± 0.01^f	2.8 ± 1.1^f	2.8

*= fitted uncertainty lower than 1%, f= fitted, c=fixed. Structural parameters: N=number of neighboring atoms, r= distance, σ^2= mean square deviation of interatomic distances, ρ= misfitting between the experimental data and the theory.

Ni K : S_0^2=0.78, Fresh ΔE_0= 9.5 $\pm$ 1.6 eV,used ΔE_0= 8.6 $\pm$ 1.1 eV, Ni ΔE_0= 6.9 $\pm$ 0.3 eV, NiO ΔE_0= -4.3 $\pm$ 4.1 eV

Cu K: S_0^2=0.91, Fresh ΔE_0= 3.2 $\pm$ 2.3 eV,used ΔE_0= 2.2 $\pm$ 1.0 eV, CuO ΔE_0=1.1 $\pm$ 1.3 eV, Cu ΔE_0=4.6 $\pm$ 0.6 eV

fresh catalyst by linear combination of Ni and NiO nanoparticle standards (Figure 6.4a), indicated that 73% of nickel was metallic and 27% oxidised. Since the catalyst was measured *ex situ* and after contact with air, a layer of oxide was formed on the particle exterior, which was confirmed also by XPS.

Since copper was in lower concentration, it was measured in fluorescence and the spectrum for the fresh catalyst is reported in Figure S10. Copper was found to be more oxidized than nickel and only Cu^0 and Cu^{2+} were identified. The quality of the fit was not improved by introducing Cu^+.

EXAFS spectroscopy gave further structural information on the nickel and copper particles (Table 6.3). The interatomic distance calculated between the nickel atoms was similar to the nickel foil (only slightly higher, 2.50 versus 2.48 Å), indicating that the nickel metallic phase in the fresh catalyst had rather more bulk features than those found for small metallic clusters. On the other hand, the Cu-Cu bond lengths were around 0.04 Å shorter than the one observed for Cu foil. This simultaneous shift of the bond length values for nickel and copper was an indication of alloying between the two metals [200]. Copper was more affected by this shift since its concentration was lower.

Regarding the oxide phase, the Ni-O and Cu-O bond distance was 0.04 Å and 0.06 Å shorter in comparison to NiO and CuO bulk. The shorter bond lengths, combined to the higher σ^2 compared to the bulk oxide and the absence of NiO

reflections in XRD analysis, suggests that a thin disordered oxide layer of nickel and copper was formed on the top of a metallic core.

For the spent catalyst at 250 °C the XANES spectrum was also fitted by a combination of metallic nickel and nickel oxide (Figure 6.4b). The catalyst was slightly more reduced than the original one (80% Ni, 20% NiO). This probably can be due to larger particles or formation of coke and other mineral deposits on the surface that prevented reoxidation in air. The XANES spectra of copper were more noisy, but qualitatively indicated that copper was more reduced than nickel, with composition around 84 % Cu and 16% CuO.

The spent catalyst at 340 °C (Figure 6.4c) indicated a similar ratio between metallic nickel and oxide (69% Ni, 31% NiO) compared to the fresh one. Copper was indicatively 77% Cu and 23% CuO. However, comparing Figure 6.4 a, b and c, the fit quality was gradually worse for the spent catalysts obtained at higher reaction temperature. Probably this indicates that another species could be present in low concentration, e.g. adsorbed sulphur on nickel or Ni_3S_2 (reference spectra [226]). In order to facilitate the indentification of this species, the spent catalyst at 250 °C was reduced at 500 °C *in situ* under hydrogen in order to eliminate nickel oxide and obtain a spectrum that should be fitted only by metallic nickel and the other compound. After the *in situ* reduction, the spent catalyst was completely reduced (Figure 6.4 d). Hence, possible other species or poisoning of the catalyst were mainly removed during regeneration under hydrogen atmosphere or their concentration was relatively low to be detected.

From XPS analysis of the region Ni 2p (Figure 6.5), nickel was mainly present in the external layer as oxide (Ni 2p3/2 855.9 eV) and only a small contribution came from metallic nickel (Ni $2p_{3/2}$ 852.3 eV). Only for the spent catalyst at 250 °C, metallic nickel had a higher contribution (confirming the results found by XAS), otherwise the signals were comparable. Considering that the attenuation length (λ) of the Ni2p electrons is circa 1 nm [227], the main information from the XPS spectra came from the top surface layers. This supported that Ni-particles are covered by a thin oxidized layer, in agreement with literature, which reported that the passivation layer of nickel is not limited to a single monolayer, but the oxidation proceeds deeper to 4-7 layers [228].

In general, XPS spectra of nickel species are difficult to be analysed, because of a complex peak structure due to satellite peaks assigned to shake-up processes [156, 229]. The peak of Ni^0 was detected at a binding energy of 852.3 eV (Ni $2p_{3/2}$) and 869.7 eV (Ni $2p_{1/2}$, spin-orbit splitting of 17.3 eV), shifted to lower energy in
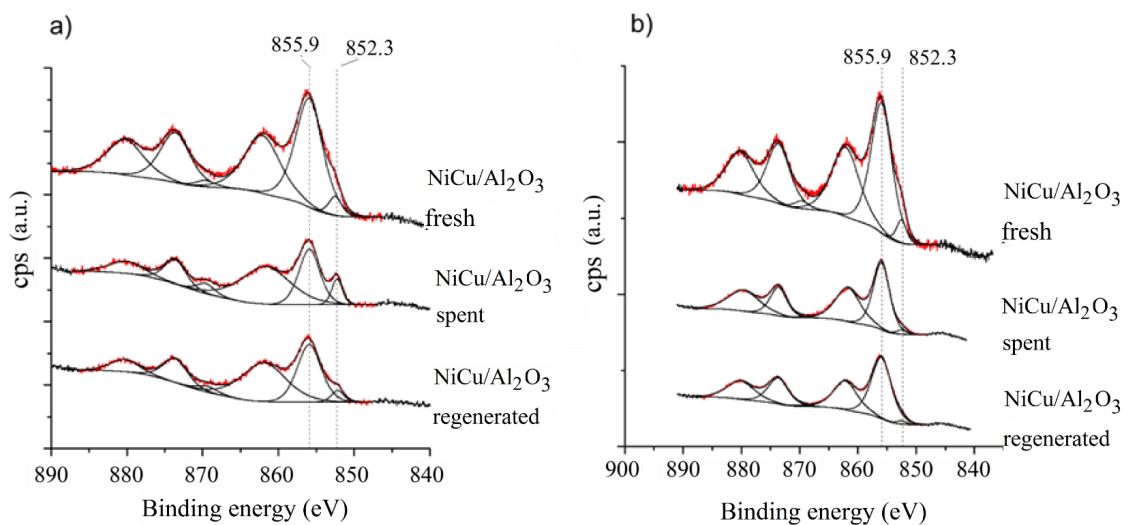
Figure 6.5: XPS regions of Ni2p of NiCu/Al$_2$O$_3$ in the fresh, spent and regenerated form for the experiment at 250 °C(a) and at 340 °C (b) (reduced *ex situ*).

comparison to bulk nickel (Ni 2p$_{3/2}$ 852.6 eV). This is probably due to the formation of an alloy with copper that increments its electron density, as reported previously in the literature [230]. The position of the peak 852.3 eV was also confirmed when the samples were partially reduced *in situ* in XPS (Figure S11). The main peaks of oxidized nickel were at 855.9 eV and at 873.3 eV, in good agreement with other values in the literature [156]. The satellite peaks were observed at 861.4 eV and 879.6 eV.

Theoretically Ni$_3$S$_2$ (Ni 2p$_{3/2}$) should have a peak at 853.0 eV [231], but in the fit it did not match, excluding that this component was present in high quantity or it is overlapped by the Ni^0 contribution. The XPS sensitivity to sulphur was too low to detect any signal in the catalyst used at 250 °C, but for the spent catalyst at 340 °C a peak at 162.1 eV was detected, indicating the presence of sulphide. The detection limit of XPS is at best 0.1 at.% and alternative surface sensitive techniques should be employed for detecting sulphur, like ToF-SIMS, which can detect in the range of ppm [232].

Cu^0 and Cu$^+$ are difficult to discriminate by XPS due to the extremely similar binding energy. Cu^{2+} was undoubtedly present in the catalysts and recognizable from its broad shake-up peak between 938-947 eV [156] (Figure 6.6). In the fresh catalyst the presence of Cu^0 was indicatively lower than in the spent one (932.0 eV Cu2p$_{3/2}$), as also confirmed by XAS. The shift of the copper peaks to lower binding energy in comparison to the bulk material Cu and CuO was also observed in the
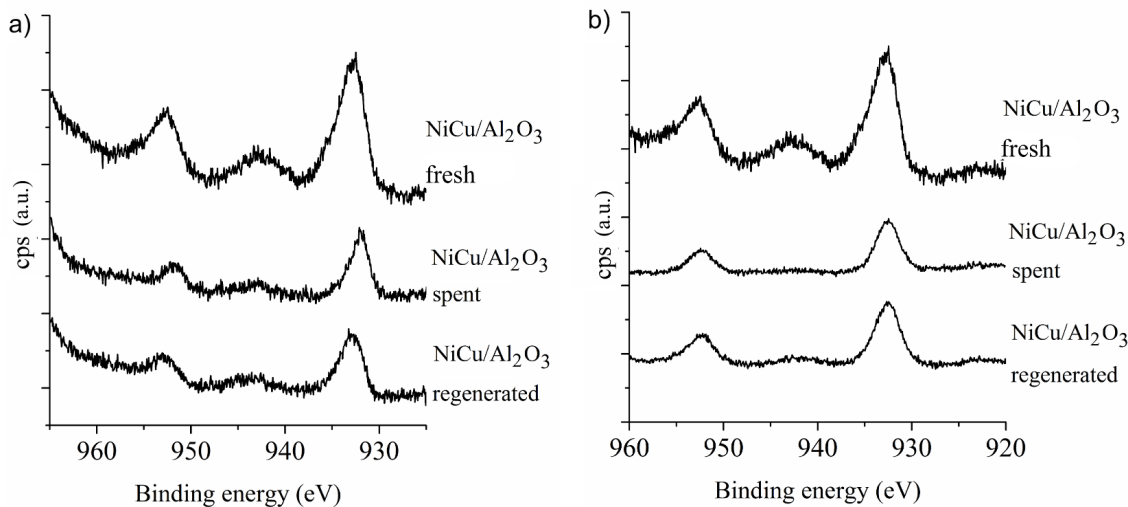
Figure 6.6: XPS regions of Cu2p of NiCu/Al$_2$O$_3$ in the fresh, spent and regenerated form for the experiment at 250 °C (a) and at 340 °C (b) (reduced *ex situ*).

literature [156, 230].

Table 6.4: Ratio between the surface atomic concentration calculated by XPS for Ni, Cu and Al on NiCu/Al$_2$O$_3$.

	Cu/Ni	Ni/Al	Cu/Al
Fresh	0.253	0.085	0.022
Spent 250 °C	0.207	0.044	0.009
Regenerated 250 °C	0.209	0.042	0.009
Spent 340 °C	0.221	0.0405	0.009
Regenerated 340 °C	0.280	0.033	0.009

In Table 6.4 the ratios between the surface atomic concentrations of nickel, copper and aluminium are reported. The ratio Cu/Ni was slightly higher for the fresh catalyst, but in all cases it is higher compared to the bulk composition: from the elemental composition Cu/Ni was circa 0.1, while on the surface was between 0.20-0.28. This affirms that copper and nickel were present as an alloy, but with segregation of copper on the surface, which can reduce the interfacial surface energy [156, 230, 233].

The Ni/Al and Cu/Al ratio (Table 6.4) changed after the reaction and the catalyst surface seemed restructured. The surface area occupied by nickel and copper decreased and this could be justified by sintering, change of the particle shape (for

example different contact angle between the surface of the active metal particle and the support) or by covering with other contaminants.
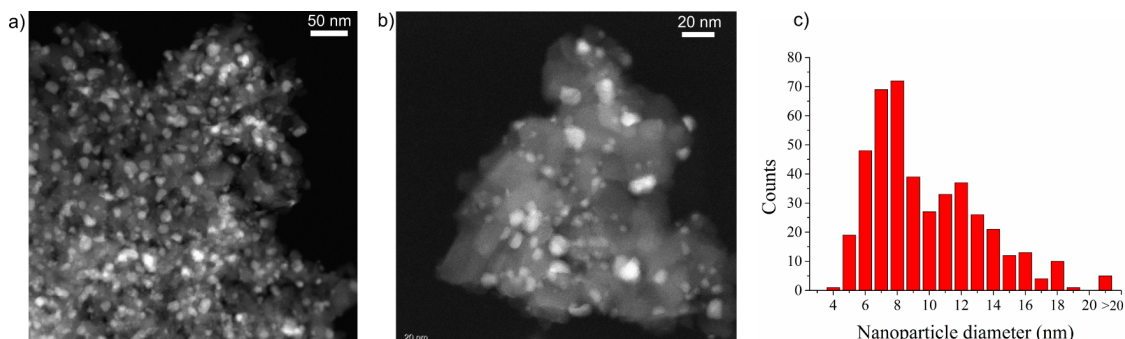
Figure 6.7: STEM pictures of fresh $NiCu/Al_2O_3$ with different magnification (a,b) and particle distribution (c).

STEM images indicated that the active metal nanoparticles had a relatively broad distribution in the fresh catalyst. In Figure 6.7, two different particle size distributions were observed: one with a relative maximum at 12 nm and one at 8 nm. Some particles with a dimension over 20 nm were also detected, but they were only a small percentage. The integration of different regions and particles of the STEM-EDX signal indicated that the composition of $NiCu/Al_2O_3$ was on average constant and circa 1:9 Cu/Ni. In addition, the linear scan by EDX of a single particle (Figure S12) and the integration of external and internal particle regions during STEM-EDX mapping showed that the ratio of the K_α signal Cu/Ni increased in proximity to the nanoparticle exterior, confirming the segregation of copper on the surface.

In the spent catalyst at 250 °C a distribution of smaller and bigger particles was still detected (Figure 6.8a,b), but the dimensions of the particles increased, as confirmed also by XRD. In the spent catalyst at 340 °C (Figure 6.8c,d), only some regions showed aggregation of the particles, indicating sintering. The integration of EDX signals in different regions and particles for the sample at 340 °C (see Section 6.5) demonstrated that the ratio Cu/Ni was not anymore constant at 1:9, but some parts were more rich in nickel and others more rich in copper (similar results were obtained by XRD, where two reflections were detected instead of one). This indicates a tendency towards phase separation at higher temperature.

Analysing the minerals contained in the aqueous phase by ICP-OES, no significant leaching was detected under the reducing reaction conditions. In the case of the catalyst used at 250 °C, 0.8% of the nickel contained in the catalyst
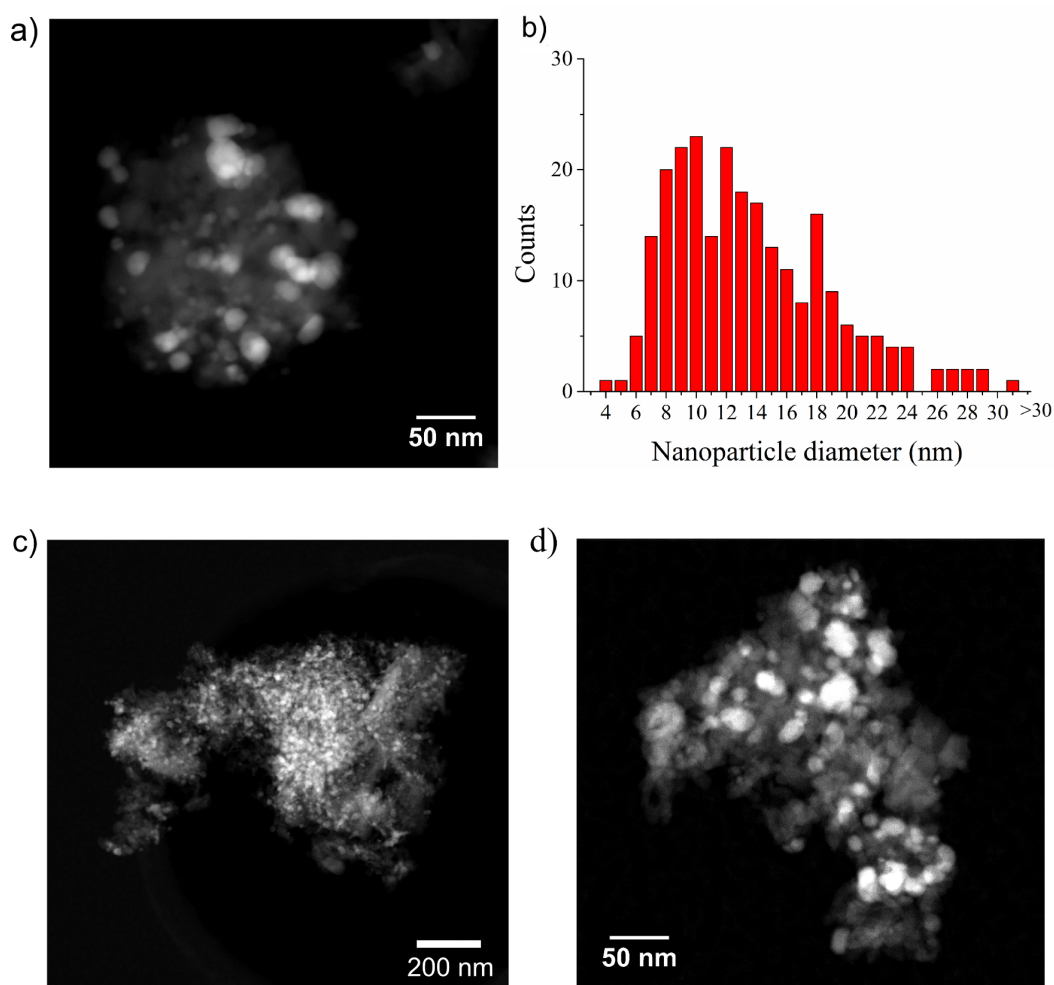
Figure 6.8: STEM imagines of NiCu/Al$_2$O$_3$ spent at 250 °C (a) and its particle distribution (b). In (c) and (d) STEM imagines of NiCu/Al$_2$O$_3$ spent at 340 °C.

was found in solution, while at 340 °C 0.24%. The lower amount detected at higher temperature may be due to a longer reaction time at 250 °C. Hence, the leaching was probably proportional to the time of the reaction or it could be also that at higher temperature and under high pressure of hydrogen the catalyst was more stable in the reduced state, and it tends less to be oxidized and therefore dissolved.

In summary, NiCu/Al$_2$O$_3$ (Ni 17.8%, Cu 2.1%) was constituted of nickel-copper nanoparticles alloyed in an average ratio of 9:1. However, the surface layer of the active nanoparticles (approx. 1-2 nm thick) was enriched in copper, increasing slightly the ratio according to XPS measurement. The active metals were affected by surface passivation when exposed to air, with a layer of oxide estimated at around 1 nm thick. This layer was supposed to be completely reduced in the highly reductive

gas atmosphere of the hydrotreatment reaction. The active particles of the spent catalysts at 250 °C and 340 °C were affected slightly by sintering, rearrangement of the metal ratio of the alloy, and sulphur adsorption, forming the structure Ni_3S_2 on the outer layer.

6.5 Deposition and adsorption of chemical species on the catalyst surface

6.5.1 Coke deposition

During the HDO reaction, polymerization can occur, favoured by the acid environment and by the temperature. Table 6.5 shows C, H, N, S elemental analysis and SEM-EDX of the spent catalyst. The value of carbon recorded by SEM-EDX was higher in comparison to elemental analysis, indicating that the coke deposition was mainly on the surface. The carbon distribution on the surface varied depending on the region analysed. The approximate surface concentration of nickel (calculated

Table 6.5: Elemental analysis and TGA of the $NiCu/Al_2O_3$ catalysts. The spent catalyst was used with the light phase of the bio-oil at 250 and 340 °C (8.0 MPa H_2 at room temperature.

Catalyst	250 °C spent	250 °C regenerated	340 °C spent	340 °C regenerated
Spent catalyst: elemental analysis (wt.%)				
C	7.7	0.1	2.7	0.1
N	0.2	0.1	0.1	0.1
S	0.8	0.9	0.7	0.7
SEM-EDX approximate surface composition (wt.%)				
C	11.9	n.d.	5.7	n.d.
Mg	0.1	0.2	0.2	0.3
P	1.0	1.5	1.2	1.2
S	0.6	0.7	0.9	0.6
Cl	n.d.	n.d	n.d.	n.d.
K	0.9	1.3	0.9	0.7
Ca	1.6	2.7	2.0	2.1
Ni	13.1	18.7	13.4	14.8
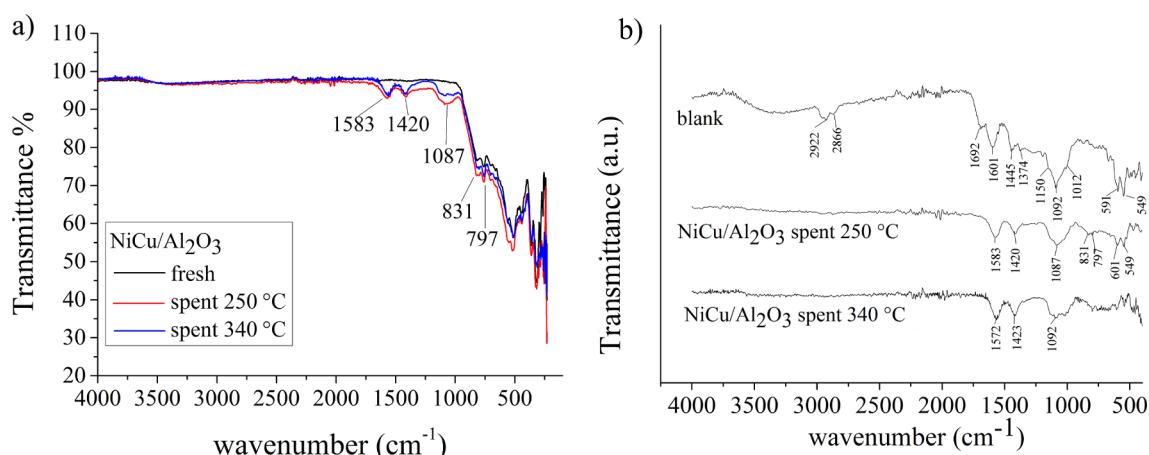
Figure 6.9: ATR-IR spectra of the catalyst fresh, spent at 250 °C and spent at 340 °C (a); ATR-IR spectrum of the coke generated in a blank experiment (without catalyst) and difference between the signal recorded for the spent catalysts (at 250 °C and at 340 °C) and the fresh catalyst (b).

by SEM-EDX and reported in Table 6.5 as a reference) was lower when carbon was on the surface, indicating that Ni was also less accessible during the reaction. When the catalyst was regenerated, the original value was restored. In general, more carbon was deposited in the experiment at 250 °C, probably due to a lower hydrogenation activity and the prevailing of polymerization reactions [100], associated to a worse stirring setup compared to the autoclave used at 340 °C. TGA analysis (Figure S13) showed that coke could be completely removed by oxidation below 500 °C, therefore this temperature was employed in the calcination step during the catalyst regeneration. After the regeneration, organic species were completely removed from the surface, but other inorganic materials (like S, Mg, P, Cl, K, Ca) remained on the surface in a similar concentration.

In order to understand better the nature of the deposited carbon, the spent catalyst was analysed by ATR-IR spectroscopy. The carbonaceous species formed at 250 and 340 °C displayed similar groups. The bands detected by ATR-IR spectroscopy (Figure 6.9) were weak, due to the relatively low amount of coke in comparison to the catalyst, but similarities with the coke produced by the blank experiment (without catalyst) were detected. The stretching bands between 1720-1650 cm^{-1} were attributed to C=O of ketones, esters and carboxylic acids, while in the range 1600-1500 cm^{-1} to symmetric stretching frequencies of COO- and C=C of aromatic groups and alkenes. Broad bands in the range 1290-1000 cm^{-1} were associated to stretching vibration of alcohols, phenols and ethers [234, 235], in

the range 900-700 cm^{-1} to bending in the aromatic ring. The structure of the coke deposited showed analogies with humic matter.

In conclusion, coke could be easily removed by oxidation, but it represents a problem during the reaction, by blocking access to the pores and the active sites. On the other hand, as already observed in industrial hydrotreatment processes [165], coke deposition reached a plateau after a period of operation and after that the catalyst activity remained constant.

6.5.2   Deactivation due to inorganic species

As reported in Table 6.5, other inorganic species contained in the pyrolysis oil tended to accumulate on the surface of the catalyst, such as S, Mg, K, Ca and P. Among these species, calcium had the highest concentration on the surface. In the presence of other anions, Ca can precipitate as a salt and deposit unselectively on the surface, thereby blocking the active sites, as verified in the case of the spent catalyst at 250 and 340 °C by the XRD reflections of $Ca_3(PO_4)_2$, $CaSO_4$ and CaO (Figure S14). The surface atomic concentration calculated by XPS (Table 6.6) showed high concentrations of calcium and potassium, comparable or superior to that of nickel. According to the integration of different regions by SEM-EDX and STEM-EDX (Table S1, S2) and mapping by ToF-SIMS (Figure S15), potassium and calcium were not homogenously distributed on the surface. They had a higher tendency to deposit on the alumina instead of covering nickel, as proven by STEM-EDX (see later). From the ToF-SIMS depth profile (Figure S16), the concentration of K and Ca was higher on the surface, but they seemed also to penetrate more deeply in the spent and regenerated catalyst.

The role of calcium is ambiguous in the catalyst activity because it can act as a poison, but it can also enhance the resistance of nickel against sulphur [42], e.g. weakening the formation of nickel sulphide for electronic reasons [236]. In addition, if nickel sulphide is formed, Ca helps the reduction to metallic nickel [237]. The formation of $CaSO_4$ or CaS is thermodynamically more favoured than NiS or $NiSO_4$, preserving the catalyst from deactivation.

Potassium was demonstrated to cause reversible poisoning in hydrodeoxygenation by influencing temporarily the deoxygenation activity but not the hydrogenation [160]. In general, potassium and calcium decrease the catalyst activity due to fouling on the surface. This could present problems for continuous operation, as observed in HDS processes [165]. However, this kind of

Table 6.6: Surface atomic concentration (in percentage with respect to the species detected) determined by XPS, considering carbon in the integration.

	Ni 2p$_{3/2}$ (at.%)	Cu 2p$_{3/2}$ (at.%)	Al 2p (at.%)	O 1s (at.%)	K 2p$_{3/2}$ (at.%)	Ca 2p$_{3/2}$ (at.%)	C 1s (at.%)	S 2p (at.%)
fresh	2.85	0.72	33.34	59.54	-	-	3.54	-
spent 250 °C	1.21	0.25	27.2	49.84	0.65	0.97	19.87	-
regenerated 250 °C	1.15	0.24	27.61	60.17	1.56	3.25	6.03	-
spent 340 °C	1.05	0.23	25.87	53.41	1.15	1.26	16.89	0.14
regenerated 340 °C	1.02	0.29	30.98	55.56	1.07	1.4	9.52	0.18

deactivation could be minimised using hot vapour filtrated pyrolysis oil that has only a low content of minerals.

ToF-SIMS analysis in Figure 6.10 gives further information on the main species adsorbed on the surface of the fresh, spent (250 °C) and regenerated (250 °C) catalysts. The concentration of the main constituents of the catalyst (Ni, Cu, Al) was lower on the surface of the spent and regenerated catalyst, due to presence of coke and other minerals that cover the surface.

The ion tropilium (C$_7$H$_7$$^+$) was identified in the spent catalyst and it was an indication of the partial aromatic character of the carbon deposits. Tropilium was not detected in the regenerated catalyst, confirming that the regeneration process was able to remove coke. According to the depth profile done by ToF-SIMS, the carbon deposits on the catalyst surface consisted of a thin layer that was eliminated after the first sputter.

Different sulphur ions were detected (Figure 6.10), confirming the presence of sulphur species on the surface, such as sulphate and sulphide detected by XRD. As demonstrated also by elemental analysis and SEM-EDX, sulphur was not completely removed after the regeneration. Na, Mg, Cl were also present on the surface, but not in such high concentrations as K and Ca.

STEM-EDX (Table 6.7) gave further important information about the distribution of elements on the surface. Quantified results of STEM-EDX spectra acquired in different regions showed a phase separation of nickel and copper, detecting regions richer in nickel and others with a higher ratio of Cu/Ni. The other elements were not homogeneously distributed on the surface and their concentration was relatively high in comparison to nickel. Quantified results of STEM-EDX spectra of a single particle (Figure 6.11, Table 6.7) showed nanoparticles with different copper contents. The alkali metals and phosphorus were in lower concentration

in comparison to the signal recorded for a region, indicating that they tended to
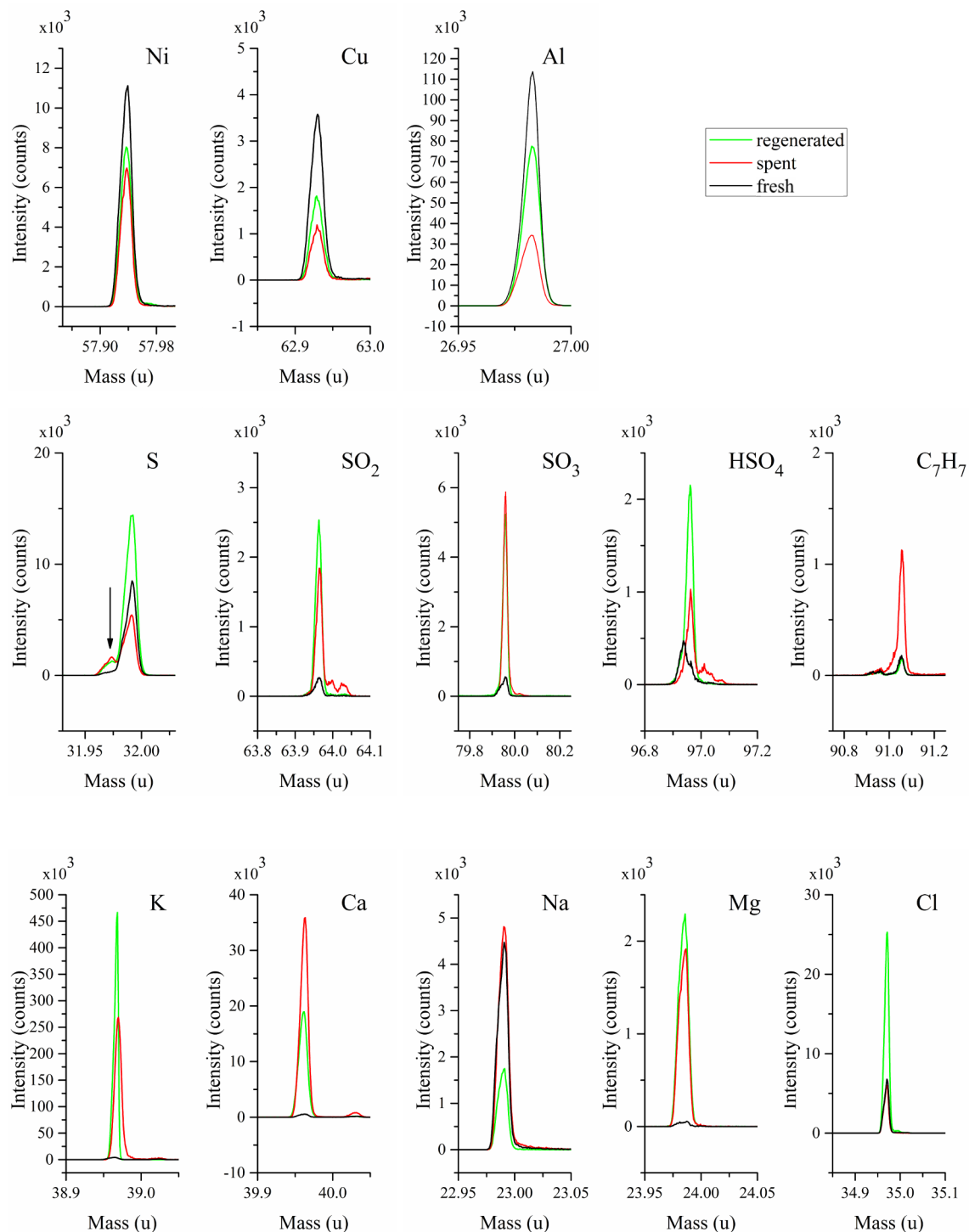
Figure 6.10: Monitoring of surface species by ToF-SIMS on the surface of the fresh catalyst, spent catalyst at 250 °C and regenerated catalyst at 250 °C.

Table 6.7: Quantified composition results (at.%) from integrated spectrums in large regions and of single particle STEM-EDX spectrum imaging for the spent catalyst at 340 °C.

	Ni	Cu	S	Mg	Fe	P	K
Region n.1	59.6	15.4	6.9	6.6	4.9	0.7	6.0
Region n.2	54.9	7.9	17.2	4.0	5.1	5.9	5.0
Region n.3	48.7	4.8	14.3	10.8	6.7	6.2	8.5
Region n.4	65.9	9.9	9.9	4.5	3.7	0.6	5.5
Particle n.1	72.4	5.5	13.5	3.1	2.5	1.7	1.4
Particle n.2	73.6	8.9	10.8	0	2.8	2.8	1.2
Particle n.3	83.5	5.7	7.3	0.6	1.9	1.0	0.1

deposit more on the alumina support, than on the nanoparticles. Sulphur was the only element detected still in high concentration on the nanoparticle surface (Table 6.7), indicating probably the formation of Ni_3S_2, also detected in some samples by XRD. Considering that the sulphur atoms on the nanoparticle were 9-19% of the nickel ones, Ni_3S_2 should have been formed in a thin outer layer, as often reported
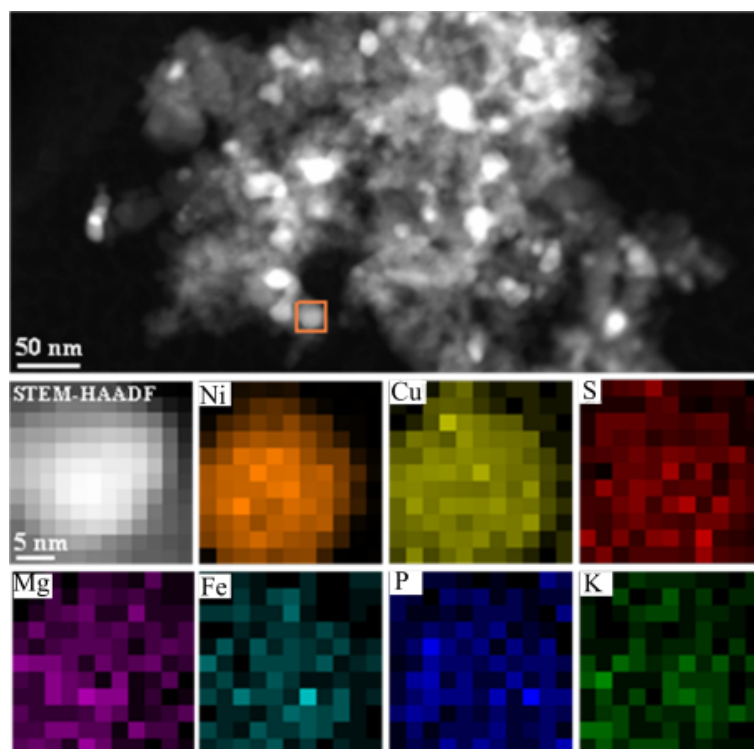
Figure 6.11: Overview STEM image of NiCu/Al₂O₃ used at 340 °C and the corresponding elemental maps obtained from STEM-EDX spectrum imaging in the area marked with box.

in literature [153, 165, 238–240]. The formation of sulphide as a surface layer or bulk seems to be dependent on the sulphur content in the feed, the hydrogen pressure and the operating temperature [238].

6.6 Comparison with other nickel-based catalysts

Different nickel-based catalysts were tested in the same conditions as $NiCu/Al_2O_3$ (Chapter 4 and 5): Ni/Al_2O_3, Ni/SiO_2, Ni/ZrO_2, NiW/AC, Ni/TiO_2 (previously characterised in Section 4.2) and Ru/C, which was used as a benchmark. Despite the other nickel-based catalysts having a slightly lower hydrogen consumption than $NiCu/Al_2O_3$, they exhibited the same selectivity towards ketones and phenolic components at 250 °C (Chapter 4) and 340 °C (Chapter 5). Ru/C was more selective towards alcohols, but also phenolic compounds were not converted with these catalysts.

In general, the poisoning affecting these catalysts was similar to $NiCu/Al_2O_3$. In the XRD patterns (Figure S17-S22), a slight sintering was observed and it was more accentuated for 340 °C than 250 °C. It was possible to calculate the average crystal size with the Scherrer equation only for catalysts with higher content of nickel. For example fresh Ni/Al_2O_3 (Figure S18) had an average crystal size of 15 nm, that increased to 17 nm after the reaction at 250 and 340 °C. For Ni/SiO_2 (Figure S19) the average dimension remained 20 nm (as originally) after the reaction at 250 °C and it changed to 22 nm at 340 °C. In case of Ni/ZrO_2 (Figure S20) and Ni/TiO_2 (Figure S22), the original catalyst did not show any reflections for nickel indicating that the particles were smaller or amorphous. After the experiments small Ni reflections were observed, which indicates some sintering (signal was too low for estimation of crystallite size). Small ruthenium reflections were detected also for Ru/C (Figure S17) after the reaction.

A peculiar case was NiW/AC (Figure S21). A real phase change happened: the fresh catalyst was characterised by reflections of a mixture of tungsten oxide, which was converted completely at 340 °C to $CaWO_4$, indicating that it could be problematic to use tungsten oxide as a catalyst if calcium is present in the feed.

In the XRD patterns of some catalysts it was possible to distinguish small reflections of Ni_3S_2, easily identifiable from the reflections at 2θ 21.81°, 49.86°and 50.26°. Note that Ni_3S_2 may be present also if no XRD reflections are detected, in case only a thin layer of sulphur not detectable by this technique was formed.

In all the catalysts and also in the solid of the blank experiment (obtained

Table 6.8: Elemental analysis (C, N, S) of the spent (250 °C and 340 °C) and regenerated catalysts.

Catalyst	Temperature of reaction (°C)	spent			regenerated		
		C (wt.%)	N (wt.%)	S (wt.%)	C (wt.%)	N (wt.%)	S (wt.%)
Ru/C	250	75.3*	1.0	1.0	-	-	-
Ni/Al₂O₃	250	7.4	0.2	0.7	0.2	<0.1	0.7
NiCu/Al₂O₃	250	7.7	0.2	0.8	0.1	0.1	0.9
Ni/SiO₂	250	5.0	0.2	0.5	0.2	<0.1	0.5
Ni/ZrO₂	250	8.4	0.3	0.7	0.2	<0.1	1.0
NiW/AC	250	74.1*	1.1	0.5	-	-	-
Ni/TiO₂	250	11.7	0.4	0.8	0.2	<0.1	0.7
Ru/C	340	77.7*	0.9	0.9	-	-	-
Ni/Al₂O₃	340	3.5	0.1	0.9	0.4	<0.1	1.1
NiCu/Al₂O₃	340	2.7	0.1	0.7	0.1	0.1	0.7
Ni/SiO₂	340	5.4	0.2	0.5	0.3	<0.1	0.8
Ni/ZrO₂	340	5.4	0.1	0.9	0.2	<0.1	1.1
NiW/AC	340	75.5*	0.9	0.8	-	-	-
Ni/TiO₂	340	4.9	0.1	0.8	0.3	<0.1	0.7

*catalyst supported on active carbon

by washing the oil in acetone), other reflections were detected and attributed to $CaSO_4$, $Ca_3(PO_4)_2$ and CaO. Also in SEM-EDX, areas with higher concentration of calcium and sulphur were detected close together. Generally, the mineral deposition monitored by SEM-EDX was similar to those of NiCu/Al₂O₃ (Table S1, S2). The concentration of sulphur was in the same range among them, indicating probably that all the catalysts were affected in a similar way by this contaminant. The deposition of minerals, especially K and Ca, was more significant at higher temperature, which could be due to the change in polarity of the pyrolysis oil and the upgraded products as an effect of the hydrodeoxygenation and the temperature (e.g. the permittivity also of the aqueous phase decreases at temperatures near the critical point). Therefore the salts can precipitate and use the catalyst surface as a nucleation center.

Carbon deposition (Table 6.8) was lower at higher temperatures, probably due to the better stirring set-up of the experiment at 340 °C, that favoured hydrogenation/hydrodeoxygenation rather than polymerization. The catalysts with an alumina support show a lower production of coke in comparison to the other catalysts. This could be explained by the use of theta alumina and corundum

instead of gamma alumina, which is more acidic and can result in polymerization reactions. In this reaction environment, the alumina phase was stable also in the presence of the water contained in pyrolysis oil, but it could be that for long term hydrotreatment tests, the conversion to boehmite could occur and therefore it could be better to support nickel on silica or other supports less sensible to water. It could be also that the deposition of the alkali metals on alumina modified its reactivity, offering a kind of protective layer. Elemental analysis (Table 6.8) confirmed also that sulphur was persistent on the surface also after regeneration, while carbon and nitrogen were mainly removed.

Table 6.9: BET surface area of the fresh, spent (after the use in the HDO of the light phase at 250 °C and 340 °C, 8.0 MPa H_2 at room temperature) and regenerated catalysts.

Catalyst	Temp. (°C)	Fresh BET surface area (m^2/g)	Spent BET surface area (m^2/g)	Regenerated BET surface area (m^2/g)
Ru/C	250	867	74	-
Ni/Al$_2$O$_3$	250	76	38	66
NiCu/Al$_2$O$_3$	250	66	55	62
Ni/SiO$_2$	250	169	28	33
Ni/ZrO$_2$	250	113	14	92
NiW/AC	250	1115	6	-
Ni/TiO$_2$	250	86	44	57
Ru/C	340	867	61	-
Ni/Al$_2$O$_3$	340	76	50	63
NiCu/Al$_2$O$_3$	340	66	55	61
Ni/SiO$_2$	340	169	28	30
Ni/ZrO$_2$	340	113	69	87
NiW/AC	340	1115	11	-
Ni/TiO$_2$	340	86	45	50

The leaching was limited to a low percentage of the nickel and as monitored for NiCu/Al$_2$O$_3$ it was more accentuated at 250 °C than 340 °C (Table S3).

According to BET model calculation, the catalyst surface area was decreased due to deposition of coke and minerals (Table 6.9). Coke deposition had a strong influence in decreasing the surface area in the spent catalyst, probably blocking some pores. After the regeneration (removal of carbonaceous species from the surface), some catalysts like the alumina and zirconia supported could recover almost completely the original surface area, while the others only partially, indicating that other irreversible structural changes happened. The porosity and surface area of

the spent catalysts supported on carbon were drastically reduced, probably because pyrolysis oil could block the micropores. Therefore a support with macro- and mesopores could be favoured.

6.7 Comparison with other pyrolysis oils from different feedstocks

From the deactivation study of the light phase of the pyrolysis oil, it emerged that sulphur was the main contaminant bound to the nickel nanoparticle surface and that it may have the greatest influence on the reactivity of this kind of catalysts. However, more minerals, especially K and Ca, were present in the light phase of the pyrolysis oil, but they were supposed to play a minor role in the selectivity of the
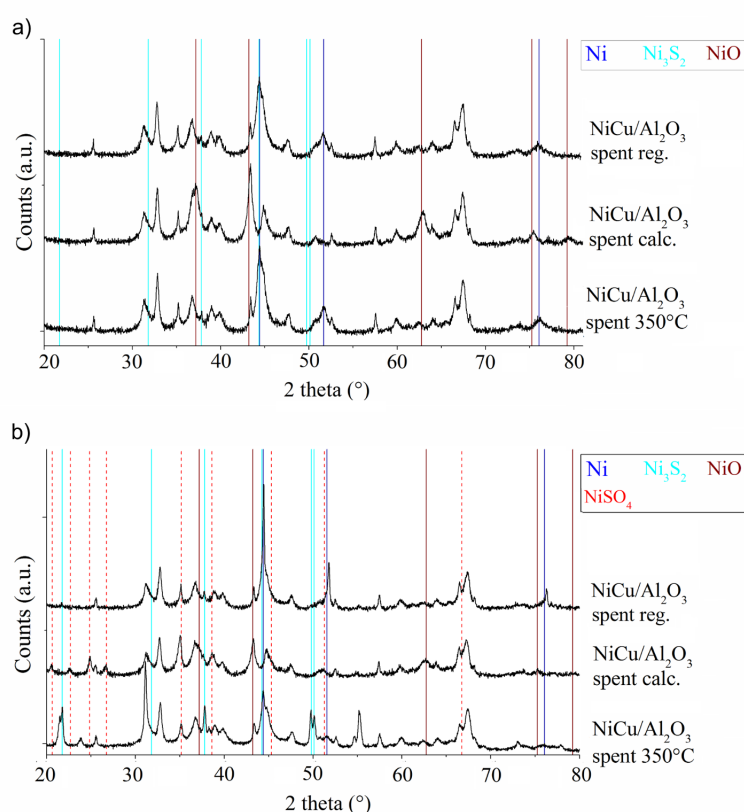
Figure 6.12: XRD patterns of the spent NiCu/Al₂O₃ used with beech 450 °C (a) and straw 450 °C (b) bio-oils (hydrotreatment at 350 °C for 2 hours with stabilisation at 150 °C for 1 hour, 14.0 MPa H₂ at room temperature) and regeneration process through calcination and reduction.

Table 6.10: Characterisation of the spent catalyst used with beech 450 °C and straw 450 °C bio-oils (hydrotreatment at 350 °C for 2 hours with stabilisation at 150°C for 1 hour, 14.0 MPa H_2 at room temperature), and the regenerated catalysts.

	beech 450 °C bio-oil	straw 450 °C bio-oil
Spent Catalyst: elemental analysis		
C (wt.%)	6.0	10.3
N (wt.%)	0.1	0.2
S (wt.%)	0.4	2.6
BET (m^2/g)	54	19
Leaching (Ni, %)	0.55	0.03
Regenerated Catalyst: elemental analysis		
C (wt.%)	0.1	0.1
N (wt.%)	< 0.1	< 0.1
S (wt.%)	0.7	2.0
BET (m^2/g)	66	60

catalyst. In order to confirm this theory, two other bio-oils produced by intermediate pyrolysis of beech wood (beech 450 °C, Section 3.4) and wheat straw (straw 450 °C, Section 3.3) were tested.

Since they were filtrated by online hot vapour filtration, char and minerals were not present. The concentration of sulphur was below the detection limit ($<0.005\%$) for the bio-oil from beech wood and 0.3% for the one from straw (Chapter 3). Testing the fresh catalyst $NiCu/Al_2O_3$ with these two bio-oils (hydrotreatment at 350 °C for 2 hours with previous stabilisation at 150°C for 1 hour, 14.0 MPa H_2 pressurised at room temperature, see Chapter 7 for further details) resulted in producing upgraded oils with a relative high percentage of ketones and phenols (Figure S23). This kind of product selectivity was also observed in the use of Ni-catalysts with the light phase, supporting the theory that sulphur may influence the catalyst activity.

From the XRD of the spent catalyst (Figure 6.12), no significant changes were detected in the case of the catalyst used with beech wood bio-oil, but a relevant amount of nickel was converted to Ni_3S_2 in the case of the straw bio-oil. According to the elemental analysis (Table 6.10), the sulphur deposited on the spent catalyst used with beech wood bio-oil was 0.4 wt.% (although the concentration in the feed was under the detection limit) and with straw bio-oil 2.6%.

The regeneration of $NiCu/Al_2O_3$ monitored by XRD (Figure 6.12) for the catalyst used with beech wood was analogous to that used with the light phase. On the other hand, the catalyst used with straw bio-oil produced during the calcination
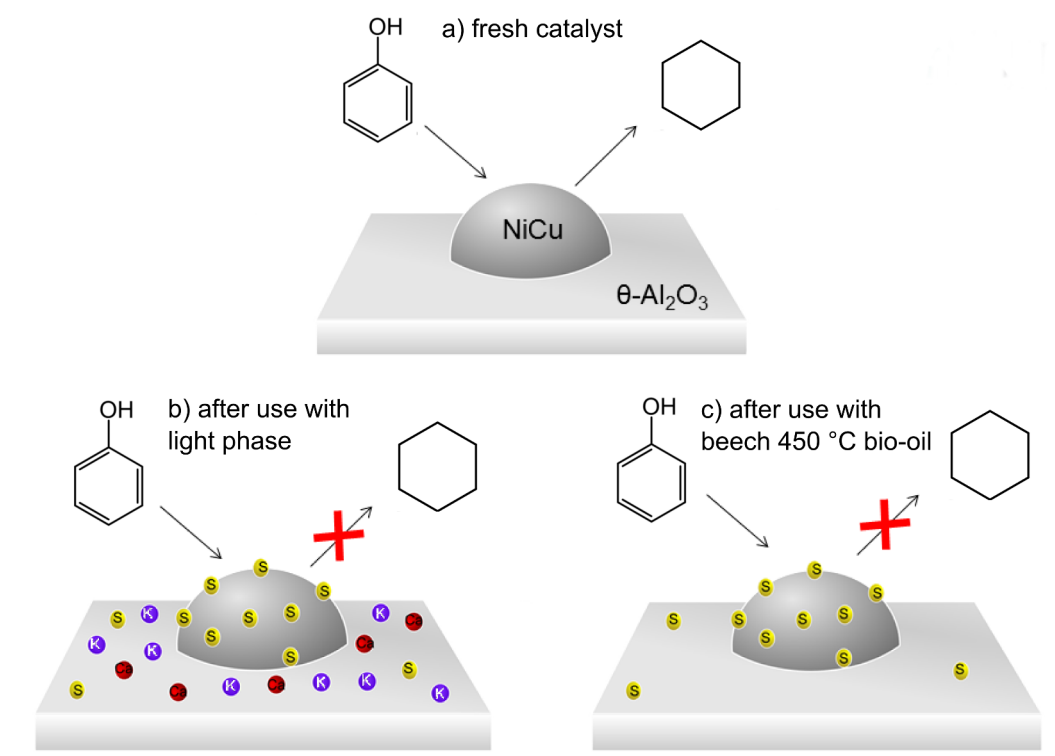
Figure 6.13: Different reactivity of phenol on fresh and regenerated NiCu/Al₂O₃ after the hydrotreatment of the light phase (340 °C, 8.0 MPa H₂) and beech 450 °C bio-oil (350 °C with stabilisation at 150 °C, 14.0 MPa H₂), and proposed structure of the regenerated catalysts.

NiO and NiSO₄ (favoured thermodynamically from Ni₃S₂ [241]) and the following reduction produced mainly Ni⁰, which was strongly sintered (circa 47 nm), but still small reflections of Ni₃S₂ were detected (sulphur on surface 2.0 wt.%). The

Table 6.11: Comparison between the upgraded oils and aqueous phase using the fresh NiCu/Al₂O₃ and the regenerated one with beech 450 °C bio-oil (hydrotreatment at 350 °C for 2 hours with stabilisation at 150°C for 1 hour, 14.0 MPa H₂ at room temperature).

	Upgraded oil fresh	Upgraded oil regenerated	Aqueous phase fresh	Aqueous phase regenerated
C (wt.%)	69.8	72.1	10.7	10.4
H (wt.%)	8.8	8.9	10.8	11.1
N (wt.%)	<0.3	< 0.3	<0.3	< 0.3
O (wt.%)	21.4	19.0	78.5	78.5
H₂O (wt.%)	5.6	5.0	76.5	77.6
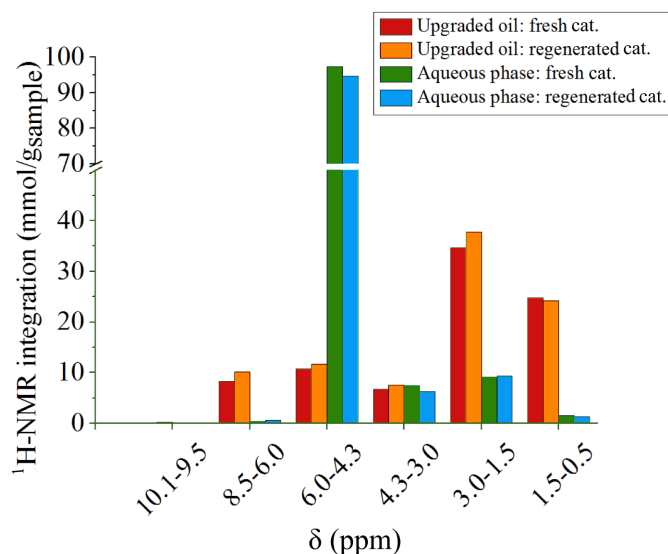
Figure 6.14: Integration of ^{1}H-NMR spectra of the upgraded oil and aqueous phase produced from the fresh and regenerated NiCu/Al$_2$O$_3$ using pyrolysis oil from beech wood (hydrotreatment at 350 °C for 2 hours with stabilisation at 150°C for 1 hour, 14.0 MPa H$_2$ at room temperature). The assignment of protons to the specific classes of compounds is reported in Table 2.1.

sintering is probably due to the lower melting temperature of nickel sulphide, that makes the mobility of the active metal higher, according to the Tamman and Hüttig temperature [165].

When the regenerated catalysts were used again in order to monitor their activity in the phenol conversion in aqueous solution, no conversion was detected, neither when sulphur was in lower concentration (summary in Figure 6.13).

When the regenerated catalyst from beech wood bio-oil was used again with the same bio-oil, the hydrogen consumption monitored was 206 NL/kg in comparison to 239 NL/kg of the fresh (86% of the activity, comparable to the percentage observed with the light phase of the pyrolysis oil). The composition of the upgraded oil was comparable between the one produced by the fresh catalyst and the regenerated one (Table 6.11). As observed by ^{1}H-NMR (Figure 6.14) and GC-MS (Figure S23), the catalyst was selective to produce ketones and phenolic compounds, confirming that sulphur changes the activity and the selectivity of nickel-based catalysts for hydrotreatment.

6.8   Conclusions

The results presented in this chapter defined the influence of different components of pyrolysis oil on the activity and the selectivity of nickel-based catalysts and in particular NiCu/Al$_2$O$_3$. Different inorganic elements present in pyrolysis oils, like S, K, Mg, Ca, P, Cl, can contribute to the deactivation of the catalyst, as well as organic compounds that can generate carbon deposits which block the surface availability. In the hydrotreatment of pyrolysis oil, nickel-based catalysts were quite selective for ketone production and did not show significant conversion of phenolic compounds. A slightly inferior activity (around 85% if the hydrogen consumption compared to the fresh catalyst), but the same selectivity was observed in the case of the regenerated catalyst. On the contrary, fresh NiCu/Al$_2$O$_3$ converted completely phenol (as a model compound) in aqueous solution mainly to cyclohexanol at 250 °C and cyclohexane at 340 °C. Once the catalyst was exposed to the pyrolysis oil, this activity was lost. This shows that phenol has the potential to undergo HDO, but that the reaction was inhibited in pyrolysis oil.

An extensive characterisation of the fresh, spent and regenerated NiCu/Al$_2$O$_3$ (17.8% Ni, 2.1% Cu) was performed by the combination of several analytical techniques in order to understand the structural and chemical differences in the distinct stages of the catalyst. In the fresh NiCu/Al$_2$O$_3$, the active nanoparticles were formed by an alloy of nickel and copper. The average atomic ratio of the alloy was 9:1, but copper was slightly more segregated on the surface. The active metals were affected by surface passivation when exposed to air, with a oxide layer estimated around 1 nm thick. This layer was supposed to be completely reduced in the highly reductive gas atmosphere of the hydrotreatment reaction. The dimensions of nickel-copper particles deposited on the alumina varied in a range between 4 and 20 nm.

Analysis of the spent and regenerated catalysts, as well as additional experiments carried out over the regenerated catalyst, suggested that the main change in activity and selectivity could be due to the adsorption of sulphur on nickel and to the formation of a thin surface layer of Ni$_3$S$_2$. Depending on the concentration of sulphur in the feed, the formation of nickel sulphide species was only limited to the surface for low content, while it proceeded to bulk Ni$_3$S$_2$ at higher concentrations of sulphur in the feed. The latter case also resulted in sintering of the nickel nanoparticles in the regeneration step. In addition, it was proven that sulphur was also non-selectively adsorbed on the support surface, mainly as sulphate salts.

Coke deposits on the surface were present in the spent catalyst, but the regeneration process (calcination and reduction at 500 °C) was able to remove these completely. Alkali and alkaline earth metals, especially K and Ca, had a higher tendency to deposit on the alumina support, more than interacting or covering the nickel nanoparticles. Theta alumina was found to be stable in the conditions tested, however the presence of water in the feed could cause problems during long term operation. Therefore, since the activity among the different nickel catalysts was similar, it is recommendable for future studies to select a support more stable in water.

Despite the deactivation process, the upgraded oils produced by nickel catalysts had a better quality than the original pyrolysis oil, showing a higher HHV, better stability and a low tendency of coking (TGA measurements). Therefore, if the deactivation by sulphur could be controlled and limited to the surface, the catalyst could be used for the production of phenolic components and ketones. In this way the hydrotreating process could be addressed to the production of chemicals instead of fuels, increasing the economic value of the products.

As an outlook, future studies should be addressed to monitor the stability of this catalyst in a long-term reaction and the feasibility of distillation for separation of valuable products.

Chapter 7

Influence of feedstock, catalyst, pyrolysis and hydrotreatment temperature on the composition of upgraded oils

Different parameters chosen during the pyrolysis process and subsequent hydrotreatment influence the quality of the final products. The dependence of the upgraded oil composition on the pyrolysis temperature, biomass feedstock, catalyst and hydrotreatment temperature was investigated systematically in this chapter. Pyrolysis temperature was responsible for the fragmentation degree, resulting in a higher quality pyrolysis oil with lower oxygen content at higher temperatures, but with decreased yield. The catalyst Ru/C generally consumed more hydrogen than NiCu/Al$_2$O$_3$, showing higher hydrogenation/hydrodeoxygenation activity with higher selectivity towards alcohols and hydrocarbons rather than ketones (typical for the nickel-based catalysts). By varying the hydrotreatment temperature (80, 150, 250, 350 °C), different classes of compounds were converted and different deoxygenation degrees were achieved. Beech wood was found to be a suitable feedstock for HDO due to its low content of heteroatoms, whereas the high sulphur content in the wheat straw bio-oil caused irreversible poisoning of the catalysts.

7.1 Introduction

Pyrolysis is known for its flexibility in processing various kinds of feedstocks, producing pyrolysis oils with variable compositions [53]. The chemical characteristics of these bio-oils are determined also by other process parameters, including the type of pyrolysis (fast or intermediate [31]), the reaction setup and especially the pyrolysis temperature [242]. In general, independently from the process used and the feedstock, bio-oils produced by biomass have a high content of oxygen, which negatively influences their properties and stability [32]. Upgrading is therefore required in case these bio-oils should further be converted into transportation fuel or chemicals. Among the various techniques, increasing attention is given to hydrodeoxygenation as an upgrading method [33, 36, 38]. However, only few studies have described a systematic investigation of the influence of pyrolysis temperature and the pyrolysis feedstock [104, 243] on the hydrotreating performance. Catalyst and hydrotreating temperature also influence the product composition and the deoxygenation degree reached. This last parameter is important and the desired value depends on the application of the upgraded oil. For example, extended studies have been addressed in determining which oxygen content in the bio-oil allows its insertion in a crude-oil refinery [34, 197, 198]. The tolerance depends on the miscibility of the pyrolysis oil with the crude-oil. Values around 10-20% are considered manageable, avoiding complete deoxygenation, which is energetically and economically expensive.

In this chapter, a systematic variation of different parameters (pyrolysis and hydrotreatment temperature, pyrolysis feedstock and catalyst) was performed in order to monitor in which way the composition of the upgraded bio-oils was affected. The influence of the pyrolysis temperature was studied using bio-oils produced by intermediate pyrolysis of beech wood (ITC/KIT). Beech wood was pyrolyzed at 350, 400, 450 and 500 °C, obtaining four one-phase bio-oils with low content of heteroatoms and no minerals (labelled beech xxx °C bio-oil, with xxx °C the corresponding temperature according to Section 3.4). Successively, the bio-oils were hydrotreated over $NiCu/Al_2O_3$ and Ru/C under the same conditions using a stabilisation for 1 hour at 150 °C and 2 hours reaction at 350 °C.

The dependency of the hydrogen consumption and the quality of the upgraded oil in relation to the hydrotreating temperature was further investigated in this study using the bio-oil from beech wood produced at 450 °C by intermediate pyrolysis (beech 450 °C bio-oil, Section 3.4). Four HDO temperatures (80, 150, 250 and 350

°C) were used over NiCu/Al$_2$O$_3$ and Ru/C in order to see the reactivity of different functional groups and the deoxygenation degree. The influence of the stabilisation step at 150 °C was also studied for HDO at 350 °C. This helps to define how much hydrogen should be invested to obtain a determinate oxygen level, which may vary depending on the required application of the bio-oil product.

The same conditions and HDO temperatures used for the beech wood oil were employed also for a bio-oil produced by intermediate pyrolysis of wheat straw at 450 °C (straw 450 °C bio-oil, Section 3.3), in order to see the influence of the feedstock. The intermediate pyrolysis oils from wheat straw were finally compared with one produced by fast pyrolysis oil in the bioliq plant (bioliq bio-oil, Section 3.3). A summary of the parameters varied in this Chapter is shown in Figure 7.1.
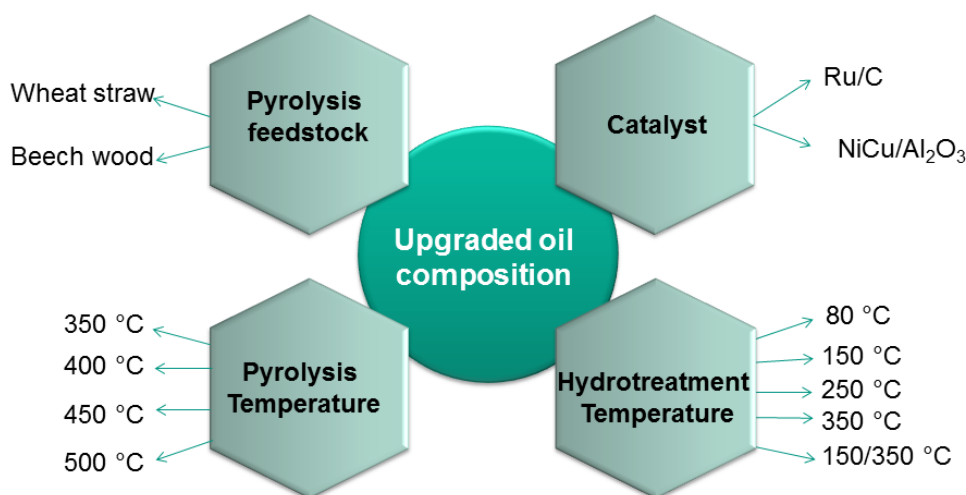
Figure 7.1: Parameters that can affect the upgraded oil composition and conditions tested in the experiments reported in this chapter.

7.2 Influence of the pyrolysis temperature on hydroprocessing

The four pyrolysis oils produced at 350, 400, 450, 500 °C from beech wood (Section 3.4) exhibited similar behavior during the hydrotreatment at 350 °C (2 hours) with previous stabilisation at 150 °C (1 hour). The hydrogen consumption of each was similar, but slightly lower for the bio-oil produced at 500 °C (Figure 7.2 a,c), due to its lower original oxygen content. NiCu/Al$_2$O$_3$ consumed less hydrogen than Ru/C under all test conditions (198-232 NL/kg$_{po}$ and 284-317 NL/kg$_{po}$ respectively). As
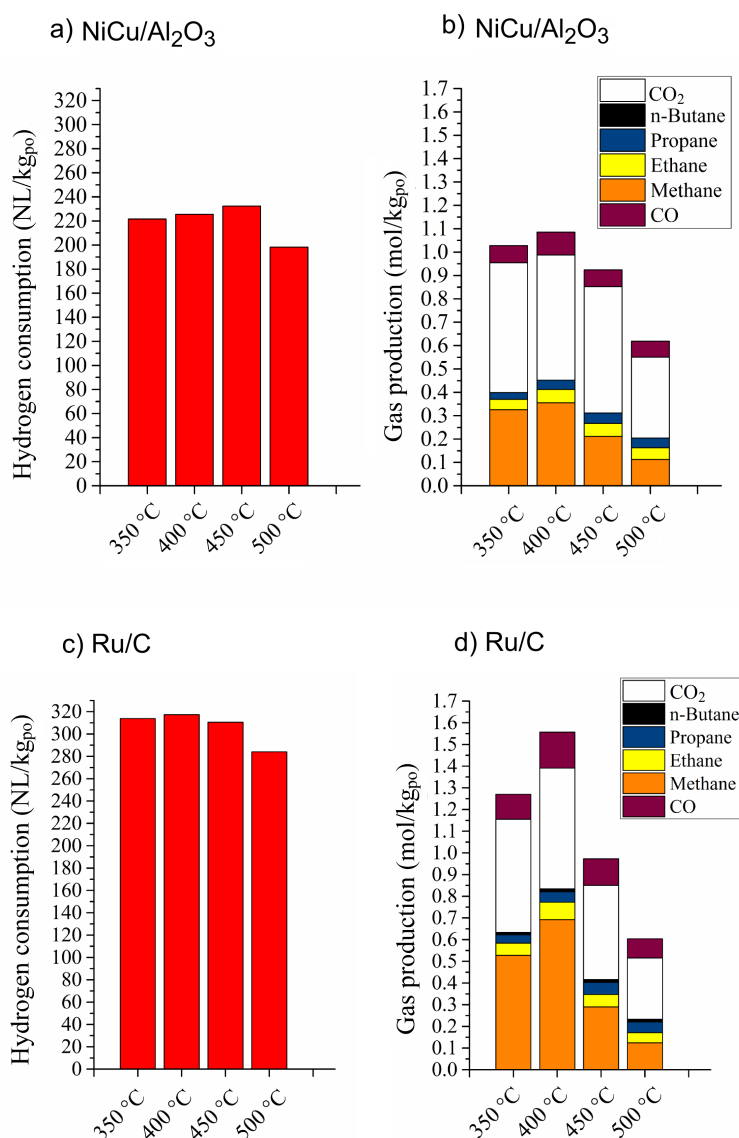
Figure 7.2: Hydrogen consumption during hydrotreatment (150 °C 1 hour, 350 °C 2 hours, 14.0 MPa H_2 at room temperature) of bio-oils produced at different pyrolysis temperatures (350, 400, 450, 500 °C) from beech wood over NiCu/Al_2O_3 (a) and Ru/C (c). The gas production during the reaction is reported in (b) for NiCu/Al_2O_3 and in (d) for Ru/C.

reported in Chapter 4 and 5, Ru/C was more active, but less convenient for hydrogen economy. Over both catalysts the main gases produced were CO_2 and methane, (see Section 4.5 and 5.4). Methane was formed in higher quantities over Ru/C, especially for bio-oils produced at 350 °C and 400 °C (Figure 7.2 b,d). According to the composition analysis (Chapter 3), more methoxy-groups were present in the

bio-oils produced at lower temperatures, therefore the high production of methane could be justified from their hydrodeoxygenation [156] favoured mainly over Ru/C.

Table 7.1: Elemental composition of the beech 350, 400, 450, 500 °C bio-oils (intermediate pyrolysis temperature, Section 3.4) and upgraded oils, and mass balance, carbon recovery and deoxygenation degree (D.O.D.) for the hydrotreatment performed over NiCu/Al$_2$O$_3$ and Ru/C (150 °C 1 hour, 350 °C 2 hours, 14.0 MPa H$_2$ at room temperature).

	Pyr. temp. (°C)	Aqueous phase (wt.%)	Upgraded oil (wt.%)	Gas (wt.%)	C (wt.%)	H (wt.%)	O (wt.%)	Water (wt.%)	Carbon recovery in oil (wt.%)	D.O.D. %
beech	350	-	-	-	49.3	7.7	43.0	17.8	-	-
beech	400	-	-	-	52.2	7.6	40.2	14.6	-	-
beech	450	-	-	-	55.4	7.1	37.5	12.4	-	-
beech	500	-	-	-	58.9	7.2	33.9	11.5	-	-
NiCu/Al$_2$O$_3$	350	32.2	66.0	3.5	65.8	8.9	25.3	6.2	88.1	36.2
NiCu/Al$_2$O$_3$	400	25.8	72.4	3.6	65.4	9.0	25.6	6.5	90.7	33.5
NiCu/Al$_2$O$_3$	450	25.4	73.6	3.3	69.8	8.8	21.4	5.6	92.7	42.4
NiCu/Al$_2$O$_3$	500	21.9	77.4	2.6	71.9	8.7	19.4	4.5	94.5	39.8
Ru/C	350	37.6	60.9	3.9	71.1	9.6	19.3	3.3	87.9	48.8
Ru/C	400	31.3	66.4	4.5	70.6	9.4	20.0	3.9	89.8	46.0
Ru/C	450	27.3	72.4	3.2	70.8	9.5	19.7	4.0	92.5	44.4
Ru/C	500	24.4	75.9	2.1	73.4	9.3	17.3	3.4	94.6	44.8

The mass balance (Table 7.1) showed that the upgraded oil yield increased with pyrolysis temperature, as well as the carbon recovery in this phase, which reached values over 90% for higher temperatures. Hydrotreatment was therefore demonstrated to be a suitable method for upgrading, losing only a limited amount of carbon. The upgraded oils produced over NiCu/Al$_2$O$_3$ and Ru/C were different in composition (Table 7.1) and in density (Figure 7.3). In the case of NiCu/Al$_2$O$_3$, the upgraded oil was more dense than the aqueous phase, while the opposite was observed for Ru/C.

On the contrary, the aqueous phase yield decreased for higher pyrolysis temperatures (Table 7.1). The water content varied from 71 to 82 wt.%, (higher values at higher temperatures), and the carbon content was limited to 4 - 9% (lower content at higher temperatures). Higher quantities of aqueous phase were produced in the case of Ru/C, indicating higher activity of Ru/C in hydrodeoxygenation as demonstrated by the deoxygenation degree (D.O.D., Table 7.1).

As reported in the van Krevelen plot (Figure 7.4), the original bio-oils had different O/C and H/C ratios, with a trend towards lower values at higher pyrolysis temperature. The upgraded oils reflected also this characteristic, however the
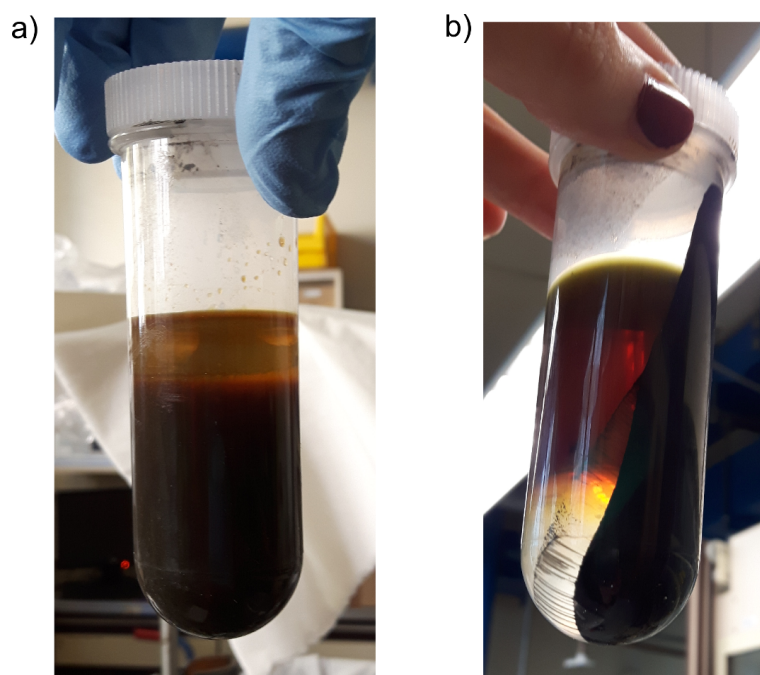
Figure 7.3: Products of the hydrotreatment of the beech wood at 450 °C bio-oil (hydrotreatment performed at 350 °C for 2 hours with previous stabilisation at 150 °C for 1 hour, 14.0 MPa H_2 at room temperature): a) over $NiCu/Al_2O_3$ (on top aqueous phase; bottom upgraded oil), b) over Ru/C (on top upgraded oil ; bottom aqueous phase).

differences were much less pronounced. Higher deoxygenation level was obtained over Ru/C and for the bio-oil produced at 500 °C. In general, the heating value was increased from the original value of 25-28 MJ/kg to 32-36 MJ/kg after the hydrotreatment. Therefore, the pyrolysis temperature plays an important role in the composition of the bio-oils, which in turn affected the upgraded oils in a smoother way. A peculiarity observed in the use of intermediate pyrolysis oil concerns the ratio H/C of the upgraded oil. For HDO of fast pyrolysis oil in similar conditions a decrease of H/C ratio was usually reported for the upgraded oil compared to the feed [113, 114, 117], as observed also the the light phase (Section 4.6 and 5.5). Regarding the beech xxx °C bio-oils, an increase of H/C ratio was observed after HDO. This could indicate a higher hydrogenation activity compared to hydrodeoxygenation. For instance, intermediate pyrolysis oils, due to the longer vapour resident time during pyrolysis, underwent more dehydration reactions, exhibiting therefore lower H/C and O/C ratio. For this characteristic composition, it is probable that hydrogenation has an important role for this kind of bio-oils. To the author's knowledge, no similar studies about HDO of intermediate pyrolysis oils were reported in the literature, as well as the dependency of upgraded oil composition on the
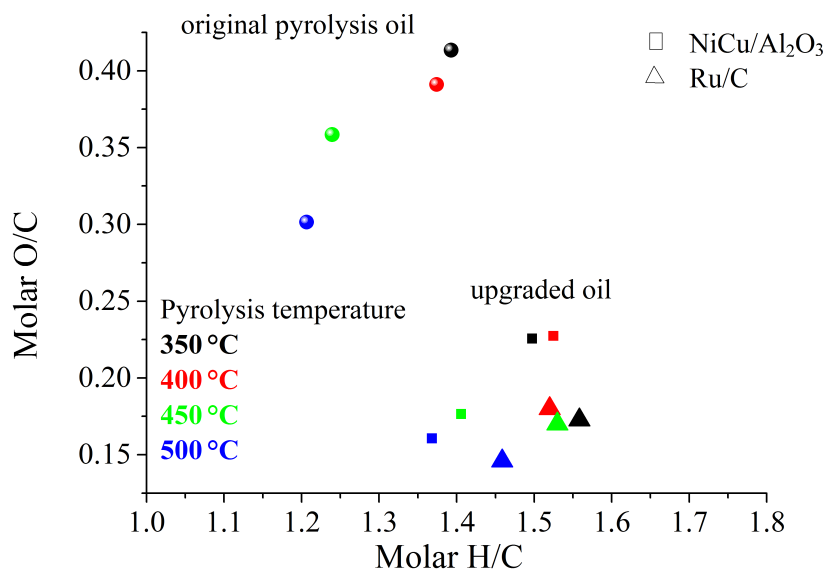
Figure 7.4: Van Krevelen plot of the upgraded oils produced from HDO (350 °C for 2 hours with previous stabilisation at 150 °C for 1 hour, 14.0 MPa H_2 at room temperature) of intermediate pyrolysis of beech wood at different pyrolysis temperatures.

pyrolysis temperature.

The differences between the upgraded oil and the aqueous phase produced over the two catalysts were investigated by ^{1}H-NMR (Figure 7.5). In both phases some trends that recall the original bio-oils were observed. In fact, the aromatic signal (8.5-6.0 ppm) increased with the pyrolysis temperature as a result of more lignin-derivatives contained in the bio-oil, while the alpha protons to alcohols/etheric bonds (4.3-3.0 ppm) decreased, due to the lower concentration of methoxy-groups. Protons alpha to carboxylic/carbonylic and unsaturated groups (3.0-1.5 ppm) constituted the main class detected in the upgraded oils over $NiCu/Al_2O_3$, but only for Ru/C the same tendency of the original oil was monitored. Ru/C had more protons in alkane groups (1.5-0.5 ppm), confirming its higher hydrodeoxygenation/hydrogenation activity. Fewer organic compounds were detected in the aqueous phase, but their protons were mainly associated to carboxylic/ carbonylic /unsaturated groups and to alcohols/ethers.

GC-MS (Figure 7.6 and 7.7) demonstrated qualitatively that the upgraded oils contained similar compounds after hydrotreatment with the same catalyst. In the case of $NiCu/Al_2O_3$, the hydrotreatment resulted in a massive production of cyclic and linear ketones, while for Ru/C more alcohols and hydrocarbons were

143

observed. The pyrolysis temperature further influenced the characteristics of the aromatic compounds produced over both catalysts. At lower temperatures more syringol and guaiacol were detected, instead of phenol and o-cresol, which were favoured at higher temperatures. Alkyl-phenols increased their concentration with higher temperatures, as reported in the original bio-oils (Section 3.4), confirming the influence of the pyrolysis temperature also in the upgraded oils.
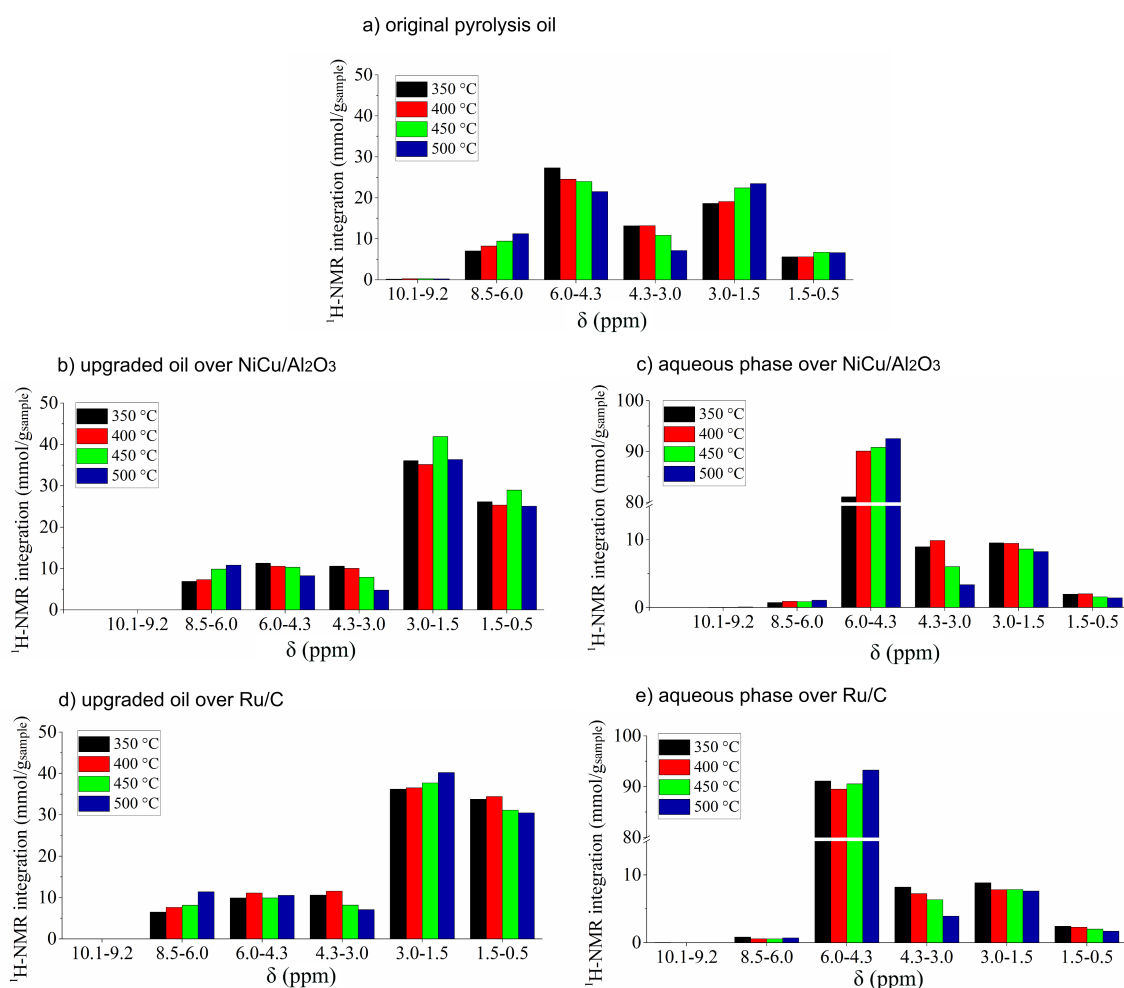
Figure 7.5: ^{1}H-NMR spectra integration of the beech wood bio-oils produced at different pyrolysis temperatures (a), of the upgraded oils over NiCu/Al$_2$O$_3$ (b) and the respective aqueous phases (c), and of the upgraded oils over Ru/C (d) and the respective aqueous phases (e).Hydrotreatment performed at 350 °C for 2 hours with previous stabilisation at 150 °C for 1 hour, 14.0 MPa H$_2$ at room temperature. The assignment of protons to the specific classes of compounds is reported in Table 2.1.
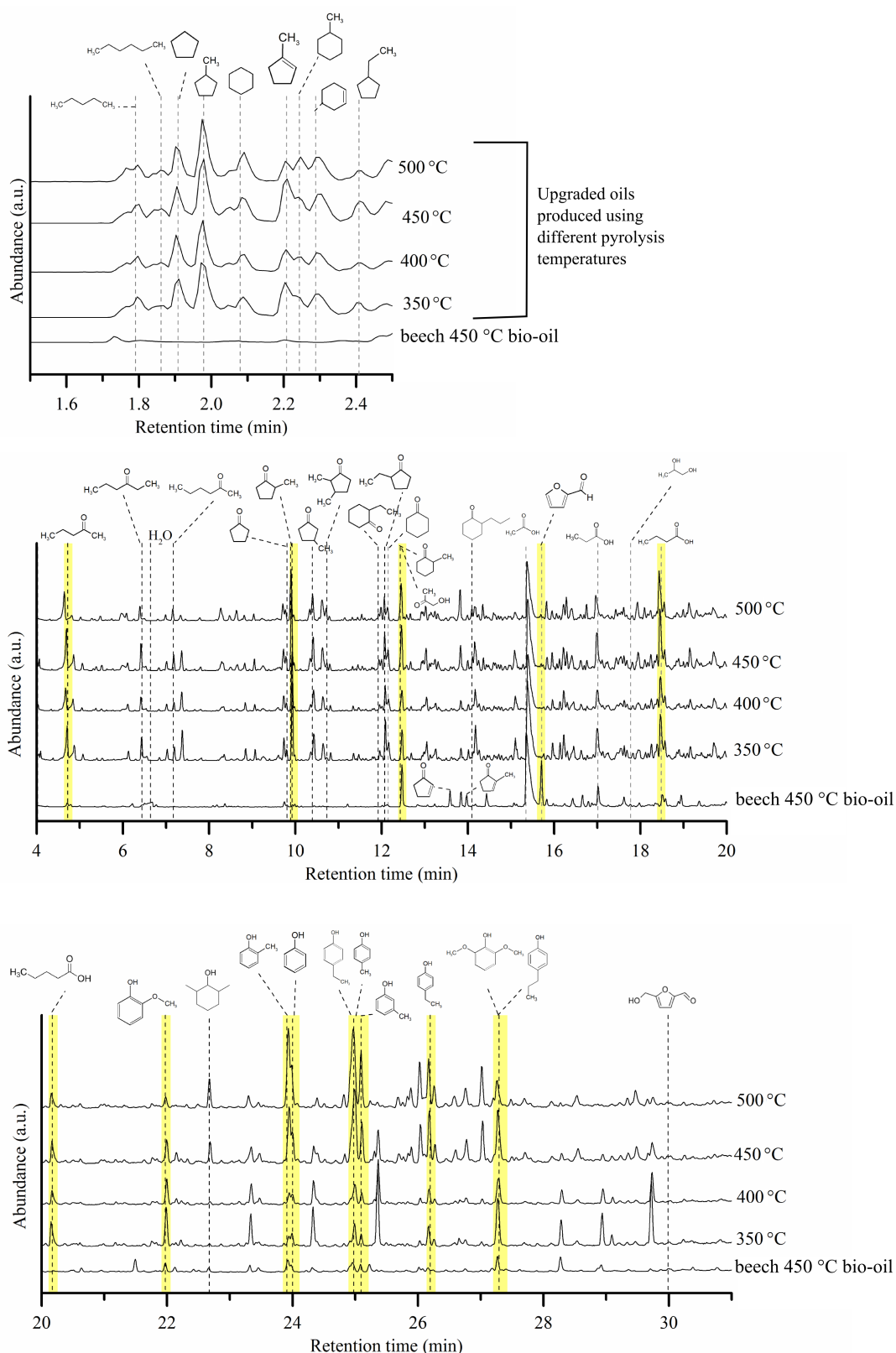
Figure 7.6: GC-MS of the upgraded oils, produced by beech wood at different pyrolysis temperatures, over NiCu/Al$_2$O$_3$ (hydrotreatment 150 °C 1 hour, 350 °C 2 hours, 14.0 MPa H$_2$ at room temperature). For comparison the chromatogram of beech 450 °C bio-oil is reported.

145
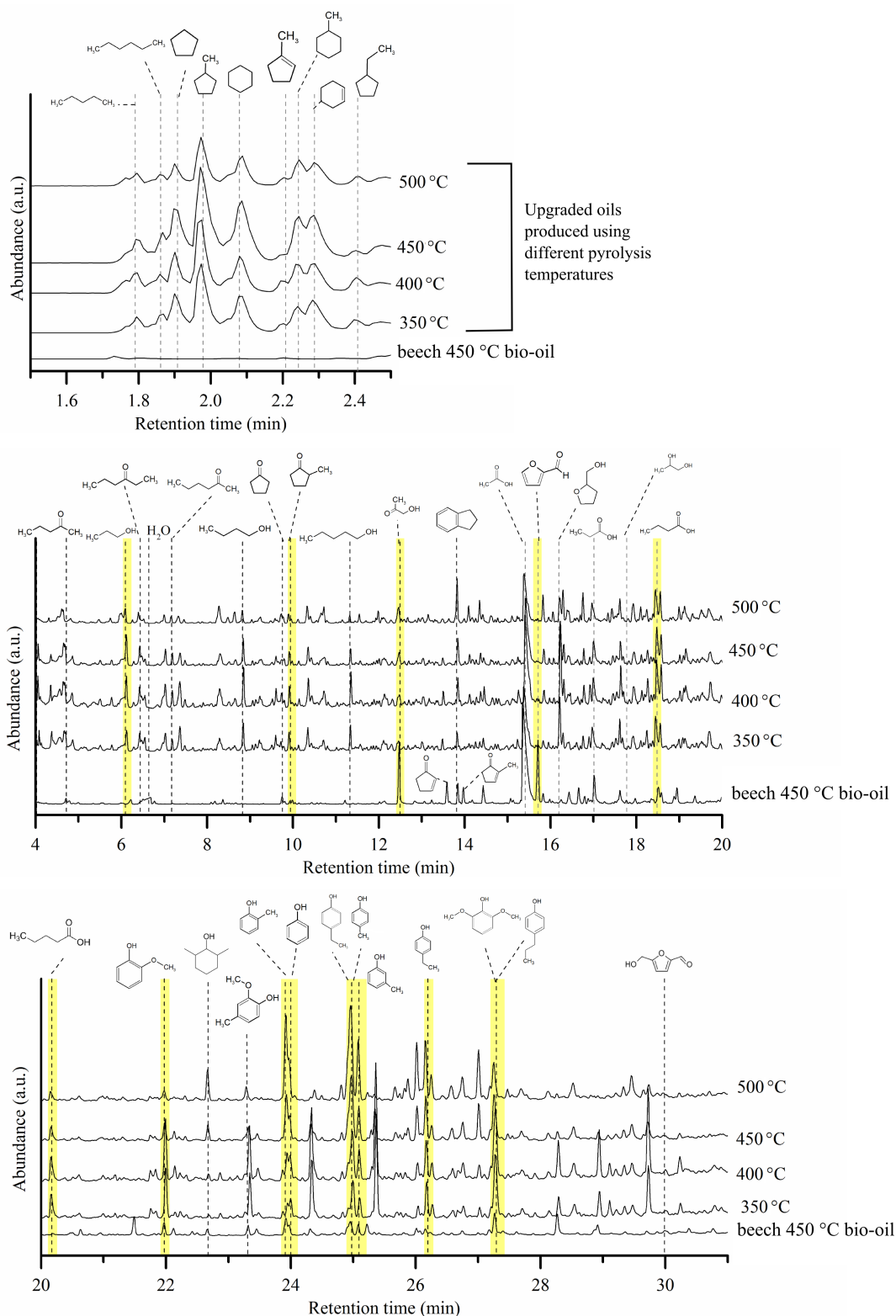
Figure 7.7: GC-MS of the upgraded oils, produced by beech wood at different pyrolysis temperatures, over Ru/C (hydrotreatment 150 °C 1 hour, 350 °C 2 hours, 14.0 MPa H_2 at room temperature). For comparison the chromatogram of beech 450 °C bio-oil is reported.

7.3 Change of the hydrotreatment temperature for beech wood bio-oils

The temperature of hydrotreatment is an important parameter, which changes the level of deoxygenation in the upgraded oil. Depending on the application, which could be a simple stabilization of the oil or insertion in a refinery, the admissible
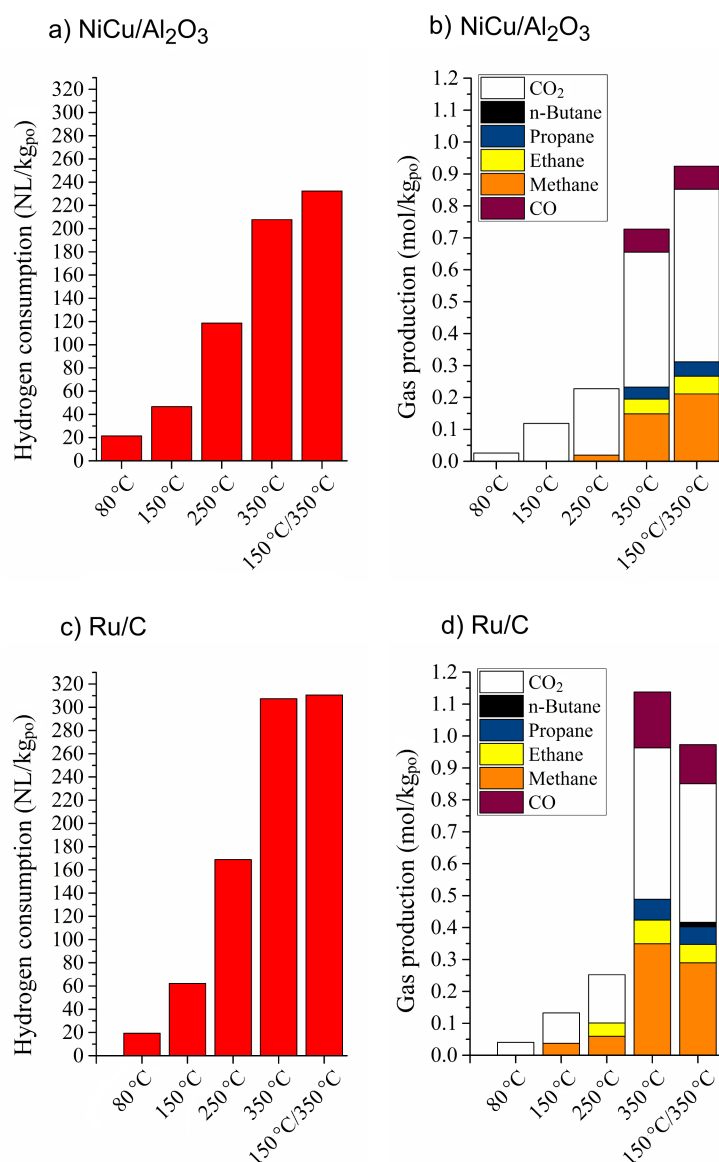
Figure 7.8: Hydrogen consumption of hydrotreatment of beech 450 °C bio-oil at different temperatures (80, 150, 250, 350 and 150/350 °C, 14.0 MPa H_2 at room temperature) over $NiCu/Al_2O_3$ (a) and Ru/C (c). The gas production during the reaction is shown in (b) for $NiCu/Al_2O_3$ and in (d) for Ru/C.

Table 7.2: Elemental composition of beech 450 °C bio-oil and upgraded oils, and mass balance, carbon recovery and deoxygenation degree for the hydrotreatment performed over NiCu/Al$_2$O$_3$ and over Ru/C (80, 150, 250, 350 and 150/350 °C, 14.0 MPa H$_2$ at room temperature).

	Temp. (°C)	Aqueous phase (wt.%)	Upgraded oil (wt.%)	Gas (wt.%)	C (wt.%)	H (wt.%)	O (wt.%)	Water (wt.%)	Carbon recovery in oil (wt.%)	D.O.D. %
beech 450	-	-	-	-	55.4	7.1	37.5	12.4	-	-
NiCu/Al$_2$O$_3$	80	1 phase	1 phase	0.1	55.5	7.5	37.0	12.1	99.9	1.2
NiCu/Al$_2$O$_3$	150	1 phase	1 phase	0.5	55.1	7.7	37.2	13.5	99.7	3.6
NiCu/Al$_2$O$_3$	250	14.1	86.1	0.9	60.4	8.1	31.5	10.7	93.9	18.5
NiCu/Al$_2$O$_3$	350	22.7	76.4	2.6	67.3	8.5	24.2	6.0	92.9	33.6
NiCu/Al$_2$O$_3$	150;350	25.4	73.6	3.3	69.8	8.8	21.4	5.6	92.7	42.4
Ru/C	80	1 phase	1 phase	0.2	55.1	7.6	37.3	12.4	99.9	0.8
Ru/C	150	1 phase	1 phase	0.5	54.7	7.7	37.6	13.8	99.7	2.8
Ru/C	250	14.8	85.8	0.9	59.6	8.4	32.0	11.5	92.3	18.6
Ru/C	350	26.7	72.2	3.7	70.8	9.2	20.0	4.4	92.3	44.3
Ru/C	150;350	27.3	72.4	3.2	70.8	9.5	19.7	4.0	92.5	44.4

oxygen content may vary. In this section the influence of the hydrotreatment temperature and the catalyst type on the quality and the characteristics of the upgraded oil are reported.

Hydrogen consumption increased with the temperature as expected [33] and it was more pronounced for Ru/C than for NiCu/Al$_2$O$_3$ (Figure 7.8). The reaction at 350 °C with a previous stabilization step at 150 °C required a slightly higher amount of hydrogen than the one without stabilisation. The hydrogen consumed at 80 and 150 °C was relatively low and at these two temperatures the bio-oils were not subjected to phase separation, making them suitable for stabilization. The gas production started already at low temperature (Figure 7.8), with a small amount of CO$_2$, which could be attributed to the decomposition of formic acid that acted as reducing agent (results verified by ^{1}H-NMR). CO$_2$ was the main gaseous product and methane evolved only at higher temperatures: 250 °C for nickel, 150 °C for Ru/C. For all the temperatures studied, Ru/C was more active in gas production. The role of the stabilization step for the reaction at 350 °C in the gas production could not finally be clarified by the experiments.

In general, the hydrotreatment produced a single phase oil at 80 °C and 150 °C, and two phases at 250 °C and at 350 °C both with and without the stabilization step. At 250 °C for both catalysts an upgraded oil with higher density and an aqueous phase were formed, while at 350 °C the upgraded oil had higher density for NiCu/Al$_2$O$_3$ and lower density than water for Ru/C. The aqueous phase production

increased with the temperature and less upgraded oil was recovered (Table 7.2). However the carbon recovery in the upgraded oil was similar and over 90% for Ru/C and NiCu/Al$_2$O$_3$. The water content of the upgraded oils was lower at high temperature. Gases and solids were negligible with respect to the overall yield (it was not possible to calculate the solid for Ru/C, but for NiCu/Al$_2$O$_3$ it was less than 0.3 wt.%). The deoxygenation degree (D.O.D) increased with the HDO temperature and reached a plateau at circa 40%.

According to the van Krevelen plot (Figure 7.9), upgraded oils from NiCu/Al$_2$O$_3$ and Ru/C had comparable oxygen content (a deviation was observed for the reaction at 350 °C without stabilization), but the H/C ratio was higher for Ru/C, indicating higher hydrogenation activity. At low temperatures (80 and 150 °C), hydrogenation was predominant (increase of H/C) and the deoxygenation was implemented for higher temperatures when phase separation was observed. The final heating value of the oil from upgrading at 350 °C with stabilization was 34 MJ/kg for NiCu/Al$_2$O$_3$ and 35 MJ/kg for Ru/C. Also in this case an increase of the H/C ratio was observed as reported in Section 7.2.

Figure 7.10 shows the results obtained by ^{1}H-NMR spectra integration. Aldehydes (10.1-9.2 ppm) were partially consumed at 80 °C and the signal disappeared completely at 150 °C. The content of aromatic protons (8.5-6.0
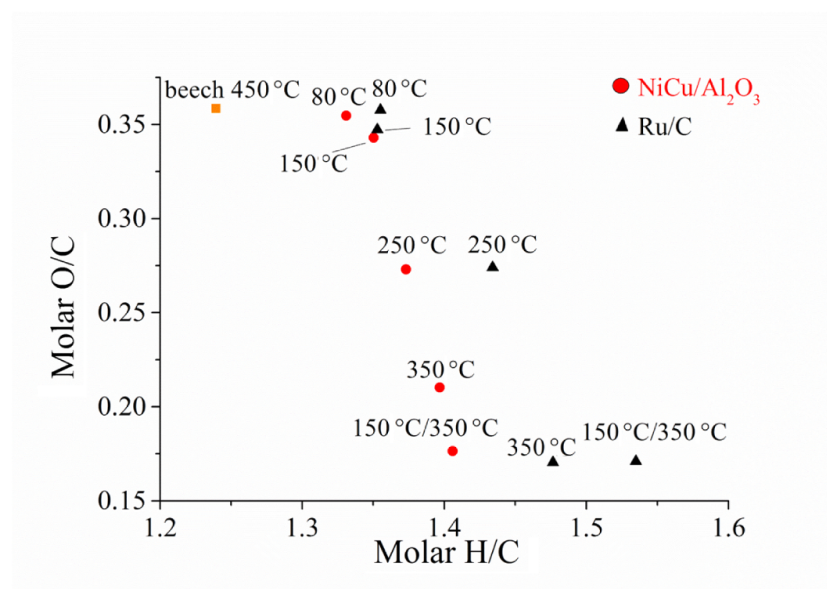
Figure 7.9: Van Krevelen plot of the upgraded oils produced at different hydrotreating temperatures (80, 150, 250, 350 and 150/350 °C, 14.0 MPa H$_2$ at room temperature) of beech 450 °C bio-oil.

ppm) decreased slightly until 250 °C, then increased again at 350 °C. Protons associated with water (or exchanging with water, 6.0-4.3 ppm) and protons alpha to alcohols/etheric bonds (4.3-3.0 ppm) increased in concentration until 150 °C, and after the phase separation occurred they were detected mainly in the aqueous phase. A contribution to this signal at low temperature was due to the hydrogenation of aldehydes. Protons alpha to carbonyl/carboxylic and unsaturated groups (3.0-1.5 ppm) had the same integral for $NiCu/Al_2O_3$ until 150 °C and they increased until reaching a maximum at 350 °C. Over Ru/C this group increased already at low temperature showing a maximum at 350 °C without stabilisation. Alkane protons (1.5-0.5 ppm) increased already at low temperature, probably due to the hydrogenation of unsaturated groups (more reactive than aldehyde, in agreement with [104]), and they reached a maximum at 350 °C. The concentration of this class in the products over Ru/C was higher, confirming higher hydrogenation/hydrodeoxygenation activity for this catalyst.

GC-MS (Figure 7.11 and 7.12) was used to establish the reactivity of various compounds at different temperatures under hydrotreating conditions. The production of alkanes started at 250 °C with a low amount of methyl-cyclopentane, and was enhanced at 350 °C with the production of other hydrocarbons. Cyclopentane and analogues derived from cyclopentenones were present in the original feed, but they disappeared already at 80 °C, with selective hydrogenation of unsaturated bonds forming cyclopentanones. Furfural was mainly converted at 150 °C, the temperature at which 2-methyl-cyclopentanone appeared, probably formed by other sugar derived components. At 250 °C cyclopentanones were converted mainly to cyclopentanols over Ru/C and at 350 °C to cyclopentanes. On the contrary, over $NiCu/Al_2O_3$ cyclopentanones concentration increased until 350 °C and only a low quantity of cyclopentanes were formed, demonstrating that this catalyst was selective for ketones.

At 350 °C Ru/C favoured the production of alcohols (some linear alcohols were detected) and hydrocarbons. Propionic, butyric and pentanoic acid were produced and higher concentrations were detected for higher temperatures. The aromatic compounds detected were similar for both Ru/C and $NiCu/Al_2O_3$, indicating that this category of compounds was not converted. Higher quantities of phenol were detected at higher temperature, due to two effects: concentration of this molecule in the upgraded oil after phase separation, and hydrodeoxygenation or other kind of cleavage of higher molecular weight components. The acid environment and the high temperature could result in the formation of alkyl phenols with substitution in

ortho and para positions, as detected at higher temperature. Guaiacol and syringol were mainly not converted at 350 °C. Compounds with higher molecular weight (retention time 28-30 min) constituted from phenolic ring with other substitutions (not easily identifiable) were converted at 350 °C.

In conclusion, the study of the influence of hydrotreating temperature permitted delineation of the reactivity of some classes of compounds over NiCu/Al$_2$O$_3$ and Ru/C, allowing the definition of the main characteristics and composition of the upgraded oil. In comparison to the reactivity reported by Elliott [35] for a sulfided NiMo catalyst (see Section 1.4.1), some differences were detected. Over NiCu/Al$_2$O$_3$ and Ru/C, olefins and aldehydes were converted at lower temperatures, but carboxylic groups and phenols were more resistant to HDO.
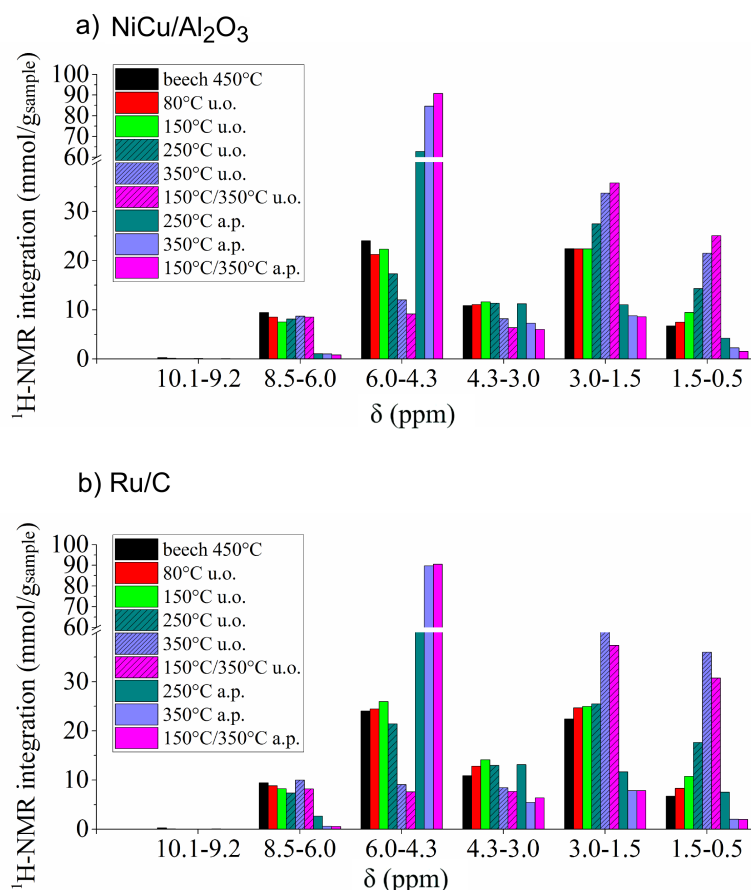
Figure 7.10: ^{1}H-NMR spectra integration of the upgraded oils (u.o.) and aqueous phase (a.p.) produced from the HDO of beech 450 °C bio-oil over NiCu/Al$_2$O$_3$ (a) and Ru/C (b). Hydrotreatment at 80, 150, 250, 350 and 150/350 °C, 14.0 MPa H$_2$ at room temperature. The assignment of protons to the specific classes of compounds is reported in Table 2.1.
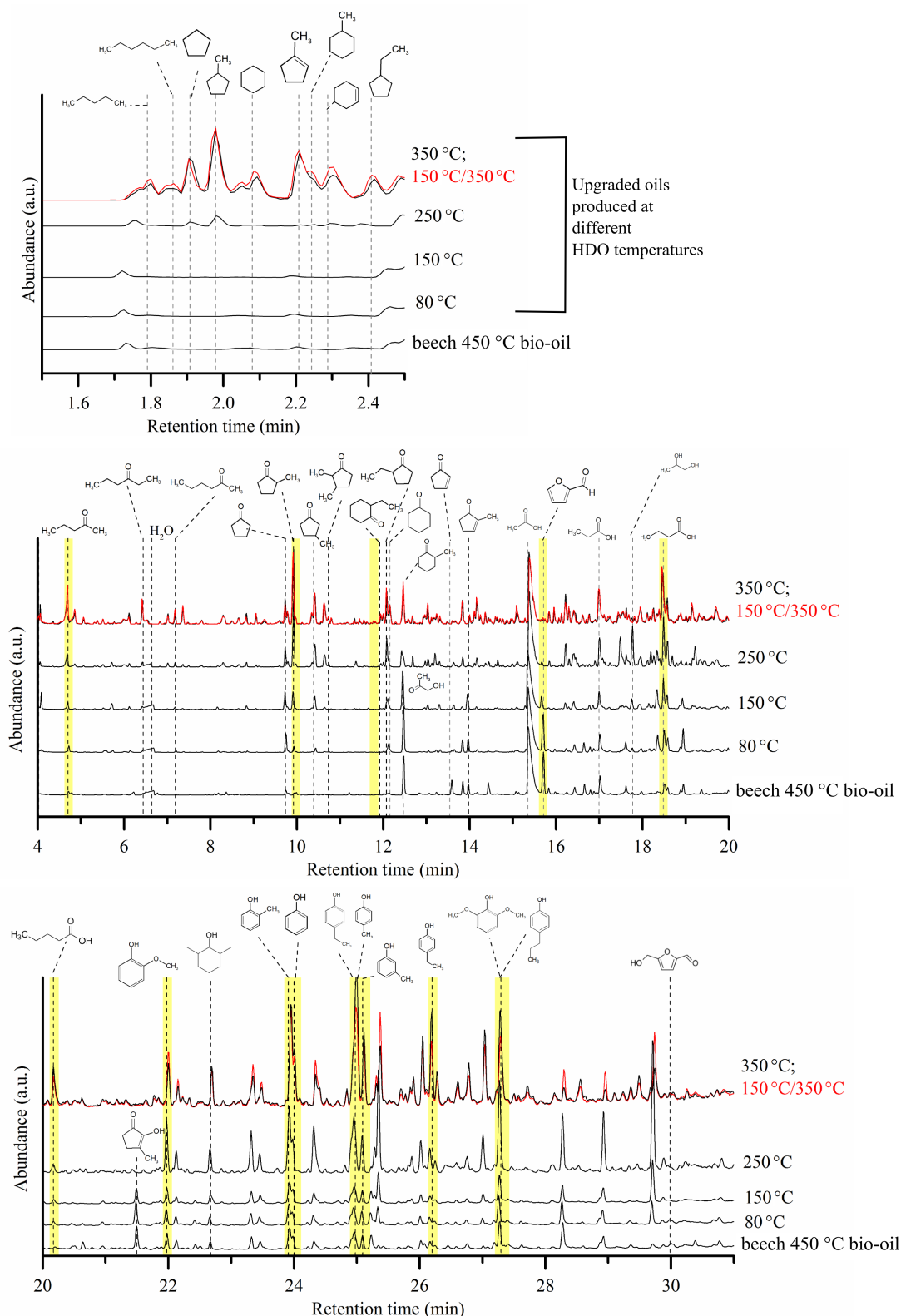
Figure 7.11: GC-MS of beech 450 °C bio-oil and the upgraded oils produced at different hydrotreatment temperatures (80, 150, 250, 350 and 150/350 °C, 14.0 MPa H_2 at room temperature) over $NiCu/Al_2O_3$.
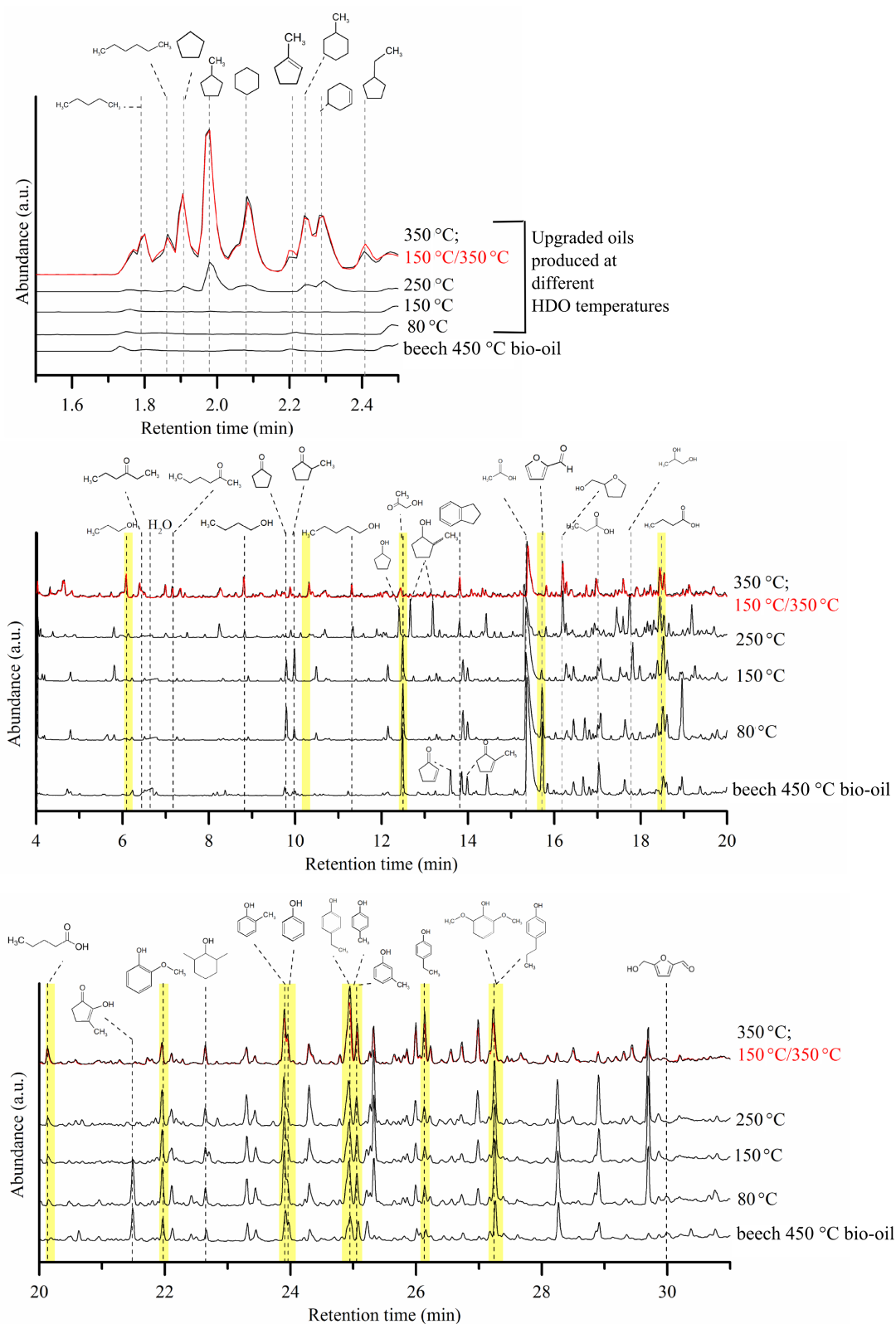
Figure 7.12: GC-MS of beech 450 °C bio-oil and the upgraded oils produced at different hydrotreatment temperatures (80, 150, 250, 350 and 150/350 °C, 14.0 MPa H_2 at room temperature) over Ru/C.

7.4 Change of the hydrotreatment temperature for wheat straw bio-oils and influence of the feedstock

The influence of the hydrotreatment temperature was also tested for an intermediate pyrolysis oil produced from wheat straw at 450 °C (straw 450 °C bio-oil, Section 3.3). In order to compare bio-oils from different processes, an additional experiment was carried out with a fast pyrolysis oil from bioliq (bioliq bio-oil, Section 3.3) for the temperature 350 °C with previous stabilization at 150 °C.

The hydrogen consumption of both bio-oils was inferior to the one recorded by beech 450 °C bio-oil. At 80 °C it was practically absent and only at 150 °C hydrogen consumption was observed (Figure 7.13). Higher hydrogen consumption was recorded at higher temperatures, with similar values for the reactions at 350 °C with and without stabilization. The intake for bioliq bio-oil was 224 Nl/kg_{po} for $NiCu/Al_2O_3$ and 269 Nl/kg_{po} for Ru/C, values that were superior to the ones for intermediate pyrolysis (147 Nl/kg_{po} for $NiCu/Al_2O_3$ versus 238 NL/kg_{po} for Ru/C at 350 °C with stabilization). The gas production of straw 450 °C bio-oil was limited in comparison to the beech 450 °C bio-oil, indicating in general a lower cracking activity of the catalyst when used with this feed. The main gaseous products were CO_2 and methane, the latter mainly produced over Ru/C. Regarding the bioliq bio-oil, contamination of ethylene glycol added during the filtration produced ethane, which appeared in higher amount (Figure 7.13).

The products recovered from the hydrotreatment of the straw 450 °C bio-oil presented different phases at different temperatures. It should be mentioned that the bio-oil was present as one phase, but if centrifuged at the same conditions used for dividing the upgraded products, a phase separation was induced forming a light aqueous phase and heavy organic phase. At HDO temperatures in the range between 80 °C and 250 °C a light aqueous phase and a heavier upgraded oil were formed. At 350 °C three phases were observed: a light upgraded oil, an aqueous phase and a heavier upgraded oil. Regarding the bioliq bio-oil, two phases were formed at 350 °C over both catalysts: a light upgraded oil and an aqueous phase.

On analysing the mass balance (Table 7.3), no trends were observed in relation to the temperature. At 350 °C it was difficult to do any kind of considerations due to the big percentage of material losses. Since three liquid phases were instead produced, it was not possible to calculate the mass balance from elemental analysis

and the collected products are reported. In general, the amount of aqueous phase and upgraded oil was not so easily correlated to the temperature as it was the case for the beech wood bio-oils. The explanation lies in the elemental composition of these two phases. In fact, water was contained in different percentages in the products and did not correlate with the temperature. The phase separation is challenging to
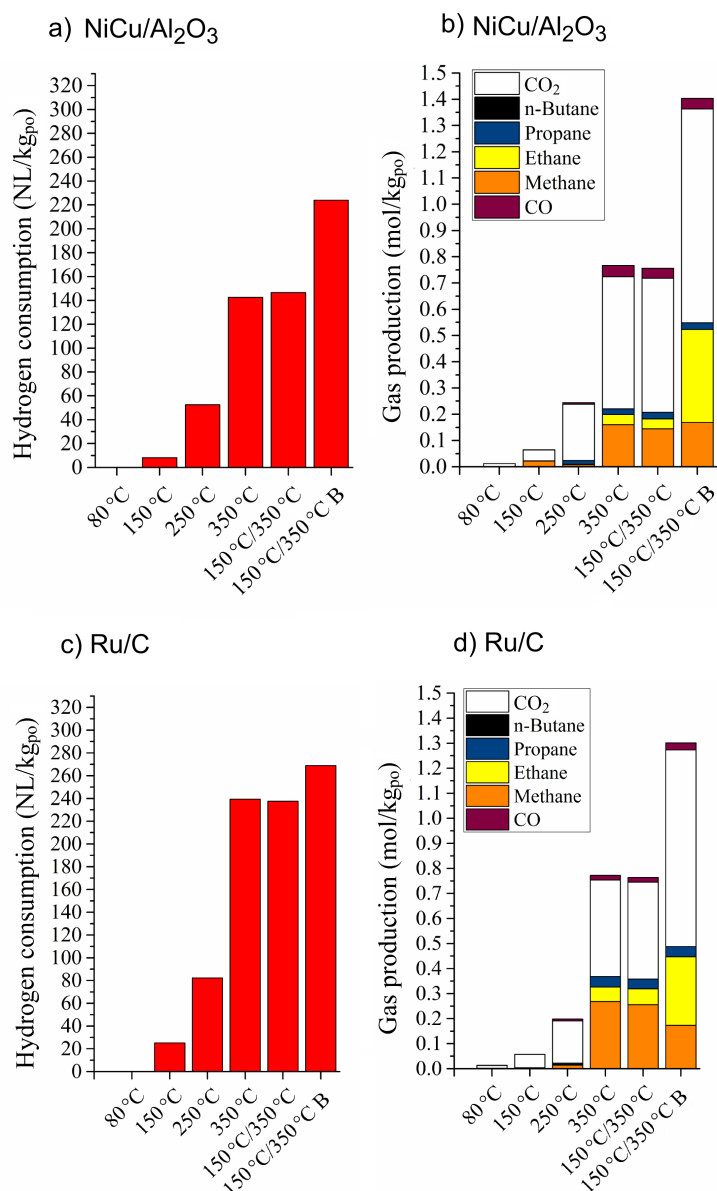
Figure 7.13: Hydrogen consumption of hydrotreatment of straw 450 °C bio-oil at different temperature (80, 150, 250, 350 and 150/350 °C, 14.0 MPa H_2 at room temperature) over $NiCu/Al_2O_3$ (a) and Ru/C (c). The gas production during the reaction is reported in (b) for $NiCu/Al_2O_3$ and in (d) for Ru/C. "B" refers to bioliq bio-oil.

explain, but it could be dependent on the complex phase equilibria established at a determined temperature. Gas and solids were a negligible amounts for the mass bilance and the main percentage of carbon was recovered in the upgraded oils.

Table 7.3: Mass balance of the hydrotreatment products (hydrotreatment temperature 80, 150, 250, 350, 150/350 °C, 14.0 MPa H_2 at room temperature) of straw 450 °C bio-oil and carbon recovery in the upgraded oil (*).

Temp. (°C)	catalyst	bio-oil	light organic (wt.%)	aqueous phase (wt.%)	heavy organic (wt.%)	gas (wt.%)	losses (wt.%)	carbon recovery* (wt.%)
80	NiCu/Al$_2$O$_3$	straw 450	-	34.1	66.5	0.1	-0.7	86.0
150	NiCu/Al$_2$O$_3$	straw 450	-	21.4	78.8	0.2	-0.4	91.8
250	NiCu/Al$_2$O$_3$	straw 450	-	31.8	67.9	1.0	-0.7	91.2
350	NiCu/Al$_2$O$_3$	straw 450	16.4	26.2	32.2	2.8	22.4	56.1
150;350	NiCu/Al$_2$O$_3$	straw 450	19.9	32.9	28.9	3.0	15.2	69.7
150;350	NiCu/Al$_2$O$_3$	bioliq	64.8	32.2	-	5.1	-2.1	86.9
80	Ru/C	straw 450	-	36.3	63.6	0.1	0.1	84.8
150	Ru/C	straw 450	-	28.9	71.1	0.2	-0.2	88.8
250	Ru/C	straw 450	-	19.7	79.9	0.8	-0.3	93.8
350	Ru/C	straw 450	17.1	29.7	28.9	2.6	21.8	61.2
150;350	Ru/C	straw 450	16.2	25.7	28.5	2.6	27.0	53.4
150;350	Ru/C	bioliq	68.2	29.1	-	4.8	-2.1	88.4

In Table 7.4, the elemental composition of the light and heavy upgraded oils is reported, together with the H/C and O/C ratio. Since the original pyrolysis oil separated during centrifugation, the starting point should be considered its heavy phase with a H/C ratio of 1.34 and O/C 0.22. The general trend observed was increasing H/C and decreasing O/C ratio with increasing temperature, producing an oil with lower oxygen content and better quality. Also in the heavier organic phase at 350 °C, the content of oxygen was decreased in a similar way to the lighter phase. In general the oxygen content in the upgraded oils was inferior to that of beech wood, probably due to the lower content in the original bio-oil. In addition, the starting phase separation helped in decreasing this content to 21%. The deoxygenation degree was reported in relation to the original bio-oil and to its heavy phase in Table 7.4. Considering the heavy phase, the D.O.D was comparable or slightly higher than those of the beech wood experiments, but if the original oil was considered it was much higher. Ru/C exhibited higher activity for higher temperatures, forming products with higher H/C ratio. The bioliq bio-oil exhibited the same trend for H/C, but less hydrodeoxygenation occurred. In summary, hydrotreatment of straw 450 °C bio-oil allowed the production of an upgraded oil with lower content of oxygen, but the products were more viscous and thus more difficult to recover compared to

Table 7.4: Elemental analysis (wet basis) of the bio-oil produced from straw 450 °C bio-oil (original= s. 450; after separation s.h.p.= straw heavy phase, s.l.p.= straw light phase) and upgraded oils at different hydrotreatment temperatures (80, 150, 250, 350, 150/350 °C, 14.0 MPa H_2 at room temperature). H/C and O/C ration are calculated on dry basis. The deoxygenation degree (D.O.D.) is reported considering the original bio-oil (s.450) or the heavy phase after centrifugation (s.h.p.).

	cat.	phase	C (%)	H (%)	O (%)	N (%)	water (%)	H/C	O/C	D.O.D (s. 450)	D.O.D (s.h.p.)
s. 450			49.7	8.5	40.6	1.2	23.7	1.42	0.3	-	-
s.h.p.			60.1	8.3	30.2	1.4	14.4	1.34	0.22	21	-
s.l.p.			21.0	9.6	68.4	1.0	60.6	1.64	0.52	-	-
80	NiCu/Al$_2$O$_3$		62.1	7.8	28.5	1.6	10.3	1.29	0.23	16	0
150	NiCu/Al$_2$O$_3$		57.9	8.6	32.0	1.5	17.4	1.38	0.21	22	1
250	NiCu/Al$_2$O$_3$		66.8	8.7	22.8	1.7	8.6	1.39	0.17	35	18
350	NiCu/Al$_2$O$_3$	light	75.6	9.4	13.7	1.3	2.9	1.44	0.11	55	44
150;350	NiCu/Al$_2$O$_3$	light	75.5	9.6	13.1	1.8	2.6	1.48	0.11	57	45
350	NiCu/Al$_2$O$_3$	heavy	48.1	9.7	41.0	1.2	35.5	1.44	0.15	43	28
150;350	NiCu/Al$_2$O$_3$	heavy	67.8	9.6	21.0	1.6	10.1	1.5	0.13	48	34
80	Ru/C		63.0	7.9	27.4	1.7	9.2	1.31	0.23	17	0
150	Ru/C		62.1	8.3	28.1	1.6	12.7	1.33	0.20	25	5
250	Ru/C		58.4	8.2	31.8	1.6	17.5	1.28	0.21	23	3
350	Ru/C	light	77.4	10.3	10.6	1.8	1.7	1.56	0.09	64	55
150;350	Ru/C	light	77.0	10.4	11.0	1.6	1.8	1.59	0.09	62	52
350	Ru/C	heavy	59.6	10.8	27.7	2.0	20.8	1.71	0.12	55	43
150;350	Ru/C	heavy	49.3	10.2	39.1	1.4	39.5	1.42	0.06	75	68
bioliq	NiCu/Al$_2$O$_3$		67.5	8.7	23.9	4.1	67.5	1.46	0.23	33	-
bioliq	Ru/C		65.1	8.8	26.1	1.95	65.1	1.58	0.28	43	-

the bioliq bio-oil.

In Figure 7.14, the ^{1}H-NMR spectra integration of the upgraded oils (light and heavy phase) and the aqueous phase are reported. In general and as observed previously by elemental analysis, the heavier upgraded oil had different characteristics from the other upgraded oil, due to the variable water content and composition. On the contrary, if the light upgraded oil is considered, some trends are visible.

The alkane region (1.5-0-5 ppm) increased with the temperature in the upgraded oil, as well for the protons alpha to carbonylic/carboxylic/unsaturated groups (3.0-1.5 ppm) with the maximum at 350 °C (similar results with and without stabilisation for the light upgraded oil). The protons alpha to alcohols/etheric bonds (4.3-3.0 ppm) decreased with temperature, as also observed by beech wood. The aromatic protons (8.5-6.0 ppm) decreased slightly with temperature. In the aqueous phase, the soluble compounds decreased with temperature and were constituted mainly by alpha to carbonylic/carboxylic/unsaturated and alpha to alcohols/etheric

bonds. Alkane groups were more concentrated in the light upgraded oil of the wheat straw than in the upgraded oil of the beech wood, but this probably was an effect of the phase separation rather than higher deoxygenation activity. In Figure 7.15, the products of bioliq bio-oil showed similar composition in the case of Ru/C and NiCu/Al$_2$O$_3$ with a higher amount of alkanes in the case of Ru/C as demonstrated by elemental analysis.
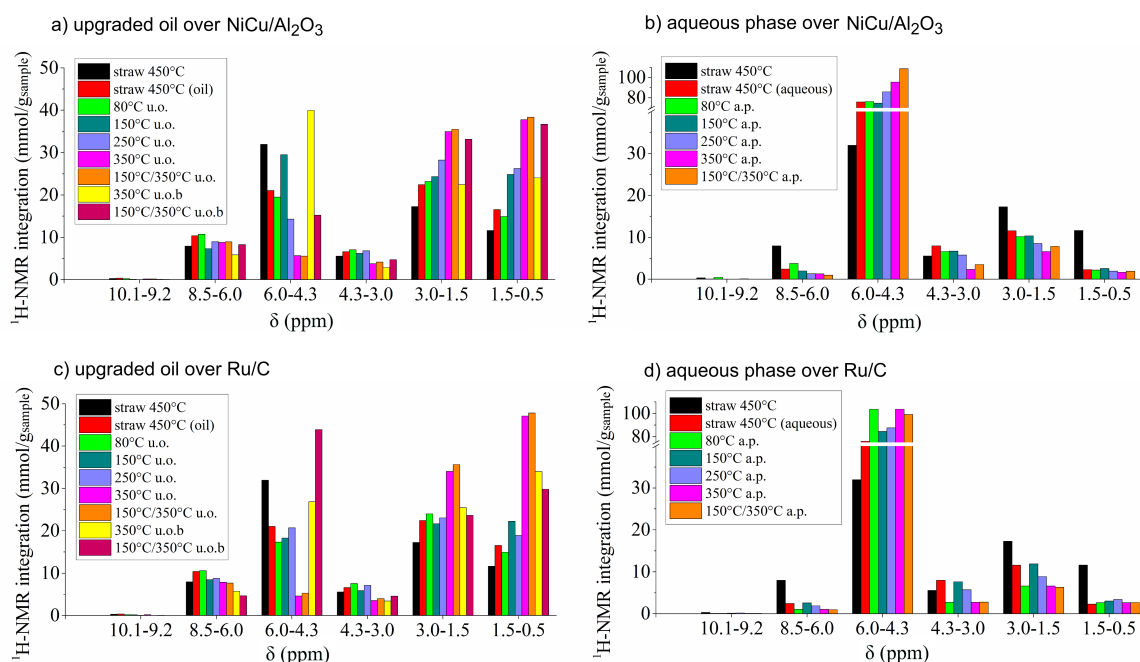
Figure 7.14: ^{1}H-NMR spectra integration of the upgraded oils over NiCu/Al$_2$O$_3$ (a) and the respective aqueous phases (b), and of the upgraded oils over Ru/C (c) and the respective aqueous phases (d) produced from HDO of straw 450 °C bio-oil. "u.o." indicates upgraded oil; "u.o.b." is the upgraded oil with higher density in the case of a three-phase liquid system. The hydrotreatment was performed at 80, 150, 250, 350, 150/350 °C, 14.0 MPa H$_2$ pressurised at room temperature. The assignment of protons to the specific classes of compounds is reported in Table 2.1.

From GC-MS (Figure 7.16 and 7.17), it was demonstrated that the lower hydrogen consumption was associated with lower reactivity of the compounds. On the contrary to beech wood, cyclopentanones were resistant to hydrogenation at 80 °C. This could be associated with poisoning of the catalyst already at low temperatures. In the case of NiCu/Al$_2$O$_3$, cyclopentenones reacted at 150 °C and were converted to cyclopentanones, while in Ru/C methyl-cyclopentanone was converted mainly at 350 °C. This is probably an effect of poisoning of the catalyst already at low temperature and this explains also the elemental composition of the
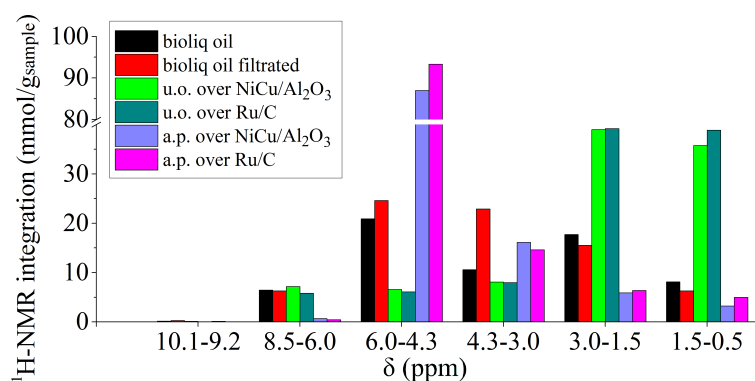
Figure 7.15: ^{1}H-NMR spectra integration of bioliq bio-oil (original and after filtration), of the upgraded oils and the aqueous phase over NiCu/Al$_2$O$_3$ and over Ru/C. Hydrotreatment at 150/350 °C, 14.0 MPa H$_2$ at room temperature. The assignment of protons to the specific classes of compounds is reported in Table 2.1.

upgraded oil over Ru/C at 250 °C, which was similar to the one at 80-150 °C. Furfural reacted at 150 °C as observed in the beech wood products. Alkanes were formed, but qualitatively in lower amounts, while toluene and ethyl-benzene were detected only in the products from wheat straw. At higher temperatures, phenol and alkyl-phenol were predominant, while guaiacol and syringol were completely converted. This tendency was confirmed also in the bioliq upgraded oil, but it was confirmed that the two upgraded oils had different compositions, despite some similarities. Similar compounds to the light upgraded oils were detected in the heavy upgraded oils, but generally the concentration was lower, probably due to the higher water content.

In general, NiCu/Al$_2$O$_3$ was selective for the production of ketones and Ru/C of alcohols-alkanes. Over both catalysts the conversion of aromatics was limited. However, the catalytic activity associated to the intermediate pyrolysis oil from straw was reduced in comparison to the beech wood or the bioliq bio-oil, probably because the heteroatoms poisoned the catalysts that changed/reduced its activity. Studies on the influence of the pyrolysis feedstock on HDO were hardly reported in literature except for Elliott et al. [104] and Elkasabi et al. [243]. Elliott et al. [104] referred mostly to various woody biomass and did not report significant differences in the upgraded oils, justified by similarities already in the original bio-oil composition. On the other hand, Elkasabi et al. [243] investigated switchgrass (herbaceous biomass) and eucalyptus (hard wood). Strikingly, higher hydrogen consumption was associated to eucalyptus, but lower oxygen content of the upgraded oil from switchgrass, although the original bio-oils had similar content. This result is analogous to the case reported in this section and it could indicate that the bio-oil

composition could favour hydrogenation (more probable in hard wood), compared to HDO (more probable in herbaceous biomass).
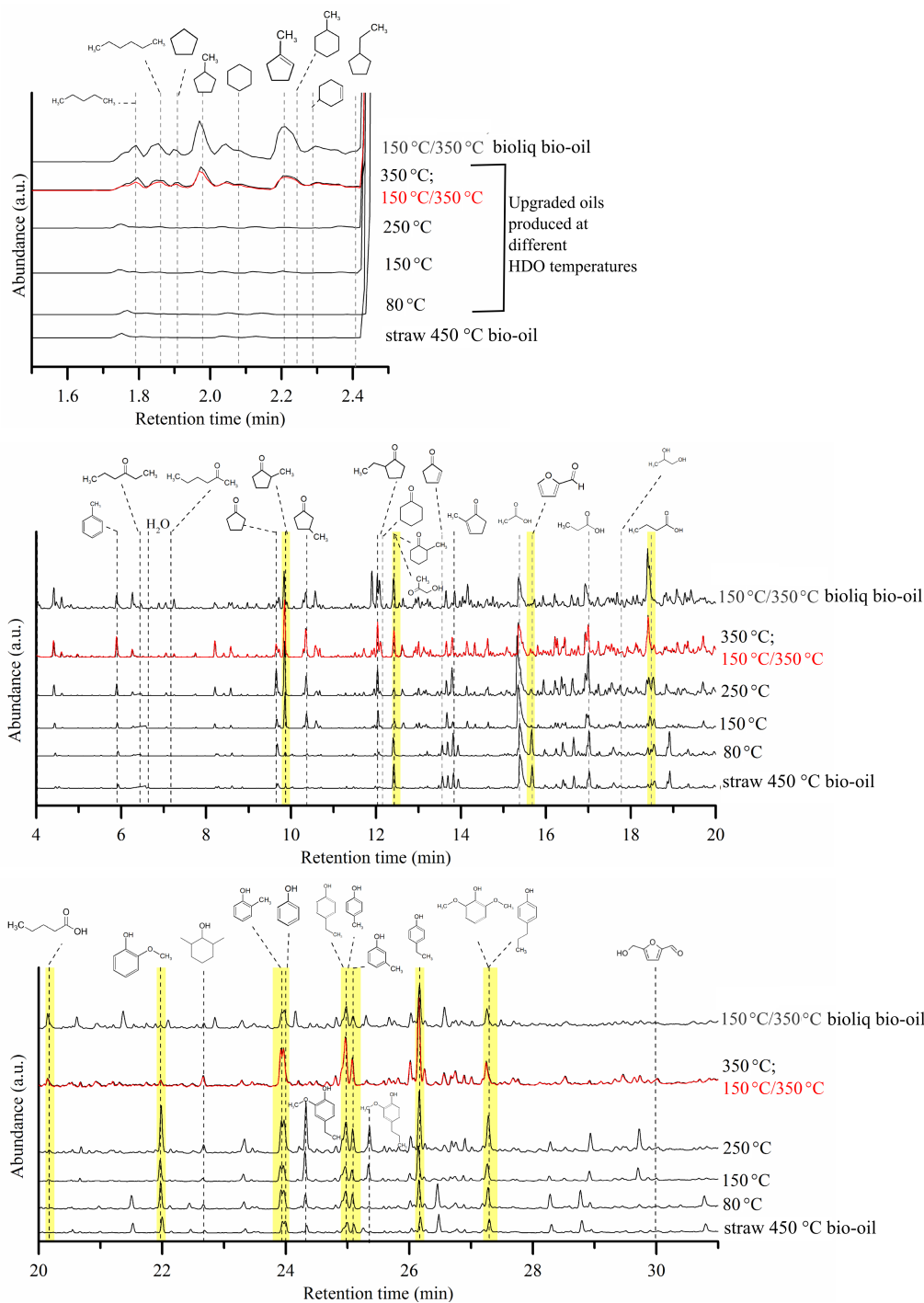
Figure 7.16: GC-MS of the original bio-oil (straw 450 °C) and the upgraded oils produced at different hydrotreatment temperatures over NiCu/Al$_2$O$_3$.
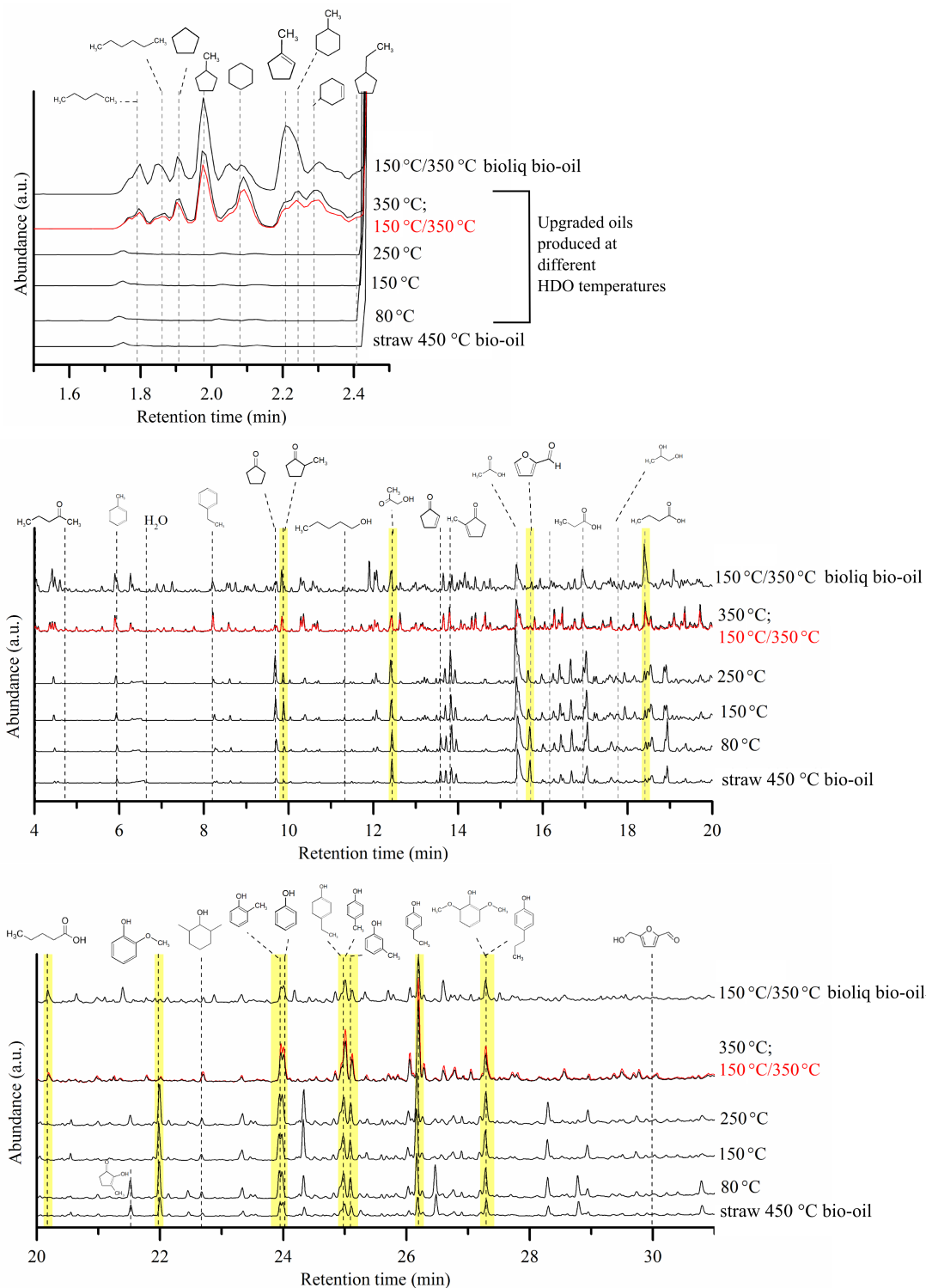
Figure 7.17: GC-MS of the original bio-oil (straw 450 °C) and the upgraded oils produced at different hydrotreatment temperatures over Ru/C.

7.5 Analysis of the spent catalysts

Analysis of the spent catalysts offered an overview about the deactivation processes which occurred. It was possible to determine the carbon deposition only for $NiCu/Al_2O_3$, since the ruthenium catalyst was supported on carbon and the weight of the recovered catalyst was similar to the original. The carbon deposits on the $NiCu/Al_2O_3$ varied from 2.7-6.3% (of the catalyst weight) for the beech wood feedstock to 8.4-16.3% for wheat straw produced by intermediate pyrolysis (Table 7.5). The pre-coat filtration of the bioliq bio-oil (fast pyrolysis) limited the solid deposit to 4.2%. The dependence on the temperature was not clear, but a minimum was observed at 250 °C.

Table 7.5: Carbon, nitrogen and sulphur deposited on the catalyst surface measured by elemental analysis and reported as percentage of the mass of the catalyst.

Bio-oil	Upgrading temperature (°C)	C (%)		N (%)		S (%)	
		$NiCu/Al_2O_3$	Ru/C	$NiCu/Al_2O_3$	Ru/C	$NiCu/Al_2O_3$	Ru/C
beech 450 °C	80	2.7	79.5	0.1	0.5	0.2	0.3
	150	6.3	81.1	0.2	0.5	0.2	0.2
	250	3.6	81.4	0.1	0.5	0.3	0.3
	350	5.0	84.2	0.1	0.5	0.4	0.4
	150;350	6.0	84.3	0.1	0.5	0.4	0.4
beech 350 °C	150;350	3.5	79.9	0.1	0.5	0.3	0.4
beech 400 °C	150;350	4.2	82.0	0.1	0.5	0.4	0.4
beech 450 °C	150;350	6.0	84.3	0.1	0.5	0.4	0.4
beech 500 °C	150;350	3.1	84.7	0.1	0.5	0.4	0.4
straw 450 °C	80	16.3	79.2	0.9	1.5	0.6	0.5
	150	13.7	80.1	0.6	1.7	1.2	0.8
	250	8.4	82.5	0.4	1.2	2.6	0.8
	350	12.8	82.9	0.2	0.9	2.8	1.1
	150;350	10.3	83.5	0.2	1.0	2.6	1.0
bioliq	150;350	4.2	82.0	0.1	0.9	1.0	0.7

Nitrogen was found in limited quantities on the catalyst surface for experiments with beech wood, but higher quantities were reported for straw 450 °C bio-oil with a decreasing tendency at higher temperatures. Sulphur was observed on the catalyst surface for both feedstocks and for both catalysts, with higher concentration at higher temperatures (Table 7.5). Beech wood pyrolysis oil had a sulfur concentration less than 0.005%, but it was present on the catalyst surface in concentration 0.2-0.4 wt.%. In XRD (Figure 7.18) no reflections of Ni_3S_2 were monitored, indicating probably that the adsorption was limited to an external layer (Chapter 6).

The pyrolysis oil from straw had higher sulphur concentration, which drove
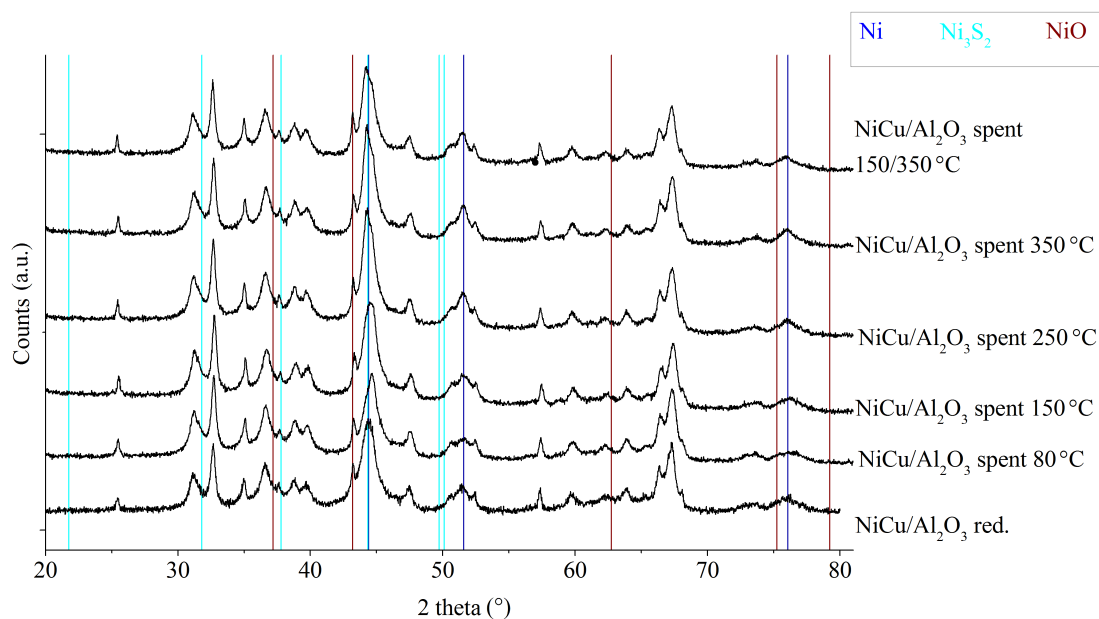
Figure 7.18: XRD pattern of the spent catalyst NiCu/Al$_2$O$_3$ used at different hydrotreatment temperatures with beech 450 °C bio-oil.
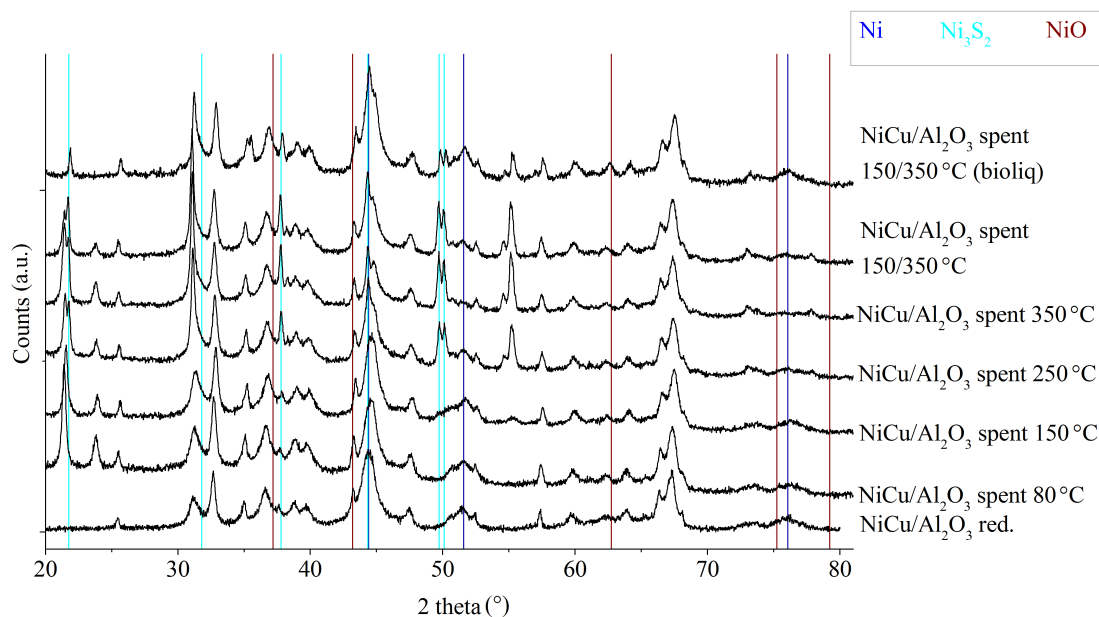
Figure 7.19: XRD pattern of the spent catalyst NiCu/Al$_2$O$_3$ used at different hydrotreatment temperatures with straw 450 °C bio-oil. In comparison the XRD pattern of the catalyst used with the bioliq bio-oil.

formation of bulk Ni_3S_2 (especially above 250 °C), observed in the XRD patterns (Figure 7.19). The formation of this mineral could result in sintering of the nanoparticles, as observed by SEM-EDX. The elemental analysis shows that Ru/C was also affected by sulphur deposition, but it was not possible to monitor it by XRD. XRD pattern showed that the alumina catalyst support was converted into boehmite when in contact with the bio-oil procuded from wheat straw. This was not observed in the beech wood pyrolysis oil, despite the water content being similar to the one of bioliq bio-oil. For further developments, other supports with greater water resistance, like silica, should be used for HDO. Leaching was a phenomenon important only at 80°C in the case of $NiCu/Al_2O_3$ (circa 20% of the active metal in case of straw bio-oil), while it was generally negligible in comparison to other deactivation processes observed (less than 1%).

7.6 Conclusions

The results presented in this chapter showed that different process parameters, like pyrolysis temperature, pyrolysis feedstock, HDO temperature and catalyst, influenced the upgraded oil composition. The pyrolysis temperature was responsible for producing bio-oil with a slightly different composition, which in turn affected the characteristics of the upgraded oils in a less accentuated way. Higher deoxygenation degree was obtained for bio-oil pyrolyzed at higher temperatures. However, taking also the bio-oil yield and the carbon recovery into account, pyrolysis at 450 °C was found to give the optimal results.

The HDO catalysts had also a fundamental role in the conversion and selectivity of the products: $NiCu/Al_2O_3$ produced mainly ketones, while Ru/C was more active in hydrogenation/hydrodeoxygenation producing more alcohols and alkanes. Both catalysts did not significantly convert aromatics, which could be theoretically separated and used as fine chemicals. The choice of one of these catalysts should be dependent on the product desired and on the hydrogen consumption, which was higher for Ru/C.

The study of the hydrotreating temperature permitted to define the main characteristics of the upgraded oil (elemental composition and deoxygenation degree) and the reactivity of different classes of compounds at 80, 150, 250, 350 °C (with/without stabilization at 150 °C). Temperatures from 80 °C to 150 °C were suitable for the stabilization of the beech wood oil, hydrogenating mainly olefins (80 °C) and aldehydes (150 °C), and obtaining a single liquid phase. The temperature

250 °C was suitable for a mild hydrotreatment, decreasing the oxygen content (D.O.D. 18.5-18.6%), but without a significant production of hydrocarbons. The temperature 350 °C resulted in higher deoxygenation degree and a significant amount of hydrocarbons. In general, the deoxygenation degree was similar for $NiCu/Al_2O_3$ and Ru/C, but higher hydrogenation activity was monitored for Ru/C. The stabilization step had only a small influence on the quality of the products.

The feedstock influenced also the quality of the upgraded oil. Beech 450 °C bio-oil had higher phase stability, showing phase separation only at temperatures above 250 °C. Phase separation for straw 450 °C bio-oil appeared already at 80 °C and at 350 °C three phases (light organic phase, aqueous phase, heavy organic phase) were collected. In addition, straw 450 °C bio-oil had the disadvantage of containing higher concentrations of heteroatoms, especially sulphur (0.3%). This was demonstrated to deactivate the catalyst forming Ni_3S_2 and to provoke sintering. In the case of beech wood, sulphur was also deposited on the nickel surface, but it was limited to a thin layer as demonstrated in Chapter 6. Sulphur deposition was also detected on Ru/C. Therefore nickel or ruthenium catalysts should be avoided when the concentration of sulphur is too high. For low amounts of sulphur the catalyst seems stable at least for tests over short periods, but long term studies should be further investigated.

Conclusions

In this thesis hydrotreatment of pyrolysis oils was considered a promising strategy to provide upgraded oils with less oxygen content, higher stability and higher quality than the original feed. The evaluation of a relatively new class of HDO catalysts with nickel as the active metal showed good prospects for producing upgraded oils that could be applied in future for the production of transport fuels and chemicals.

A central facet of the thesis dealt with hydrotreatment of pyrolysis oil produced from wheat straw. As a non-woody biomass, pyrolysis of wheat straw offers a potential route to valorisation of a widely available agricultural residue. However, the bio-oils produced usually exhibit phase instability. As reported in this work, a bio-oil produced by fast pyrolysis of wheat straw in the bioliq plant showed spontaneous phase separation, resulting in a light phase (containing mainly sugar derivatives and water) and a heavy phase (containing mainly lignin derivatives). Although the phase separation can be considered as a disadvantage at first sight for further hydroprocessing, it turned out to be a possible strategy for treating two different compound classes separately with two distinct optimal sets of conditions. However, the excessive solid content in the heavy phase excludes the possibility for its hydrotreatment and makes this feed more suitable for gasification. On the other hand the light phase was an easier system to characterise compared to the whole bio-oil and was more suitable for a study of the reactivity of certain classes of compounds.

Different nickel-based catalysts were tested in HDO of the light phase at 250 °C and 340 °C: Ni/Al_2O_3, $NiCu/Al_2O_3$, Ni/SiO_2, Ni/ZrO_2, NiW/AC and Ni/TiO_2. Ru/C was used as a benchmark. All nickel catalysts showed similar activity with a slightly superior performance of $NiCu/Al_2O_3$, enhanced by the presence of copper that probably promoted hydrogen spill over. Ru/C provided a similar deoxygenation degree of the products, but the upgraded oils had higher H/C ratios, leading to a higher hydrogen consumption. The oxygen content was generally decreased from 40% in the original feed, to 20-26% for HDO at 250 °C and to 12-15% at 340 °C.

The upgraded oil yields were not more than 18 wt.%, but in this phase the main amount of carbon content (R.C. 50% at 250 °C and 60% at 340 °C) and the energy (HHV of the upgraded oils 30-37 MJ/kg) of the light phase were concentrated. Using GC-MS and quantitative ^{1}H-NMR, nickel catalysts were found to be active for the production of ketones, and prevented further hydrogenation of this compound class and of the aromatic ring at both temperatures studied. Ru/C showed higher activity during HDO, producing mostly alcohols at 250 °C and a significant percentage of hydrocarbons at 340 °C. Hydrotreatment over nickel catalysts and Ru/C was successful in converting a non-valuable fraction containing mainly sugar derivatives and water, into an upgraded oil with lower oxygen content which could be suitable for further processing in a refinery.

A comparison between model compounds and pyrolysis oils over NiCu/Al$_2$O$_3$ and Ru/C showed different reactivity for the same components in the two different environments. For example NiCu/Al$_2$O$_3$ was an effective HDO catalyst for the conversion of phenol in aqueous solution, obtaining selectivity of 85% to cyclohexane at 340 °C. Under the same conditions, phenol in pyrolysis oil was mainly resistant to HDO. The reactivity in pyrolysis oil was more profoundly investigated using phenol-d$_6$. These studies showed that the main fraction of phenol was not converted and exhibited only proton exchange in ortho- and para-positions of the aromatic ring with the medium, as a result of the high temperature and acid environment. The HDO of D-glucose, representative of sugar derivatives, was analogously investigated in aqueous solution and in pyrolysis oil. In aqueous solution, D-glucose was converted selectively to methane, showing that the conditions used favored hydrocracking and that this temperature (340 °C) was too high for HDO. On the contrary D-glucose in pyrolysis oil was converted to a complex mixture of liquid components, recovered mainly in the upgraded oil as a result of dehydration, HDO and hydrogenation processes. Therefore the reaction environment (solvent, acidity, impurities, etc.) played a crucial role in HDO and these parameters should be considered and included in future HDO studies with model compounds.

For further exploring the reasons for the discrepancy between the reactivity of model compounds in the two different media, a comparison of the physical and chemical characteristics of the NiCu/Al$_2$O$_3$ catalyst before and after the reaction was conducted. The fresh catalyst was composed of nickel-copper alloyed nanoparticles (in the range of 4-20 nm) supported on theta alumina. The ratio of Ni:Cu was on average 9:1, but with a slightly higher accumulation of copper in proximity to the surface. Analysis of the spent catalysts showed that the catalyst surface was

covered by coke and other inorganic elements like K, Ca, Mg, P and S. Sulphur adsorbed on the nickel-nanoparticle surface and formed a thin layer of Ni_3S_2, which was identified as the main poison affecting the conversion and selectivity of the catalyst. In particular, this inhibited the further conversion of phenolic compounds and ketones. The regeneration procedure adopted (calcination followed by reduction at 500 °C) permitted removal of coke from the surface, but minerals and sulphur were still present. The presence of calcium on the surface could have a dual role: it could block the catalyst sites, but it could also prevent irreversible deactivation of the catalyst by forming a calcium salt with sulphur and facilitating nickel reduction under hydrogen pressure. To avoid the problem of minerals obstructing the surface during HDO, hot vapour filtration downstream to pyrolysis is a good solution that can prolong the catalyst lifespan. The regenerated catalyst used again with pyrolysis oil showed a slightly lower activity in term of hydrogen consumption (circa 85% of the fresh catalyst), but the same selectivity towards ketones and no significant conversion of phenolic compounds. This demonstrated that the catalyst activity was similar, showing that probably pyrolysis oil affected the catalyst performance already at the beginning of the reaction for the fresh and regenerated catalyst. When Ni_3S_2 was present only as a thin layer, minimal structural change were observed, however when the feed contained high concentration of sulphur, bulk Ni_3S_2 was formed and intense sintering affected the catalyst structure. Therefore, if sulphur adsorption could be controlled and limited to the surface, nickel catalysts could potentially be used for the production of phenolic components and ketones from biomass. In general the upgraded oils produced by nickel catalysts were of higher quality than the original pyrolysis oil, showing higher HHV, better stability and lower coking tendency (TGA measurements), properties which could allow product separation by distillation. Considering these results, hydrotreating processes could be addressed to the production of chemicals from biomass, with higher economic value than fuels and employing at the same time less hydrogen.

In the last section of the thesis, different process parameters of pyrolysis and hydrotreatment, including feedstock, pyrolysis temperature, HDO temperature and catalyst type were systematically varied in order to monitor their influence on the upgraded products. Different pyrolysis oils were used for this target and they were produced from wheat straw and beech wood, by fast and intermediate pyrolysis, and at different pyrolysis temperatures in the case of beech wood. Bio-oils produced from beech wood were easier to handle than those from wheat straw, thanks to their phase stability and the low content of minerals and heteroatoms, which otherwise

would affect the catalytic activity of $NiCu/Al_2O_3$ and Ru/C. Bio-oils produced by intermediate pyrolysis showed lower molecular weight compounds and lower viscosity than those produced by fast pyrolysis, but the bio-oil yield of the former process was lower. Hot vapour filtration performed downstream to intermediate pyrolysis provided an oil with negligible amount of solids and minerals, offering therefore a better substrate for HDO. Pyrolysis temperature was responsible for producing bio-oil with a slightly different composition, resulting in a oil with lower oxygen content at higher temperatures (oxygen range 33.1-26.8% between 350-500 °C). In general the bio-oil composition affected in turn, but in a less accentuated way, the characteristics of the upgraded oils. However, using a bio-oil from intermediate pyrolysis at 450 °C instead of 500 °C (despite containing more oxygen) was more advantageous in terms of bio-oil yield and carbon recovery, since pyrolysis at higher temperature has higher gaseous product yield at the expense of liquid yield. The catalyst had an important role in the conversion and selectivity of the products: $NiCu/Al_2O_3$ produced upgraded oils containing mainly ketones, whereas Ru/C resulted in upgraded oils with higher concentration of alcohols and alkanes. Both catalysts did not significantly convert aromatics, which could be theoretically separated and used as fine chemicals. Hydrotreating temperature had a pronounced influence on the products formed and on the deoxygenation degree. Studying the reactivity of different functional groups depending on the temperature permitted definition of the upgraded oil quality obtained at each temperature. Therefore, depending on the quality requested for a specific application, an optimal hydrotreatment temperature could be chosen. Olefins were mainly hydrogenated at 80 °C, aldehydes at 150 °C. These two low temperatures can be considered for stabilisation. At 250 °C mainly ketones were produced over $NiCu/Al_2O_3$ and alcohols over Ru/C, and in general the pyrolysis oil had a significant decrement in the oxygen content with a D.O.D. between 18-35%. At 350 °C the main products over $NiCu/Al_2O_3$ were still ketones, while for Ru/C alcohols and a significant percentage of hydrocarbons. The D.O.D at this temperature was between 34-75%.

In future, studies should be addressed to monitor the stability of nickel catalysts in a long-term reaction, and the feasibility of distillation as a separation method for valuable products. For long-term operation, a trickle bed reactor for HDO was planned and is currently under construction at IKFT/KIT. It will be online in the next year, with an operational range up to 400 °C and 40 MPa. Concerning the catalyst, theta alumina was found in the majority of cases to be resistant to water, but in some it was converted to boehmite. For this reason, the use

of inorganic supports with higher resistance to water is encouraged. However, the combination of copper and nickel was found to be a good system and this combination of active metals should be further investigated. At first, experiments should be run with model compounds in order to optimise the conditions and determine the main parameters of the reaction in the continuous reactor. Following this, hydrodeoxygenation should be performed with pyrolysis oil, preferentially hot vapour filtrated in order to avoid deposition of minerals. The catalyst deactivation should be monitored and characterised by the combination of several complementary characterisation techniques. Apart from those shown in this thesis, further studies could exploit XAS for detailed characterisation of the catalyst structure. *Operando* studies could be very interesting in order to understand the origin of the deactivation processes, but limitations related to the reaction cell for the measurement are usually present for the range of temperature and pressure employed. In case the catalyst is not stable to sulphur for long periods, alternative solutions should be proposed and tested, like the use of promoters to make Ni more stable or adsorbers that could bind sulphur selectively and preferentially, such as Mo, B (reported in literature) or maybe Ca as observed in this work.

References

[1] R. Wurzel and J. Connelly, *The European Union as a Leader in International Climate Change Politics.* Routledge, 2010.

[2] W. P. M. v. Swaaij, S. R. A. Kersten, and W. Palz, *Biomass Power for the World.* CRC Press, 2015.

[3] G. W. Huber, S. Iborra, and A. Corma, "Synthesis of Transportation Fuels from Biomass: Chemistry, Catalysts, and Engineering," *Chemical Reviews*, vol. 106, no. 9, pp. 4044–4098, 2006.

[4] A. V. Bridgwater and D. G. B. Boocock, *Developments in Thermochemical Biomass Conversion.* Springer, 1996.

[5] M. Fatih Demirbas, "Biorefineries for biofuel upgrading: A critical review," *Applied Energy*, vol. 86, Supplement 1, pp. S151–S161, 2009.

[6] M. J. Groeneveld, "The change from fossil to solar and biofuels needs our energy," *Inaugural Lecture. University of Twente, Enchede*, 2008. *doc.utwente.nl/67339/1/rede_Groeneveld.pdf*, accessed on October 2016.

[7] A. Bridgwater and G. Peacocke, "Fast pyrolysis processes for biomass," *Renewable and Sustainable Energy Reviews*, vol. 4, no. 1, pp. 1–73, 2000.

[8] H. Chen, T. N. Cong, W. Yang, C. Tan, Y. Li, and Y. Ding, "Progress in electrical energy storage system: A critical review," *Progress in Natural Science*, vol. 19, no. 3, pp. 291–312, 2009.

[9] B. Kamm, P. R. Gruber, and M. Kamm, *Biorefineries – Industrial Processes and Products: Status Quo and Future Directions.* Wiley, 2010.

[10] N. Dahmen, E. Dinjus, T. Kolb, U. Arnold, H. Leibold, and R. Stahl, "State of the art of the bioliq® process for synthetic biofuels production," *Environmental Progress & Sustainable Energy*, vol. 31, no. 2, pp. 176–181, 2012.

[11] N. Dahmen, U. Arnold, N. Djordjevic, T. Henrich, T. Kolb, H. Leibold, and J. Sauer, "High Pressure in Synthetic Fuels Production," *The Journal of Supercritical Fluids*, vol. 96, pp. 124 – 132, 2015.

[12] A. J. Ragauskas, C. K. Williams, B. H. Davison, G. Britovsek, J. Cairney, C. A. Eckert, W. J. Frederick, J. P. Hallett, D. J. Leak, C. L. Liotta, J. R. Mielenz, R. Murphy, R. Templer,

and T. Tschaplinski, "The path forward for biofuels and biomaterials," *Science*, vol. 311, no. 5760, pp. 484–489, 2006.

[13] L. Gustavsson, P. Börjesson, B. Johansson, and P. Svenningsson, "Reducing CO_2 emissions by substituting biomass for fossil fuels," *Energy*, vol. 20, no. 11, pp. 1097–1113, 1995.

[14] S. N. Naik, V. V. Goud, P. K. Rout, and A. K. Dalai, "Production of first and second generation biofuels: A comprehensive review," *Renewable and Sustainable Energy Reviews*, vol. 14, no. 2, pp. 578–597, 2010.

[15] R. A. Lee and J.-M. Lavoie, "From first– to third–generation biofuels: Challenges of producing a commodity from a biomass of increasing complexity," *Animal Frontiers*, vol. 3, no. 2, pp. 6–11, 2013.

[16] V. Balan, "Current Challenges in Commercially Producing Biofuels from Lignocellulosic Biomass," *International Scholarly Research Notices, International Scholarly Research Notices*, vol. 2014, pp. 31, ID e463074, 2014.

[17] T. Damartzis and A. Zabaniotou, "Thermochemical conversion of biomass to second generation biofuels through integrated process design—A review," *Renewable and Sustainable Energy Reviews*, vol. 15, no. 1, pp. 366–378, 2011.

[18] R. E. H. Sims, W. Mabee, J. N. Saddler, and M. Taylor, "An overview of second generation biofuel technologies," *Bioresource Technology*, vol. 101, no. 6, pp. 1570–1580, 2010.

[19] A. Alaswad, M. Dassisti, T. Prescott, and A. G. Olabi, "Technologies and developments of third generation biofuel production," *Renewable and Sustainable Energy Reviews*, vol. 51, pp. 1446–1460, 2015.

[20] A. Singh and S. I. Olsen, "A critical review of biochemical conversion, sustainability and life cycle assessment of algal biofuels," *Applied Energy*, vol. 88, no. 10, pp. 3548–3555, 2011.

[21] L. Brennan and P. Owende, "Biofuels from microalgae—A review of technologies for production, processing, and extractions of biofuels and co-products," *Renewable and Sustainable Energy Reviews*, vol. 14, no. 2, pp. 557–577, 2010.

[22] I. Hariskos and C. Posten, "Biorefinery of microalgae – opportunities and constraints for different production scenarios," *Biotechnology Journal*, vol. 9, no. 6, pp. 739–752, 2014.

[23] J. J. Milledge and S. Heaven, "A review of the harvesting of micro-algae for biofuel production," *Reviews in Environmental Science and Bio/Technology*, vol. 12, no. 2, pp. 165–178, 2012.

[24] S. Nanda, R. Azargohar, A. K. Dalai, and J. A. Kozinski, "An assessment on the sustainability of lignocellulosic biomass for biorefining," *Renewable and Sustainable Energy Reviews*, vol. 50, no. C, pp. 925–941, 2015.

[25] D. A. Bulushev and J. R. H. Ross, "Catalysis for conversion of biomass to fuels via pyrolysis and gasification: A review," *Catalysis Today*, vol. 171, no. 1, pp. 1–13, 2011.

[26] A. Kumar, D. D. Jones, and M. A. Hanna, "Thermochemical Biomass Gasification: A Review of the Current Status of the Technology," *Energies*, vol. 2, no. 3, pp. 556–581, 2009.

[27] P.L. Spath and D. Dayton, *Preliminary Screening–Technical and Economic Assessment of Synthesis Gas to Fuels and Chemicals with Emphasis on the Potential for Biomass-Derived Syngas.* DIANE Publishing, 2003.

[28] H. Schulz, "Short history and present trends of Fischer–Tropsch synthesis," *Applied Catalysis A: General*, vol. 186, no. 1–2, pp. 3–12, 1999.

[29] P. Forzatti, E. Tronconi, and I. Pasquon, "Higher Alcohol Synthesis," *Catalysis Reviews*, vol. 33, no. 1-2, pp. 109–168, 1991.

[30] K. M. Walter, M. Schubert, W. Kleist, and J.-D. Grunwaldt, "Effect of the addition of ethanol to synthesis gas on the production of higher alcohols over Cs and Ru modified Cu/ZnO catalysts," *Industrial & Engineering Chemistry Research*, vol. 54, no. 5, pp. 1452–1463, 2015.

[31] A. Bridgwater, "Review of fast pyrolysis of biomass and product upgrading," *Biomass and Bioenergy*, vol. 38, pp. 68–94, 2012.

[32] P. Mortensen, J.-D. Grunwaldt, P. Jensen, K. Knudsen, and A. Jensen, "A review of catalytic upgrading of bio-oil to engine fuels," *Applied Catalysis A: General*, vol. 407, no. 1–2, pp. 1–19, 2011.

[33] R. Venderbosch, A. Ardiyanti, J. Wildschut, A. Oasmaa, and H. Heeres, "Stabilization of biomass-derived pyrolysis oils," *Journal of Chemical Technology & Biotechnology*, vol. 85, no. 5, pp. 674–686, 2010.

[34] F. de Miguel Mercader, *Pyrolysis oil upgrading for co-processing in standard refinery units.* PhD thesis, University Twente, 2010.

[35] D. C. Elliott, "Historical Developments in Hydroprocessing Bio-oils," *Energy & Fuels*, vol. 21, no. 3, pp. 1792–1815, 2007.

[36] D. C. Elliott, "Biofuel from fast pyrolysis and catalytic hydrodeoxygenation," *Current Opinion in Chemical Engineering*, vol. 9, pp. 59–65, 2015.

[37] D. C. Elliott, "Transportation fuels from biomass via fast pyrolysis and hydroprocessing," *Wiley Interdisciplinary Reviews: Energy and Environment*, vol. 2, no. 5, pp. 525–533, 2013.

[38] A. H. Zacher, M. V. Olarte, D. M. Santosa, D. C. Elliott, and S. B. Jones, "A review and perspective of recent bio-oil hydrotreating research," *Green Chemistry*, vol. 16, no. 2, pp. 491–515, 2014.

[39] D. B. S. Arbogast, "Advanced biofuels from pyrolysis oil… Opportunities for cost reduction," *Fuel Processing Technology*, vol. 106, pp. 518–525, 2013.

[40] E. Butler, G. Devlin, D. Meier, and K. McDonnell, "A review of recent laboratory research and commercial developments in fast pyrolysis and upgrading," *Renewable & Sustainable Energy Reviews*, vol. 15, no. 8, pp. 4171–4186, 2011.

[41] M. Bykova, D. Ermakov, S. Khromova, A. Smirnov, M. Lebedev, and V. Yakovlev, "Stabilized Ni-based catalysts for bio-oil hydrotreatment: Reactivity studies using guaiacol," *Catalysis Today*, vol. 220–222, pp. 21 – 31, 2014.

[42] Z. He and X. Wang, "Hydrodeoxygenation of model compounds and catalytic systems for pyrolysis bio-oils upgrading," *Catalysis for Sustainable Energy*, vol. 1, pp. 28–52, 2012.

[43] S. Czernik and A. V. Bridgwater, "Overview of Applications of Biomass Fast Pyrolysis Oil," *Energy & Fuels*, vol. 18, no. 2, pp. 590–598, 2004.

[44] F. de Miguel Mercader, M. J. Groeneveld, S. R. A. Kersten, N. W. J. Way, C. J. Schaverien, and J. A. Hogendoorn, "Production of advanced biofuels: Co-processing of upgraded pyrolysis oil in standard refinery units," *Applied Catalysis B: Environmental*, vol. 96, no. 1–2, pp. 57–66, 2010.

[45] M. J. Antal, *Biomass Pyrolysis: A Review of the Literature Part 1—Carbohydrate Pyrolysis*, pp. 61–111. Boston, MA: Springer New York, 1985.

[46] M. J. Antal, *Biomass Pyrolysis: A Review of the Literature Part 2—Lignocellulose Pyrolysis*, pp. 175–255. Boston, MA: Springer US, 1985.

[47] A. Bridgwater, D. Meier, and D. Radlein, "An overview of fast pyrolysis of biomass," *Organic Geochemistry*, vol. 30, no. 12, pp. 1479–1493, 1999.

[48] H. Yang, R. Yan, H. Chen, D. H. Lee, and C. Zheng, "Characteristics of hemicellulose, cellulose and lignin pyrolysis," *Fuel*, vol. 86, no. 12–13, pp. 1781–1788, 2007.

[49] A. Bridgwater, "Principles and practice of biomass fast pyrolysis processes for liquids," *Journal of Analytical and Applied Pyrolysis*, vol. 51, no. 1–2, pp. 3–22, 1999.

[50] D. Meier and O. Faix, "State of the art of applied fast pyrolysis of lignocellulosic materials — a review," *Bioresource Technology*, vol. 68, no. 1, pp. 71–77, 1999.

[51] S. R. A. Kersten, X. Wang, W. Prins, and W. P. M. van Swaaij, "Biomass pyrolysis in a fluidized bed reactor. part 1: Literature review and model simulations," *Industrial & Engineering Chemistry Research*, vol. 44, no. 23, pp. 8773–8785, 2005.

[52] S. Kersten and M. Garcia-Perez, "Recent developments in fast pyrolysis of ligno-cellulosic materials," *Current Opinion in Biotechnology*, vol. 24, no. 3, pp. 414–420, 2013.

[53] M. I. Jahirul, M. G. Rasul, A. A. Chowdhury, and N. Ashwath, "Biofuels production through biomass pyrolysis —a technological review," *Energies*, vol. 5, no. 12, p. 4952, 2012.

[54] M. Tomasi Morgano, H. Leibold, F. Richter, and H. Seifert, "Screw pyrolysis with integrated sequential hot gas filtration," *Journal of Analytical and Applied Pyrolysis*, vol. 113, pp. 216–224, 2015.

[55] A. Hornung, ed., *Transformation of Biomass: Theory to Practice.* Wiley, 2014.

[56] R. Venderbosch and W. Prins, "Fast pyrolysis technology development," *Biofuels, Bioproducts and Biorefining*, vol. 4, no. 2, pp. 178–208, 2010.

[57] "http://www.ensyn.com/," accessed on 20 October 2016.

[58] "http://www.dynamotive.com/," accessed on 20 October 2016.

[59] "https://www.btg-btl.com/en/company/projects/empyro," accessed on 20 October 2016.

[60] "http://www.pyne.co.uk/," accessed on 20 October 2016.

[61] M. S. Talmadge, R. M. Baldwin, M. J. Biddy, R. L. McCormick, G. T. Beckham, G. A. Ferguson, S. Czernik, K. A. Magrini-Bair, T. D. Foust, P. D. Metelski, C. Hetrick, and M. R. Nimlos, "A perspective on oxygenated species in the refinery integration of pyrolysis oil," *Green Chem.*, vol. 16, pp. 407–453, 2014.

[62] A. Oasmaa, E. Kuoppala, A. Ardiyanti, R. H. Venderbosch, and H. J. Heeres, "Characterization of Hydrotreated Fast Pyrolysis Liquids," *Energy & Fuels*, vol. 24, no. 9, pp. 5264–5272, 2010.

[63] A. Oasmaa and C. Peacocke, *Properties and fuel use of biomass-derived fast pyrolysis liquids A guide.* VTT Publications 731, 2010.

[64] A. Oasmaa and E. Kuoppala, "Solvent fractionation method with brix for rapid characterization of wood fast pyrolysis liquids," *Energy & Fuels*, vol. 22, no. 6, pp. 4245–4248, 2008.

[65] A. Oasmaa, C. Peacocke, S. Gust, D. Meier, and R. McLellan, "Norms and Standards for Pyrolysis Liquids. End-User Requirements and Specifications," *Energy & Fuels*, vol. 19, no. 5, pp. 2155–2163, 2005.

[66] A. Oasmaa, E. Kuoppala, and D. C. Elliott, "Development of the Basis for an Analytical Protocol for Feeds and Products of Bio-oil Hydrotreatment," *Energy & Fuels*, vol. 26, no. 4, pp. 2454–2460, 2012.

[67] D. Meier and M. Windt, "Analysis of bio-oil," in *Transformation of biomass - Theory to practise*, pp. 227–256, Chichester, UK: John Wiley & Sons Ltd., 2014.

[68] D. Meier and O. Faix, "State of the art of applied fast pyrolysis of lignocellulosic materials — a review," *Bioresource Technology*, vol. 68, no. 1, pp. 71–77, 1999.

[69] A. Oasmaa, I. Fonts, M. R. Pelaez-Samaniego, M. E. Garcia-Perez, and M. Garcia-Perez, "Pyrolysis oil multiphase behavior and phase stability: A review," *Energy & Fuels*, vol. 30, no. 8, pp. 6179–6200, 2016.

[70] A. Oasmaa, A. Källi, C. Lindfors, D. C. Elliott, D. Springer, C. Peacocke, and D. Chiaramonti, "Guidelines for Transportation, Handling, and Use of Fast Pyrolysis Bio-Oil. 1. Flammability and Toxicity," *Energy & Fuels*, vol. 26, no. 6, pp. 3864–3873, 2012.

[71] J. Lehto, A. Oasmaa, Y. Solantausta, M. Kytö, and D. Chiaramonti, "Review of fuel oil quality and combustion of fast pyrolysis bio-oils from lignocellulosic biomass," *Applied Energy*, vol. 116, pp. 178–190, 2014.

[72] J. Lehto, A. Oasmaa, Y. Solantausta, M. Kytö, and D. Chiaramonti, "Fuel oil quality and combustion of fast pyrolysis bio-oils," tech. rep., VTT Publications, 2013.

[73] J. Scahill, J. P. Diebold, and C. Feik, *Removal of Residual Char Fines from Pyrolysis Vapors by Hot Gas Filtration*, pp. 253–266. Dordrecht: Springer Netherlands, 1997.

[74] R. M. Baldwin and C. J. Feik, "Bio-oil stabilization and upgrading by hot gas filtration," *Energy & Fuels*, vol. 27, no. 6, pp. 3224–3238, 2013.

[75] D. C. Elliott, H. Wang, R. French, S. Deutch, and K. Iisa, "Hydrocarbon liquid production from biomass via hot-vapor-filtered fast pyrolysis and catalytic hydroprocessing of the bio-oil," *Energy & Fuels*, vol. 28, no. 9, pp. 5909–5917, 2014.

[76] E. Hoekstra, K. J. A. Hogendoorn, X. Wang, R. J. M. Westerhof, S. R. A. Kersten, W. P. M. van Swaaij, and M. J. Groeneveld, "Fast pyrolysis of biomass in a fluidized bed reactor: In situ filtering of the vapors," *Industrial & Engineering Chemistry Research*, vol. 48, no. 10, pp. 4744–4756, 2009.

[77] J. P. Diebold and S. Czernik, "Additives to lower and stabilize the viscosity of pyrolysis oils during storage," *Energy & Fuels*, vol. 11, no. 5, pp. 1081–1091, 1997.

[78] T. P. Vispute and G. W. Huber, "Production of hydrogen, alkanes and polyols by aqueous phase processing of wood-derived pyrolysis oils," *Green Chem.*, no. 11, pp. 1433–1445, 2009.

[79] T. P. Vispute, H. Zhang, A. Sanna, R. Xiao, and G. W. Huber, "Renewable Chemical Commodity Feedstocks from Integrated Catalytic Processing of Pyrolysis Oils," *Science*, vol. 330, no. 6008, pp. 1222–1227, 2010.

[80] F. de Miguel Mercader, M. J. Groeneveld, S. R. A. Kersten, C. Geantet, G. Toussaint, N. W. J. Way, C. J. Schaverien, and K. J. A. Hogendoorn, "Hydrodeoxygenation of pyrolysis oil fractions: process understanding and quality assessment through co-processing in refinery units," *Energy & Environmental Science*, vol. 4, no. 3, pp. 985–997, 2011.

[81] T. L. Marker and J. A. Petri, "Gasoline and diesel production from pyrolytic lignin produced from pyrolysis of cellulosic waste,," 2009. US Patent 7578927.

[82] A. Preau, "Process for upgrading a pyrolysis oil, in particular in a refinery," 2014. US Patent 8912376.

[83] D. Chiaramonti, M. Bonini, E. Fratini, G. Tondi, K. Gartner, A. Bridgwater, H. Grimm, I. Soldaini, A. Webster, and P. Baglioni, "Development of emulsions from biomass pyrolysis liquid and diesel and their use in engines—Part 1 : emulsion production," *Biomass and Bioenergy*, vol. 25, no. 1, pp. 85–99, 2003.

[84] D. Chiaramonti, M. Bonini, E. Fratini, G. Tondi, K. Gartner, A. Bridgwater, H. Grimm, I. Soldaini, A. Webster, and P. Baglioni, "Development of emulsions from biomass pyrolysis liquid and diesel and their use in engines—Part 2: tests in diesel engines," *Biomass and Bioenergy*, vol. 25, no. 1, pp. 101–111, 2003.

[85] J.-J. Wang, J. Chang, and J. Fan, "Upgrading of bio-oil by catalytic esterification and determination of acid number for evaluating esterification degree," *Energy & Fuels*, vol. 24, no. 5, pp. 3251–3255, 2010.

[86] F. Mahfud, I. Melián-Cabrera, R. Manurung, and H. Heeres, "Biomass to fuels: Upgrading of flash pyrolysis oil by reactive distillation using a high boiling alcohol and acid catalysts," *Process Safety and Environmental Protection*, vol. 85, no. 5, pp. 466–472, 2007.

[87] R. Hilten, K. Das, J. Kastner, and B. Bibens, "Production of higher quality bio-oils by in-line esterification of pyrolysis vapor," 2014. US Patent 8900416.

[88] L. Moens, S. K. Black, M. D. Myers, and S. Czernik, "Study of the neutralization and stabilization of a mixed hardwood bio-oil," *Energy & Fuels*, vol. 23, no. 5, pp. 2695–2699, 2009.

[89] L. Ciddor, J. A. Bennett, J. A. Hunns, K. Wilson, and A. F. Lee, "Catalytic upgrading of bio-oils by esterification," *Journal of Chemical Technology Biotechnology*, vol. 90, no. 5, pp. 780–795, 2015.

[90] J. D. Adjaye, S. P. Katikaneni, and N. N. Bakhshi, "Catalytic conversion of a biofuel to hydrocarbons: effect of mixtures of HZSM-5 and silica-alumina catalysts on product distribution," *Fuel Processing Technology*, vol. 48, no. 2, pp. 115–143, 1996.

[91] J. D. Adjaye and N. N. Bakhshi, "Production of hydrocarbons by catalytic upgrading of a fast pyrolysis bio-oil. Part I: Conversion over various catalysts," *Fuel Processing Technology*, vol. 45, no. 3, pp. 161–183, 1995.

[92] T. R. Carlson, G. A. Tompsett, W. C. Conner, and G. W. Huber, "Aromatic production from catalytic fast pyrolysis of biomass-derived feedstocks," *Topics in Catalysis*, vol. 52, no. 3, pp. 241–252, 2009.

[93] A. Bridgwater, "Catalysis in thermal biomass conversion," *Applied Catalysis A: General*, vol. 116, no. 1, pp. 5–47, 1994.

[94] M. Balat, M. Balat, E. Kirtay, and H. Balat, "Main routes for the thermo-conversion of biomass into fuels and chemicals. part 1: Pyrolysis systems," *Energy Conversion and Management*, vol. 50, no. 12, pp. 3147–3157, 2009.

[95] T. Dickerson and J. Soria, "Catalytic fast pyrolysis: A review," *Energies*, vol. 6, no. 1, pp. 514–538, 2013.

[96] F. L. Resende, "Recent advances on fast hydropyrolysis of biomass," *Catalysis Today*, vol. 269, pp. 148 – 155, 2016. Transformations of Biomass and its derivatives to Fuels and Chemicals.

[97] P. M. Mortensen, J.-D. Grunwaldt, P. A. Jensen, and A. D. Jensen, "Screening of catalysts for hydrodeoxygenation of phenol as a model compound for bio-oil," *ACS Catalysis*, vol. 3, no. 8, pp. 1774–1785, 2013.

[98] S. Echeandia, P. Arias, V. Barrio, B. Pawelec, and J. Fierro, "Synergy effect in the HDO of phenol over Ni–W catalysts supported on active carbon: Effect of tungsten precursors," *Applied Catalysis B: Environmental*, vol. 101, no. 1–2, pp. 1–12, 2010.

[99] M. Hellinger, H. W. Carvalho, S. Baier, D. Wang, W. Kleist, and J.-D. Grunwaldt, "Catalytic hydrodeoxygenation of guaiacol over platinum supported on metal oxides and zeolites," *Applied Catalysis A: General*, vol. 490, pp. 181 – 192, 2015.

[100] F. De Miguel Mercader, P. J. J. Koehorst, H. Heeres, S. R. A. Kersten, and J. A. Hogendoorn, "Competition between hydrotreating and polymerization reactions during pyrolysis oil hydrodeoxygenation," *AIChE Journal*, vol. 57, no. 11, pp. 3160–3170, 2011.

[101] D. C. Elliott, G. G. Neuenschwander, T. R. Hart, J. Hu, A. E. Solana, and C. Cao, *Science in Thermal and Chemical Biomass Conversion*, ch. Hydrogenation of Bio-oil for Chemicals and Fuels Production, pp. 1536–1546. CPL Press, Newbury, 2006.

[102] D. C. Elliott and T. R. Hart, "Catalytic Hydroprocessing of Chemical Models for Bio-oil," *Energy & Fuels*, vol. 23, no. 2, pp. 631–637, 2009.

[103] P. Grange, E. Laurent, R. Maggi, A. Centeno, and B. Delmon, "Hydrotreatment of pyrolysis oils from biomass: reactivity of the various categories of oxygenated compounds and preliminary techno-economical study," *Catalysis Today*, vol. 29, no. 1, pp. 297–301, 1996.

[104] D. C. Elliott, T. R. Hart, G. G. Neuenschwander, L. J. Rotness, and A. H. Zacher, "Catalytic hydroprocessing of biomass fast pyrolysis bio-oil to produce hydrocarbon products," *Environmental Progress & Sustainable Energy*, vol. 28, no. 3, pp. 441–449, 2009.

[105] D. van Krevelen, "Graphical-statistical method for the study of structure and reaction processes of coal," *Fuel*, vol. 29, pp. 269–284, 1950.

[106] S. R. A. Kersten, W. P. M. van Swaaij, L. Lefferts, and K. Seshan, *Options for Catalysis in the Thermochemical Conversion of Biomass into Fuels*, pp. 119–145. Wiley-VCH Verlag GmbH & Co. KGaA, 2007.

[107] J. Wildschut, M. Iqbal, F. H. Mahfud, I. M. Cabrera, R. H. Venderbosch, and H. J. Heeres, "Insights in the hydrotreatment of fast pyrolysis oil using a ruthenium on carbon catalyst," *Energy & Environmental Science*, vol. 3, no. 7, pp. 962–970, 2010.

[108] M. McCall and T. Brandvold, "Fuel and fuel blending components from biomass derived pyrolysis oil," 2009. US Patent App. 12/419,005.

[109] D. Elliott and E. Baker, "Process for upgrading biomass pyrolyzates," 1989. US Patent 4,795,841.

[110] D. C. Elliott, T. R. Hart, G. G. Neuenschwander, L. J. Rotness, M. V. Olarte, A. H. Zacher, and Y. Solantausta, "Catalytic hydroprocessing of fast pyrolysis bio-oil from pine sawdust," *Energy & Fuels*, vol. 26, no. 6, pp. 3891–3896, 2012.

[111] J. Wildschut, J. Arentz, C. Rasrendra, R. Venderbosch, and H. Heeres, "Catalytic hydrotreatment of fast pyrolysis oil: Model studies on reaction pathways for the carbohydrate fraction," *Environmental Progress & Sustainable Energy*, vol. 28, no. 3, pp. 450–460, 2009.

[112] J. Wildschut, F. H. Mahfud, R. H. Venderbosch, and H. J. Heeres, "Hydrotreatment of Fast Pyrolysis Oil Using Heterogeneous Noble-Metal Catalysts," *Industrial & Engineering Chemistry Research*, vol. 48, no. 23, pp. 10324–10334, 2009.

[113] A. Ardiyanti, S. Khromova, R. Venderbosch, V. Yakovlev, and H. Heeres, "Catalytic hydrotreatment of fast-pyrolysis oil using non-sulfided bimetallic Ni-Cu catalysts on a δ-Al_2O_3 support," *Applied Catalysis B: Environmental*, vol. 117–118, pp. 105–117, 2012.

[114] A. Ardiyanti, S. Khromova, R. Venderbosch, V. Yakovlev, I. Melián-Cabrera, and H. Heeres, "Catalytic hydrotreatment of fast pyrolysis oil using bimetallic Ni–Cu catalysts on various supports," *Applied Catalysis A: General*, vol. 449, pp. 121–130, 2012.

[115] A. Ardiyanti, A. Gutierrez, M. Honkela, A. Krause, and H. Heeres, "Hydrotreatment of wood-based pyrolysis oil using zirconia-supported mono- and bimetallic (Pt, Pd, Rh) catalysts," *Applied Catalysis A: General*, vol. 407, no. 1–2, pp. 56–66, 2011.

[116] A. R. Ardiyanti, R. H. Venderbosch, W. Yin, and H. J. Heeres, "Chapter 7 catalytic hydrotreatment of fast pyrolysis oils using supported metal catalysts," in *Catalytic Hydrogenation for Biomass Valorization*, pp. 151–173, The Royal Society of Chemistry, 2015.

[117] A. Ardiyanti, M. V. Bykova, S. A. Khromova, W. Yin, R. Venderbosch, V. Yakovlev, and H. Heeres, "Ni-based catalysts for the hydrotreatment of fast pyrolysis oil," *Energy & Fuels*, vol. 30 (3), pp. 1544–1554, 2016.

[118] E. Furimsky, "Catalytic hydrodeoxygenation," *Applied Catalysis A: General*, vol. 199, no. 2, pp. 147–190, 2000.

[119] Y. Romero, F. Richard, and S. Brunet, "Hydrodeoxygenation of 2-ethylphenol as a model compound of bio-crude over sulfided mo-based catalysts: Promoting effect and reaction mechanism," *Applied Catalysis B: Environmental*, vol. 98, no. 3–4, pp. 213–223, 2010.

[120] D. James Speight Editor, "A review of: "hydrotreating catalysis science and technology" Topsøe, H., Clausen, B.S., and Massoth, F.E., Springer-Verlag New York, 1996.," *Fuel Science and Technology International*, vol. 14, no. 10, pp. 1465–1465, 1996.

[121] H. Topsøe, B. S. Clausen, and F. E. Massoth, *Hydrotreating Catalysis*, pp. 1–269. Springer Berlin Heidelberg, 1996.

[122] M. Brorson, A. Carlsson, and H. Topsøe, "The morphology of MoS_2, WS_2, Co–Mo–S, Ni–Mo–S and Ni–W–S nanoclusters in hydrodesulfurization catalysts revealed by HAADF-STEM," *Catalysis Today*, vol. 123, no. 1–4, pp. 31–36, 2007.

[123] H. Topsøe, "The role of Co–Mo–S type structures in hydrotreating catalysts," *Applied Catalysis A: General*, vol. 322, pp. 3–8, 2007.

[124] P. G. Moses, B. Hinnemann, H. Topsøe, and J. K. Nørskov, "The effect of Co-promotion on MoS_2 catalysts for hydrodesulfurization of thiophene: A density functional study," *Journal of Catalysis*, vol. 268, no. 2, pp. 201–208, 2009.

[125] Y. Zhu, Q. M. Ramasse, M. Brorson, P. G. Moses, L. P. Hansen, H. Topsøe, C. F. Kisielowski, and S. Helveg, "Location of Co and Ni promoter atoms in multi-layer MoS_2 nanocrystals for hydrotreating catalysis," *Catalysis Today*, vol. 261, pp. 75–81, 2016.

[126] R. R. Chianelli, G. Berhault, and B. Torres, "Unsupported transition metal sulfide catalysts: 100 years of science and application," *Catalysis Today*, vol. 147, no. 3–4, pp. 275–286, 2009.

[127] V. N. Bui, D. Laurenti, P. Afanasiev, and C. Geantet, "Hydrodeoxygenation of guaiacol with CoMo catalysts. part i: Promoting effect of cobalt on HDO selectivity and activity," *Applied Catalysis B: Environmental*, vol. 101, no. 3–4, pp. 239–245, 2011.

[128] Y.-C. Lin, C.-L. Li, H.-P. Wan, H.-T. Lee, and C.-F. Liu, "Catalytic hydrodeoxygenation of guaiacol on Rh-based and sulfided CoMo and NiMo catalysts," *Energy & Fuels*, vol. 25, no. 3, pp. 890–896, 2011.

[129] E. Laurent and B. Delmon, "Study of the hydrodeoxygenation of carbonyl, carboxylic and guaiacyl groups over sulfided CoMo/γ-Al_2O_3 and NiMo/γ-Al_2O_3 catalysts," *Applied Catalysis A: General*, vol. 109, no. 1, pp. 77–96, 1994.

[130] E. G. Baker and D. C. Elliott, *Catalytic Hydrotreating of Biomass-Derived Oils*, ch. 21, pp. 228–240. American Chemical Society, 1988.

[131] E. Laurent and B. Delmon, "Deactivation of a sulfided NiMo/γ-Al$_2$O$_3$ during the hydrodeoxygenation of bio-oils: Influence of a high water pressure," in *Catalyst Deactivation 1994 - Proceedings of the 6th International Symposium* (B. Delmon and G. Froment, eds.), vol. 88 of *Studies in Surface Science and Catalysis*, pp. 459–466, Elsevier, 1994.

[132] M. Badawi, J. Paul, S. Cristol, E. Payen, Y. Romero, F. Richard, S. Brunet, D. Lambert, X. Portier, A. Popov, E. Kondratieva, J. Goupil, J. E. Fallah, J. Gilson, L. Mariey, A. Travert, and F. Maugé, "Effect of water on the stability of Mo and CoMo hydrodeoxygenation catalysts: A combined experimental and DFT study," *Journal of Catalysis*, vol. 282, no. 1, pp. 155–164, 2011.

[133] B. Pawelec and J. L. G. Fierro, "Chapter 8 Hydrodeoxygenation of Biomass-Derived Liquids over Transition-Metal-Sulfide Catalysts," in *Catalytic Hydrogenation for Biomass Valorization*, The Royal Society of Chemistry, 2014.

[134] H. Kobayashi, H. Ohta, and A. Fukuoka, "Conversion of lignocellulose into renewable chemicals by heterogeneous catalysis," *Catalysis Science & Technology*, vol. 2, no. 5, pp. 869–883, 2012.

[135] O. Şenol, T.-R. Viljava, and A. Krause, "Effect of sulphiding agents on the hydrodeoxygenation of aliphatic esters on sulphided catalysts," *Applied Catalysis A: General*, vol. 326, no. 2, pp. 236–244, 2007.

[136] O. Şenol, E.-M. Ryymin, T.-R. Viljava, and A. Krause, "Effect of hydrogen sulphide on the hydrodeoxygenation of aromatic and aliphatic oxygenates on sulphided catalysts," *Journal of Molecular Catalysis A: Chemical*, vol. 277, no. 1–2, pp. 107–112, 2007.

[137] T.-R. Viljava, R. Komulainen, and A. Krause, "Effect of H$_2$S on the stability of CoMo/Al$_2$O$_3$ catalysts during hydrodeoxygenation," *Catalysis Today*, vol. 60, no. 1–2, pp. 83–92, 2000.

[138] O. Şenol, T.-R. Viljava, and A. Krause, "Hydrodeoxygenation of aliphatic esters on sulphided NiMo/γ-Al$_2$O$_3$ and CoMo/γ-Al$_2$O$_3$3 catalyst: The effect of water," *Catalysis Today*, vol. 106, no. 1–4, pp. 186–189, 2005.

[139] E. Laurent and B. Delmon, "Study of the hydrodeoxygenation of carbonyl, carboxylic and guaiacyl groups over sulfided CoMo/γ-Al$_2$O$_3$ and NiMo/γ-Al$_2$O$_3$ catalyst," *Applied Catalysis A: General*, vol. 109, no. 1, pp. 97–115, 1994.

[140] V. Yakovlev, S. Khromova, O. Sherstyuk, V. Dundich, D. Ermakov, V. Novopashina, M. Lebedev, O. Bulavchenko, and V. Parmon, "Development of new catalytic systems for upgraded bio-fuels production from bio-crude-oil and biodiesel," *Catalysis Today*, vol. 144, no. 3–4, pp. 362–366, 2009.

[141] M. V. Olarte, D. C. Elliott, G. G. Neuenschwander, L. G. Rotness, S. D. Burton, B. Schwenzer, A. Padmaperuma, and A. H. Zacher, "Towards long-term fast pyrolysis oil caatalytic upgrading," *Prep. Pap. -Am. Chem. Soc.: Div. Energy Fuels*, no. 58, pp. 230–231, 2013.

[142] D. R. Moberg, T. J. Thibodeau, F. G. Amar, and B. G. Frederick, "Mechanism of hydrodeoxygenation of acrolein on a cluster model of MoO_3," *The Journal of Physical Chemistry C*, vol. 114, no. 32, pp. 13782–13795, 2010.

[143] V. M. L. Whiffen and K. J. Smith, "Hydrodeoxygenation of 4-methylphenol over unsupported MoP, MoS_2, and MoO_x catalysts," *Energy & Fuels*, vol. 24, no. 9, pp. 4728–4737, 2010.

[144] D. C. Elliott and T. R. Hart, "Catalytic hydroprocessing of chemical models for bio-oil," *Energy & Fuels*, vol. 23, no. 2, pp. 631–637, 2009.

[145] R. Maggi and B. Delmon, "A review of catalytic hydrotreating processes for the upgrading of liquids produced by flash pyrolysis," in *Hydrotreatment and Hydrocracking of Oil FractionsProceedings of the 1st International Symposium/6th European Workshop* (B. D. G.F. Froment and P. Grange, eds.), vol. 106 of *Studies in Surface Science and Catalysis*, pp. 99–113, Elsevier, 1997.

[146] M. Mendes, O. Santos, E. Jordão, and A. Silva, "Hydrogenation of oleic acid over ruthenium catalysts," *Applied Catalysis A: General*, vol. 217, no. 1–2, pp. 253–262, 2001.

[147] R. Pestman, R. Koster, J. Pieterse, and V. Ponec, "Reactions of carboxylic acids on oxides," *Journal of Catalysis*, vol. 168, no. 2, pp. 255–264, 1997.

[148] T. Mallat and A. Baiker, "Selectivity enhancement in heterogeneous catalysis induced by reaction modifiers," *Applied Catalysis A: General*, vol. 200, no. 1–2, pp. 3–22, 2000.

[149] A. Gutierrez, R. Kaila, M. Honkela, R. Slioor, and A. Krause, "Hydrodeoxygenation of guaiacol on noble metal catalysts," *Catalysis Today*, vol. 147, no. 3–4, pp. 239–246, 2009.

[150] J. Wildschut, I. Melián-Cabrera, and H. Heeres, "Catalyst studies on the hydrotreatment of fast pyrolysis oil," *Applied Catalysis B: Environmental*, vol. 99, no. 1–2, pp. 298–306, 2010.

[151] J. Wildschut, M. Iqbal, F. H. Mahfud, I. M. Cabrera, R. H. Venderbosch, and H. J. Heeres, "Insights in the hydrotreatment of fast pyrolysis oil using a ruthenium on carbon catalyst," *Energy Environ. Sci.*, vol. 3, pp. 962–970, 2010.

[152] D. Elliott, J. Hu, T. Hart, and G. Neuenschwander, "Palladium catalyzed hydrogenation of bio-oils and organic compounds," 2008. US Patent 7425657.

[153] C. H. Bartholomew, "Mechanisms of catalyst deactivation," *Applied Catalysis A: General*, vol. 212, no. 1–2, pp. 17–60, 2001.

[154] V. A. Yakovlev, M. V. Bykova, and S. A. Khromova, "Stability of nickel-containing catalysts for hydrodeoxygenation of biomass pyrolysis products," *Catalysis in Industry*, vol. 4, no. 4, pp. 324–339, 2012.

[155] C. Zhao, Y. Kou, A. A. Lemonidou, X. Li, and J. A. Lercher, "Hydrodeoxygenation of bio-derived phenols to hydrocarbons using RANEY$^{®}$ Ni and Nafion/SiO_2 catalysts," *Chemical Communications*, vol. 46, no. 3, pp. 412–414, 2010.

[156] M. Bykova, D. Ermakov, V. Kaichev, O. Bulavchenko, A. Saraev, M. Lebedev, and V. Yakovlev, "Ni-based sol–gel catalysts as promising systems for crude bio-oil upgrading: Guaiacol hydrodeoxygenation study," *Applied Catalysis B: Environmental*, vol. 113–114, pp. 296–307, 2012.

[157] M. V. Bykova and O. A. Bulavchenko, "Guaiacol hydrodeoxygenation in the presence of Ni-containing catalysts," *Catalysis in Industry*, vol. 3, no. 1, pp. 15–22, 2011.

[158] M. V. Bykova, S. G. Zavarukhin, L. I. Trusov, and V. A. Yakovlev, "Guaiacol hydrodeoxygenation kinetics with catalyst deactivation taken into consideration," *Kinetics and Catalysis*, vol. 54, no. 1, pp. 40–48, 2013.

[159] S. A. Khromova, M. V. Bykova, O. A. Bulavchenko, D. Y. Ermakov, A. A. Saraev, V. V. Kaichev, R. H. Venderbosch, and V. A. Yakovlev, "Furfural Hydrogenation to Furfuryl Alcohol over Bimetallic Ni–Cu Sol–Gel Catalyst: A Model Reaction for Conversion of Oxygenates in Pyrolysis Liquids," *Topics in Catalysis*, pp. 1–11, 2016.

[160] P. M. Mortensen, D. Gardini, H. W. P. d. Carvalho, C. D. Damsgaard, J.-D. Grunwaldt, P. A. Jensen, J. B. Wagner, and A. D. Jensen, "Stability and resistance of nickel catalysts for hydrodeoxygenation: carbon deposition and effects of sulfur, potassium, and chlorine in the feed," *Catalysis Science & Technology*, vol. 4, no. 10, pp. 3672–3686, 2014.

[161] T. M. Huynh, U. Armbruster, M.-M. Pohl, M. Schneider, J. Radnik, D.-L. Hoang, B. M. Q. Phan, D. A. Nguyen, and A. Martin, "Hydrodeoxygenation of phenol as a model compound for bio-oil on non-noble bimetallic nickel-based catalysts," *ChemCatChem*, vol. 6, no. 7, pp. 1940–1951, 2014.

[162] P. M. Mortensen, J.-D. Grunwaldt, P. A. Jensen, and A. D. Jensen, "Influence on nickel particle size on the hydrodeoxygenation of phenol over Ni/SiO$_2$," *Catalysis Today*, vol. 259, Part 2, pp. 277–284, 2016.

[163] W. Yin, A. Kloekhorst, R. H. Venderbosch, M. V. Bykova, S. A. Khromova, V. A. Yakovlev, and H. J. Heeres, "Catalytic hydrotreatment of fast pyrolysis liquids in batch and continuous set-ups using a bimetallic Ni-Cu catalyst with a high metal content," *Catal. Sci. Technol.*, vol. 6, pp. 5899–5915, 2016.

[164] E. Furimsky and F. E. Massoth, "Deactivation of hydroprocessing catalysts," *Catalysis Today*, vol. 52, no. 4, pp. 381–495, 1999.

[165] J. Moulijn, A. van Diepen, and F. Kapteijn, "Catalyst deactivation: is it predictable?," *Applied Catalysis A: General*, vol. 212, no. 1-2, pp. 3–16, 2001.

[166] E. Furimsky, "Hydroprocessing challenges in biofuels production," *Catalysis Today*, vol. 217, pp. 13–56, 2013.

[167] E. Laurent and B. Delmon, "Influence of water in the deactivation of a sulfided NiMoγ-Al$_2$O$_3$ catalyst during hydrodeoxygenation," *Journal of Catalysis*, vol. 146, no. 1, pp. 281–291, 1994.

[168] Q. Song, F. Wang, J. Cai, Y. Wang, J. Zhang, W. Yu, and J. Xu, "Lignin depolymerization (LDP) in alcohol over nickel-based catalysts via a fragmentation-hydrogenolysis process," *Energy Environ. Sci.*, vol. 6, pp. 994–1007, 2013.

[169] Q. Song, F. Wang, and J. Xu, "Hydrogenolysis of lignosulfonate into phenols over heterogeneous nickel catalysts," *Chem. Commun.*, vol. 48, pp. 7019–7021, 2012.

[170] Y. Elkasabi, C. A. Mullen, A. L. Pighinelli, and A. A. Boateng, "Hydrodeoxygenation of fast-pyrolysis bio-oils from various feedstocks using carbon-supported catalysts," *Fuel Processing Technology*, vol. 123, pp. 11–18, 2014.

[171] P. Scherrer, "Bestimmung der größe und der inneren struktur von kolloidteilchen mittels röntgenstrahlen.," *Nachrichten Von Ges Wiss Zu Gött Math-Phys Kl*, p. 98–100, 1918.

[172] A. L. Patterson, "The Scherrer Formula for X-Ray Particle Size Determination," *Physical Review*, vol. 56, no. 10, pp. 978–982, 1939.

[173] "http://www.casaxps.com," accessed on 20 October 2016.

[174] J.-D. Grunwaldt, M. Caravati, S. Hannemann, and A. Baiker, "X-ray absorption spectroscopy under reaction conditions: suitability of different reaction cells for combined catalyst characterization and time-resolved studies," *Phys. Chem. Chem. Phys.*, vol. 6, pp. 3037–3047, 2004.

[175] J.-D. Grunwaldt, N. Vegten, and A. Baiker, "Insight into the structure of supported palladium catalysts during the total oxidation of methane," *Chem. Commun.*, pp. 4635–4637, 2007.

[176] B. Ravel and M. Newville, "*ATHENA, ARTEMIS, HEPHAESTUS*: data analysis for X-ray absorption spectroscopy using *IFEFFIT*," *Journal of Synchrotron Radiation*, vol. 12, no. 4, pp. 537–541, 2005.

[177] J. J. Rehr and R. C. Albers, "Theoretical approaches to x-ray absorption fine structure," *Rev. Mod. Phys.*, vol. 72, pp. 621–654, 2000.

[178] J. Rehr, J. Kas, M. Prange, A. Sorini, Y. Takimoto, and F. Vila, "Ab initio theory and calculations of X-ray spectra," *Comptes Rendus Physique*, vol. 10, pp. 548–559, 2009.

[179] C. Boscagli, K. Raffelt, T. A. Zevaco, W. Olbrich, T. N. Otto, J. Sauer, and J.-D. Grunwaldt, "Mild hydrotreatment of the light fraction of fast-pyrolysis oil produced from straw over nickel-based catalysts," *Biomass and Bioenergy*, vol. 83, pp. 525–538, 2015. http://dx.doi.org/10.1016/j.biombioe.2015.11.003.

[180] G. Soave, "Equilibrium constants from a modified Redlich-Kwong equation of state," *Chemical Engineering Science*, vol. 27, no. 6, pp. 1197–1203, 1972.

[181] R. H. Perry, D. W. A. Green, and J. O. Maloney, *Perry's Chemical Engineers' Handbook*. McGraw-Hill Professional Publishing, 1997.

[182] M. K. Hrnčič, R. H. Venderbosch, M. Škerget, L. Ilić, and e. Knez, "Phase equilibrium data of hydrogen in pyrolysis oil and hydrogenated pyrolysis oil at elevated pressures," *The Journal of Supercritical Fluids*, vol. 80, pp. 86–89, 2013.

[183] S. A. Channiwala and P. P. Parikh, "A unified correlation for estimating HHV of solid, liquid and gaseous fuels," *Fuel*, vol. 81, no. 8, pp. 1051–1063, 2002.

[184] T. Saito, S. Nakaie, M. Kinoshita, T. Ihara, S. Kinugasa, A. Nomura, and T. Maeda, "Practical guide to accurate quantitative solution state NMR analysis," *Metrologia*, vol. 41, pp. 213–218, 2004.

[185] C. A. Mullen, G. D. Strahan, and A. A. Boateng, "Characterization of various fast-pyrolysis bio-oils by NMR spectroscopy," *Energy & Fuels*, vol. 23, no. 5, pp. 2707–2718, 2009.

[186] A. Oasmaa, T. Sundqvist, E. Kuoppala, M. Garcia-Perez, Y. Solantausta, C. Lindfors, and V. Paasikallio, "Controlling the phase stability of biomass fast pyrolysis bio-oils," *Energy & Fuels*, vol. 29, no. 7, pp. 4373–4381, 2015.

[187] K. Raveendran, A. Ganesh, and K. C. Khilar, "Pyrolysis characteristics of biomass and biomass components," *Fuel*, vol. 75, no. 8, pp. 987–998, 1996.

[188] S. V. Vassilev, D. Baxter, L. K. Andersen, and C. G. Vassileva, "An overview of the composition and application of biomass ash. Part 1. Phase–mineral and chemical composition and classification," *Fuel*, vol. 105, pp. 40–76, 2013.

[189] C. Heitner, D. Dimmel, and J. Schmidt, *Lignin and Lignans: Advances in Chemistry*. CRC Press, 2016.

[190] K. Raveendran, A. Ganesh, and K. C. Khilar, "Influence of mineral matter on biomass pyrolysis characteristics," *Fuel*, vol. 74, no. 12, pp. 1812–1822, 1995.

[191] R. Fahmi, A. Bridgwater, I. Donnison, N. Yates, and J. Jones, "The effect of lignin and inorganic species in biomass on pyrolysis oil yields, quality and stability," *Fuel*, vol. 87, no. 7, pp. 1230–1240, 2008.

[192] A. Bridgwater, "Production of high grade fuels and chemicals from catalytic pyrolysis of biomass," *Catalysis Today*, vol. 29, no. 1, pp. 285–295, 1996.

[193] A. Oasmaa, I. Fonts, M. R. Pelaez-Samaniego, M. E. Garcia-Perez, and M. Garcia-Perez, "Pyrolysis oil multiphase behavior and phase stability: A review," *Energy & Fuels*, vol. 30, no. 8, pp. 6179–6200, 2016.

[194] D. Mohan, C. U. Pittman, and P. H. Steele, "Pyrolysis of wood/biomass for bio-oil: A critical review," *Energy Fuels*, vol. 20, no. 3, pp. 848–889, 2006.

[195] J.-Y. Liu, S.-B. Wu, and R. Lou, "Chemical structure and pyrolysis response of β-o-4 lignin model polymer," *BioResources*, vol. 6, no. 2, pp. 1079–1093, 2011.

[196] C. Liu, Y. Deng, S. Wu, M. Lei, and J. Liang, "Experimental and theoretical analysis of the pyrolysis mechanism of a dimeric lignin model compound with α-o-4 linkage," *BioResources*, vol. 11, no. 2, pp. 3626–3636, 2016.

[197] R. J. French, S. K. Black, M. Myers, J. Stunkel, E. Gjersing, and K. Iisa, "Hydrotreating the Organic Fraction of Biomass Pyrolysis Oil to a Refinery Intermediate," *Energy & Fuels*, vol. 29, no. 12, pp. 7985–7992, 2015.

[198] R. J. French, J. Hrdlicka, and R. Baldwin, "Mild hydrotreating of biomass pyrolysis oils to produce a suitable refinery feedstock," *Environmental Progress & Sustainable Energy*, vol. 29, no. 2, pp. 142–150, 2010.

[199] T. R. Wilken, W. R. Morcom, C. A. Wert, and J. B. Woodhouse, "Reduction of tungsten oxide to tungsten metal," *Metallurgical Transactions B*, vol. 7, no. 4, pp. 589–597, 1976.

[200] Q. Wu, L. D. L. Duchstein, G. L. Chiarello, J. M. Christensen, C. D. Damsgaard, C. F. Elkjær, J. B. Wagner, B. Temel, J.-D. Grunwaldt, and A. D. Jensen, "In Situ Observation of Cu–Ni Alloy Nanoparticle Formation by X-Ray Diffraction, X-Ray Absorption Spectroscopy, and Transmission Electron Microscopy: Influence of Cu/Ni Ratio," *ChemCatChem*, vol. 6, no. 1, pp. 301–310, 2014.

[201] A. C. Dimian and C. Sorin Bildea, eds., *Chemical Process Design: Computer-Aided Case Studies*. Wiley, 2008.

[202] S. Sitthisa and D. E. Resasco, "Hydrodeoxygenation of Furfural Over Supported Metal Catalysts: A Comparative Study of Cu, Pd and Ni," *Catalysis Letters*, vol. 141, no. 6, pp. 784–791, 2011.

[203] M. Hronec and K. Fulajtarová, "Selective transformation of furfural to cyclopentanone," *Catalysis Communications*, vol. 24, pp. 100–104, 2012.

[204] Y. Yang, Z. Du, Y. Huang, F. Lu, F. Wang, J. Gao, and J. Xu, "Conversion of furfural into cyclopentanone over Ni–Cu bimetallic catalysts," *Green Chemistry*, vol. 15, no. 7, pp. 1932–1940, 2013.

[205] P. K. Kanaujia, Y. K. Sharma, M. O. Garg, D. Tripathi, and R. Singh, "Review of analytical strategies in the production and upgrading of bio-oils derived from lignocellulosic biomass," *Journal of Analytical and Applied Pyrolysis*, vol. 105, pp. 55–74, 2014.

[206] X. Zhang, J. Long, W. Kong, Q. Zhang, L. Chen, T. Wang, L. Ma, and Y. Li, "Catalytic Upgrading of Bio-oil over Ni-Based Catalysts Supported on Mixed Oxides," *Energy & Fuels*, vol. 28, no. 4, pp. 2562–2570, 2014.

[207] M. Hellinger, H. W. P. d. Carvalho, S. Baier, L. Gharnati, and J.-D. Grunwaldt, "Solvent Influence on the Hydrodeoxygenation of Guaiacol over Pt/SiO$_2$ and Pt/H-MFI 90 Catalysts," *Chemie Ingenieur Technik*, vol. 87, no. 12, pp. 1771–1780, 2015.

[208] M. Zhou, G. Xiao, K. Wang, and J. Jiang, "Catalytic conversion of aqueous fraction of bio-oil to alcohols over CNT-supported catalysts," *Fuel*, vol. 180, pp. 749–758, 2016.

[209] A. A. Dwiannoko, S. Lee, H. C. Ham, J.-W. Choi, D. J. Suh, and J.-M. Ha, "Effects of Carbohydrates on the Hydrodeoxygenation of Lignin-Derived Phenolic Compounds," *Acs Catalysis*, vol. 5, no. 1, pp. 433–437, 2015.

[210] Y. Xu, S. Qiu, J. Long, C. Wang, J. Chang, J. Tan, Q. Liu, L. Ma, T. Wang, and Q. Zhang, "In situ hydrogenation of furfural with additives over a RANEY® Ni catalyst," *RSC Advances*, vol. 5, no. 111, pp. 91190–91195, 2015.

[211] R. S. Weber, M. V. Olarte, and H. Wang, "Modeling the Kinetics of Deactivation of Catalysts during the Upgrading of Bio-oil," *Energy & Fuels*, vol. 29, no. 1, pp. 273–277, 2015.

[212] A. Sanna, T. P. Vispute, and G. W. Huber, "Hydrodeoxygenation of the Aqueous Fraction of Bio-oil with Ru/C and Pt/C catalysts," *Applied Catalysis B: Environmental*, vol. 165, pp. 446 – 456, 2015.

[213] Y. Yao and D. W. Goodman, "Direct evidence of hydrogen spillover from Ni to Cu on Ni–Cu bimetallic catalysts," *Journal of Molecular Catalysis A: Chemical*, vol. 383–384, pp. 239–242, 2014.

[214] W. Olbrich, C. Boscagli, K. Raffelt, H. Zang, N. Dahmen, and J. Sauer, "Catalytic hydrodeoxygenation of pyrolysis oil over nickel-based catalysts under H_2 /CO_2 atmosphere," *Sustainable Chemical Processes*, vol. 4, no. 1, p. 1, 2016.

[215] G. Li, N. Li, X. Wang, X. Sheng, S. Li, A. Wang, Y. Cong, X. Wang, and T. Zhang, "Synthesis of Diesel or Jet Fuel Range Cycloalkanes with 2-Methylfuran and Cyclopentanone from Lignocellulose," *Energy & Fuels*, vol. 28, no. 8, pp. 5112–5118, 2014.

[216] R. Fang, H. Liu, R. Luque, and Y. Li, "Efficient and selective hydrogenation of biomass-derived furfural to cyclopentanone using Ru catalysts," *Green Chemistry*, vol. 17, no. 8, pp. 4183–4188, 2015.

[217] R. K. M. R. Kallury, T. T. Tidwell, D. G. B. Boocock, and D. H. L. Chow, "High temperature catalytic hydrogenolysis and alkylation of anisole and phenol," *Canadian Journal of Chemistry*, vol. 62, no. 11, pp. 2540–2545, 1984.

[218] L. Nie and D. E. Resasco, "Improving carbon retention in biomass conversion by alkylation of phenolics with small oxygenates," *Applied Catalysis A: General*, vol. 447–448, pp. 14–21, 2012.

[219] T. N. Pham, D. Shi, and D. E. Resasco, "Evaluating strategies for catalytic upgrading of pyrolysis oil in liquid phase," *Applied Catalysis B-Environmental*, vol. 145, pp. 10–23, 2014.

[220] Y. Matsumura, S. Yanachi, and T. Yoshida, "Glucose decomposition kinetics in water at 25 mpa in the temperature range of 448–673 k," *Industrial & Engineering Chemistry Research*, vol. 45, no. 6, pp. 1875–1879, 2006.

[221] Q. Jing and X. Lü, "Kinetics of Non-catalyzed Decomposition of Glucose in High-temperature Liquid Water," *Chinese Journal of Chemical Engineering*, vol. 16, no. 6, pp. 890–894, 2008.

[222] K. Murata, M. Inaba, I. Takahara, and Y. Liu, "Selective hydrocarbon production by the hydrocracking of glucose," *Reaction Kinetics, Mechanisms and Catalysis*, vol. 110, no. 2, pp. 295–307, 2013.

[223] V. H. Pomin, *Unravelling Glycobiology by NMR Spectroscopy*. INTECH Open Access Publisher, 2012.

[224] S. A. Khromova, A. A. Smirnov, O. A. Bulavchenko, A. A. Saraev, V. V. Kaichev, S. I. Reshetnikov, and V. A. Yakovlev, "Anisole hydrodeoxygenation over Ni-Cu bimetallic catalysts: The effect of Ni/Cu ratio on selectivity," *Applied Catalysis a-General*, vol. 470, pp. 261–270, 2014.

[225] P. M. Mortensen, J.-D. Grunwaldt, P. A. Jensen, and A. D. Jensen, "Influence on nickel particle size on the hydrodeoxygenation of phenol over Ni/SiO2," *Catalysis Today*, vol. 259, pp. 277–284, 2016.

[226] L. L. Van Loon, C. Throssell, and M. D. Dutton, "Comparison of nickel speciation in workplace aerosol samples using sequential extraction analysis and X-ray absorption near-edge structure spectroscopy," *Environmental Science. Processes & Impacts*, vol. 17, no. 5, pp. 922–931, 2015.

[227] C. J. Powell and A. Jablonski, "Evaluation of Calculated and Measured Electron Inelastic Mean Free Paths Near Solid Surfaces," *Journal of Physical and Chemical Reference Data*, vol. 28, no. 1, pp. 19–62, 1999.

[228] A. Gil, A. Diaz, and M. Montes, "Passivation and reactivation of nickel catalysts," *Journal of the Chemical Society, Faraday Transactions*, vol. 87, no. 5, pp. 791–795, 1991.

[229] P. Braos-Garcia, P. Maireles-Torres, E. Rodriguez-Castellon, and A. Jimenez-Lopez, "Gas-phase hydrogenation of acetonitrile over nickel supported on alumina- and mixed alumina/gallium oxide-pillared tin phosphate catalysts," *Journal of Molecular Catalysis A: Chemical*, vol. 168, no. 1–2, pp. 279–287, 2001.

[230] A. R. Naghash, T. H. Etsell, and S. Xu, "XRD and XPS Study of Cu-Ni Interactions on Reduced Copper-Nickel-Aluminum Oxide Solid Solution Catalysts," *Chemistry of Materials*, vol. 18, no. 10, pp. 2480–2488, 2006.

[231] D. L. Legrand, H. W. Nesbitt, and G. M. Bancroft, "X-ray photoelectron spectroscopic study of a pristine millerite (NiS) surface and the effect of air and water oxidation," *American Mineralogist*, vol. 83, no. 11-12 Part 1, pp. 1256–1265, 1998.

[232] L.-T. Weng, "Advances in the surface characterization of heterogeneous catalysts using ToF-SIMS," *Applied Catalysis A: General*, vol. 474, pp. 203–210, 2014.

[233] M. Lortie, R. Isaifan, Y. Liu, and S. Mommers, "Synthesis of CuNi/C and CuNi/-Al$_2$O$_3$ Catalysts for the Reverse Water Gas Shift Reaction," *International Journal of Chemical Engineering*, vol. 2015, p. e750689, 2015.

[234] J. Pertusatti and A. G. Prado, "Buffer capacity of humic acid: Thermodynamic approach," *Journal of Colloid and Interface Science*, vol. 314, no. 2, pp. 484–489, 2007.

[235] A. Rodrigues, A. Brito, P. Janknecht, M. F. Proença, and R. Nogueira, "Quantification of humic acids in surface water: effects of divalent cations, pH, and filtration," *J. Environ. Monit.*, vol. 11, no. 2, pp. 377–382, 2009.

[236] I. Chen and D. W. Shiue, "Resistivity to sulfur poisoning of nickel-alumina catalysts," *Industrial & Engineering Chemistry Research*, vol. 27, no. 8, pp. 1391–1396, 1988.

[237] T. C. Tan and J. D. Ford, "Hydrogen reduction kinetics of nickel sulfide in the presence of calcium oxide," *Metallurgical Transactions B*, vol. 15, no. 4, pp. 719–723, 1984.

[238] E. K. Poels, W. P. van Beek, W. den Hoed, and C. Visser, "Deactivation of fixed-bed nickel hydrogenation catalysts by sulfur," *Fuel*, vol. 74, no. 12, pp. 1800–1805, 1995.

[239] Y. Zhang, C. Wu, M. A. Nahil, and P. Williams, "Pyrolysis–Catalytic Reforming/Gasification of Waste Tires for Production of Carbon Nanotubes and Hydrogen," *Energy & Fuels*, vol. 29, no. 5, pp. 3328–3334, 2015.

[240] R. P. W. J. Struis, T. J. Schildhauer, I. Czekaj, M. Janousch, S. M. A. Biollaz, and C. Ludwig, "Sulphur poisoning of Ni catalysts in the SNG production from biomass: A TPO/XPS/XAS study," *Applied Catalysis A: General*, vol. 362, no. 1–2, pp. 121–128, 2009.

[241] Z. Asaki, K. Hajika, T. Tanabe, and Y. Kondo, "Oxidation of nickel sulfide," *Metallurgical Transactions B*, vol. 15, no. 1, pp. 127–133, 1984.

[242] A. V. Bridgwater and G. V. C. Peacocke, "Fast pyrolysis processes for biomass," *Renewable and Sustainable Energy Reviews*, vol. 4, no. 1, pp. 1–73, 2000.

[243] Y. Elkasabi, C. A. Mullen, A. L. M. T. Pighinelli, and A. A. Boateng, "Hydrodeoxygenation of fast-pyrolysis bio-oils from various feedstocks using carbon-supported catalysts," *Fuel Processing Technology*, vol. 123, pp. 11–18, 2014.

Appendix

Supplementary figures
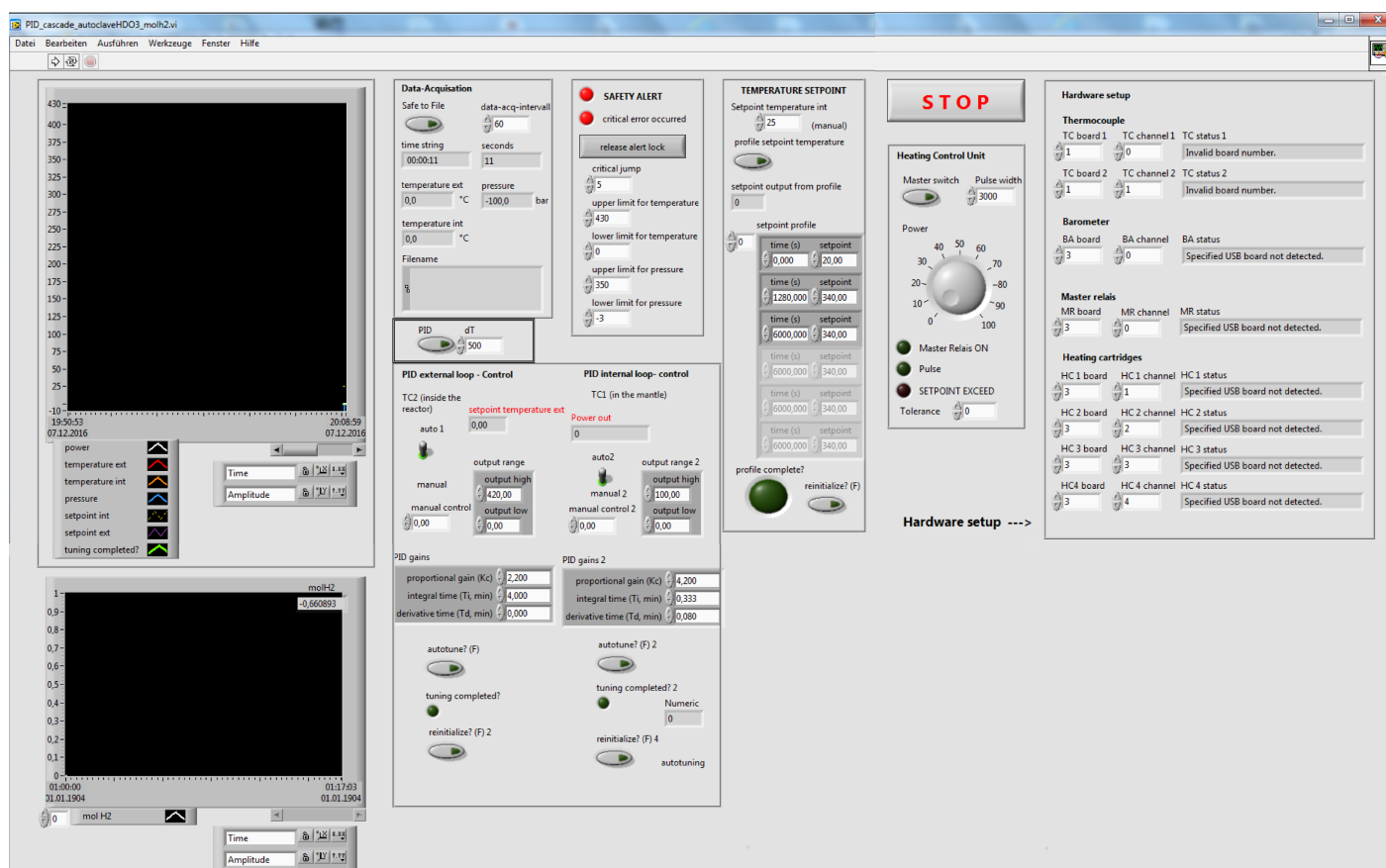
Figure S1: Graphical interface of the Labview program used for controlling the internal and external temperature of the autoclave by cascade PID controllers and for recording temperature and pressure.
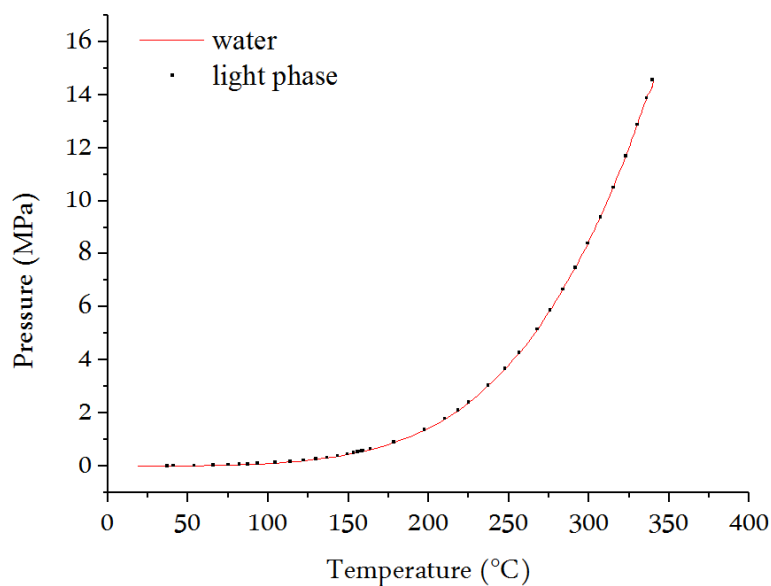
Figure S2: Partial pressure of the light phase of pyrolysis oil (56.7% water) compared to the one of water as a function of temperature in an autoclave (50 ml of light phase in 200 ml autoclave).
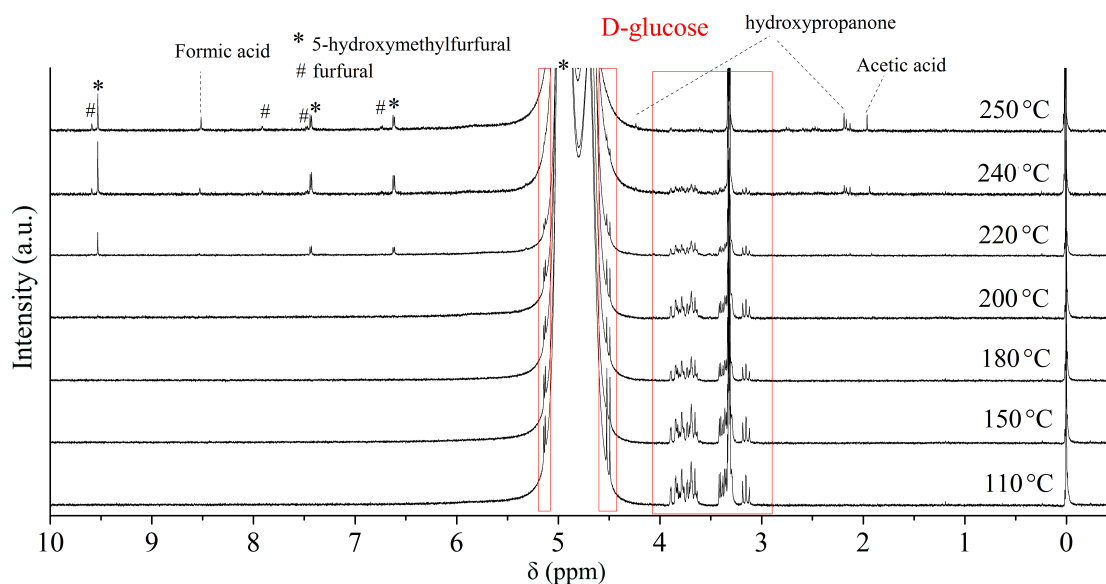
Figure S3: Decomposition of glucose (10 wt.% in water) followed by ^{1}H-NMR. The reaction was monitored using the autoclave in Figure 2.1 inserting a sampling valve for collecting a sample at different temperatures and after 5 minutes of stabilization at this temperature (heating ramp 5 °C/min).
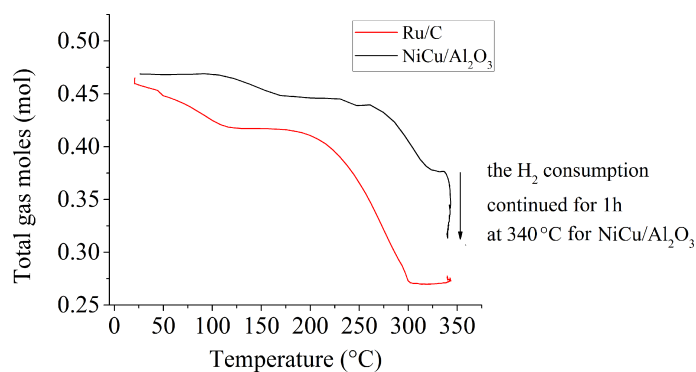
Figure S4: Variation of the total moles of gas (calculated by ideal gas equation, subtracting the partial pressure of water) during hydrotreatment of a solution 10 wt.% of glucose in water over Ru/C and NiCu/Al$_2$O$_3$ (340 °C, 8.0 MPa hydrogen at room temperature).
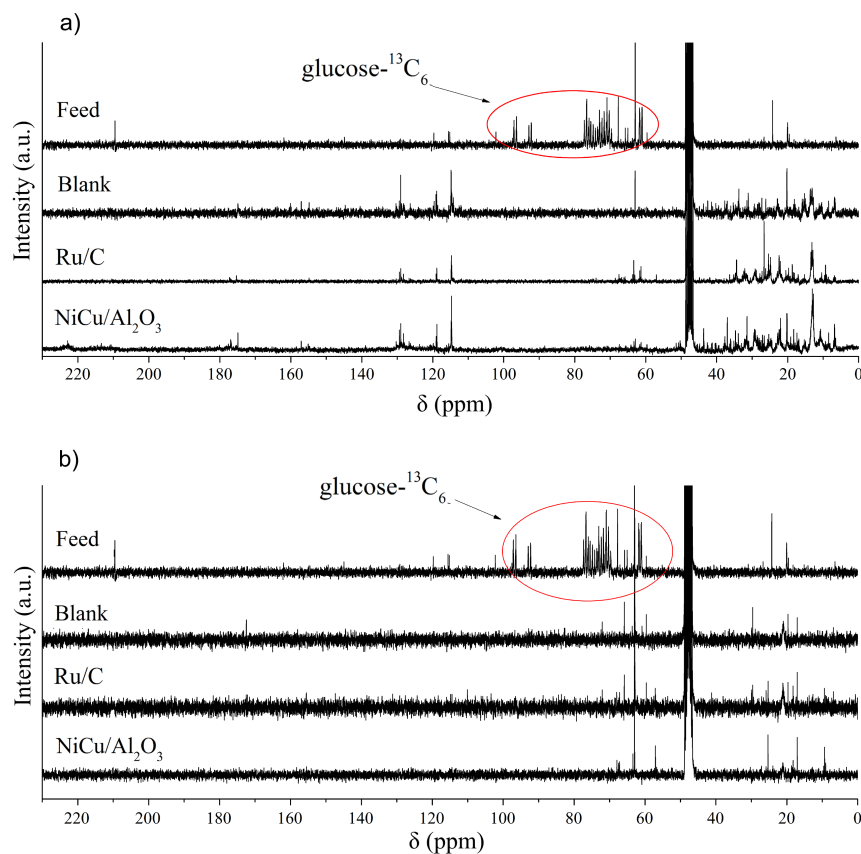
Figure S5: ^{13}C-NMR spectra of the light phase of pyrolysis oil (feed) with D-glucose-^{13}C$_6$ (60-100 ppm), compared to the upgraded oils (a) and the aqueous phases (b) produced during the experiment with no catalyst (blank), over Ru/C and NiCu/Al$_2$O$_3$ (hydrotreatment at 340 °C, 8.0 MPa of hydrogen at room temperature).
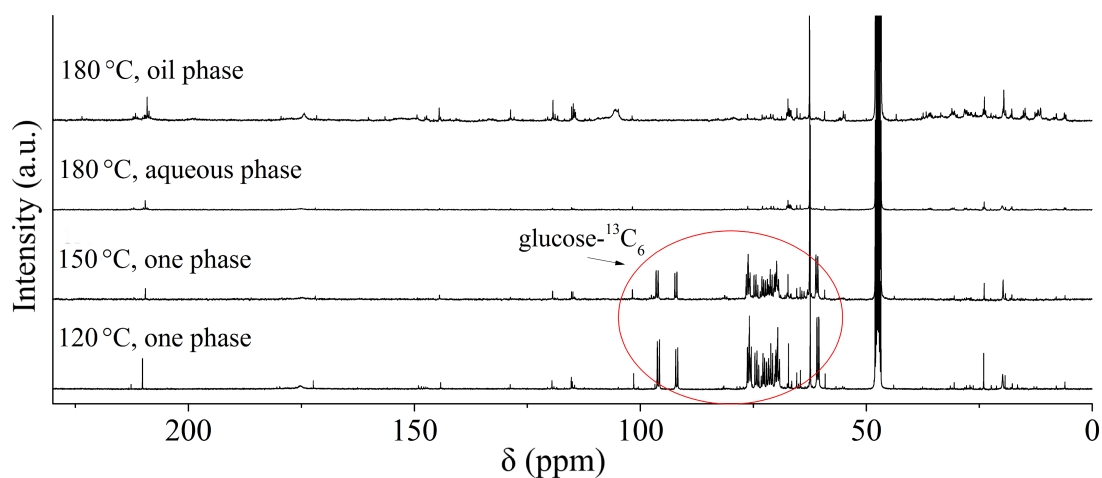
Figure S6: Decomposition of glucose-$^{13}C_6$ (10 wt.% in water) followed by ^{13}C-NMR. The reaction was monitored using the autoclave reported in Figure 2.1 inserting a sampling valve for collecting a sample at different temperatures and after 5 minutes of stabilization at this temperature (heating ramp 5 °C/min).
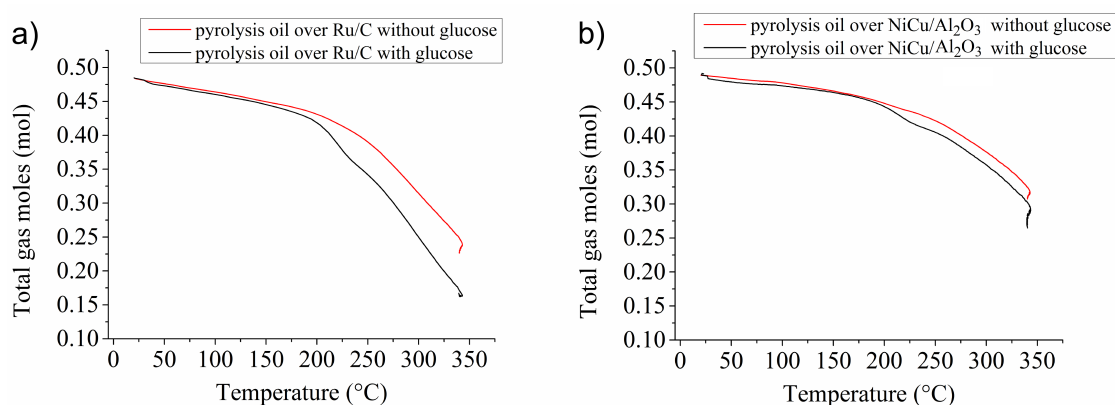
Figure S7: Variation of the total moles of gas (calculated by ideal gas equation, subtracting the partial pressure of pyrolysis oil) during hydrotreatment of a mixture 10 wt.% of glucose in pyrolysis oil over Ru/C and NiCu/Al$_2$O$_3$ (340 °C, 8.0 MPa hydrogen at room temperature).
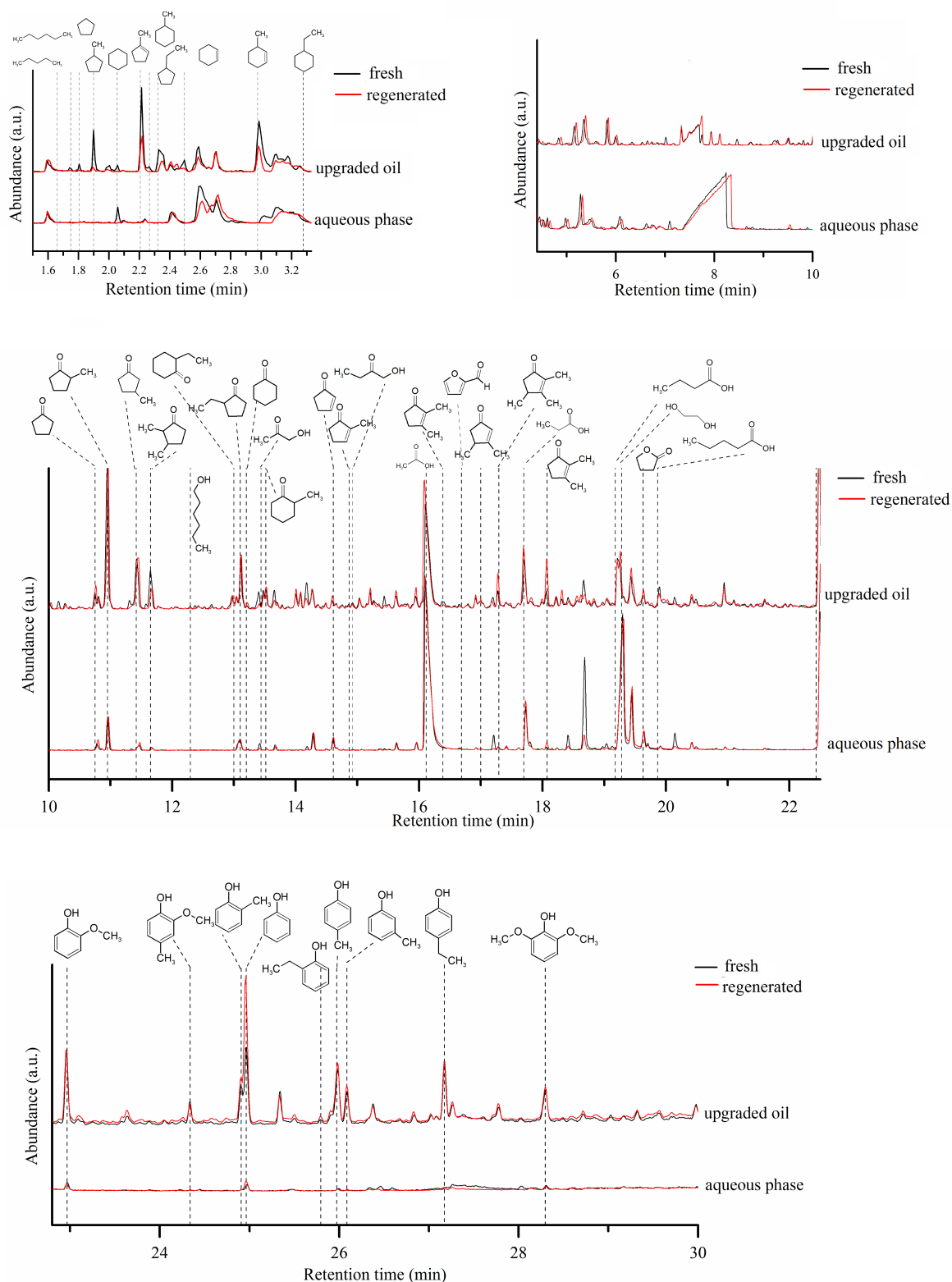
Figure S8: GC-MS of upgraded oil produced from the fresh and regenerated NiCu/Al$_2$O$_3$ (HDO of light phase at 250 °C, 8.0 MPa hydrogen at room temperature).

Figure S9: GC-MS of upgraded oil produced from the fresh and regenerated NiCu/Al$_2$O$_3$ (HDO of light phase at 340 °C, 8.0 MPa hydrogen at room temperature).
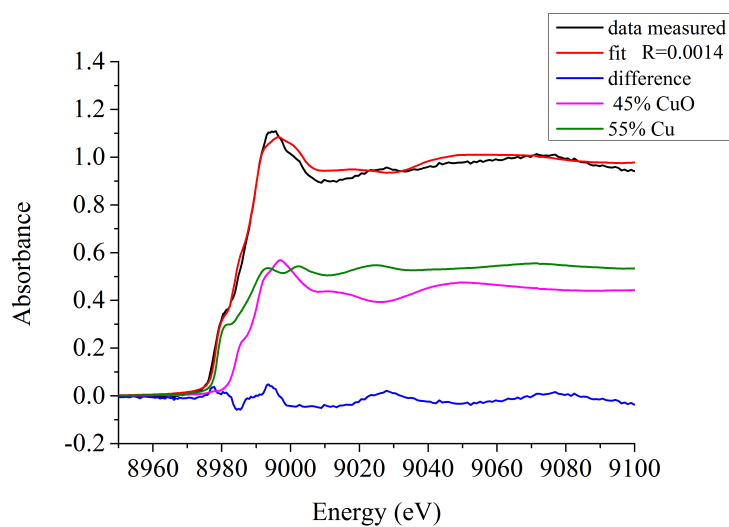
Figure S10: Cu-K edge X-ray fluorescence spectrum of the fresh catalyst NiCu/Al$_2$O$_3$.
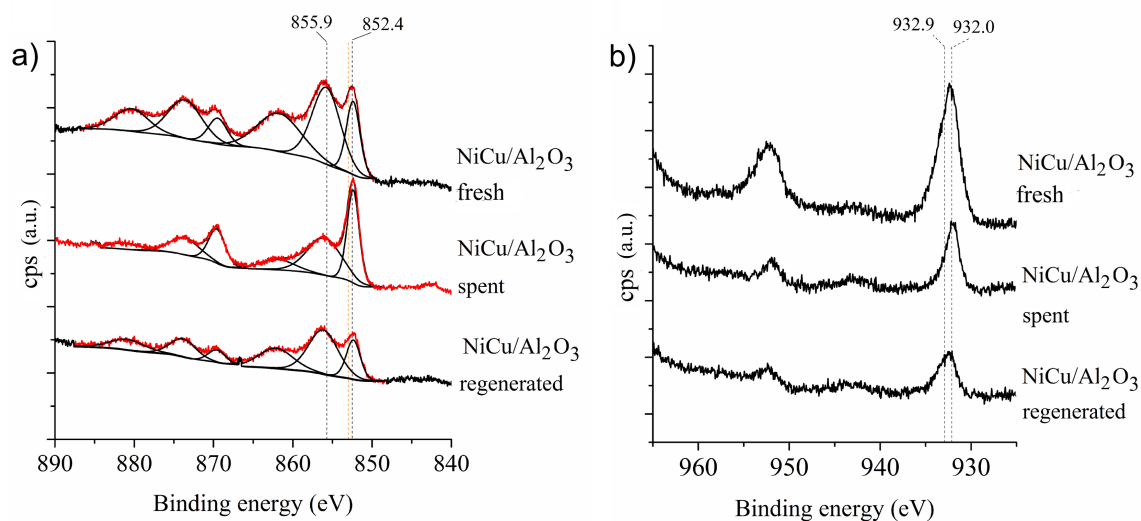
Figure S11: XPS regions of Ni2p (a) and Cu2p (b) of NiCu/Al$_2$O$_3$ in the fresh form, spent at 250 °C and regenerated (partially reduced in situ (5.0 x 10^{-5} mbar H$_2$ for 1 hour at 500 °C)
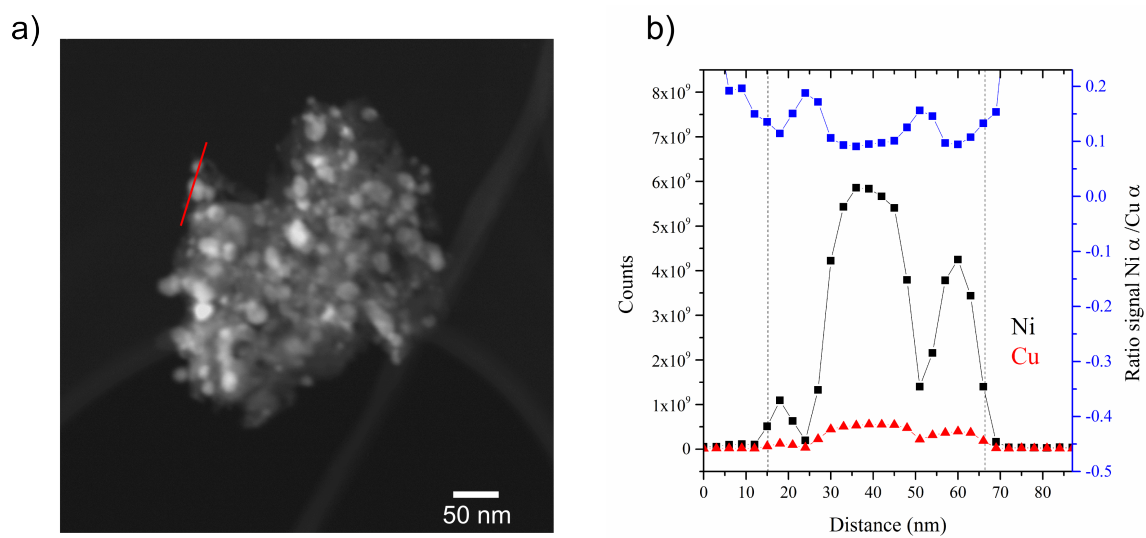
Figure S12: STEM pictures of fresh NiCu/Al$_2$O$_3$, with indicated in red the line scan measured by EDX (a) and signal ratio of Ni and Cu Kα (b).
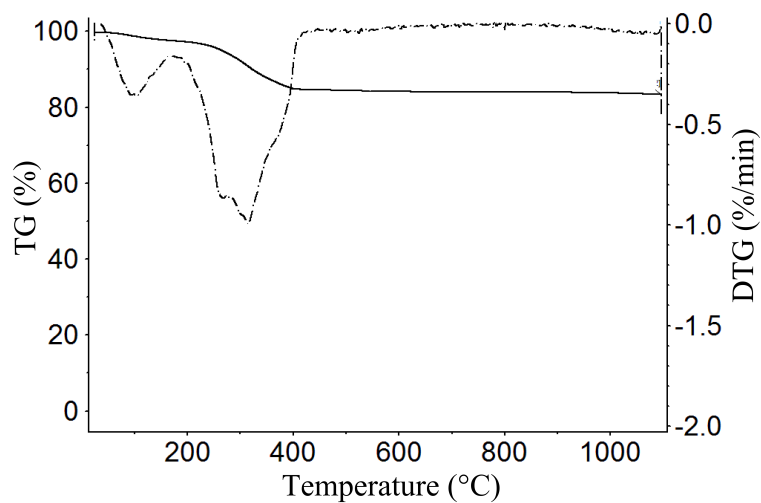
Figure S13: Oxidation of the spent NiCu/Al$_2$O$_3$ produced at 250 °C followed by TGA (atmospheric pressure, 21% oxygen).
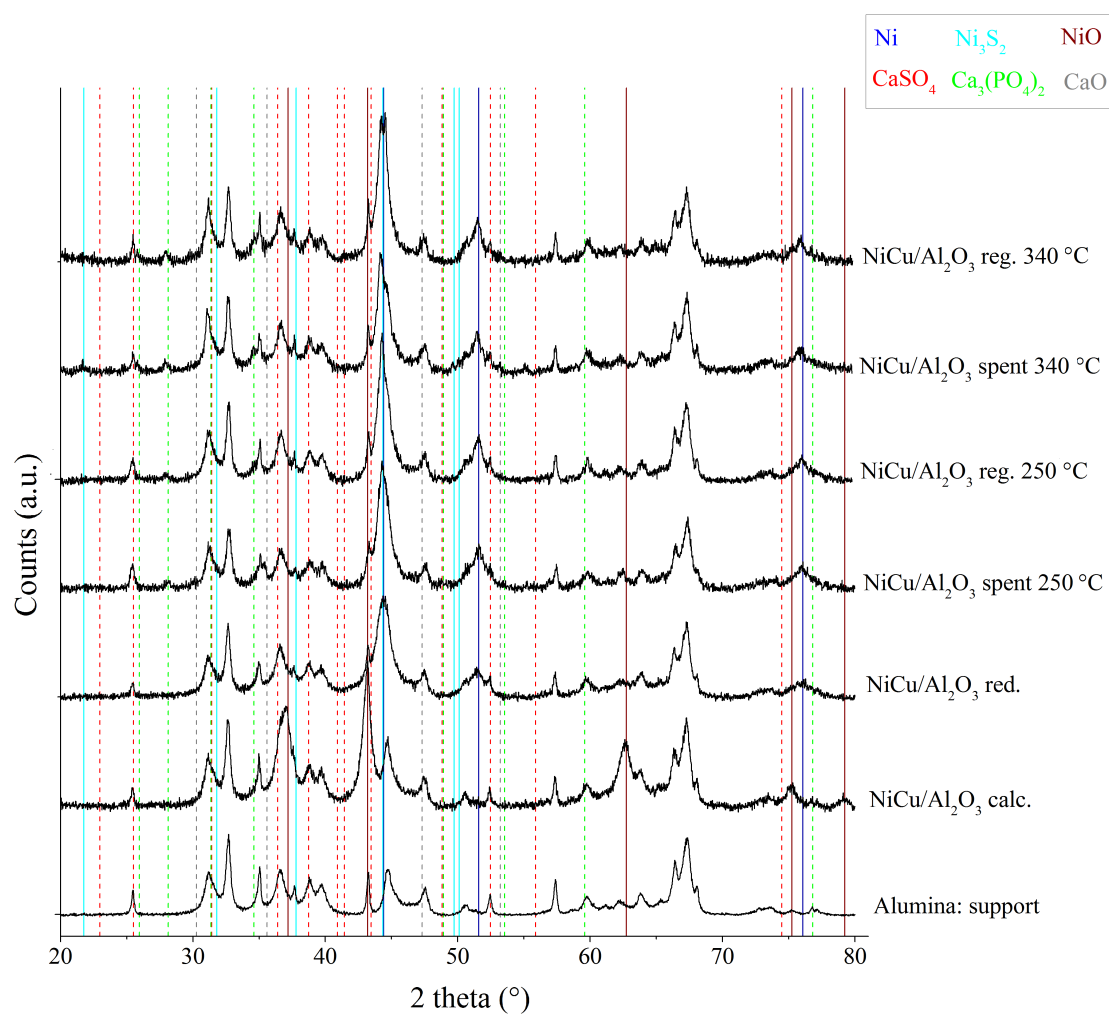
Figure S14: Deposition of calcium salt on the surface of NiCu/Al$_2$O$_3$ detected by XRD (after HDO of light phase at 250 and 340 °C, 8.0 MPa hydrogen at room temperature).
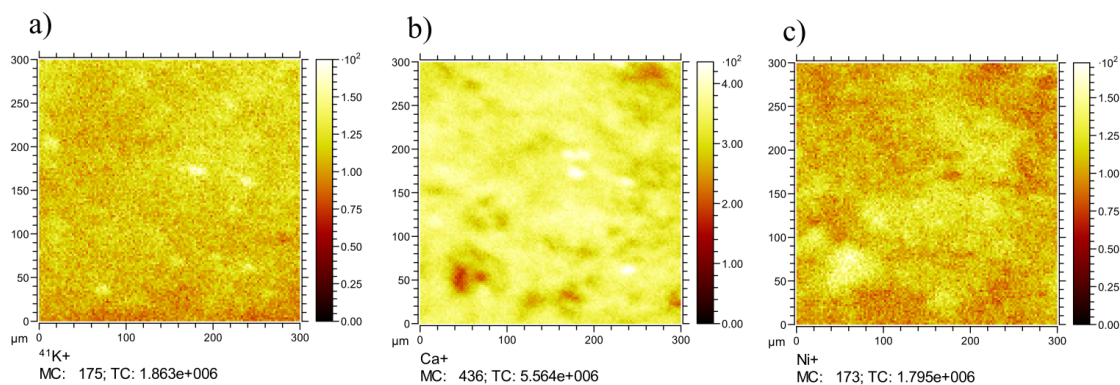
Figure S15: Mapping of potassium, calcium and nickel in the regenerated catalyst NiCu/Al$_2$O$_3$ at 250 °C by ToF-SIMS (after HDO of light phase at 250 °C, 8.0 MPa hydrogen at room temperature.
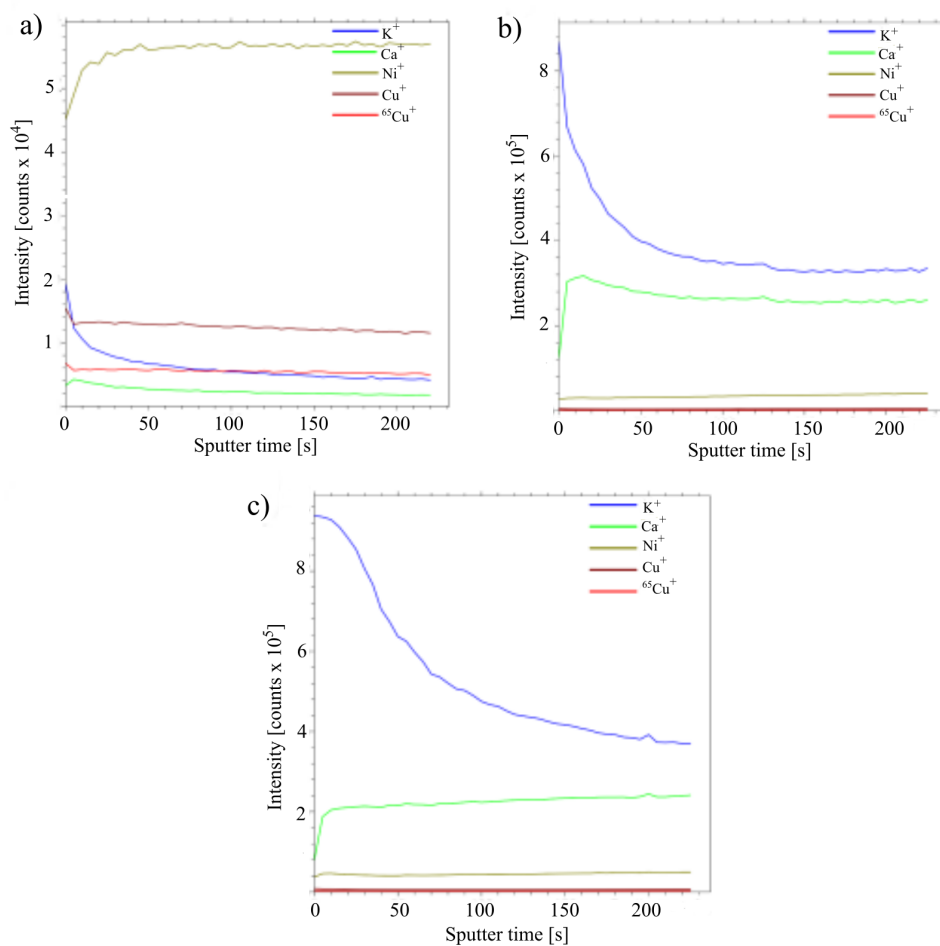
Figure S16: ToF-SIMS depth profile for the fresh catalyst NiCu/Al$_2$O$_3$ (a), the spent at 250 °C (b), the regenerated at 250 °C (c).
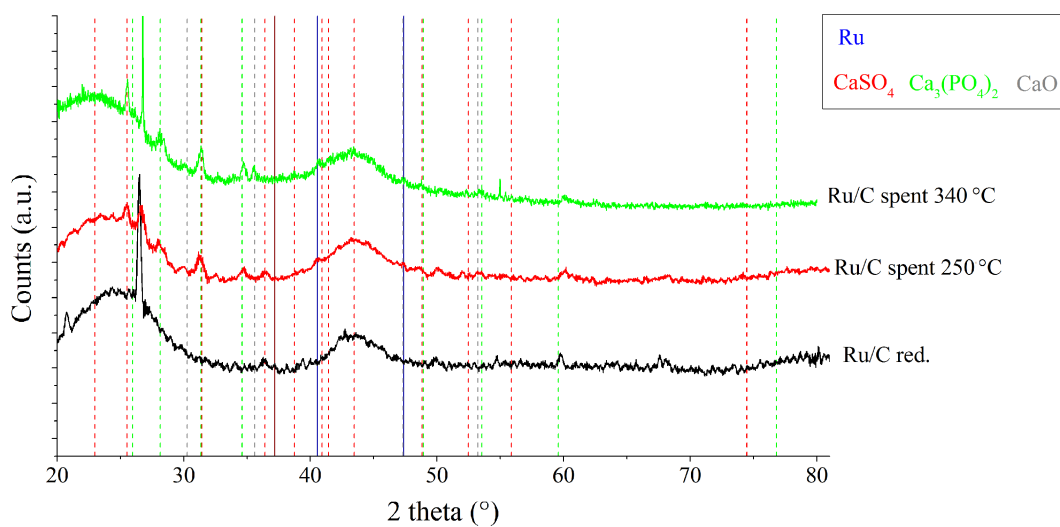
Figure S17: XRD patterns of fresh Ru/C (red.), spent at 250 °C and spent at 340 °C (after HDO of light phase at 250 and 340 °C, 8.0 MPa hydrogen at room temperature).
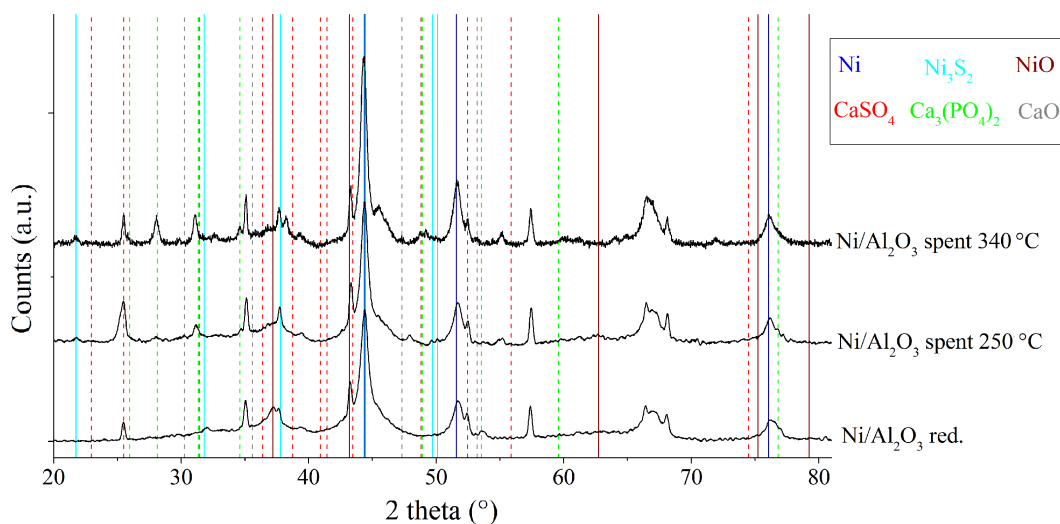
Figure S18: XRD patterns of fresh Ni/Al$_2$O$_3$ (red.), spent at 250 °C and spent at 340 °C (after HDO of light phase at 250 and 340 °C, 8.0 MPa hydrogen at room temperature).
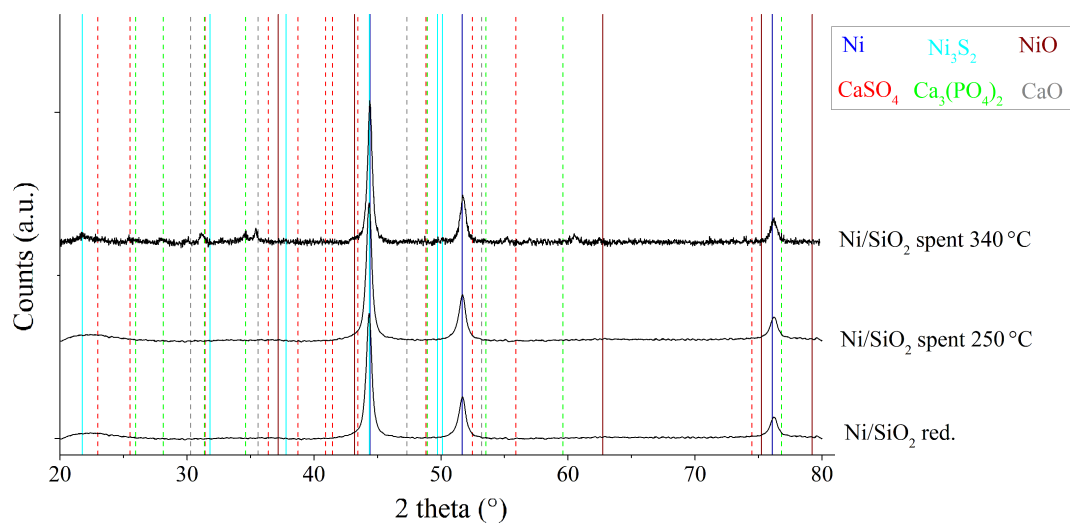
Figure S19: XRD patterns of fresh Ni/SiO₂ (red.), spent at 250 °C and spent at 340 °C (after HDO of light phase at 250 and 340 °C, 8.0 MPa hydrogen at room temperature).
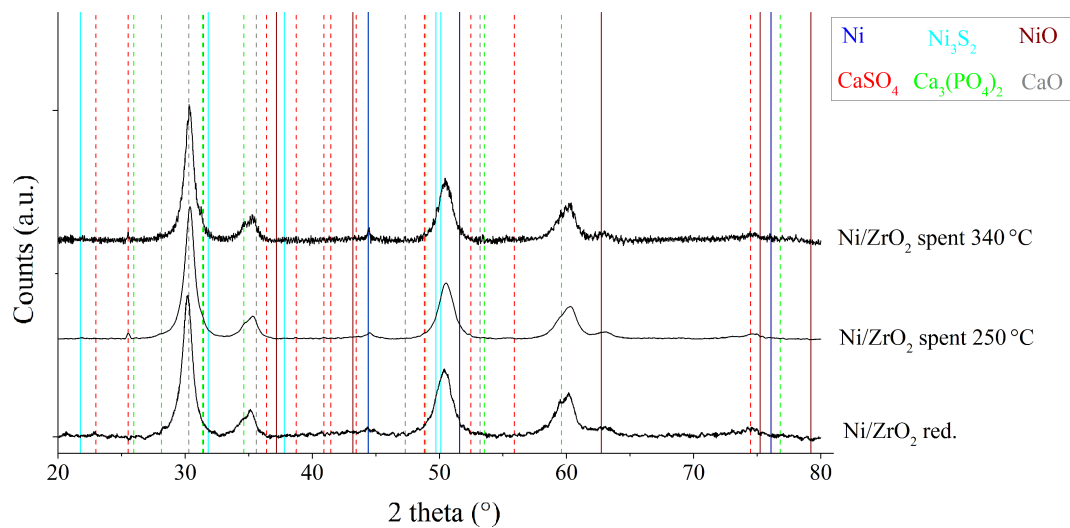
Figure S20: XRD patterns of fresh Ni/ZrO₂ (red.), spent at 250 °C and spent at 340 °C (after HDO of light phase at 250 and 340 °C, 8.0 MPa hydrogen at room temperature).
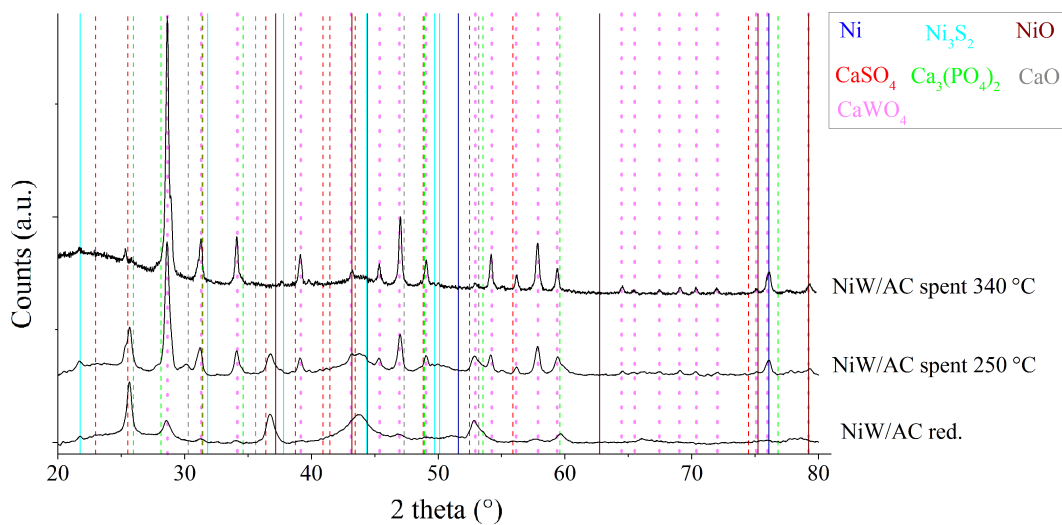
Figure S21: XRD patterns of fresh NiW/AC (red.), spent at 250 °C and spent at 340 °C (after HDO of light phase at 250 and 340 °C, 8.0 MPa hydrogen at room temperature).
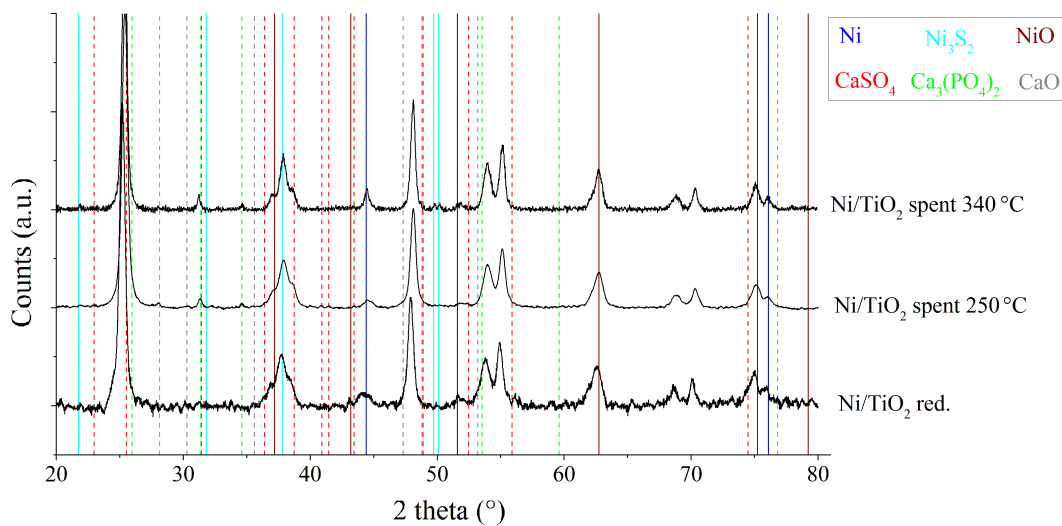
Figure S22: XRD patterns of fresh Ni/TiO$_2$ (red.), spent at 250 °C and spent at 340 °C (after HDO of light phase at 250 and 340 °C, 8.0 MPa hydrogen at room temperature).

Figure S23: GC-MS of upgraded oil produced by the fresh and regenerated NiCu/Al$_2$O$_3$ using beech 450 °C bio-oil (HDO at 350 °C with previous stabilisation at 150 °C, 14.0 MPa H$_2$ at room temperature).

Supplementary tables

Table S1: Superficial concentration (wt.%) of spent catalysts at 250 °C determined by SEM-EDX.

	C	Mg	P	S	Cl	K	Ca	Ni
Ru/C	78.9	0.1	0.7	0.7	0.2	0.5	1.3	-
Ni/Al$_2$O$_3$	16.2	0.2	1.2	0.5	0.1	0.9	2.1	11.6
NiCu/Al$_2$O$_3$	11.9	0.1	1.0	0.6	n.d.	0.9	1.6	13.1
Ni/SiO$_2$	10.2	0.2	0.9	0.6	n.d.	0.9	1.7	18.6
Ni/ZrO$_2$	20.0	n.d.	n.d.	0.4	n.d.	0.3	1.4	4.3
NIW/AC	69.4	0.2	1.2	0.5	n.d.	0.3	2.6	2.5
Ni/TiO$_2$	20.1	0.1	0.7	0.8	n.d.	0.5	1.3	3.0

Table S2: Superficial concentration (wt.%) of spent catalysts at 340 °C determined by SEM-EDX.

	C	Mg	P	S	Cl	K	Ca	Ni
Ru/C	75.0	0.5	0.7	0.9	0.3	0.7	1.8	-
Ni/Al$_2$O$_3$	5.1	0.3	1.0	0.8	0.2	1.0	2.4	13.9
NiCu/Al$_2$O$_3$	5.7	0.2	1.2	0.9	0	0.9	2.0	13.4
Ni/SiO$_2$	10.8	1.8	1.6	0.9	0.2	0.7	2.8	11.6
Ni/ZrO$_2$	14.8	0.4	0.6	0.6	0	0.2	1.8	3.1
NIW/AC	57.2	0.7	1.2	1.4	0.4	1.1	4.5	3.3
Ni/TiO$_2$	7.2	0.2	1.0	0.7	0.1	0.5	1.4	2.5

Table S3: Percentage of the nickel leached in the experiment at 250 °C and 340 °C with light phase.

	250 °C (wt.%)	340 °C (wt.%)
Ru/C	0.2	0
Ni/Al$_2$O$_3$	2.5	0.31
NiCu/Al$_2$O$_3$	0.8	0.24
Ni/SiO$_2$	0.9	0.21
Ni/ZrO$_2$	0.6	0.43
NiW/AC	1.1	0.1
Ni/TiO$_2$	1.3	0.07

List of abbreviations

AC	Activated carbon
ANKA	Angströmquelle Karlsruhe
a.p.	aqueous phase
at.%	atom percentage
ATR-IR	Attenuated Total Reflectance - Infrared Spectroscopy
BET	Brunauer, Emmett and Teller model
calc.	calcined
DFT	Density Functional Theory
D.O.D.	Deoxygenation Degree
EXAFS	Extended X-ray Absorption Fine Structure
FCC	Fluid Catalytic Cracking
FE-SEM	Field Emission - Scanning Electron Microscopy
FID	Flame Ionization Detector
FT-IR	Fourier Transform - Infrared Spectroscopy
GC	Gas Chromatography
HDO	Hydrodeoxygenation
HDS	Hydrodesulfurisation
HHV	Higher Heating Value
HMM	High Molecular Mass
HPTT	High Pressure Thermal Treatment
IAM	Institute of Advance Materials
ICP-OES	Inductively Coupled Plasma - Optical Emission Spectroscopy
IFG	Institute of Functional Interfaces
IKFT	Institute of Catalysis Research and Technology
INT	Institute of Nanotechnology
ITC	Institute of Technical Chemistry
ITCP	Institute for Chemical Technology and Polymer Chemistry

KIT	Karlsruhe Institute of Technology
LMM	Low Molecular Mass
MAT	Micro-Activity Test
MS	Mass Spectroscopy
n.d.	not detected
NMR	Nuclear Magnetic Resonance
PID	Proportional–Integral–Derivative controller
R.C.	Recovery of Carbon
red.	reduced
reg.	regenerated
RSF	Relative Sensitivity Factor
SEM-EDX	Scanning Electron Microscopy - Energy Dispersive X-Ray
STEM	Scanning Transmission Electron Microscopy
TCD	Thermal Conductivity Detector
TEM	Transmission Electron Microscopy
TGA	Thermogravimetric Analysis
ToF-SIMS	Time of Flight - Secondary Ion Mass Spectrometry
TPR	Temperature Programmed Reduction
UHV	Ultra High Vacuum
u.o.	upgraded oil
u.o.b	upgraded oil bottom phase
VGO	Vacuum Gas Oil
wt.%	Weight percentage
WIS	Water InSoluble
WS	Water Soluble
WIS-DIS	Water InSoluble - Dichloromethane InSoluble
WIS-DS	Water InSoluble - Dichloromethane Soluble
WS-DDIS	Water Soluble - Diethyl ether/Dichloromethane InSoluble
WS-DDS	Water Soluble - Diethyl ether/Dichloromethane Soluble
WIS-DS#	WIS-DS without extractives
WS-DDIS*	WS-DDIS without water
XAS	X-ray Absorption Spectroscopy
XANES	X-ray Absorption Near Edge Structure
XPS	X-ray Photoelectron Spectroscopy
XRD	X-Ray Diffraction

List of symbols

C_{H2}	fraction in volume of hydrogen in a mixture of gases
C_i	fraction in volume of a i-component in a mixture of gases
C_{oil}	carbon percentage measured by elemental analysis in the upgraded oil
C_w	carbon percentage measured by elemental analysis in the aqueous phase
K	Crystallite shape factor
m_{feed}	Mass of the feed
m_{oil}	Mass of the upgraded oil
$molH_{2c}$	mol of hydrogen consumed
$molH_{2f}$	mol of hydrogen after the reaction
$molH_{2i}$	mol of hydrogen before the reaction
mol_i	mol of the i-component after the reaction
mol_{tot}	total mol of gases
O_{oil}	oxygen percentage measured by elemental analysis in the upgraded oil
C_w	oxygen percentage measured by elemental analysis in the aqueous phase
TotC	quantity of carbon theoretically recovered in the liquid products
TotO	quantity of oxygen theoretically recovered in the liquid products
Y_{oil}	Yield of the upgraded oil
wt.%C_{feed}	Weight percentage of the Carbon contained in the feed
wt.%C_{oil}	Weight percentage of the Carbon contained in the upgraded oil
wt.%O_{feed}	Weight percentage of the Oxygen contained in the feed
wt.%O_{oil}	Weight percentage of the Oxygen contained in the upgraded oil
δ	chemical shift
θ	Bragg angle
μ	Dynamic viscosity
ρ	Density
%oil	quantity in weight percentage of the upgraded oil produced
%wp	quantity in weight percentage of the aqueous phase produced

List of publications

Publications in this thesis

C. Boscagli, K. Raffelt, T.A. Zevaco, W. Olbrich, T.N. Otto, J.Sauer, J.-D. Grunwaldt
Mild hydrotreatment of the light fraction of fast-pyrolysis oil produced from straw over nickel-based catalysts
Biomass Bioenergy. 83 (2015) pp. 525–538.

Publications submitted to journals and in preparation related to this thesis

C. Boscagli, K. Raffelt, J.-D. Grunwaldt
Deep hydrotreatment of pyrolysis oil and platform molecules over nickel and ruthenium catalysts.
submitted for publication.

C. Boscagli, C. Wang, A. Welle, W. Wang, S. Behrens, K. Raffelt, J.-D. Grunwaldt
Effect of pyrolysis oil components on the activity and selectivity of nickel-based catalysts during hydrotreatment.
submitted for publication.

C. Boscagli, M.Tomasi Morgano, K. Raffelt, H. Leibold, J.-D. Grunwaldt
Influence of feedstock, catalyst, pyrolysis and hydrotreatment temperature on the composition of upgraded oils.
in preparation.

Further publications

W. Olbrich, C. Boscagli, K. Raffelt, H. Zang, N. Dahmen, J. Sauer
Catalytic hydrodeoxygenation of pyrolysis oil over nickel-based catalysts under H_2/CO_2 atmosphere
Sustain. Chem. Process. 4 (2016) pp. 1-9.

C. Weber, C. Boscagli, K. Raffelt, D. Richter, T. Zevaco
Fast Pyrolysis of Fresh Bio Waste and Ensiled Municipal Green Cut
Chem. Ing. Tech. 87 (2015) pp. 1696–1706.

Oral presentations

C. Boscagli, K. Raffelt, J.-D. Grunwaldt
Study of the reactivity of platform molecules in aqueous solution and in the pyrolysis oil during hydrotreatment
Pyro2016, 9-12 May 2016, Nancy (France).

C. Boscagli, K. Raffelt, T. Zevaco, J. Sauer, J.-D. Grunwaldt
Hydrotreatment of pyrolysis oil using nickel-based catalysts
24th European Biomass Conference and Exhibition, 1-5 June 2015, Wien (Austria).

M. Tomasi Morgano, C. Boscagli, L. Jampolski, H. Leibold, F. Richter, H. Seifert, D. Stapf
Production and Conditioning of Wood Pyrolysis Oil from a Screw Reactor with Integrated Hot Gas Filtration
Advanced Biofuels Symposium 2016, July 6-8 2016, Vancouver (Canada).

W. Olbrich, C. Boscagli, K. Raffelt, J. Sauer, N. Dahmen
Catalytic hydrodeoxygenation of pyrolysis oil over nickel-based catalysts under H_2/CO_2 atmosphere
3rd Iberoamerican Congress on Biorefineries (CIAB), 4th Latin American Congress on Biorefineries and 2nd International Symposium on Lignocellulosic Materials, 23-25 November 2015, Concepción (Chile).

Poster presentations

C. Boscagli, K. Raffelt, J.-D. Grunwaldt
Upgrading of fast pyrolysis oil by hydrotreatment over nickel-based catalysts
24th European Biomass Conference and Exhibition 2016, 6-9 June 2016, Amsterdam (The Netherlands).

C. Boscagli, K. Raffelt, T. Zevaco, J. Sauer, J.-D. Grunwaldt
Nickel-Based Catalysts for Upgrading of Pyrolysis Oils
NAM24, 14-19 June 2015, Pittsburg (USA).

C. Boscagli, K. Raffelt, T. Zevaco, J. Sauer, J.-D. Grunwaldt
Evaluation of catalytic hydrotreatment as an upgrading method for bioliq®-condensates
WasteEng2014 Conference, 25-28 August 2014, Rio de Janeiro (Brasil)
Award for the best student poster.

C. Boscagli, K. Raffelt, T. Zevaco, J. Sauer, J.-D. Grunwaldt
Evaluation and development of upgrading methods for bioliq-condensate
22nd European Biomass Conference and Exhibition 2014, 23-26 June 2014, Hamburg (Germany).

C. Weber, C. Boscagli, E. Dinjus, A. Niebel, K. Raffelt, T. Zevaco
Fast pyrolysis of fresh biowaste and ensiled municipal green cut waste
21st European Biomass Conference and Exhibition 2013, 3-7 June 2013, Copenhagen (Denmark).

Eidesstattliche Erklärung

Hiermit versichere ich, die vorliegende Doktorarbeit selbständig angefertigt und keine anderen als die von mir angegebenen Quellen und Hilfsmittel verwendet, sowie wörtliche und sinngemäße Zitate als solche gekennzeichnet zu haben. Die Arbeit wurde in gleicher oder anderer Form keiner anderen Prüfungsbehörde zur Erlangung eines akademischen Grades vorgelegt.

Karlsruhe, den _____

Datum und Unterschrift